A THEORY AND METHOD OF PREDICTING THE STABILITY DERIVATIVES Cl_β, Cl_r, Cn_p, AND CY_p FOR WINGS OF ARBITRARY PLANFORM IN SUBSONIC FLOW

by

M. J. Queijo

Thesis submitted to the Graduate Faculty of the

Virginia Polytechnic Institute

in candidacy for the degree of

DOCTOR OF PHILOSOPHY

in

ENGINEERING MECHANICS

June 1963

Blacksburg, Virginia

II. TABLE OF CONTENTS

CHAPTER PAGE

III. LIST OF TABLES AND FIGURES

A. TABLES

B. FIGURES

FIGURE PAGE

FIGURE PAGE

IV. SYMBOLS AND DEFINITIONS

A	aspect ratio, b^2/S
a	speed of sound, feet per second
b	wing span, feet
c	wing local chord, feet
$\bar{c}$	wing average chord, feet
c_r	wing root chord, feet
c_t	wing tip chord, feet
d	spanwise distance from wing centerline to center of rotation of yawing wing
F_i	force vector
L	lift, pounds
L'	rolling moment, foot pounds
M	free-stream Mach number
M'	pitching moment, foot pounds
N	yawing moment, foot pounds
P	rate of roll, radians per second
p'	pressure, pounds per square foot
q	pitching velocity, radians per second
R	universal gas constant
r	yawing angular velocity, radians per second
S	wing area, square feet
S'	perpendicular distance to vortex line for case of zero sideslip
T	absolute temperature, degrees Rankine

t	time, seconds
u	wind velocity in x-direction, feet per second
u_i	velocity vector
V	free-stream wind velocity, feet per second
V_0	velocity at moment center for yawing wing, feet per second
v	wind velocity in y-direction, feet per second
v'	specific volume, cubic feet per slug
w	wind velocity in z-direction, and also downwash velocity feet per second
$\bar{X}$	chordwise distance between aerodynamic center (a. c.) and moment center (or center of gravity, c. g., in flight), positive when c. g. is upstream of a. c., feet
x_i	displacement vector
x,y,z	displacements along reference axes, feet
$(x)_{c/4}$	x-distance to quarter-chord line, feet
$(x)_c$	x-distance to wing trailing edge, feet
Y	side force, pounds
$\bar{y}$	spanwise position of centroid of the angle-of-attack span loading, feet
$\tilde{y}$	radius of gyration of angle-of-attach span loading, feet
α	angle of attack (or incidence), radians
α_i	induced angle of attack, radians
β	sideslip angle, radians
Γ	circulation or vortex strength

Γ_y	circulation strength related to spanwise position
Γ_ξ	circulation strength related to displacement along quarter-chord line
∇	del operator
Λ	sweep angle of quarter-chord line, radians
λ	wing taper ratio, c_t/c_r
ξ	distance along the quarter-chord line, measured from wing centerline, feet
ρ	mass density, slugs per cubic foot
ϕ	velocity potential
l	lift per unit length of vortex
l_1	lift per unit span of quarter-chord-line vortex, pounds
l_2	lift per unit length of chordwise-bound vortex, pounds
$\left(\frac{cc_l}{\bar{c}C_L}\right)_0$	angle-of-attack span-load parameter at zero Mach number
$\left(\frac{cc_l}{\bar{c}C_L}\right)_r$	span-load parameter associated with yawing
$\left(\frac{cc_l}{\bar{c}C_L}\right)_\beta$	span-load parameter associated with sideslip
C_D	drag coefficient, $D/\frac{1}{2}\rho V^2S$
C_L	lift coefficient, $L/\frac{1}{2}\rho V^2S$
C_l	rolling-moment coefficient, $L'/\frac{1}{2}\rho V^2Sb$
C_m	pitching-moment coefficient, $M'/\frac{1}{2}\rho V^2S\bar{c}$
C_n	yawing moment coefficient, $N/\frac{1}{2}\rho V^2Sb$

C_Y side-force coefficient, $Y/\frac{1}{2}\rho V^2 S$

$C_{D_\alpha} = \frac{\partial C_D}{\partial \alpha}$

$C_{D_q} = \frac{\partial C_D}{\partial \frac{qc}{2V}}$

$C_{L_\alpha} = \frac{\partial C_L}{\partial \alpha}$

$C_{l_\beta} = \frac{\partial C_l}{\partial \beta}$

$C_{l_P} = \frac{\partial C_l}{\partial \frac{Pb}{2V}}$

$C_{m_\alpha} = \frac{\partial C_m}{\partial \alpha}$

$C_{n_\beta} = \frac{\partial C_n}{\partial \beta}$

$C_{n_P} = \frac{\partial C_n}{\partial \frac{Pb}{2V}}$

$C_{Y_\beta} = \frac{\partial C_Y}{\partial \beta}$

$C_{Y_P} = \frac{\partial C_Y}{\partial \frac{Pb}{2V}}$

c_l section-lift coefficient, $l/\frac{1}{2}\rho V^2 c$

$c_{l_\alpha} = \frac{\partial c_l}{\partial \alpha}$

$$C_{L_q} = \frac{\partial C_L}{\partial \frac{q\bar{c}}{2V}}$$

$$C_{m_q} = \frac{\partial C_m}{\partial \frac{q\bar{c}}{2V}}$$

$$C_{l_r} = \frac{\partial C_L}{\partial \frac{rb}{2V_0}}$$

$$C_{n_r} = \frac{\partial C_n}{\partial \frac{rb}{2V_0}}$$

$$C_{Y_r} = \frac{\partial C_Y}{\partial \frac{rb}{2V_0}}$$

Note: A star (*) superscript indicates that the quantity has been nondimensionalized by division by $b/2$; for example

$$y^* = \frac{y}{b/2}$$

V. INTRODUCTION

A. The Problem

The safety of an aircraft and its occupants depends to a large extent on the structural integrity and inherent stability characteristics of the aircraft. Both the structural requirements and the inherent (or natural) stability characteristics depend on the aerodynamic characteristics and the expected or probable flight envelope of the aircraft. Therefore, in order not to excessively penalize the aircraft by overdesign based on uncertainties of aerodynamic loading, and in order to predict stability characteristics during the design stage, an accurate knowledge of aerodynamics of the proposed aircraft is necessary. The aerodynamic characteristics of aircraft are predicted by estimating the characteristics of the aircraft components (wing, fuselage, tail, etc.) and by proper addition of the characteristics of the components with due regard for interference effects. In this process, the basic ingredient is the accurate prediction of the aerodynamics of the aircraft components. The lifting surfaces (wing and tail surfaces) generally produce the predominant aerodynamic forces, therefore much effort has been expended in developing methods of predicting the aerodynamics of lifting surfaces. Most of this effort, however, has been directed toward determination of aerodynamic characteristics associated with angle of attack. Aerodynamics associated with other aircraft motions (rolling, yawing, pitching, sideslipping) have been investigated to a lesser degree, and generally by somewhat cruder methods. This is particularly true for the low speed regime. The nature of the governing equations for supersonic

speeds is such that it has been possible to obtain equations for loads and aerodynamic derivatives for wings performing various modes of motion (see refs. 1 through 4, for example).

The purpose of the present paper is to examine the problem of wing characteristics in subsonic compressible flow and to develop a theory and method for computing these characteristics.

B. Background for the Present Study

There are a number of problems associated with attempting to predict aerodynamic characteristics of wings performing the possible modes of motion. One problem is that of finding an adequate mathematical model for the wing, and the second is that associated with solution of the equations which arise from use of the mathematical models. Throughout the years, various methods for predicting certain aerodynamic characteristics of unswept wings having fairly high aspect ratio, and taper ratios in the range from about 0.25 to 1.0 have been developed by a number of investigators, and numerous reports published from which certain characteristics can be obtained for specific wings (see refs. 5 and 6, for example).

The use of high-aspect ratio, unswept wings for aircraft was acceptable for a number of years, primarily because the low thrust-to-weight ratio of aircraft engines seriously limited the speed of aircraft. As engine efficiency increased, however, aircraft velocities increased and reached the region where Mach number effects become important. The designer was now faced with a new phenomenon, the

"transonic drag rise" (fig. 1). Aerodynamic theory indicated that wing drag (for a specific wing incidence) would begin to rise quite rapidly as the Mach number increased beyond about 0.9, and would become infinitely great at Mach number 1. Experimental data showed similar trends, but the maximum drag coefficient reached some finite limit, as shown in the example of figure 1. The transonic drag rise was sufficiently great that it appeared that aircraft speeds would be limited to Mach numbers less than unity unless (a) some means were found to reduce the transonic drag rise, or (b) extremely powerful light-weight aircraft propulsion systems could be developed.

A close examination of aerodynamic theory indicated that the Mach number of the flow normal to the wing leading edge, rather than the free-stream Mach number, was the important parameter in determining compressibility effects. In other words, the transonic drag rise could be delayed to higher aircraft speeds by resorting to sweptback wings (see ref. 7, for example).

The aerodynamacist and aircraft designer were now faced with an additional variable, sweep, in predicting the aerodynamic characteristics of wings. Three general approaches were used in determining the aerodynamics of swept wings, these were:

(a) Computations based on mathematical models associated with the use of vortices, sources, sinks, or other concepts to represent the wing. (Refs. 8 through 12, for example.)

(b) Determination of approximate equations based on treating each wing semispan as one half of an unswept wing. The

"unswept" panels are skewed relative to each other to simulate a swept wing. (Refs. 13 through 15, for example.)

(c) Development of design charts based on tests of a great number of wings of various sweep angles, aspect ratio, and taper ratio. (Ref. 16, for example.)

The first of these approaches is very difficult, and for this reason only a few aerodynamic parameters (primarily C_{l_r} and C_{l_p}) have been attacked by fairly rigorous mathematical methods.

The second approach has been quite successful in predicting trends and, with some modifications, has been used to obtain good quantative results for certain aerodynamic characteristics. (See ref. 17, for example.) These approximate methods, however, are not mathematically rigorous and do not give a good insight into the basic aerodynamics involved.

The third approach is adequate for engineering data provided the available data envelope the range of geometric variables of interest. Unfortunately, the amount of data available for some of the wing derivatives is very limited because of the scarcity of experimental facilities for determining such derivatives. One might ask, for example, how many facilities are currently available which can be used to measure yawing or pitching derivatives?

There is, then, a requirement for a theory which will permit accurate estimation of the important wing derivatives by a rigorous method which provides an insight regarding the origin of the derivatives.

C. Purpose of the Present Study

The preceeding discussion points out the desirability of the development of a theory which will permit the use of a fairly simple, consistent method of predicting the aerodynamic characteristics of wings of arbitrary planform with little computational effort. The present thesis develops such a theory and method, based on a simplified vortex system representation of a wing. It is shown that the theory and method are applicable to wings of arbitrary planform. In addition, the developed methods are used to prepare charts from which various aerodynamic parameters of arbitrary wings can be obtained. Numerous comparisons between results of the theory developed herein, and those of other theories and experimental results are shown. Most of the experimental results used in the comparisons were obtained in the former Langley Stability Tunnel. This facility, which is presently located on the VPI campus in Blacksburg, Virginia, is unique in that it can be used to obtain experimental data under conditions simulating linear, rolling, pitching, or yawing flight under steady-state conditions. In addition, several mechanisms have been developed which permit tests of airplane model components under oscillating conditions. References containing descriptions of the tunnel and complementary mechanisms will be mentioned in those sections concerned with comparisons of experimental and theoretical results.

VI. REVIEW OF THE LITERATURE

A. Aerodynamic Forces and Moments

In classical aerodynamic theory, the forces and moments on a body immersed in a moving fluid are assumed to depend on the fluid velocity and the angle between the free-stream velocity and some reference plane or references planes in the body. For example, the lift on a wing is dependent on the airspeed and on the angle of attack. If one assigns a set of orthogonal axes to the body, then there is the possibility of obtaining a force and a moment component related to each axis as shown in figure 2. In determining the motions or stability of a body in a moving fluid, one is generally concerned with motion following a small disturbance from an equilibrium condition. A basic assumption made in such an analysis is that the resulting additional forces and moments acting on the body are linear functions of the resulting change in incidence of the airstream relative to the body. The six equations of motion of the rigid body can then be written, that is - one force and one moment equation related to each axis. The equations of motion for a purely arbitrary body can be quite complex. However, because aerodynamic shapes of interest, particularly aircraft, have a plane of symmetry, some simplifications are possible. A full development of the equations can be found in many publications on the dynamic stability of aircraft (ref. 18, for example). The equations show that the forces and moments acting on the aircraft are functions of certain aerodynamic derivatives, namely, C_{L_α}, C_{m_α}, C_{D_α}, C_{Y_β}, C_{l_β}, C_{n_β}, C_{Y_p}, C_{n_p}, C_{l_p}, C_{Y_r}, C_{n_r}, C_{l_r}, C_{L_q}, C_{m_q}, C_{D_q}. The importance of

the various derivatives in estimating airplane stability depends to a large extent on the airplane geometry and the flight speed. This is pointed out quite clearly in reference 19, which is an excellent summary of the current state of the art in estimation of derivatives. Since the geometry of current aircraft varies from that of high-aspect-ratio-wing, thin-body, low speed craft, to low-aspect-ratio-wing, thick-body craft it is apparent that there exists a need for methods of accurately predicting most, if not all, of the derivatives.

B. Estimation of the Aerodynamic Forces, Moments, and Derivatives

1. Governing equations of fluid motion.- The forces and moments acting on a body immersed in a moving fluid can be determined by use of the classical inviscid-fluid-flow equations. The pertinent equations are given here in index or summation notation as a matter of convenience. This notation is not used elsewhere in the thesis. The pertinent equations are:

Euler's equations of motion

$$F_i = \frac{Du_i}{Dt} + \frac{1}{\rho}\frac{\partial p'}{\partial x_i} \qquad i = 1, 2, 3$$

Continuity equation

$$\frac{\partial \rho}{\partial t} + \frac{\partial(\rho u_i)}{\partial x_i} = 0 \qquad i = 1, 2, 3$$

and the equation of state for a perfect gas

$$p' = \rho RT$$

The following assumptions are commonly made in classical aerodynamics:

1. No body forces exist, therefore, the equations of motion reduce to

$$\frac{Du_i}{Dt} + \frac{1}{\rho}\frac{\partial p'}{\partial x_i} = 0 \qquad i = 1, 2, 3$$

2. The flow is isentropic, so that a unique pressure-density relationship exist, that is

$$a^2 = \frac{\partial p'}{\partial \rho}$$

3. The fluid is initially at rest or moving with uniform velocity and is, therefore, initially irrotational. Consequently, from Kelvin's circulation theorem, the flow will remain irrotational. The flow, therefore, is always irrotational, and the concept of the velocity potential is applicable.

With these assumptions, the equations of motion and continuity can be manipulated to yield the governing equation for the velocity potential

$$\nabla^2\phi = \frac{1}{a^2}\frac{\partial^2\phi}{\partial t^2}$$

which is the vector form of the three-dimensional wave equation. For steady flows, which is of primary interest in this study, the above equation reduces to Laplace's equation

$$\nabla^2\phi = 0$$

The boundary conditions which are used with the governing equations to solve specific flow problems are:

1. There is no component of flow velocity normal to the wing.

2. The flow has finite velocity infinitely far from the wing.

The Laplace equation and the above two boundary conditions are, in principle, sufficient to solve specific flow problems (and have been used for a large number of flow problems).

2. Aerodynamic forces on unswept wings.- The direct approach of attempting to solve the linear Laplace equation for steady-state flows, subject to the proper boundary conditions, is quite complex. Therefore, a common practice is to attempt a solution by investigating the characteristics of flows built up by addition of elementary solutions of the Laplace equation. The vortex potential is a solution of the Laplace equation and satisfies the second boundary condition stated above. Since the Laplace equation is a linear differential equation, the principle of superposition of solutions is applicable. In dealing with lifting wings, the general approach is to construct a solution by use of a free-stream potential and a suitable distribution of vortices. In classical aerodynamics solutions are obtained for very thin wings at low angles of attack, and these restrictions permit placement of the vortices in the plane of the free stream, and permit the boundary condition, $\vec{v} \cdot \vec{n} = 0$, to be satisfied in the same plane. The boundary condition can be restated as requiring that the flow direction over the wing be parallel to the actual wing surface. This condition is to be satisfied over the wing surface. Before proceeding with the solution of wing aerodynamics, a few fundamental questions must be answered

(a) What vortex distribution should be used to represent the wing, and how should the vortices be placed relative to the wing?

(b) Is it necessary to satisfy the boundary condition condition at all points on the wing?

(c) How does one determine the strength of the vortices, and

(d) How is the vortex strength related to the wing lift?

a. Two-dimensional airfoils

One of the earliest aerodynamic problems attempted was that of lift on a wing at some angle of incidence. The fundamental law relating lift, stream velocity, and circulation is given by the Kutta-Joukowski law

$$l = \rho V \Gamma \tag{1}$$

where l is the lift per unit length of vortex, V is the velocity component normal to the vortex, and Γ is the strength of the vortex. The lift, and circulation, can be related to the angle of incidence of a two-dimensional airfoil as follows. The lift per unit span of a two-dimensional airfoil is related to incidence by

$$l = c l_\alpha \alpha \frac{1}{2} \rho V^2 c$$

Therefore, the circulation is related to incidence by

$$\Gamma = \frac{1}{2} V c \, c l_\alpha \alpha \tag{2}$$

Aerodynamic theory gives a value for the two-dimensional lift-curve-slope $c l_\alpha$ of 2π, therefore, the circulation strength is given by

$$\Gamma = \pi V c \alpha \tag{3}$$

A few observations should now be made. Experimental pressure

on two-dimensional airfoils have shown that the centroid of lift is

located close to the wing quarter-chord line. It appears reasonable, therefore, to locate the lifting vortex at the wing quarter-chord line. One could now ask where, if any place, is the boundary condition satisfied for a single-vortex representation of the wing? This can be considered as follows. The velocity distribution around a two-dimensional vortex is given by

$$v = \frac{\Gamma}{2\pi s'}$$

Therefore, in the wing plane, the flow angle is given by

$$\alpha = \frac{v}{V} = \frac{\Gamma}{2\pi s' V} \qquad (4)$$

Combining equations (3) and (4) results in

$$\Gamma = \pi V c \frac{\Gamma}{2\pi s' V}$$

from which

$$s' = \frac{c}{2}$$

This shows that the flow direction is parallel to the wing at one-half chord from the lifting vortex, or at a distance of three-quarter chord from the wing leading edge. The application of this observation will be pointed out in a later section.

b. Three-dimensional airfoils; Prandtl wing theory

In the case of a two-dimensional wing, the flow is identical in all planes perpendicular to the span. This obviously is not true for three-dimensional wings since the lift is known to drop off rapidly

near the tips. A treatment of the problem of the three-dimensional flow over an unswept wing of finite span was given by Prandtl in 1918, although the basic concepts were discussed by him in 1911 and realized still earlier by Lancaster. Prandtl's wing theory is closely related to the important laws for vortices

1. A vortex filament cannot have an end, but must continue to infinity or form a closed path.
2. The strength of a vortex filament is constant along its length.
3. Vortices in a fluid always remain attached to the same particles of fluid.

These are the Helmholtz vortex theorems and were first given by him in eighteen fifty-eight.

The vortex filament which replaces the wing in two-dimensional wing theory was called the "lifting line" or "bound vortex" by Prandtl. His basic conception was to realize that Helmholtz vortex laws applied to such bound vortices just as if they were ordinary vortices having a physical existence in the fluid. Vortex theorems 1 and 2 indicate that the bound vortex cannot end at the wing tip, nor can the vortex become weaker as the wing tip is approached. The only possibility of making the load drop to zero at the wing tip appeared to be to permit the vortex to turn 90° and extend downstream parallel to the free-stream velocity. This resulted in the Prandtl horseshoe vortex shown in figure 3. It is apparent that the "bound" vortex will produce constant lift across the span, and that the "trailing" or free vortices will produce no lift. This simple representation of the wing has two glaring faults, (1) the constant spanwise load which is equal to that of a two-dimensional

vortex, and (b) the infinite downwash at the wing tips. The first of these difficulties was met, in part, by assuming that the downwash due to the tip vortices reduced the effective angle of attack. Since the downwash varied with spanwise position, a value often used is that associated with the center of the bound vortex. The section lift on the wing now remained constant, but had a lower magnitude, and was given by

$$c_l = 2\pi(\alpha - \alpha_i) \qquad (5)$$

where α_i is the induced angle at the wing (bound vortex center) and numerically equal to

$$\alpha_i = \frac{w}{V}$$

The objections regarding constant lift across the span and infinite downwash at the wing tips remained.

Prandtl's group was finally able to resolve these difficulties by proposing that a series of horseshoe vortices be used to represent the wing. The vortices were placed so that the lifting lines were coincident (see fig. 4). The circulation strength along the quarter-chord line at any position along the span is then equal to the sum of the circulations of the individual vortices at that spanwise position. The superposition principle can be carried to the limit in which an infinite number of horseshoe vortices, each of infinitesimal strength is used to represent the wing. This results in a trailing vortex sheet instead of a number of discrete vortices, and in a continuous distribution of circulation over the span. Since the strength of each vortex is infinitesimal, there is no infinite value of downwash on the wing. Thus the difficulties associated with the one-horseshoe-vortex

representation were eliminated.

The vortex pattern described above is very flexible and can be used to determine a circulation distribution which corresponds to any desired lift distribution over the wing. The spanwise circulation distribution determines the distribution of the strength of the trailing vortices, and also the local downwash distribution. Therefore, the lift, downwash velocity, and effective angle of attack are all closely related. Working out this complex set of interrelationships to obtain the characteristics of a given wing involve very lengthy and elaborate calculations.

The lifting-line theory described above has been used extensively to determine the characteristics of unswept wings of fairly large aspect ratio (see ref. 5, for example). However, the vortex system described above cannot adequately predict the characteristics of wings having sweep and low aspect ratio. Consequently, it has been found necessary to turn to more complex lifting-surface theories or modifications to the lifting-line theory.

C. Lifting-Surface Theories for Computing Span Loads due to Angle of Attack

A number of methods have been developed for predicting the load due to angle of attack (and consequently the lifting-curve-slope C_{L_α}) for wings of arbitrary planform and sweep. Of these, three have been used quite extensively; that of V. M. Falkner (ref. 10), of Wm. Mutterperl (ref. 11), and of Weissinger (ref. 12). These methods involve vortex systems to represent the wing, with the bound vortex producing lift. However, the methods depart from lifting-line concepts

by consideration of downwash away from the lifting line, and satisfying boundary conditions at various locations. These methods can be considered to be lifting-surface methods or modified lifting-line theories. Here again the basic assumptions of the theories are:

(1) The fluid is incompressible

(2) The flow is potential

(3) The circulation is such that the Kutta condition exists at the trailing edge

(4) The wing is represented by a thin vortex sheet in the wing plane

(5) All vertical displacements are ignored

In these methods, the wing is replaced by a vortex system and the strength of the vorticity is related to the differential pressure or lift at any point by the Kutta-Joukowski equation

$$l = \rho V \Gamma$$

The problem of determining the loading or pressure distribution is that of finding the distribution of vorticity Γ within the wing planform. The boundary condition is that no flow can occur through the vorticity sheet - that is, the resultant flow direction is parallel to the wing surface. This means that the local downwash velocity must be equal and of opposite sense to the normal velocity component due to angle of attack. The determination of Γ would be exact if its distribution were considered to be continuous and if the boundary condition were satisfied at all points on the wing. Such an exact determination is impractical (if not impossible), hence simplifying assumptions must be made. The usual simplifying assumptions are those of

(1) concentrating the continuous vorticity spanwise and/or chordwise

(2) representing the vorticity distribution by a mathematical expression, usually a series containing a finite number of unknown coefficients

(3) limiting the number of points at which the boundary condition is satisfied.

The differences in the various methods which have been developed for determining vorticity distribution, therefore, arise from

(a) the manner of concentrating the vorticity

(b) the differences in the form of the mathematical expression for vorticity distribution

(c) the choice in number and location of the control points

(d) the mathematical procedure used to obtain a solution.

The vortex distribution and control points used in the methods of Falkner, Mutterperl, and Weissinger are shown in figures 5, 6, and 7, respectively. The mathematics of the three methods is quite complex. These methods are explained in some detail and compared in reference 20. Note that the control points for the methods of Weissinger and Mutterperl are at the three-quarter chord line. The comparison presented in reference 20, based on comparing experimental spanload distributions of five swept wings with distributions computed by each of the three methods, indicated that the Falkner method gave the best accuracy but at a considerable expense in computing effort. The Weissinger method would be best suited for overall studies of wing characteristics and gave good results with by far the least computing effort. The Mutterperl method offered no advantages in accuracy or facility over either of the other methods.

The Weissinger method, therefore, has been extensively used in computing span loads due to angle of attack (ref. 8, for example), and span loads due to roll (ref. 21). Direct use of the Weissinger method or other available methods to the computation of the other wing aerodynamic characteristics proved to be quite difficult and sometimes inaccurate, consequently other methods for determining these characteristics (or derivatives) were sought.

D. Approximate Relations for Stability Derivatives of Swept Wings

One of the earliest papers giving approximate equations for the derivatives of swept wings was authored by Toll and Queijo (ref. 13). The basic concept of reference 13 is that a rough approximation of any wing derivative can be obtained by strip theory (load distribution is proportional to local geometric angle of attack). Further, although strip theory yields crude results, the ratio of a derivative of a swept wing to an unswept one of the same taper ratio and aspect ratio should be fairly accurate. An analogy to this concept, for example, is that if one has a rubber scale which has been extended so that the inch marks no longer represent inches, one may still obtain the correct ratio of the lengths of two objects even though one cannot find the actual length of either object. If one now has the correct ratio of

$$\frac{\text{Derivative of swept wing for specified } A \text{ and } \lambda}{\text{Derivative of unswept wing for same } A \text{ and } \lambda}$$

he could use this ratio and accurate values of unswept wing characteristics (obtained by a better theory) to obtain swept wing characteristics. Accurate unswept wing charecteristics were available in several

papers (ref. 5, for example). Although this method generally predicted proper trends, it was not as accurate as might be desired in many cases. One of the basic difficulties of the method was that strip theory predicted certain derivatives for which there were no corresponding values for unswept wings. Another difficulty, which appeared somewhat later and which will be mentioned in a later section, was in the method of determining the wing aspect ratio on which induction effects should be based. Nevertheless, reference 13 proved to be quite useful and is still used for estimates of certain derivatives for which more exact methods are not available (see ref. 19). The strip analysis method has been extended to study effects of dihedral (ref. 14), twist and camber (ref. 22) and is a very useful tool.

A survey of current literature on aerodynamic derivatives indicates that rigorous estimates of certain derivatives are still lacking, and that there is no general vortex representation which has been used for estimating all or most of the wing derivatives. An initial start in this direction was made by the author in NACA TR 1269 (ref. 23), for the estimation of the derivative C_{l_β}. The purpose of the present thesis is to extend the theory of reference 23 and develop it to permit estimation of several other stability derivatives. In addition, the present thesis includes the effects of compressibility, whereas reference 23 was limited to incompressible flow.

A. General Consideration

The first step in devising a theory and method for obtaining wing characteristics is that of selecting a suitable vortex system for representing the wing.

1. Unswept wings.- At this point, it is well to review vortex systems as used to represent unswept wings at some small angle of attack in straight flight. As a general case, the wing could be represented by a system of many spanwise and chordwise vortices as shown in figure 8(a). For wings of high aspect ratio, the spanwise vortices are generally replaced by a vortex, and the resulting system is the common lifting-line-theory representation of the wing (fig. 8(b)). It should be noted that the chordwise vortices are parallel to the free-stream direction and, therefore, can produce no pressure differential (or lift).

At this point, one might ask how these vortex systems should be changed if the wing had some motion other than straight symmetric flight. Consider, for example, the wing in sideslip. One plausible vortex arrangement would be that shown in figure 8(c). Here the trailing vortices depart from the lifting line in a direction parallel to the free stream. The lifting line produces lift per unit span according to the equation

$$l = \rho \Gamma_\zeta V \cos \beta$$

The only factor which could produce a resultant rolling moment would be caused by the unsymmetric downwash distribution due to the skewed

vortices. This arrangement was used by Blenk (ref. 24), however, the estimated resulting rolling moments were not verified either in sign or magnitude by experiment.

A different vortex system was tried by Weissinger (ref. 6) and this is illustrated in figure 8(d). In this case, it was assumed that the trailing vortices remained parallel to the wing [illegible] vortex position (c/4) to the wing trailing edge, and then were bent so as to be parallel to the airstream. The fact that part of the trailing vortices were essentially fixed to the wing meant that they could develop lift due to the lateral (or sideslip) velocity component. This vortex system yielded rolling moments due to sideslip which were in good agreement with experiment.

2. Swept wings.- The early analyses of swept wings characteristics reverted to use of the Weissinger method and vortex system of reference 12, where the vortices from the quarter-chord line were permitted to follow the free-stream velocity direction. The success of the Weissinger approach for angle-of-attack load computations led to its use in estimating the rolling moment of rolling wings in reference 21, which also permitted the trailing vortices to be parallel to the free stream. The analytical results of reference 21 compared favorably with experimental results. However, the range of planforms investigated was somewhat limited, and the comparisons with experiment generally were for wings of moderate and high aspect ratio. Reference 21 also presents rolling moments due to sideslip for wings with geometric dihedral, but does not predict the rolling moments of plane wings in sideslip. A general vortex system applicable to wings of arbitrary planform which could be used to estimate various derivatives still was lacking.

B. Selection of a Vortex System

The above discussion of vortex systems leads one to wonder if a system based on modified lifting-line-concepts, and utilizing the chordwise "bound" vortices as used by Weissinger (ref. 6) for unswept wings might be suitable for determining aerodynamic characteristics of swept wings. Such a vortex system was proposed by the author (ref. 23) and is shown in figure 9. This system was applied to sideslipping wings in reference 23, and proved to be very successful in predicting values of the parameter C_{l_β} for a wide range of wing planforms for which experimental results were available. The priority of other work prevented the extension of the work of reference 23. However, a recent appraisal of this vortex system indicated that it would be applicable to the estimation of several other wing derivatives. The vortex system shown in figure 9, therefore, is used in the present paper.

C. General Considerations of Relationships Between Circulation Distribution, Wind Velocity Components, and Load Distribution

The vortex system adopted for this study allows the possibility of generating lift by the bound vortices, which are:

a. the quarter-chord-line vortex, which extends across the entire wing span, and

b. the chordwise-bound vortices, which are parallel to the wing plane of symmetry and extend from the wing quarter-chord line to the wing-trailing edge.

The trailing vortices behind the wing are "free"vortices which are parallel to the free-stream velocity and hence develop no lift. The

strength of the chordwise-bound vortices is determined by the strength distribution of the quarter-chord-line vortex; therefore the lift distribution of the wing can be determined if the vortex strength distribution of the quarter-chord-line is known, and if the wind velocity components are known. The distribution of the wind velocity components relative to the wing can be determined easily for each possible motion of the wing. The basic problem in determining wing load distribution, therefore, is that of determining the vortex (or circulation) distribution for all wing motions. The three types of motion to be considered in this paper are sideslip, yawing, and rolling. The problem now is to determine the circulation distribution associated with each of these motions.

1. Circulation distribution for wings in sideslip.- This case was studied in reference 23, however, a review of that study is helpful in subsequent discussions.

Assume a wing at some angle of attack and at zero sideslip. The circulation distribution can be determined by the methods of references 10, 11, or 12, or by use of available charts generated from these methods (see refs. 8 or 9, for example). One now asks, "How will the circulation distribution be altered if the wing maintains its geometric angle of attack, but is given a lateral (sideslip) velocity?" The following arguments indicate that for small sideslip angles (consistent with linear theory) the change in circulation due to sideslip is very small. The vortex system for a wing in sideslip is shown in figure 10. Consider an element of the quarter-chord-line vortex of the right wing semispan. The lift per unit length of vortex of a swept wing in sideslip is given by

$$l_1 = \rho V \cos(\Lambda - \beta)\Gamma_\zeta \tag{6}$$

and also by

$$l_1 = \frac{1}{2}\rho\left[V^2\cos^2(\Lambda - \beta)\right] c_{l_\alpha} \frac{\alpha - \alpha_1}{\cos(\Lambda - \beta)} \tag{7}$$

From these equations it is seen that the circulation Γ_ζ is given by

$$\Gamma_\zeta = \frac{1}{2} Vc\, c_{l_\alpha}(\alpha - \alpha_1) \tag{8}$$

Similarly, for the wing at zero sideslip angle, the circulation is given by

$$(\Gamma_\zeta)_{\beta=0} = \frac{1}{2} Vc\, c_{l_\alpha}(\alpha - \alpha_1)_{\beta=0} \tag{9}$$

The relationship between circulation at a sideslip angle and circulation at zero sideslip, therefore, is given by

$$\Gamma_\zeta = (\Gamma_\zeta)_{\beta=0} \frac{\alpha - \alpha_1}{(\alpha - \alpha_1)_{\beta=0}} \tag{10}$$

It appears, therefore, that the local circulation of the quarter-chord-line vortex at a given angle of attack will be changed by sideslip only if sideslip changes the induced angle of attack. Now consider the following arguments:

a. A fundamental assumption of Prandtl's lifting line theory is that the downwash velocity is very small (see p. 45 of ref. 25). Since the methods in use for computing span loads are based on applications or modifications of Prandtl's theory, the same assumption

should be valid. There does exist a possibility that this assumption might be violated for very low aspect ratios. At infinite aspect ratios the induced angle is, of course, equal to zero since the circulation is constant across the span and there are no trailing vortices. If α_i is small in comparison with α, then

$$\frac{\alpha - \alpha_i}{(\alpha - \alpha_i)_\beta}$$

b. In lifting-line theory, the induced angle of attack at any point on the wing is due to the downwash at that point caused by all of the vortices of the system, in accordance with the Biot-Savart law. In most current methods of computing span loads, the boundary condition is satisfied at the three-quarter-chord line. Therefore, one must consider how downwash at the three-quarter-chord line might be altered by sideslip. According to the vortex system adopted in this study, the only change in vortex pattern caused by sideslip is that the trailing vortices behind the wing trailing edge bend to follow the free-stream direction. As a crude estimate of the effect of the bent vortices, consider the two sets of trailing vortices in the following sketch, and a control point as shown

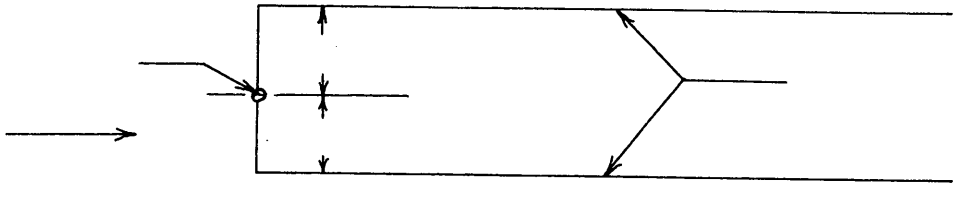

In this case, the downwash at the control point due to the two infinitely long vortices is given by

$$(w)_{\beta=0} = \frac{\Gamma}{2\pi S'}$$

For the same control point, and a sideslip angle β, the following sketch is applicable

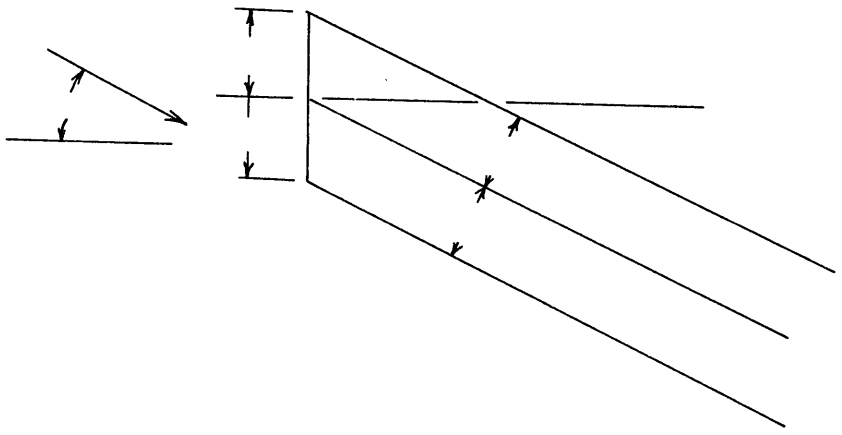

In this case, the downwash velocity is given by

$$w = \frac{\Gamma}{2\pi S' \cos \beta}$$

or for small sideslip angles

$$w \quad \frac{\Gamma}{2\pi S'}\left(1 + \frac{\beta^2}{2}\right)$$

It appears then that the downwash angle is affected as β^2 and therefore negligible when β is small. Note that this discussion neglects the mutual interaction between Γ and β but this effect should be quite small and was, in fact, investigated by Weissinger as will be pointed out next.

c. When the author was developing the theory of sideslipping swept wings (ref. 23) he neglected the effects of the bent vortices. He then checked his theory against experiment by plotting on one graph the estimated value of C_{l_β}/C_L against the experimental value for a great many wings. The results plotted as a 45° line as would be expected for correlation, however, the experimental points fell around a line which was almost exactly 0.05 too negative, that is for all wings the average estimated value of C_{l_β}/C_L was too negative by 0.05. At this stage, Weissinger's report on unswept wings in sideslip was brought to the author's attention. A careful study of the report showed the similarity in concepts of the vortex patterns, and further, indicated that Weissinger had computed the effects of the bent trailing vortices on the circulation and on C_{l_β}/C_L for a wide range of aspect ratio and taper ratio of unswept wings. His results showed that the effects of the bent trailing vortices was to make C_{l_β}/C_L more positive (or less negative) by a value which was, for all practical purposes, independent of aspect ratio and taper ratio, and in fact, made C_{l_β}/C_L more positive by a value of 0.05. This is a relatively small correction, and again indicates that the effect of the bend in the vortices on the circulation distribution is small. Based on the above arguments, it is a basic assumption of the present theory that <u>the circulation distribution for a wing in sideslip is essentially the same as that of the wing at zero sideslip angle</u>.

2. <u>Circulation distribution for a yawing wing</u>. The bound vortex pattern of a yawing wing is, of course, the basic system shown in

figure 9. The free trailing vortices, however, are curved to match the air flow stream lines (fig. 11). The geometry of the flow shows that there is a lateral velocity component over the wing, and that the magnitude of the component varies over the wing surface. The wing, therefore, can be considered to be in sideslip, where the effective sideslip angle varies over the wing. The arguments presented with regard to the circulation distribution of the wing in sideslip can be carried over in principle to the yawing wing. Therefore, the conclusion and assumption of the present theory is that the circulation distribution for a yawing wing is essentially the same as that of the nonyawing wing.

3. Circulation distribution for a rolling wing. The rolling wing presents a somewhat different problem than do the sideslipping and yawing wing with regard to circulation distribution. As pointed out above, the geometric angle of attack is not affected by sideslipping or yawing, it is only the induced angle which might be slightly altered. However, in the case of the rolling wing, the local geometric angle of attack is increased by

$$\Delta\alpha = \frac{pb}{2V}\frac{y}{\frac{b}{2}}$$

Therefore the primary cause of circulation and hence the circulation itself is altered by rolling. The net circulation of a rolling wing therefore is made up of

a. Circulation due to the symmetric angle of attack, and

b. Circulation due to the antisymmetric angle of attack distribution associated with rolling velocity.

The assumed wing vortex system, and the circulation distributions discussed above form the basis for the present theory for the computation of certain wing aerodynamic characteristics.

D. Derivation of Equations for Various Aerodynamic Derivatives for Wings in Incompressible Flow

1. Sideslipping wing.- The equations pertaining to wings in sideslip were derived by the author in reference 23, but will be repeated in somewhat more detail here since it will aid in the development of the more complicated yawing wing concepts and also for the sake of completeness.

a. General equations

In the following derivations, all equations refer to the right wing semispan unless otherwise noted. As pointed out in the section entitled "General Consideration of Relationships Between Circulation Distribution, Wind Velocity Components, and Load Distribution," forces can be obtained from interaction of the wind velocity components with the quarter-chord-line and the chordwise-bound vortices. By referring to figure 12, it is seen that the lift per element of length of the quarter-chord-line vortex is given by the interaction of the vortex and the stream velocity normal to the vortex;

$$l_1 = \rho V \cos (\Lambda - \beta)\Gamma_\zeta \qquad (11)$$

or, per unit length of wing span, by

$$l_1 = \rho V \cos (\Lambda - \beta)\Gamma_\zeta \frac{1}{\cos \Lambda} \tag{12}$$

The lift due to one chordwise-bound vortex is caused by interaction of the vortex and the lateral velocity component

$$l_2 = -\rho V \sin \beta \frac{3}{4} c \frac{d\Gamma_\zeta}{d\zeta} \tag{13}$$

For small sideslip angles, such that $\sin \beta \approx \beta$ and $\cos \beta \approx 1.0$, the two lift components can be written as

$$l_1 = \rho V \Gamma_\zeta (1 + \beta \tan \Lambda) \tag{14}$$

and

$$l_2 = -\frac{3}{4} \rho V c\beta \frac{d\Gamma_\zeta}{d\zeta} \tag{15}$$

Wing span load distributions are generally given in terms of spanwise position, y, rather than in distance along the quarter-chord-line vortex ζ. The next step is to recast the equations for the lift components in terms of spanwise load distribution. Consider a wing at zero sideslip angle. The lift per unit span is given by

$$(l)_{\beta=0} = \rho V \Gamma_y \tag{16}$$

and also by

$$(l)_{\beta=0} = \rho(V \cos \Lambda)\Gamma_\zeta \frac{1}{\cos \Lambda}$$

Comparison of these equations shows that Γ_y and Γ_ζ are equal for the wing at zero sideslip. Since a basic premise of the

present theory is that sideslip will not alter the spanwise circulation distribution, then Γ_y and Γ_ζ are also equal for the wing in sideslip. Equations (14) and (15) therefore can be written as

$$l_1 = \rho V \Gamma_y (1 + \beta \tan \Lambda) \tag{17}$$

$$l_2 = -\frac{3}{4} \rho V c\beta \frac{d\Gamma_y}{dy} \tag{18}$$

The circulation distribution Γ_y for a wing at angle of attack can be determined in terms of the span load. Span load distributions are generally given in terms of the parameter $\frac{cc_l}{cC_L}$. The quantities $\frac{cc_l}{cC_L}$ and Γ_y can be related through equation (16) as follows

$$l = \rho V \Gamma_y$$

$$c\tfrac{1}{2} \rho V^2 c = \rho V \Gamma_y$$

$$\left(\frac{cc_l}{cC_L}\right) = \frac{2\Gamma_y}{Vc C_L}$$

or

$$\Gamma_y = \frac{1}{2} Vc C_L \left(\frac{cc_l}{cC_L}\right)$$

Substituting this into equations (17) and (18) results in

$$l_1 = \frac{1}{2} \rho V^2 C_L \bar{c} \left(\frac{cc_l}{cC_L}\right) (1 + \beta \tan \Lambda) \tag{19}$$

and

$$l_2 = -\frac{3}{8} \rho V^2 c \beta C_L \frac{d\left(\frac{cc_l}{cC_L}\right)}{dy} \tag{20}$$

The load parameter corresponding to l_1 and l_2 can now be formed

$$\left[\left(\frac{cc_l}{\bar{c}C_L}\right)_1\right]_\beta = \frac{cl_1}{\bar{c}C_L\left(\frac{1}{2}\rho V^2 c\right)} = \left[\left(\frac{cc_l}{\bar{c}C_L}\right)_1\right](1 + \beta \tan \Lambda) \qquad (21)$$

$$\left[\left(\frac{cc_l}{\bar{c}C_L}\right)_2\right]_\beta \frac{cl_2}{\bar{c}C_L\left(\frac{1}{2}\rho V^2 c\right)} = -\frac{3}{4} c\beta \frac{d\left(\frac{cc_l}{\bar{c}C_L}\right)}{dy} \qquad (22)$$

The total load per unit span of the right wing semispan is given by the sum of these two terms, that is

$$\left(\frac{cc_l}{\bar{c}C_L}\right)_\beta = \left(\frac{cc_l}{\bar{c}C_L}\right)(1 + \beta \tan \Lambda) - \frac{3}{4} c\beta \frac{d\left(\frac{cc_l}{\bar{c}C_L}\right)}{dy} \qquad (23)$$

Similarly, the load parameter for the left semispan is given by

$$\left(\frac{cc_l}{\bar{c}C_L}\right)_\beta = \left(\frac{cc_l}{\bar{c}C_L}\right)(1 - \beta \tan \Lambda) - \frac{3}{4} c\beta \frac{d\left(\frac{cc_l}{\bar{c}C_L}\right)}{dy} \qquad (24)$$

The span load for a wing in sideslip therefore, can be determined by use of equations (23) and (24).

The rolling moment of a wing can be determined by an integration of the span load multiplied by the proper moment arm. A general form of a rolling-moment equation can be obtained from equations (23) and (24), to which must be added the increment determined analytically by Weissinger in reference 6, and by the author from empirical data (see section on "Circulation Distribution for Wings in Sideslip"). The rolling-moment equation (neglecting the correction just mentioned) can be derived as follows:

$$L' = -\int_{-b/2}^{b/2} l_y \, dy = -\int_{-b/2}^{b/2} \frac{1}{2}\rho V^2 c \, \frac{l}{\frac{1}{2}\rho V^2 c} \, y \, dy$$

or, in coefficient form

$$C_l = \frac{L'}{\frac{1}{2}\rho V^2 S b} = -\frac{1}{Sb}\int_{-b/2}^{b/2} cc_l y \, dy = -\frac{\bar{c}C_L}{Sb}\int_{-b/2}^{b/2} \frac{cc_l}{\bar{c}C_L} \, y \, dy$$

The dimension y can be nondimensionalized in terms of the semi-span so that the rolling-moment equation becomes

$$C_l = -\frac{b^2 \bar{c} C_L}{4Sb}\int_{-1}^{1} \frac{cc_l}{\bar{c}C_L} \frac{y}{b/2} \, d\frac{y}{b/2} \qquad (25)$$

Now

$$b = b\bar{c}$$

and by definition

$$\frac{y}{b/2} = y^*$$

therefore

$$C_l = -\frac{1}{4} C_L \int_{-1}^{1} \frac{cc_l}{\bar{c}C_L} \, y^* \, dy^* \qquad (26)$$

The load parameters given by equations (23) and (24) can now be substituted into equation (26) to yield the rolling moment of a wing in sideslip

$$C_l = -\frac{1}{4} C_L \int_{-1}^{0} \left[\left(\frac{cc_l}{\bar{c}C_L} \right)_0 (1 - \beta \tan \Lambda) - \frac{2}{b} c^* \beta \frac{d\left(\frac{cc_l}{\bar{c}C_L} \right)_0}{dy^*} \right] y^* \, dy^* \Bigg] \qquad (27)$$

$$-\frac{1}{4} C_L \int_0^1 \left[\left(\frac{cc_l}{\bar{c} C_L} \right)_0 (1 + \beta \tan \Lambda) - \frac{3}{4} c^* \beta \frac{d\left(\frac{cc_l}{\bar{c} C_L} \right)_0}{dy^*} \right] y^* \, dy^* \Bigg| \qquad (27)$$

This equation can be simplified by physical consideration.

First consider the terms $\int \left(\frac{cc_l}{\bar{c} C_L} \right)_0 y^* \, dy^*$ on each panel. It is obvious that this load term is symmetric over the wing and therefore, will produce no resultant moment. The terms $\int \left(\frac{cc_l}{\bar{c} C_L} \right)_0 (\beta \tan \Lambda) \, y^* \, dy^*$ result in a negative (downward) load on the left panel and hence, a negative moment increment; and in a positive load on the right panel and hence, also a negative moment increment. These terms therefore, are additive. The terms $\int c^* \beta \frac{d\left(\frac{cc_l}{\bar{c} C_L} \right)_0}{dy^*} y^* \, dy^*$ are a little more complex; however, the following sketch showing a typical vortex pair and lateral velocity direction indicates that a negative rolling moment will be obtained from each semispan.

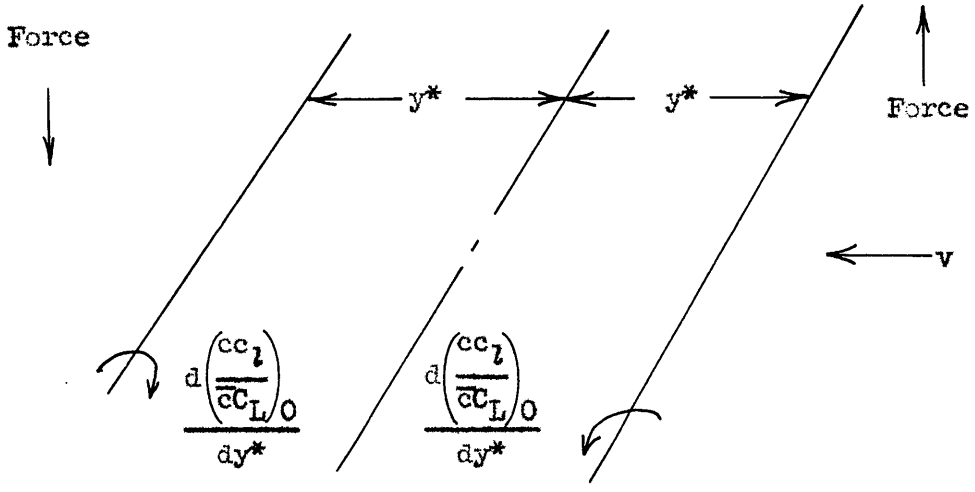

Equation (27) therefore, can be written as

$$C_{l} = -\frac{1}{2} C_L \int_0^1 \left[\left(\frac{cc_l}{\bar{c}C_L} \right)_0 \beta \tan \Lambda - \frac{3}{4} c^* \beta \frac{d\left(\frac{cc_l}{\bar{c}C_L} \right)_0}{dy^*} \right] y^* \, dy^* \quad (28)$$

The desired equation for $C_{l_\beta} C_L$ can now be obtained by differentiating with respect to β, dividing through by C_L, and adding the increment 0.05 to account for the effects of the skewed trailing vortices. The general equation therefore, is

$$\frac{C_{l_\beta}}{C_L} = -\frac{1}{2} \int_0^1 \left[\left(\frac{cc_l}{\bar{c}C_L} \right)_0 \tan \Lambda - \frac{3}{4} c^* \frac{d\left(\frac{cc_l}{\bar{c}C_L} \right)_0}{dy^*} \right] y^* \, dy^* + 0.05 \quad (29)$$

In a very general case, if sweep Λ is a function of spanwise position, then the above equation will probably have to be solved by a mechanical integration or a summation process (ref. 23).

There are at least two families of wings for which equation (29) can be integrated readily, and these are the elliptic wing and the wing with linear taper (that is, straight leading and trailing edge).

b. Elliptic Wing

These wings have interesting geometric and aerodynamic characteristics. They have elliptic planform and therefore, a varying quarter-chord sweep angle (as will be shown), and also have elliptic span load distribution due to angle of attack. These characteristics combine to make equation (29) readily integrable. First, it is instructive to derive the terms

required in equation (29). Consider the span load distribution. Since the distribution is elliptic, one can immediately write

$$\frac{\left(\frac{cc_l}{\bar{c}C_L}\right)^2}{\left[\left(\frac{cc_l}{\bar{c}C_L}\right)_{y=0}\right]^2} + \frac{y^2}{(b/2)^2} = 1$$

or

$$\frac{cc_l}{\bar{c}C_L} = \left(\frac{cc_l}{\bar{c}C_L}\right)_{y=0} \sqrt{1 - \left(\frac{y}{b/2}\right)^2}$$

$$\frac{cc_l}{\bar{c}C_L} = \left(\frac{cc_l}{\bar{c}C_L}\right)_{y=0} \sqrt{1 - (y^*)^2} \qquad (30)$$

The term $\left(\frac{cc_l}{\bar{c}C_L}\right)_{y=0}$ of equation (30) can be evaluated by considering the lift on an arbitrary wing:

$$L = 2\int_0^{b/2} l\, dy = 2\int_0^{b/2} \frac{l}{\frac{1}{2}\rho V^2 c}\left(\frac{1}{2}\rho V^2 c\right) dy$$

$$C_L = \frac{L}{\frac{1}{2}\rho V^2 S} = \frac{2}{S}\int_0^1 cc_l\, dy = \frac{2}{S}\int \frac{cc_l}{\bar{c}}\frac{b}{2}\bar{c}\, dy^*$$

Dividing then by C_L, and noting that $S = b\bar{c}$,

$$1 = \int_0^1 \frac{cc_l}{\bar{c}C_L}\, dy^* \qquad (31)$$

Note that equation is still perfectly general and does not apply to any specific planform. This equation will be found very useful in later developments.

If one now specifies an elliptic load distribution, equation (30) can be substituted into equation (31) and the result is

$$1 = \int_0^1 \left(\frac{cc_l}{\bar{c}C_L}\right)_{y=0} \sqrt{1 - (y^*)^2}\, dy^*$$

This integral is a standard form which can be evaluated immediately, and results in

$$\left(\frac{cc_l}{\bar{c}C_L}\right)_{y=0} = \frac{4}{\pi} \tag{32}$$

Combining equations (30) and (32) results in

$$\frac{cc_l}{\bar{c}C_L} = \frac{4}{\pi} \sqrt{1 - (y^*)^2} \tag{33}$$

The equation for the local chord of an elliptic wing is of the same form as equation (30) and is

$$c = (c)_{y=0} \sqrt{1 - (y^*)^2} \tag{34}$$

Now the area of an elliptic wing is given by

$$S = \frac{1}{4} \pi b (c)_{y=0}$$

Solving for $(c)_{y=0}$ and substituting into equation (34),

$$c = \frac{4S}{\pi b} \sqrt{1 - (y^*)^2}$$

Nondimensionalizing c by dividing through by $b/2$ and noting that the aspect ratio A is given by $A = \frac{b^2}{S}$, one obtains

$$c^* = \frac{8}{\pi A}\sqrt{1 - (y^*)^2} \tag{35}$$

The tangent of the sweep of the quarter-chord line is, of course, equal to the negative of the slope of that line. The equation of the quarter-chord line is obtained from equation (35) and is

$$\frac{c^*}{4} = \frac{2}{\pi A}\sqrt{1 - (y^*)^2}$$

hence,

$$\tan \Lambda = -\frac{1}{4}\frac{dc^*}{dy^*} = \frac{2}{\pi A}\frac{y^*}{\sqrt{1 - (y^*)^2}} \tag{36}$$

From equation (33) one obtains

$$\frac{d\left(\frac{cc_l}{\bar{c}C_L}\right)}{dy^*} = -\frac{4}{\pi}\frac{y^*}{\sqrt{1 - (y^*)^2}} \tag{37}$$

Equations (33), (35), (36), and (37) can be substituted into equation (29) to obtain

$$\frac{C_{l_\beta}}{C_L} = -\frac{1}{2}\int_0^1 \left[\left(\frac{4}{\pi}\sqrt{1 - (y^*)^2}\right)\left(\frac{2}{\pi A}\frac{y^*}{\sqrt{1 - (y^*)^2}}\right)\right.$$

$$\left. + \frac{3}{4}\left(\frac{8}{\pi A}\right)\sqrt{1 - y(^*)^2}\left(\frac{4}{\pi}\right)\frac{y^*}{\sqrt{1 - y^{*2}}}\right] y^*\, dy^* + 0.05$$

This equation can be simplified and integrated to obtain the following simple equation for elliptic wings

$$\frac{C_{l_\beta}}{C_L} = -\frac{16}{3\pi^2 A} + 0.05 \tag{38}$$

c. Swept Wings

If the leading edge and trailing edge of a wing are straight lines, then the quarter-chord-line is straight also, that is, the sweep angle is constant over a semispan. Equation (29) therefore, can be evaluated as follows. The first term can be written as

$$\tan \Lambda \int_0^1 \left(\frac{cc_l}{\bar{c}C_L}\right)_0 y^* \, dy^*$$

The integral is exactly the definition of the first moment of the span load about the $y^* = 0$ line, that is

$$\tan \Lambda \int_0^1 y^* \left(\frac{cc_l}{\bar{c}C_L}\right)_0 dy^* = \tan \Lambda \left[\int_0^1 \left(\frac{cc_l}{\bar{c}C_L}\right)_0 dy^*\right] \bar{y}^*$$

The integral can be evaluated by use of equation (31) and therefore

$$\tan \Lambda \int_0^1 \left[\left(\frac{cc_l}{\bar{c}C_L}\right)_0\right] y^* \, dy^* = \bar{y}^* \tan \Lambda \tag{39}$$

The second integral of equation (29) can be integrated by parts as follows

$$\int_0^1 c^* \frac{d\left(\frac{cc_l}{\bar{c}c_L}\right)_0}{dy^*} y^* \, dy^* = \int_0^1 c^* y^* \, d\left(\frac{cc_l}{\bar{c}c_L}\right)_0 = \left[c^* y^* \left(\frac{cc_l}{\bar{c}c_L}\right)_0\right]_0^1$$

$$- \int_0^1 \left(\frac{cc_l}{\bar{c}c_L}\right)_0 \left[c^* + y^* \frac{dc^*}{dy^*}\right] dy^*$$

The first term in brackets is zero at the upper limit since $\left(\frac{cc_l}{\bar{c}c_L}\right)_0 = 0$ when $y^* = 1$, that is, the span load must drop to zero at the wing tip. The value at the lower limit is also zero since y^* is zero. Therefore, the second integral of equation (29) becomes

$$\int c^* \frac{d\left(\frac{cc_l}{\bar{c}c_L}\right)_0}{dy^*} y^* \, dy^* = - \int_0^1 \left(\frac{cc_l}{\bar{c}c_L}\right)_0 \left[c^* + y^* \frac{dc^*}{dy^*}\right] dy^* \qquad (40)$$

Equation (29) therefore, becomes (using equations (39) and (40))

$$\frac{C_{l_\beta}}{C_L} = - \frac{1}{2} \bar{y}^* \tan \Lambda - \frac{3}{5} \int_0^1 \left(\frac{cc_l}{\bar{c}c_L}\right)_0 \left[c^* + y^* \frac{dc^*}{dy^*}\right] dy^* + 0.05 \qquad (41)$$

The remaining integral can be evaluated in the following manner. First, the local chord can be obtained as a function of spanwise position from

$$c = c_r - \frac{c_r - c_t}{b/2} y = c_r \left[1 - (1 - \lambda)\right] \frac{y}{b/2}$$

or

$$c^* = c_r^*\left[1 - (1 - \lambda)y^*\right] \tag{42}$$

However, the wing area is given by

$$S = b\bar{c} = b\left(\frac{c_r + c_t}{2}\right) = \frac{b}{2}c_r(1 + \lambda) = \frac{b^2}{4}c_r^*(1 + \lambda)$$

so that

$$c_r^* = \frac{4S}{b^2}\left(\frac{1}{1 + \lambda}\right)$$

or, finally

$$c_r^* = \frac{4}{A}\ \frac{1}{1 + \lambda}$$

Substituting into equation (42) results in

$$c^* = \frac{4}{A(1 + \lambda)}\left[1 - (1 - \lambda)y^*\right] \tag{43}$$

Equations (41) and (43) can now be combined, and this results in the following

$$\frac{C_{l_\beta}}{C_L} = -\frac{1}{2}\bar{y}^* \tan\Lambda - \frac{3}{2A(1 + \lambda)}\int_0^1 \left(\frac{cc_l}{\bar{c}C_L}\right)_0\left[1 - 2(1 - \lambda)y^*\right]dy^* + 0.05$$

The integral can be evaluated readily using equation (31) and the concept of first moment used in deriving equation (39). The final equation becomes

$$\frac{C_{l_\beta}}{C_L} = -\frac{1}{2}\left\{\frac{3}{A(1 + \lambda)} + \bar{y}^*\left[\tan\Lambda - \frac{6}{A}\left(\frac{1 - \lambda}{1 + \lambda}\right)\right]\right\} + 0.05 \tag{44}$$

2. Yawing wing.- The analysis of the yawing wing follows closely that of the wing in sideslip, but is somewhat more complex because the wind velocity and direction relative to the vortices vary with both the spanwise and chordwise position on the wing.

a. General Equations

The pertinent wind velocity components can be determined from the geometry of figure 13. The total wind velocity at any point on the wing is given by

$$V = r\,(d - y)\,\frac{1}{\cos\delta}$$

The components parallel and normal to the wing plane of symmetry are

$$u = -V\cos\delta = -r\,(d - y) \tag{45}$$

and

$$v = -V\sin\delta = -r\,(d - y)\tan\delta = -rx \tag{46}$$

Considering the right span of the wing, the component of velocity normal to the wing quarter-chord line is given by

$$V_N = -u\cos\Lambda - v\sin\Lambda$$

or, using equations (45) and (46)

$$V_N = r\,(d - y)\cos\Lambda + r\,(x)_{c/4}\sin\Lambda \tag{47}$$

Denoting the velocity at the wing center of gravity by V_0, then

$$V_0 = rd$$

and equation (47) can be rewritten as

$$V_N = \left(V_0 - ry\right) \cos \Lambda + r \left(x\right)_{c/4} \sin \Lambda \tag{48}$$

The lift per unit length of the quarter-chord-line vortex is given by use of the Kutta-Joukowski equation ($l = \rho V_N \Gamma$) and equation (48), so that

$$l_1 = \rho \left[\left(V_0 - ry\right) \cos \Lambda + r \left(x\right)_{c/4} \sin \Lambda\right] \Gamma_\xi$$

Using this equation and equation (8) one obtains

$$l_1 = \rho \left[\left(V_0 - ry\right) \cos \Lambda + r \left(x\right)_{c/4} \sin \Lambda\right]\left[\frac{1}{2} V_0 \, cc_{l_\alpha} \left(\alpha - \alpha_1\right)\right]$$

per unit length of vortex, or

$$l_1 = \frac{1}{2} \rho \left[\left(V_0 - ry\right) + r \left(x\right)_{c/4} \tan \Lambda\right]\left[V_0 \left(\frac{cc_l}{\bar{c}}\right)_0 \bar{c}\right] \tag{49}$$

per unit of span.

The lift of each chordwise-bound vortex must be found through an integration since the lateral velocity (which is the velocity component normal to the vortex) varies in magnitude along the length of the vortex. The lift is given by

$$l_2 = \int_{(x)_c}^{(x)_{c/4}} \rho v \frac{df_y}{dy} \, dx$$

or, using equation (46) and the relations of page 54

$$l_2 = \int_{(x)_c}^{(x)_{c/4}} \rho \left(-rx\right) \left[\frac{1}{2} V_0 \, \bar{c} \, \frac{d\left(\frac{cc_l}{\bar{c}}\right)_0}{dy}\right] dx \tag{50}$$

The local load coefficient is given by

$$\left(\frac{cc_l}{\bar{c}}\right)_r = \frac{c}{\bar{c}}\left(\frac{l_1 + l_2}{\frac{1}{2}\rho V_0^2 c}\right)$$

or, using equations (49) and (50)

$$\left(\frac{cc_l}{\bar{c}}\right)_r = \left[\left(1 - \frac{ry}{V_0}\right) + \frac{r\,(x)_{c/4}}{V_0}\tan\Lambda\right]\left(\frac{cc_l}{\bar{c}}\right)_0 - \int_{(x)_c}^{(x)_{c/4}} \frac{rx}{V_0}\,\frac{d\left(\frac{cc_l}{\bar{c}}\right)_0}{dy}\,dx \qquad (51)$$

Similarly, for the left wing span, it can be shown that

$$\left(\frac{cc_l}{\bar{c}}\right)_r = \left[1 - \frac{ry}{V_0} - \frac{r\,(x)_{c/4}}{V_0}\tan\Lambda\right]\left(\frac{cc_l}{\bar{c}}\right)_0 - \int_{(x)_c}^{(x)_{c/4}} \frac{rx}{V_0}\,\frac{d\left(\frac{cc_l}{\bar{c}}\right)_0}{dy}\,dx \qquad (52)$$

The rolling moment can now be determined by

$$L' = -\int_{-b/2}^{b/2}\left(\frac{cc_l}{\bar{c}}\right)_r\left(\frac{1}{2}\rho V_0^2\right)\frac{\bar{c}}{c}\,y\,dy$$

and the rolling moment coefficient is given by

$$C_l = \frac{L'}{\frac{1}{2}\rho V_0^2 Sb} = -\frac{1}{b^2}\int_{-b/2}^{b/2}\left(\frac{cc_l}{\bar{c}}\right)_r y\,dy$$

or

$$c_l = -\frac{1}{b}\int_{-1}^{1}\left(\frac{cc_l}{\bar{c}}\right)_r y^* \, dy^* \tag{53}$$

Before attempting to integrate equation (53), it is advisable to eliminate the integrals of equations (51) and (52). This can be done quite easily since in the integral the term r is taken as a constant and the term $\frac{d\left(\frac{cc_l}{\bar{c}}\right)_0}{dy}$ is a function of y but not of x. Therefore

$$\int_{(x)_c}^{(x)_{c/4}} \frac{x}{V_0}\frac{d\left(\frac{cc_l}{\bar{c}}\right)_0}{dy}\,dx = \frac{r}{V_0}\frac{d\left(\frac{cc_l}{\bar{c}}\right)_0}{dy}\frac{x^2}{2}\Bigg|_{(x)_c}^{(x)_{c/4}}$$

$$= \frac{r}{2V_0}\frac{d\left(\frac{cc_l}{\bar{c}}\right)_0}{dy}\left[(x)_{c/4}^2 - (x)_c^2\right] \tag{54}$$

Using equations (51), (52), and (54) with equation (53) results in the following expression

$$c_l = -\frac{1}{4}\int_{-1}^{0}\left\{\left[1 - \frac{2y}{V_0} - \frac{r\,(x)_{c/4}}{V_0}\tan\Lambda\right]\left(\frac{cc_l}{\bar{c}}\right)_0 - \frac{r}{2V_0}\frac{d\left(\frac{cc_l}{\bar{c}}\right)}{dy}\left[(x)_{c/4}^2 - (x)_c^2\right]\right\} y^*\,dy^* - \frac{1}{4}\int_{0}^{1}\left\{\left[1 - \frac{2y}{V_0} + \frac{r\,(x)_{c/4}}{V_0}\tan\Lambda\right]\left(\frac{cc_l}{\bar{c}}\right)_0 - \frac{r}{2V_0}\frac{d\left(\frac{cc_l}{\bar{c}}\right)_0}{dy}\left[(x)_{c/4} - (x)_c^2\right]\right\} y^*\,dy^* \tag{55}$$

Equation (55) can be simplified to some extent from physical and geometric considerations. Consider the term

$$\int \frac{xr}{V_0}\left(\frac{cc_l}{\bar{c}}\right)_0 y^* \, dy^*$$

This term gives rise to a positive force on the left panel and a negative force on the right panel (see fig. 14(a)). These forces result in rolling moments which are additive. Similarly it can be shown that the remaining terms involving the yawing velocity are additive (see fig. 14(b) and 14(c)). Therefore, retaining only those terms depending on yawing velocity, equation (55) can be rewritten as

$$c_l = \frac{1}{\bar{c}} \int_0^1 \left\{ \left[\frac{xr}{V_0} - \frac{r\,(x)_{c/4}}{V_0} \tan \Lambda \right] \left(\frac{cc_l}{\bar{c}}\right)_0 + \frac{1}{2} \frac{r}{V_0} \frac{d\left(\frac{cc_l}{\bar{c}}\right)_0}{dy} \left[(x)^2_{c/4} - (x)^2_c \right] \right\} y^* \, dy^*$$

Nondimensionalizing x and y and converting the rate of yawing r to the yawing parameter $\frac{rb}{2V_0}$ results in

$$c_l = \frac{1}{\bar{c}} \int_0^1 \left\{ \left[\frac{rb}{2V_0} y^* - \frac{rb}{2V_0} (x^*)_{c/4} \tan \Lambda \right] \left(\frac{cc_l}{\bar{c}}\right)_0 + \frac{1}{2} \frac{rb}{2V_0} \frac{d\left(\frac{cc_l}{\bar{c}}\right)_0}{dy^*} \left[(x^*)^2_{c/4} - (x^*)^2_c \right] \right\} y^* \, dy^*$$

Taking the derivative with respect to $\frac{rb}{2V_0}$ and dividing through by C_L results in the desired general equation

$$\frac{C_{l_r}}{C_L} = \frac{1}{2}\int_0^1 \left\{ \left[y^* - (x^*)_{c/4} \tan \Lambda \right] \left(\frac{cc_l}{\bar{c}C_L} \right)_0 + \frac{1}{2} \left[(x^*)^2_{c/4} - (x^*)^2_c \right] \frac{d\left(\frac{cc_l}{\bar{c}C_L} \right)_0}{dy^*} \right\} y^* \, dy^* \tag{56}$$

b. Swept Wing

Equation (56) is perfectly general and is somewhat complex for an arbitrary wing. Some simplification is possible for the ordinary swept wing. In this case the x^*-dimensions can be rewritten in terms of y^* from geometric considerations (see fig. 13).

$$(x)_{c/4} = \bar{y} \tan \Lambda - y \tan \Lambda - \bar{X}$$

or

$$(x^*)_{c/4} = (\bar{y}^* - y^*) \tan \Lambda - \bar{X}^* \tag{57}$$

Also,

$$(x^*)_c = (x^*)_{c/4} - \frac{2}{4} c^*$$

therefore it is easy to show that

$$(x^*)^2_{c/4} - (x^*)^2_c = c^*\left[\frac{3}{2}(\bar{y}^* - y^*)\tan\Lambda - \frac{3}{2}\bar{X}^* - \frac{9}{16} c^*\right] \qquad (58)$$

Substituting equations (57) and (58) into equation (56) results in the following

$$\frac{C_{l_r}}{C_L} = \frac{1}{2}\int_0^1 \left\{\left[y^*(1 + \tan^2\Lambda) - (\bar{y}^* \tan\Lambda - \bar{X}^*)\tan\Lambda\right]\left(\frac{cc_l}{\bar{c}C_L}\right)_0\right.$$

$$\left. + \frac{c^*}{2}\left[\frac{3}{2}(\bar{y}^* - y^*)\tan\Lambda - \frac{3}{2}\bar{X}^* - \frac{9}{16} c^*\right]\frac{d\left(\frac{cc_l}{\bar{c}C_L}\right)_0}{dy^*}\right\} y^* dy^* \qquad (59)$$

Evaluation of equation (59) is quite tedious, but can be accomplished step by step. Consider the first integral, which can be written as

$$(1 + \tan^2\Lambda)\int_0^1 \left(\frac{cc_l}{\bar{c}C_L}\right)_0 (y^*)^2 dy^* - (\bar{y}^* \tan\Lambda - \bar{X}^*)\tan\Lambda \int_0^1 \left(\frac{cc_l}{\bar{c}C_L}\right)_0 y^* dy^*$$

Note that the integral

$$\int_0^1 \left(\frac{cc_l}{\bar{c}C_L}\right)_0 (y^*)^2 dy^*$$

is in the form of the definition of the moment of inertia of the span load parameter about the axis $y^* = 0$, and therefore can be written as

$$\int_0^1 \left(\frac{cc_l}{\bar{c}C_L}\right)_0 (y^*)^2 dy^* = (\bar{y}^*)^2 \int_0^1 \left(\frac{cc_l}{\bar{c}C_L}\right)_0 \tag{60}$$

This last integral is equal to unity (eq. (51)), therefore

$$\int_0^1 \left(\frac{cc_l}{\bar{c}C_L}\right)_0 (y^*)^2 dy^* = (\bar{y}^*)^2 \tag{61}$$

Also note that the integral $\int_0^1 \left(\frac{cc_l}{\bar{c}C_L}\right)_0 y^* dy^*$ was previously evaluated (eq. (39)). Therefore, using equations (39) and (61), the first integral of equation (59) becomes

$$\frac{1}{2}\int_0^1 \left[y^*(1 + \tan^2\Lambda) - (\bar{y}^* \tan\Lambda - \bar{X}^*)\tan\Lambda \right]\left(\frac{cc_l}{\bar{c}C_L}\right)_0 y^* dy^*$$

$$= \frac{1}{2}\left[(1 + \tan^2\Lambda)(\bar{y}^*)^2 - (\bar{y}^* \tan\Lambda - \bar{X}^*)\bar{y}^* \tan\Lambda\right] \tag{62}$$

The second integral of equation (59) can be rewritten, so that

$$\frac{1}{2}\int_0^1 \frac{c^*}{2}\left[\frac{3}{2}(\bar{y}^* - y^*)\tan\Lambda - \frac{3}{2}\bar{X}^* - \frac{9}{16}c^*\right]\frac{d\left(\frac{cc_l}{\bar{c}C_L}\right)_0}{dy^*} y^* dy^*$$

$$= \frac{3}{8}(\bar{y}^* \tan\Lambda - \bar{X}^*)\int_0^1 c^* \frac{d\left(\frac{cc_l}{\bar{c}C_L}\right)_0}{dy^*} y^* dy^*$$

$$- \frac{3}{8}\tan\Lambda \int_0^1 c^* \frac{d\left(\frac{cc_l}{\bar{c}C_L}\right)_0}{dy^*}(y^*)^2 dy^* - \frac{9}{64}\int_0^1 (c^*)^2 \frac{d\left(\frac{cc_l}{\bar{c}C_L}\right)_0}{dy^*} y^* dy^* \tag{63}$$

The first integral on the right was manipulated previously (eq. (40)), so that one can write

$$\frac{2}{b}(\bar{y}^* \tan \Lambda - \bar{x}^*) \int_0^1 c^* \frac{d\left(\frac{cc_l}{\bar{c}C_L}\right)_0}{dy^*} y^* dy^*$$

$$= -\frac{2}{b}(\bar{y}^* \tan \Lambda - \bar{x}^*) \int_0^1 \left(c^* + y^* \frac{dc^*}{dy^*}\right)\left(\frac{cc_l}{\bar{c}C_L}\right)_0 dy^* \qquad (64)$$

The second integral on the right side of equation (63) can be integrated by parts as follows

$$\int_0^1 c^*(y^*)^2 \frac{d\left(\frac{cc_l}{\bar{c}C_L}\right)_0}{dy^*} dy^* = \int_0^1 \frac{d\left[c^*(y^*)^2\left(\frac{cc_l}{\bar{c}C_L}\right)_0\right]}{dy^*} dy^*$$

$$- \int_0^1 \left(\frac{cc_l}{\bar{c}C_L}\right)_0 \frac{d\left[c^*(y^*)^2\right]}{dy^*} dy^*$$

from which

$$\int_0^1 c^*(y^*)^2 \frac{d\left(\frac{cc_l}{\bar{c}C_L}\right)_0}{dy^*} dy^* = c^*(y^*)^2\left(\frac{cc_l}{\bar{c}C_L}\right)_0 \Bigg|_0^1$$

$$- \int_0^1 \left(\frac{cc_l}{\bar{c}C_L}\right)_0 \left[2c^*y^* + (y^*)^2 \frac{dc^*}{dy^*}\right] dy^*$$

The first term on right is equal to zero. (See pg. 63.) Therefore,

$$- \frac{3}{8} \tan \Lambda \int_0^1 c^* \frac{d\left(\frac{cc_l}{\bar{c}C_L}\right)_0}{dy^*} (y^*)^2 dy^*$$

$$= \frac{3}{8} \tan \Lambda \int_0^1 \left(\frac{cc_l}{\bar{c}C_L}\right)_0 \left[2c^*y^* + (y^*)^2 \frac{dc^*}{dy^*}\right] dy^* \qquad (65)$$

The last integral on the right side of equation (63) also can be integrated by parts as follows

$$- \frac{9}{64} \int_0^1 (c^*)^2 y^* \frac{d\left(\frac{cc_l}{\bar{c}C_L}\right)_0}{dy^*} dy^*$$

$$= - \frac{9}{64} \left\{ \int_0^1 \frac{d\left[\left(\frac{cc_l}{\bar{c}C_L}\right)_0 (c^*)^2 y^*\right]}{dy^*} dy^* - \int_0^1 \left(\frac{cc_l}{\bar{c}C_L}\right)_0 \frac{d\left[(c^*)^2 y^*\right]}{dy^*} dy^* \right\}$$

$$= - \frac{9}{64} \left(\frac{cc_l}{\bar{c}C_L}\right)_0 (c^*)^2 y^* \Big|_0^1 + \frac{9}{64} \int_0^1 \left(\frac{cc_l}{\bar{c}C_L}\right)_0 \left[2c^*y^* \frac{dc^*}{dy^*} + (c^*)^2\right] dy^* \qquad (66)$$

Substituting equations (64), (65), and (66) into eqaution (63) results in

$$\frac{1}{2}\int_0^1 \frac{c^*}{2}\left[\frac{3}{2}(\bar{y}^* - y^*)\tan\Lambda - \frac{2\bar{X}^*}{2} - \frac{9}{16}c^*\right]\frac{d\left(\frac{cc_l}{\bar{c}C_L}\right)_0}{dy^*}\,y^*dy^*$$

$$= -\frac{3}{8}(\bar{y}^*\tan\Lambda - \bar{X}^*)\int_0^1\left(c^* + y^*\frac{dc^*}{dy^*}\right)\left(\frac{cc_l}{\bar{c}C_L}\right)_0 dy^*$$

$$+\frac{3}{8}\tan\Lambda\int_0^1\left(\frac{cc_l}{\bar{c}C_L}\right)_0\left[2c^*y^* + (y^*)^2\frac{dc^*}{dy^*}\right]dy^*$$

$$+\frac{9}{64}\int_0^1\left[2c^*y^*\frac{dc^*}{dy^*} + (c^*)^2\right]\left(\frac{cc_l}{\bar{c}C_L}\right)_0 dy^* \qquad (67)$$

Substitution of equations (62) and (67) into equation (59) results in the following

$$\frac{c_{l_r}}{C_L} = \frac{1}{2}\left[\left(1 + \tan^2\Lambda\right)(\bar{y}^*)^2 - (\bar{y}^*\tan\Lambda - \bar{X}^*)\bar{y}^*\tan\Lambda\right]$$

$$-\frac{3}{8}(\bar{y}^*\tan\Lambda - \bar{X}^*)\int_0^1\left(c^* + y^*\frac{dc^*}{dy^*}\right)\left(\frac{cc_l}{\bar{c}C_L}\right)_0 dy^*$$

$$+\frac{3}{8}\tan\Lambda\int_0^1\left(\frac{cc_l}{\bar{c}C_L}\right)_0\left[2c^*y^* + (y^*)^2\frac{dc^*}{dy^*}\right]dy^*$$

$$+\frac{9}{64}\int_0^1\left[(c^*)^2 + 2c^*y^*\frac{dc^*}{dy^*}\right]\left(\frac{cc_l}{\bar{c}C_L}\right)_0 dy^* \qquad (68)$$

The first integral of equation (68) can be expanded by making use of equation (43), so that

$$\int_0^1 \left(c^* + y^* \frac{dc^*}{dy^*} \right) \left(\frac{cc_l}{\bar{c}C_L} \right)_0 dy^*$$

$$= \frac{4}{A(1 + \lambda)} \int_0^1 \left[1 - (1 - \lambda)y^* - (1 - \lambda)y^* \right] \left(\frac{cc_l}{\bar{c}C_L} \right)_0 dy^*$$

$$= \frac{4}{A(1 + \lambda)} \int_0^1 \left[1 - 2(1 - \lambda)y^* \right] \left(\frac{cc_l}{cC_L} \right)_0 dy^*$$

or, finally,

$$\int_0^1 \left(c^* + y^* \frac{dc^*}{dy^*} \right) \left(\frac{cc_l}{\bar{c}C_L} \right)_0 dy^* = \frac{4}{A(1 + \lambda)} - \frac{8}{A} \left(\frac{1 - \lambda}{1 + \lambda} \right) \bar{y}^* \qquad (69)$$

The second and third integrals of equation (68) can be integrated in a similar manner, and the results are

$$\int_0^1 \left(\frac{cc_l}{\bar{c}C_L} \right)_0 \left[2c^*y^* + (y^*)^2 \frac{dc^*}{dy^*} \right] dy^* = \frac{8}{A(1 + \lambda)} \bar{y}^* - \frac{12}{A} \left(\frac{1 - \lambda}{1 + \lambda} \right) (y^*)^2 \qquad (70)$$

and

$$\int_0^1 \left[(c^*)^2 + 2c^*y^* \frac{dc^*}{dy^*} \right] \left(\frac{cc_l}{\bar{c}C_L} \right)_0 dy^*$$

$$= \frac{16}{A^2(1 + \lambda)^2} \left[1 - 4(1 - \lambda)\bar{y}^* + 3(1 - \lambda)^2 (\bar{y}^*)^2 \right] \qquad (71)$$

Substitution of equations (69), (70), and (71) into equation (68) yields, after some manipulation, the desired equation for C_{l_i}/C_L,

$$\frac{C_{l_r}}{C_L} = \left[\frac{1}{2}(1 + \tan^2\Lambda) - \frac{9 \tan \Lambda}{2A}\left(\frac{1 - \lambda}{1 + \lambda}\right) + \frac{27}{4A^2}\left(\frac{1 - \lambda}{1 + \lambda}\right)^2\right](\tilde{y}^*)^2$$

$$+ \left[\frac{3}{A}\left(\frac{1 - \lambda}{1 + \lambda}\right)\tan \Lambda - \frac{1}{2}\tan^2\Lambda\right](\bar{y}^*)^2$$

$$+ \left[\frac{3 \tan \Lambda}{2A(1 + \lambda)} - \frac{9(1 - \lambda)}{A^2(1 + \lambda)^2}\right]\bar{y}^*$$

$$+ \left[\frac{\tan \Lambda}{2} - \frac{3}{A}\left(\frac{1 - \lambda}{1 + \lambda}\right)\right]\bar{x}^*\bar{y}^* + \frac{3\bar{x}^*}{2A(1 + \lambda)} + \frac{9}{4A^2(1 + \lambda)^2} \qquad (72)$$

3. Rolling wing.- The analysis of the rolling wing must consider the basic angle-of-attack circulation and the additional circulation associated with rolling. It is therefore necessary to consider the possibility of forces and moments from two sources

(a) Interaction of the free-stream velocity with the additional circulation due to rolling.

(b) Interaction of the rolling-velocity components with the angle-of-attack circulation distribution.

a. General Equations

The geometry of figure 15 shows that the first of these interactions results in a rolling moment. This is essentially a change in loading associated with a change in local wing incidence, and is the type of loading which can be handled well by the Weissinger method (ref. 9 for example).

In this study, therefore, the emphasis will be on the interaction of the basic angle-of-attack circulation and the velocity components associated with rolling velocity. The additional velocity component is simply

$$w = Py \tag{73}$$

which is, of course, normal to the wing or vortex plane. Note that the boundary condition of no flow perpendicular to the vortex plane precludes any interaction of the additional velocity with the chordwise-bound vortices. Therefore, it is necessary to consider only the forces arising from interaction of the quarter-chord-line vortex and the additional velocity Py. This force is given by

$$l = \rho(Py)\Gamma_{\xi}$$

per unit vortex length, or

$$l = \rho(Py)\frac{\Gamma}{\cos \Lambda} \tag{74}$$

per unit span. Combining equations (74) and (2) results in

$$l = \frac{1}{2}\rho PyV\left(\frac{cc_l}{\bar{c}}\right)_0 \frac{\bar{c}}{\cos \Lambda} \tag{75}$$

Note that this force is normal to the quarter-chord-line vortex and is in the wing plane. The force indicated by equation (75) results in a side force which is given by

$$Y = \int_{-b/2}^{b/2} l \sin \Lambda \, dy$$

or, using equation (75),

$$Y = \int_{-b/2}^{b/2} \frac{1}{2}\rho PyV\left(\frac{cc_l}{\bar{c}}\right)_0 \bar{c} \tan \Lambda \, dy$$

Geometric and physical considerations (see fig. 15) show that this force for the entire wing is twice that of one semispan, so that it is proper to write

$$Y = \frac{1}{2}\rho PV\bar{c}\int_0^{b/2} 2\left(\frac{cc_l}{\bar{c}}\right)_0 \tan\Lambda y dy$$

This equation can be nondimensionalized and the side force coefficient formed, so that

$$C_Y = \frac{Y}{\frac{1}{2}\rho V^2 S} = \frac{Pb}{2V}\int_0^1 \left(\frac{cc_l}{\bar{c}}\right)_0 \tan\Lambda y^* dy^*$$

Taking the derivative with respect to $Pb/2V$ and dividing through by C_L results in

$$\frac{C_{Y_p}}{C_L} = \int_0^1 \left(\frac{cc_l}{\bar{c}C_L}\right)_0 \tan\Lambda y^* dy^* \qquad (76)$$

The force indicated by equation (74) also gives rise to a yawing moment which can be determined from the following equation (see figure 15 also)

$$N = 2\int_0^{b/2} \rho(Py)(\Gamma_0)\left[(x)_{c/4}\sin\Lambda - y\cos\Lambda\right]\frac{1}{\cos\Lambda}dy$$

or

$$N = 2\int_0^{b/2} \rho(Py)\,\frac{1}{2}V\left(\frac{cc_l}{\bar{c}}\right)_0(\bar{c})\left[(x)_{c/4}\sin\Lambda - y\cos\Lambda\right]\frac{1}{\cos\Lambda}dy$$

This can be nondimensionalized, and the yawing moment coefficient obtained as

$$C_n = \frac{N}{\frac{1}{2}\rho V^2 Sb} = \frac{1}{2}\frac{Pb}{2V}\int_0^1 \left(\frac{cc_l}{\bar{c}}\right)_0\left[(x^*)_{c/4}\tan\Lambda - y^*\right]y^* dy^*$$

Taking the derivative with respect to $Pb/2V$ and dividing through by C_L results in

$$\frac{C_{n_P}}{C_L} = \frac{1}{2} \int_0^1 \left(\frac{cc_l}{\bar{c}C_L}\right)_0 \left[(x^*)_{c/4} \tan \Lambda - y^*\right] y^* dy^* \qquad (77)$$

This equation can be integrated, in part, by use of equation (61), so that

$$\frac{C_{n_P}}{C_L} = -\frac{1}{2} (\tilde{y}^*)^2 + \frac{1}{2} \int_0^1 \left(\frac{cc_l}{\bar{c}C_L}\right)_0 (x^*)_{c/4} \tan \Lambda \, y^* dy^* \qquad (78)$$

Equations (76) and (78) are quite general for the parameters C_{Y_P}/C_L and C_{n_P}/C_L, respectively.

b. Swept Wings

The usual swept wing has a straight leading and trailing edge, and in such a case the sweep of the quarter-chord line is a constant across the span. In such cases equations (76) and (78) can be rewritten as

$$\frac{C_{Y_P}}{C_L} = \tan \Lambda \int_0^1 \left(\frac{cc_l}{\bar{c}C_L}\right)_0 y^* dy^* \qquad (79)$$

and

$$\frac{C_{n_P}}{C_L} = -\frac{1}{2}(\tilde{y}^*)^2 + \frac{1}{2} \tan \Lambda \int_0^1 \left(\frac{cc_l}{\bar{c}C_L}\right)_0 (x^*)_{c/4} \, y^* dy^* \qquad (80)$$

Equation (79) can be integrated immediately (see eq. (39)), so that

$$\frac{C_{Y_P}}{C_L} = \bar{y}^* \tan \Lambda$$

which is the desired equation for the side force coefficient associated with rolling velocity.

The yawing moment equation can be expanded, by use of equation (57) to obtain

$$\frac{C_{n_p}}{C_L} = -\frac{1}{2}(\bar{y}^*)^2 + \frac{1}{2}\int_0^1 \left(\frac{cc_l}{\bar{c}C_L}\right)_0 \left[(\bar{y}^* - y^*)\tan\Lambda - \bar{X}^*\right] y^* \tan\Lambda dy^*$$

or

$$\frac{C_{n_p}}{C_L} = -\frac{1}{2}(\tilde{y}^*)^2 + \frac{1}{2}\tan^2\Lambda\left[\bar{y}^* \int_0^1 \left(\frac{cc_l}{\bar{c}C_L}\right)_0 y^* dy^* - \int_0^1 \left(\frac{cc_l}{\bar{c}C_L}\right)_0 (y^*)^2 dy^*\right]$$

$$-\frac{1}{2}\bar{X}^* \tan\Lambda \int_0^1 \left(\frac{cc_l}{\bar{c}C_L}\right)_0 y^* dy^*$$

The three integrals have been integrated previously (see eqs. (59) and (60)), and the final result is

$$\frac{C_{n_p}}{C_L} = -\frac{1}{2}(\tilde{y}^*)^2 + \frac{1}{2}(\bar{y}^*)^2\tan^2\Lambda - \frac{1}{2}(\tilde{y}^*)^2\tan^2\Lambda - \frac{1}{2}\bar{X}^*\bar{y}^* \tan\Lambda$$

The terms can be combined to yield

$$\frac{C_{n_p}}{C_L} = -\frac{1}{2}\left\{(\tilde{y}^*)^2 + \left[(\tilde{y}^*)^2 - (\bar{y}^*)^2\right]\tan^2\Lambda + \bar{X}^*\bar{y}^* \tan\Lambda\right\} \qquad (82)$$

E. Equations for Span Load Distributions

The equations derived thus far have been for parameters which are important from considerations of aircraft static and dynamic stability. Since the derivatives apply to the wing as a whole, they can be used to obtain forces and moments at the root chord. The structural engineer, however, is also interested in local forces and moments, hence the span

load distribution should be of use. Very little theoretical or experimental work exists on the estimation of span load distributions for the side-slipping or yawing wing. Experimentally, such information is obtained from pressure distribution investigations. Such investigations are very time consuming from construction of the model, through testing and data reduction. Existing theoretical methods for computing span loads appear to be restricted to span loads associated with local changes in angle of attack. Thus, for example, reference 9 can be used to determine additional span loads due to rolling velocity, aileron deflection, or sideslip of wings with dihedral. Since sideslip or yawing does not cause a local change in angle of attack for a plane wing, it appears that aerodynamicists have generally neglected this area. The equations derived herein can be used to estimate span loads for sideslipping or yawing wings. The loads on rolling wings are associated with local change in angle of attack due to roll, and can be obtained from several papers (ref. 9 for example).

1. Sideslipping wing

a. General Equations

The total local span load parameter for a wing in sideslip is given by equation (23) for the right semispan, and by equation (24) for the left semispan

$$\left(\frac{cc_l}{\bar{c}C_L}\right)_\beta = \left(\frac{cc_l}{\bar{c}C_L}\right)_0 (1 + \beta \tan \Lambda) - \frac{3}{4} c^* \beta \frac{d\left(\frac{cc_l}{\bar{c}C_L}\right)_0}{dy^*} \qquad (23)$$

$$\left(\frac{cc_l}{\bar{c}C_L}\right)_\beta = \left(\frac{cc_l}{\bar{c}C_L}\right)_0 (1 - \beta \tan \Lambda) - \frac{3}{4} c^* \beta \frac{d\left(\frac{cc_l}{\bar{c}C_L}\right)_0}{dy^*} \tag{24}$$

The additional loading due to sideslip therefore is given by (for right semispan)

$$\Delta\left(\frac{cc_l}{\bar{c}C_L}\right)_\beta = \left[\left(\frac{cc_l}{\bar{c}C_L}\right)_0 \tan \Lambda - \frac{3}{4} c^* \frac{d\left(\frac{cc_l}{\bar{c}C_L}\right)_0}{dy^*}\right]\beta$$

or

$$\frac{\left(\frac{cc_l}{\bar{c}C_L}\right)_\beta}{\beta} = \left(\frac{cc_l}{\bar{c}C_L}\right)_0 \tan \Lambda - \frac{3}{4} c^* \frac{d\left(\frac{cc_l}{\bar{c}C_L}\right)_0}{dy^*} \tag{33}$$

The load due to sideslip is antisymmetric over the wing.

b. Swept Wing

For wings having constant sweep angle, equation (43) can be used to eliminate c^* from the general equations (23) and (24), therefore one obtains for the total local load

$$\left(\frac{cc_l}{\bar{c}C_L}\right)_\beta = \left(\frac{cc_l}{\bar{c}C_L}\right)_0 (1 + \beta \tan \Lambda) - \frac{3}{A(1 + \lambda)}\left[1 - (1 - \lambda)y^*\right]\beta \frac{d\left(\frac{cc_l}{\bar{c}C_L}\right)_0}{dy^*} \tag{34}$$

for the right semispan, and

$$\left(\frac{cc_l}{\bar{c}C_L}\right)_\beta = \left(\frac{cc_l}{\bar{c}C_L}\right)_0 (1 - \beta \tan \Lambda) - \frac{3}{A(1 + \lambda)}\left[1 - (1 - \lambda)y^*\right]\beta \frac{d\left(\frac{cc_l}{\bar{c}C_L}\right)_0}{dy^*} \tag{35}$$

for the left semispan. The additional loading due to sideslip is, for the right semispan

$$\frac{\left(\frac{cc_l}{\bar{c}C_L}\right)_\beta}{\beta} = \left(\frac{cc_l}{\bar{c}C_L}\right)_0 \tan\Lambda - \frac{3}{A(1+\lambda)}\left[1 - (1-\lambda)y^*\right]\frac{d\left(\frac{cc_l}{\bar{c}C_L}\right)_0}{dy^*} \qquad (86)$$

2. Yawing wing

a. General Equations

The total local span load for a yawing wing is given by equation (51), which can be written as (for right semispan)

$$\left(\frac{cc_l}{\bar{c}C_L}\right)_r = \left[1 - \frac{rb}{2V_0}y^* + \frac{rb}{2V_0}(x^*)_{c/4}\tan\Lambda\right]\left(\frac{cc_l}{\bar{c}C_L}\right)_0 - \int_{(x)_c}^{(x)_{c/4}} \frac{rx}{V_0}\frac{d\left(\frac{cc_l}{\bar{c}C_L}\right)_0}{dy^*}\,dx$$

Using equation (54) to eliminate the integral results in the following

$$\left(\frac{cc_l}{\bar{c}C_L}\right)_r = \left[1 - \frac{rb}{2V_0}y^* + \frac{rb}{2V_0}(x^*)_{c/4}\tan\Lambda\right]\left(\frac{cc_l}{\bar{c}C_L}\right)_0 - \frac{r}{2V_0}\frac{d\left(\frac{cc_l}{\bar{c}C_L}\right)_0}{dy}\left[(x)^2_{c/4} - (x)^2_c\right]$$

This equation can be nondimensionalized to yield the following for the right semispan

$$\left(\frac{cc_l}{\bar{c}C_L}\right)_r = \left[1 - \frac{rb}{2V_0} y^* + \frac{rb}{2V_0}(x^*)_{c/4} \tan \Lambda\right]\left(\frac{cc_l}{\bar{c}C_L}\right)_0 - \frac{1}{2}\frac{rb}{2V_0}\left[(x^*)^2_{c/4} - (x^*)^2_c\right]\frac{d\left(\frac{cc_l}{\bar{c}C_L}\right)_0}{dy^*} \tag{87}$$

Similarly, for the left semispan,

$$\left(\frac{cc_l}{\bar{c}C_L}\right)_r = \left[1 - \frac{rb}{2V_0} y^* - \frac{rb}{2V_0}(x^*)_{c/4} \tan \Lambda\right]\left(\frac{cc_l}{\bar{c}C_L}\right)_0 - \frac{1}{2}\frac{rb}{2V_0}\left[(x^*)^2_{c/4} - (x^*)^2_c\right]\frac{d\left(\frac{cc_l}{\bar{c}C_L}\right)_0}{dy^*}$$

The span load associated with yawing is given by (for right semispan)

$$\frac{\left(\frac{cc_l}{\bar{c}C_L}\right)_r}{rb/2V_0} = -\left[y^* - (x^*)_{c/4} \tan \Lambda\right]\left(\frac{cc_l}{\bar{c}C_L}\right)_0 - \frac{1}{2}\left[(x^*)^2_{c/4} - (x^*)^2_c\right]\frac{d\left(\frac{cc_l}{\bar{c}C_L}\right)_0}{dy^*} \tag{88}$$

The additional loading due to yawing is also antisymmetric over the wing span.

b. Swept Wing

The span load equations applicable to swept wings can be obtained from equations (87) and (88) by using equations (43), (57), and (58) to put the $\bar{X}^*$ factors in terms of spanwise position, so that the total local load is given by (for right semispan)

$$\left(\frac{cc_l}{\bar{c}C_L}\right)_r = \left\{1 - \frac{rb}{2V_0}y^* + \frac{rb}{2V_0}\left[(\bar{y}^* - y^*)\tan\Lambda - \bar{X}^*\right]\tan\Lambda\right\}\left(\frac{cc_l}{\bar{c}C_L}\right)_0$$

$$- \frac{2}{A(1+\lambda)}\left(\frac{rb}{2V_0}\right)\left[1 - (1-\lambda)y^*\right]\left\{\frac{3}{2}(\bar{y}^* - y^*)\tan\Lambda\right.$$

$$\left. - \frac{9}{4A(1+\lambda)}\left[1 - (1-\lambda)y^*\right]\right\}\left\{\frac{d\,\frac{cc_l}{\bar{c}C_L}_0}{dy^*}\right\} \qquad (89)$$

The additional local loading due to yawing is given by (for right semispan)

$$\frac{\left(\frac{cc_l}{\bar{c}C_L}\right)_r}{rb/2V_0} = -\left\{y^* - \left[(\bar{y}^* - y^*)\tan\Lambda - \bar{X}^*\right]\tan\right\}\left(\frac{cc_l}{\bar{c}C_L}\right)_0$$

$$- \frac{2}{A(1+\lambda)}\left[1 - (1-\lambda)y^*\right]\left\{\frac{3}{2}(\bar{y}^* - y^*)\tan\Lambda - \frac{3}{2}\bar{X}^*\right.$$

$$\left. - \frac{9}{4A(1+\lambda)}\left[1 - (1-\lambda)y^*\right]\right\}\frac{d\left(\frac{cc_l}{\bar{c}C_L}\right)_0}{dy^*} \qquad (90)$$

3. Rolling wing

The additional local span load produced by rolling is associated with the incremental local angle of attack due to rolling velocity. This type of loading has been studied extensively by various authors (see ref. 9, for example), and will not be covered in the present paper.

VIII. COMPRESSIBILITY EFFECTS

A. General Considerations

The various wing parameters derived in this paper arise from two sources,

1. Interaction of the quarter-chord-line vortex and the air stream velocity component normal to the vortex
2. Interaction of the chordwise-bound vortices and the air stream velocity component normal to the vortices

In the latter case the velocity component is very small compared with the free-stream velocity, i.e., ($V\beta$) for sideslip, and (rx) for yawing flow as given by equations (13) and (46) respectively. It would be expected, therefore, that so long as the free stream remains subsonic, there would be no compressibility effects on the contribution of the chordwise-bound vortices to the various derivatives.

The effects of compressibility on the contribution of the quarter-chord-line vortex to the derivatives can be estimated by proper use of the Prandtl-Glauert transformation. One of the forms of the transformation states that the effects of compressibility on a given wing at a specified incidence can be estimated by assuming that the wing section lift curve slope is increased by the factor $\frac{1}{\sqrt{1 - M_y^2}}$ where M_y is the Mach number of the free-stream velocity component which is normal to the quarter-chord-line vortex; that is,

$$(c l_\alpha)_M = \frac{(c l_\alpha)_{M=0}}{\sqrt{1 - M_y^2}}$$

or, since the incidence α is constant,

$$(c_l)_M = \frac{(c_l)_{M=0}}{\sqrt{1 - M_N^2}} \tag{91}$$

The span load parameter can also be formed

$$\left(\frac{cc_l}{\bar{c}C_L}\right)_M = \frac{1}{\sqrt{1 - M_N^2}} \left(\frac{cc_l}{\bar{c}C_L}\right)_0 \tag{92}$$

At zero sideslip angle, the Mach number normal to the quarter-chord line is $M \cos \Lambda$, so that equation (92) can be written as

$$\left(\frac{cc_l}{\bar{c}C_L}\right)_M = \frac{1}{\sqrt{1 - M^2 \cos^2 \Lambda}} \left(\frac{cc_l}{\bar{c}C_L}\right)_0 \tag{93}$$

This fundamental relationship can be used to determine compressibility effects on the various derivatives and span loads as shown in the following sections.

The simplest procedure of incorporating the compressibility effects in the incompressible-flow equations derived thus far is to note that only the forces or span load due to the quarter-chord-line vortex is to have a compressibility correction. The span load of the quarter-chord line appears in the various general equations as $\left(\frac{cc_l}{\bar{c}C_L}\right)_0$ multiplied by certain geometric parameters of the wing, hence this span load factor must be increased by $\frac{1}{\sqrt{1 - M^2 \cos^2 \Lambda}}$ as shown by equation (93). The forces and loads on the chordwise-bound vortices are associated with the parameter $\frac{d\left(\frac{cc_l}{\bar{c}C_L}\right)_0}{dy^*}$ and have no compressibility effect.

B. Aerodynamic Derivatives

The procedure for incorporating compressibility effects in the equations for the various aerodynamic derivatives is straight-forward, and is shown in the next few sections.

1. Sideslipping wing.- The parameter derived for the wing in sideslip was C_{l_β}/C_L.

a. General Equations

The general equation for C_{l_β}/C_L in incompressible flow is given in equation (29), that is,

$$\frac{C_{l_\beta}}{C_L} = -\frac{1}{2}\int_0^1 \left[\left(\frac{cc_l}{\overline{c}C_L}\right)_0 \tan\Lambda - \frac{3}{4}\frac{d\left(\frac{cc_l}{\overline{c}C_L}\right)_0}{dy^*}\right] y^*\,dy^* + 0.05 \qquad (29)$$

Application of the compressibility correction according to equation (93) is straightforward, except for treatment of the constant 0.05 which occurs in equation (29). As discussed in the section "Circulation Distribution for Wings in Sideslip" (pages 46-51), the term 0.05 represents an increment to C_{l_β}/C_L due to alteration of the span load distribution caused by skewing the trailing vortices behind the wing. Perhaps the simplest way of assessing the compressibility effect on this term is to note that the Prandtl-Glauert correction for compressibility effects can be treated in any of several ways for wings in symmetric flow. In the present case an applicable treatment is to assume that compressibility effects can be accounted for by stating that a wing in compressible flow at Mach number M has

the same aerodynamic characteristics as it would have in incompressible flow if its dimensions in the free-stream direction were shrunk by the factor $\sqrt{1 - M^2}$.

In other words the wing x-dimensions are changed so that

$$(x)_{\text{compressible}} = \frac{(x)_{\text{incompressible}}}{\sqrt{1 - M^2}}$$

The change in wing geometry therefore would account for Mach number effects on the aerodynamic characteristics. Therefore, one could presume that if a certain wing characteristic (in incompressible flow) varied with geometric shape, it would also vary with Mach number. Conversely, if a parameter is independent of wing geometry, it should also be independent of Mach number. As was pointed out in the discussion of the origin of the increment 0.05 (pages), the increment was found to be independent (for all practical purposes) of wing geometry. Based on the above arguments, the term 0.05 appearing in the equation for Cl_β/C_L will not be altered by compressibility.

The general equation for Cl_β/C_L therefore becomes

$$\frac{Cl_\beta}{C_L} = -\frac{1}{2}\int_0^1 \left[\left(\frac{cc_l}{\bar{c}C_L}\right)_0 \frac{\tan \Lambda}{\sqrt{1 - M^2 \cos^2 \Lambda}} - \frac{3}{4} \frac{d\left(\frac{cc_l}{\bar{c}C_L}\right)_0}{dy^*} \right] y^* \, dy^* + 0.05 \qquad (94)$$

b. Swept Wing

The compressible-flow equation for swept wings can be

obtained from equation (94). Since sweep is constant for the wings under consideration, tan Λ and the compressibility factor $\frac{1}{\sqrt{1 - M^2 \cos^2 \Lambda}}$ are constants and do not effect the indicated integrations. The integrals of equation (94) can therefore be evaluated as done previously (see work from equations (39) through (44), and the result is

$$\frac{Cl_\beta}{C_L} = -\frac{1}{2}\left\{\frac{3}{A(1+\lambda)} + \bar{y}^*\left[\frac{\tan \Lambda}{\sqrt{1 - M^2 \cos^2 \Lambda}} - \frac{6}{A}\left(\frac{1-\lambda}{1+\lambda}\right)\right]\right\} + 0.05 \qquad (95)$$

2. Yawing wing.— The parameter derived for yawing wings was Cl_r/C_L.

a. General Equations

The general equation for Cl_r/C_L in incompressible flow is given by equation (56), which is repeated here for convenience

$$\frac{Cl_r}{C_L} = \frac{1}{2}\int_0^1 \left\{\left[y^* - (x^*)_{\frac{c}{4}} \tan \Lambda\right]\left(\frac{cc_l}{\bar{c}C_L}\right)_0 + \frac{1}{2}\left[(x^*)^2_{\frac{c}{4}} - (x^*)^2_c\right]\frac{d\left(\frac{cc_l}{\bar{c}C_L}\right)_0}{dy^*}\right\} y^*\, dy^* \qquad (56)$$

Application of equation (93) to account for compressibility effects results in

$$\frac{Cl_r}{C_L} = \frac{1}{2}\int_0^1 \left\{\left[y^* - (x^*)^2_{\frac{c}{4}} \tan \Lambda\right]\left(\frac{1}{\sqrt{1 - M^2 \cos^2 \Lambda}}\right)\left(\frac{cc_l}{\bar{c}C_L}\right)_0 + \frac{1}{2}\left[(x^*)^2_{\frac{c}{4}} - (x^*)_c\right]\frac{d\left(\frac{cc_l}{\bar{c}C_L}\right)_0}{dy^*}\right\} y^*\, dy^* \qquad (96)$$

b. Swept Wing

A suitable equation for application of compressibility effects for the swept wing is equation (59), which is repeated here for convenience.

$$\frac{c_{l_r}}{C_L} = \frac{1}{2}\int_0^1 \left\{ \left[y^* (1 + \tan^2 \Lambda) - (\bar{y}^* \tan \Lambda - \bar{X}^*) \tan \Lambda \right] \left(\frac{cc_l}{cC_L} \right)_0 + \frac{c^*}{2} \left[\frac{3}{2} (\bar{y}^* - y^*) \tan \Lambda - \frac{3}{2} \bar{X}^* - \frac{9}{16} c^* \right] \frac{d \left(\frac{cc_l}{cC_L} \right)_0}{dy^*} \right\} y^* \, dy^* \tag{59}$$

Application of the compressibility correction given by equation (93) results in

$$\frac{c_{l_r}}{C_L} = \frac{1}{2}\int_0^1 \left\{ \left[y^* (1 + \tan^2 \Lambda) - (\bar{y}^* \tan \Lambda - \bar{X}^*) \tan \Lambda \right] \frac{1}{\sqrt{1 - M^2 \cos^2 \Lambda}} \left(\frac{cc_l}{cC_L} \right)_0 + \frac{c^*}{2} \left[\frac{3}{2} (\bar{y}^* - y^*) \tan \Lambda - \frac{3}{2} (\bar{X}^*) - \frac{9}{16} c^* \right] \frac{d \left(\frac{cc_l}{cC_L} \right)_0}{dy^*} \right\} y^* \, dy^* \tag{97}$$

The various integrals of equation (97) have been evaluated previously (see equations (62) and (67)), so that equation (97) can be rewritten as

$$\begin{aligned} \frac{c_{l_r}}{C_L} = {} & \frac{1}{2} \left[(1 + \tan^2 \Lambda)(\bar{y}^*)^2 - (y^* \tan \Lambda - \bar{X}^*) \bar{y}^* \tan \Lambda \right] \frac{1}{\sqrt{1 - M^2 \cos^2 \Lambda}} \\ & - \frac{3}{8} (\bar{y}^* \tan \Lambda - \bar{X}^*) \int_0^1 (c^* + y^* \frac{dc^*}{dy^*}) \left(\frac{cc_l}{cC_L} \right)_0 \, dy^* \\ & + \frac{3}{8} \tan \Lambda \int_0^1 \left(\frac{cc_l}{cC_L} \right)_0 \left[2c^* y^* + (y^*)^2 \frac{dc^*}{dy^*} \right] dy^* \\ & + \frac{9}{64} \int_0^1 \left[(c^*)^2 + 2c^* y^* \frac{dc^*}{dy^*} \right] \left(\frac{cc_l}{cC_L} \right)_0 dy^* \end{aligned} \tag{98}$$

The integrals of equation (98) also have been evaluated previously (see equations (69), (70), and (71)), hence equation (98) becomes

$$\frac{Cl_r}{C_L} = \frac{1}{2}\left[(1 + \tan^2\Lambda)(\tilde{y}^*)^2 - (\bar{y}^* \tan\Lambda - \bar{x}^*)\,\bar{y}\,\tan\Lambda\right]\frac{1}{\sqrt{1 - M^2\cos^2\Lambda}}$$

$$- \frac{3}{2}(\bar{y}^* \tan\Lambda - \bar{x}^*)\left[\frac{1}{A(1+\lambda)} - \frac{2}{A}\left(\frac{1-\lambda}{1+\lambda}\right)\bar{y}^*\right]$$

$$+ \frac{3}{2}\tan\Lambda\left[\frac{2}{A(1+\lambda)}\,\bar{y}^* - \frac{3}{A}\left(\frac{1-\lambda}{1+\lambda}\right)(\tilde{y}^*)^2\right]$$

$$+ \frac{9}{4}\left[\frac{1}{A^2(1+\lambda)^2}\right]\left[1 - 4(1-\lambda)\,\bar{y}^* + 3(1-\lambda)^2\,(\tilde{y}^*)^2\right]$$

Various terms of the above equation can be combined to result in the following equation

$$\frac{Cl_r}{C_L} = \left[\frac{1}{2}\left(\frac{1 + \tan^2\Lambda}{\sqrt{1 - M^2\cos^2\Lambda}}\right) - \frac{9}{2A}\left(\frac{1-\lambda}{1+\lambda}\right)\tan\Lambda + \frac{27}{4A^2}\left(\frac{1-\lambda}{1+\lambda}\right)^2\right](\tilde{y}^*)^2$$

$$+ \left[\frac{3}{A}\left(\frac{1-\lambda}{1+\lambda}\right)\tan\Lambda - \frac{\tan^2\Lambda}{2\sqrt{1 - M^2\cos^2\Lambda}}\right](\bar{y}^*)^2$$

$$+ \left[\frac{3\tan\Lambda}{2A(1+\lambda)} - \frac{9(1-\lambda)}{A^2(1+\lambda)^2}\right]\bar{y}^*$$

$$+ \left[\left(\frac{1}{2}\right)\frac{\tan\Lambda}{\sqrt{1 - M^2\cos^2\Lambda}} - \frac{3}{A}\left(\frac{1-\lambda}{1+\lambda}\right)\right]\bar{x}^*\,\bar{y}^*$$

$$+ \frac{3\bar{x}^*}{2A(1+\lambda)} + \frac{9}{4A^2(1+\lambda)^2} \qquad (99)$$

3. Rolling wing.- The derivatives which were determined for the rolling wing were dependent only on the load associated with the quarter-chord-line vortex, therefore the effects of compressibility can be determined easily.

a. General Equations

The general equations determined for the wing characteristics in incompressible flow were presented as equations (76) and (77),

$$\frac{C_{Y_p}}{C_L} = \int_0^1 \left(\frac{cc_l}{\bar{c}C_L}\right)_0 \tan\Lambda \, y^* \, dy^* \tag{76}$$

$$\frac{C_{n_p}}{C_L} = \frac{1}{2}\int_0^1 \left(\frac{cc_l}{\bar{c}C_L}\right)_0 \left[(x^*)_{\frac{c}{4}} \tan\Lambda - y^*\right] y^* \, dy^* \tag{77}$$

Applying the compressibility correction results in

$$\frac{C_{Y_p}}{C_L} = \int_0^1 \left(\frac{cc_l}{\bar{c}C_L}\right)_0 \frac{\tan\Lambda}{\sqrt{1 - M^2\cos^2\Lambda}} \, y^* \, dy^* \tag{100}$$

$$\frac{C_{n_p}}{C_L} = \frac{1}{2}\int_0^1 \left(\frac{cc_l}{\bar{c}C_L}\right)_0 \left[(x^*)_{\frac{c}{4}} \tan\Lambda - y^*\right] \frac{y^*}{\sqrt{1 - M^2\cos^2\Lambda}} \, dy^* \tag{101}$$

b. Swept Wing

The equations derived for the swept wing in incompressible flow were

$$\frac{C_{Y_p}}{C_L} = \bar{y}^* \tan\Lambda \tag{81}$$

and

$$\frac{C_{np}}{C_L} = -\frac{1}{2}\left\{(\tilde{y}^*)^2 + \left[(\tilde{y}^*)^2 - (\bar{y}^*)^2\right]\tan^2\Lambda + \bar{X}^*\,\bar{y}^*\tan\Lambda\right\} \quad (82)$$

In this case, the simplest way of determining the compressibility effects is to note that for constant sweep the general equations (equations (100) and (101)) show that the compressibility parameter simply multiplies the derivatives. Therefore, the equations for the swept wing in compressible flow can be immediately written as

$$\frac{C_{Y_p}}{C_L} = \frac{\bar{y}^*\tan\Lambda}{\sqrt{1 - M^2\cos^2\Lambda}} \quad (102)$$

and

$$\frac{C_{np}}{C_L} = -\frac{1}{2\sqrt{1 - M^2\cos^2\Lambda}}\left\{(\tilde{y}^*)^2 + \left[(\tilde{y}^*)^2 - (\bar{y}^*)^2\right]\tan^2\Lambda + \bar{X}^*\,\bar{y}^*\tan\Lambda\right\} \quad (103)$$

C. Span Load Distribution

Compressibility effects on the span load distribution can be determined by the concept that only the load associated with the quarter-chord line is effected.

1. Sideslipping wing.—

a. General Equations

The total local span load on a sideslipping wing in incompressible flow is given by equation (23). Applying the compressibility correction as noted previously results in

$$\left(\frac{cc_l}{\bar{c}C_L}\right)_\beta = \left(\frac{cc_l}{\bar{c}C_L}\right)_0 \frac{1 + \beta \tan \Lambda}{\sqrt{1 - M^2 \cos^2 \Lambda}} - \frac{3}{4} c^* \beta \frac{d\left(\frac{cc_l}{\bar{c}C_L}\right)_0}{dy^*} \qquad (104)$$

for the right semispan, and in

$$\left(\frac{cc_l}{\bar{c}C_L}\right)_\beta = \left(\frac{cc_l}{\bar{c}C_L}\right)_0 \frac{1 - \beta \tan \Lambda}{\sqrt{1 - M^2 \cos^2 \Lambda}} - \frac{3}{4} c^* \beta \frac{d\left(\frac{cc_l}{\bar{c}C_L}\right)_0}{dy^*} \qquad (105)$$

for the left semispan. The additional loading due to sideslip therefore is given by

$$\frac{\left(\frac{cc_l}{\bar{c}C_L}\right)_\beta}{\beta} = \left(\frac{cc_l}{\bar{c}C_L}\right)_0 \frac{\tan \Lambda}{\sqrt{1 - M^2 \cos^2 \Lambda}} - \frac{3}{4} c^* \frac{d\left(\frac{cc_l}{\bar{c}C_L}\right)_0}{dy^*} \qquad (106)$$

for the right semispan. This additional loading is antisymmetric over the wing

b. Swept Wings

The span load equations for swept wings can be determined from the general equations. Equation (43) is used to eliminate c^*, therefore the total local load on the swept wing in sideslip is

$$\left(\frac{cc_l}{\bar{c}C_L}\right)_\beta = \left(\frac{cc_l}{\bar{c}C_L}\right)_0 \frac{1 + \beta \tan \Lambda}{\sqrt{1 - M^2 \cos^2 \Lambda}} - \frac{3\beta}{A(1 + \lambda)} \left[1 - (1 - \lambda) y^*\right] \frac{d\left(\frac{cc_l}{\bar{c}C_L}\right)_0}{dy^*} \qquad (107)$$

The additional load due to sideslip is given by

$$\frac{\left(\frac{cc_l}{\bar{c}C_L}\right)_\beta}{\beta} = \left(\frac{cc_l}{\bar{c}C_L}\right)_0 \frac{\tan \Lambda}{\sqrt{1 - M^2 \cos^2 \Lambda}} - \frac{3}{\Lambda(1 + \lambda)}\left[1 - (1 - \lambda)\, y^*\right] \frac{d\left(\frac{cc_l}{\bar{c}C_L}\right)_0}{dy} \tag{108}$$

for the right semispan.

2. Yawing wing.-

a. General Equations

The total local span load on a yawing wing in compressible flow can be obtained by applying the compressibility correction to equation (87), and the result is, for the right semispan,

$$\left(\frac{cc_l}{\bar{c}C_L}\right)_r = \left[1 - \frac{rb}{2V_0}\left(y^* - (x^*)_{\frac{c}{4}} \tan \Lambda\right)\right] \frac{\left(\frac{cc_l}{\bar{c}C_L}\right)_0}{\sqrt{1 - M^2 \cos^2 \Lambda}} - \frac{1}{2} \frac{rb}{2V_0}\left[(x^*)^2_{\frac{c}{4}} - (x^*)^2_c\right] \frac{d\left(\frac{cc_l}{\bar{c}C_L}\right)_0}{dy^*} \tag{109}$$

The additional loading due to yawing is given by (for right semispan)

$$\frac{\left(\frac{cc_l}{\bar{c}C_L}\right)_r}{\frac{rb}{2V_0}} = -\left[y^* - (x^*)_{\frac{c}{4}} \tan \Lambda\right] \frac{\left(\frac{cc_l}{\bar{c}C_L}\right)_0}{\sqrt{1 - M^2 \cos^2 \Lambda}} - \frac{1}{2}\left[(x^*)^2_{\frac{c}{4}} - (x^*)^2_c\right] \frac{d\left(\frac{cc_l}{\bar{c}C_L}\right)_0}{dy^*} \tag{110}$$

The additional loading due to yawing is antisymmetric over the wing.

b. Swept Wings

The load parameters for swept wings in compressible flow can be obtained by applying the compressibility corrections to equations (89) and (90), which pertain to the right semispan. The results are, for total local load,

$$\left(\frac{cc_l}{\bar{c}C_L}\right)_r = \left\{1 - \frac{rb}{2V_0}\,y^* + \frac{rb}{2V_0}\left[(\bar{y}^* - y^*)\tan\Lambda - \bar{X}^*\right]\tan\Lambda\right\}\frac{\left(\frac{cc_l}{\bar{c}C_L}\right)_0}{\sqrt{1 - M^2\cos^2\Lambda}}$$
$$- \frac{2}{A(1+\lambda)}\left(\frac{rb}{2V_0}\right)\left[1 - (1-\lambda)y^*\right]\left\{\frac{3}{2}(\bar{y}^* - y^*)\tan\Lambda\right.$$
$$\left. - \frac{3}{2}\bar{X}^* - \frac{9}{4A(1+\lambda)}\left[1 - (1-\lambda)y^*\right]\right\}\frac{d\left(\frac{cc_l}{\bar{c}C_L}\right)_0}{dy^*} \qquad (111)$$

and for the additional load due to yawing,

$$\frac{\left(\frac{cc_l}{\bar{c}C_L}\right)_r}{\frac{rb}{2V_0}} = -\left\{y^* - \left[(\bar{y}^* - y^*)\tan\Lambda - \bar{X}^*\right]\tan\Lambda\right\}\frac{\left(\frac{cc_l}{\bar{c}C_L}\right)_0}{\sqrt{1 - M^2\cos^2\Lambda}}$$
$$- \frac{2}{A(1+\lambda)}\left[1 - (1-\lambda)y^*\right]\left\{\frac{3}{2}(\bar{y}^* - y^*)\tan\Lambda\right.$$
$$\left. - \frac{3}{2}\bar{X}^* - \frac{9}{4A(1+\lambda)}\left[1 - (1-\lambda)y^*\right]\right\}\frac{d\left(\frac{cc_l}{\bar{c}C_L}\right)_0}{dy^*} \qquad (112)$$

IX. PRESENTATION OF RESULTS

A. General Remarks

The theory and methods developed in this thesis permit the computation of certain aerodynamic derivatives and span load characteristics for sideslipping, yawing, and rolling wings of arbitrary planform in subsonic flow. The method requires that the angle-of-attack loading be known in incompressible flow for the wing under consideration. This information is available for a wide range of wing planforms, hence such a requirement should not seriously restrict the application of the present method. Span loads for wings of unusual [illegible] such as M or W, wings can be obtained by the method of finite-span horseshoe vortices as outlined in references 26 or 27.

Most of the equations derived herein involve the spanwise position of the centroid and radius of gyration of the angle-of-attack loading of the wing semispan. The centroid position for angle-of-attack loadings has been determined for a wide range of wing planforms and is readily available in the literature (see references 8, 9, 28, and 29 for example). The present theory appears to be the only one in the literature in which the radius of gyration appears as a factor in determining aerodynamic characteristics. The centroid and radius of gyration were determined for use in this thesis as explained in the two following sections.

1. Centroid of angle-of-attack loading.- As explained above, the centroid of wing span loadings are available for swept wings in various references. This information is replotted in figure 16 in a form suitable for use in the methods and equations of this

paper. The spanwise position of the centroid, $\bar{y}^*$, is given as a function of sweep, aspect ratio, and taper ratio.

2. Radius of gyration of angle-of-attack loading.- Since the radius of gyration of span loads has not previously been used as a factor in determining aerodynamic derivatives, its values for various wings do not appear in the literature. It was necessary, therefore, to compute the radius of gyration, $\tilde{y}^*$, for use in this paper. The values were determined by plotting the angle-of-attack span loading (i.e., $\left(\frac{cc_l}{\bar{c}C_L}\right)_0$ plotted against y^*) for a large number of wings and performing a mechanical integration to obtain $\tilde{y}^*$ by use of equation (61),

$$(\tilde{y}^*)^2 = \int_0^1 \left(\frac{cc_l}{\bar{c}C_L}\right)_0 (y^*)^2 \, dy^* \tag{61}$$

A total of 160 such integrations were performed to obtain the desired coverage of wing planforms. Values of $\tilde{y}^*$ are plotted in figure 17 as functions of sweep, aspect ratio, and taper ratio for use in this paper and for general information. Data for the span loads was obtained from reference 8.

B. Aerodynamic Derivatives

1. Summary of equations for the wing derivatives.- The equations derived for the various aerodynamic derivatives are presented in tables 1 and 2 for convenient reference. The equations of Table I are general equations which are applicable to wings of arbitrary planform. These equations should be used if sweep varies across

the wing span. If sweep is constant, the equations of Table II are applicable.

2. Figures for the wing derivatives as functions of wing geometry and Mach number.- The equations of Table II have been used to construct a series of figures from which numerical values of the various derivative can be obtained as functions of sweep, aspect ratio, taper ratio, and Mach numbers from zero to about 0.95. The derivatives have been computed for a value of $\bar{X}^*$ of zero, and are presented in the following figures:

Parameter	Figures
Cl_β/C_L	18 through 22
Cl_r/C_L	23 through 27
C_{Y_p}/C_L	28 through 32
C_{n_p}/C_L	33 through 37

Two of the parameters, Cl_r/C_L and C_{n_p}/C_L vary linearly with $\bar{X}^*$ for a given wing as can be seen by examination of the equations of Table II. It would be a simple matter to evaluate the dependence of the parameters Cl_r/C_L and C_{n_p}/C_L on $\bar{X}^*$. However, as will be pointed out in the discussion, this is not required since these increments can be evaluated very simply in terms of the parameters Cl_β/C_L and C_{Y_p}/C_L.

C. Span Load Distributions

The span-load equations derived in this thesis are applicable for the determination of the additional load due to sideslip and yawing velocity of a wing for which the span load in symmetric flight is known at zero Mach number. The span-load equations are summarized

in Table III and Table IV. The equations of Table III are very general, and should be used if the sweep angle varies across the wing span. In such instances it may not be possible to find in the literature the corresponding angle-of-attack loading of the wing. In these instances, as noted previously, the angle-of-attack loading can be determined in a straight-forward manner (solution of simultaneous algebraic equations) by the method of reference 26 or 27.

If sweep is constant across the span, which is so in by far the majority of cases, the equations of Table IV are applicable and convenient. In these cases the angle-of-attack span-load distribution can be obtained from a number of sources, such as reference 8.

Most of the theoretical angle-of-attack span-load distributions available in the literature have been determined by use of the Weissinger method. It is of interest and significance to note that the use of finite horseshoe vortices to determine angle-of-attack span loadings (as in ref. 26 or 27) will closely approximate loadings from the Weissinger method if a minimum of about 20 horseshoe vortices are used to represent the wing (see ref. 26). The finite-horseshoe vortex method is applicable for representing wings having discontinuities in sweep distribution (for example M- or W-wings), where the applicability of the Weissinger method is doubtful. This method was used in reference 29 to determine the span loads of some M- and W-wings, and can be used for wings of arbitrary planform. Note that the system of finite horseshoe vortices was also used in reference 25 to obtain

the load on wings in sideslip. In such a case, the loads are obtained from either a mechanical integration or from a series expansion (ref. 23).

X. DISCUSSION OF RESULTS

A. General Remarks

The equations derived herein permit the computation of the aerodynamic derivatives C_{l_β}, C_{l_r}, C_{Y_p}, and C_{n_p} for wings of arbitrary planform. One might ask at this point why the theory predicts these particular derivatives and not the remaining ones. The reasons are not obvious, but can be explained as follows. The forces which result in the above derivatives arise from interaction of the various wind velocity components and the vortices used to represent the wing. The local vortex strength is directly proportional to the wing lift coefficient. Hence the various forces are directly proportional to the total wing lift (or lift coefficient). The various aerodynamic derivatives obtained by use of the present methods are therefore those directly proportional to C_L. This is the reason that the equations for the derivatives are extracted in the form $\frac{C_{l_\beta}}{C_L}$, $\frac{C_{l_r}}{C_L}$, $\frac{C_{Y_p}}{C_L}$, and $\frac{C_{n_p}}{C_L}$. Examination of the equations for wing derivatives as given by other methods (see for example reference 13) shows that indeed the above derivatives are the only common derivatives linearly dependent on C_L. The other derivatives are either independent of C_L (for example, C_{l_p}) or are dependent on C_L^2 (for example, C_{n_β}).

B. Comparison of Various Theories and Experimental Results for the Aerodynamic Derivatives of Wings in Incompressible Flow

Various methods have been used in the past in determining mathematical expressions for estimating wing derivatives in incompressible flow. In general, the methods result in similar variations of each derivative with any particular variable. However, the methods generally do not give identical results as will be shown.

1. Sideslipping wing. - The derivative determined for the wing in sideslip is C_{l_β}. This derivative has been the subject of several analytical studies (references 6, 13, and 15 for example). It is interesting to compare the results of the various methods. This has been done to a small extent in reference 23. That comparison will be repeated here briefly, and brought up to date.

a. Elliptic Wings

The variation of C_{l_β}/C_L with aspect ratio for elliptic wings is shown in figure 38 as determined by the present theory and also by equation (4) of reference 6 with $K = 1.5$. Note that the values given by reference 6 are somewhat lower than those given by equation (38) of this thesis. The primary reason for this is that reference 6 did not include the contribution of the quarter-chord-line vortex. If this contribution is neglected in the present analysis, the agreement with reference 6 is much closer. The fact that the quarter-chord-line vortex was not considered in reference 6 is not surprising, since elliptic wings

are not generally treated as swept wings. If one places the bound vortex along the quarter-chord-line, however, the elliptic wing must be treated as a swept wing with the sweep angle varying across the wing span as was done in reference 23 and this thesis.

b. Swept Wing

The term "swept wing" as used herein is also used to include the wing having zero sweep as a limiting case. This is pointed out because there are certain theories which apply specifically to unswept wings and are not applicable to swept wings. There are currently at least three sources from which theoretical values of C_{l_β}/C_L may be obtained for unswept wings, and these are references 6, 13, and 15. It is instructive to examine the applicable equations of each of these references to determine why differences exist.

The equation for C_{l_β}/C_L given in reference 6 is

$$\frac{C_{l_\beta}}{C_L} = -\frac{K}{A}\frac{0.71\lambda + 0.29}{1 + \lambda} + 0.05 \qquad (113)$$

Several remarks concerning this equation are in order. According to Weissinger, the theoretical value for K is 1.5. However, when Weissinger compared his estimated values with available data, the theory gave values which were too negative. He therefore suggested an empirical value of $K = 1.0$ to provide closer agreement with data.

The unswept-wing values of reference 13 are those given by the Weissinger equation (eq. (113)) with $K = 1.0$, hence the applicable equation for reference 13 is

$$\frac{C_{l_\beta}}{C_L} = -\frac{1}{A}\frac{0.71\lambda + 0.29}{1 + \lambda} + 0.05 \qquad (114)$$

The unswept-wing values of C_{l_β}/C_L of reference 15 were determined empirically from available data and are given as functions of aspect ratio for taper ratios of 1.0 and zero in figure 8 of reference 15.

The applicable equation from the theory presented in this thesis is equation (95), with $M = 0$, and $\Lambda = 0$, that is,

$$\frac{C_{l_\beta}}{C_L} = -\frac{1}{2}\left[\frac{3}{A(1 + \lambda)} - \frac{6\bar{y}^*}{A}\left(\frac{1 - \lambda}{1 + \lambda}\right)\right] + 0.05 \qquad (115)$$

Note that equations (115) and (113) are identical for $\lambda = 1.0$ if a value of $K = 1.5$ is used in equation (113). In other words, the present theory agrees with Weissinger's method if the theoretically correct value of $K = 1.5$ is used in Weissinger's equation, and if the wings are untapered. Reference 13 would also have given identical results except for Weissinger's recommendation that a value of $K = 1.0$ be used in his equation.

A comparison of the results obtained from the various theories reviewed above is shown in figure 39 for untapered wings. Also shown are experimental values taken from reference 30. Two points are to be noted from this comparison. First, equation (95)

of the present theory, Weissinger's equation (113) with K = 1.5, and the method of reference 15 all agree closely with the experimental data. The Weissinger equation with K = 1.0 yields values of C_{l_β}/C_L which are substantially lower than the experimental points. One is then led to wonder why Weissinger's comparisons with data lead him to recommend that a value K = 1.0 be used in his equation. One plausible explanation is that the wing planforms generally in use at the time Weissinger developed his theory (1938) had tips which were rounded (viewed from the top), whereas current wings, and those of reference 30 have essentially straight tips. Rounding the tips would tend to reduce tip loading and thereby also the derivative C_{l_β}.

Swept wing values of C_{l_β}/C_L can be estimated by the methods developed in references 13, 15 and equation (95) of the present theory. Results from the various theories are shown in figure 40 for untapered wings. Also shown are experimental values from reference 30. The results of reference 15 and equation (95) are in good agreement with experiment, whereas values predicted by reference 13 are somewhat low. The poor agreement shown by reference 13 is traceable to the fact that the applicable equation of reference 13 is given by

$$\frac{C_{l_\beta}}{C_L} = \left(\frac{C_{l_\beta}}{C_L}\right)_{\Lambda=0} - \bar{y}^* \frac{A + 2\cos\Lambda}{A + 4\cos\Lambda} \frac{\tan\Lambda}{2} \qquad (116)$$

where, as noted previously, $\left(\frac{C_{l_\beta}}{C_L}\right)_{\Lambda=0}$ is the unswept-wing value and was obtained from Weissinger's equation with K = 1.0. Note that if equation (95) is written in a form corresponding to equation (116) the result is

$$\frac{C_{l_\beta}}{C_L} = \left(\frac{C_{l_\beta}}{C_L}\right)_{\Lambda=0} - \frac{\bar{y}^*}{2} \tan \Lambda \qquad (117)$$

The equations now differ in form only in that the sweep effect is modified by the term $\frac{A + 2 \cos \Lambda}{A + 4 \cos \Lambda}$ in equation (116). This term had its origin in the concept that since the additional load due to sideslip is antisymmetric, induction effects should be based on the aspect ratio of the wing semispan rather than of the entire span. The present theory has no such effect because it was argued that the circulation is symmetric even when the wing is sideslipping.

The theories of reference 13 and 15 are limited to taper ratios close to 1.0. The present theory does not have this restriction. The theory predicts the effects of taper ratio as shown by a comparison of the theory with experimental data from reference 31 (see figure 41). The theory also predicts the proper variation of $\frac{C_{l_\beta}}{C_L}$ with aspect ratio for triangular wings as shown in figure 42 where a comparison is made with data from references 32 and 33. Triangular wings have a unique relationship between sweep of the quarter-chord-line and the aspect ratio. This relationship, which will be used in a later section, is given by

$$\tan \Lambda = \frac{3}{A}$$

2. Yawing wing.- The derivative extracted for the yawing wing was C_{l_r}. In spite of the importance of this derivative in the dynamic lateral stability of aircraft, there is little published information on theoretical or experimental values of C_{l_r}. A review of the literature indicates that theoretical values may be obtained from references 5, 13, 16, 34, and 35. References 34 and 35 are unpublished and therefore of little value to the aerodynamicist. References 5 and 16 apply only to unswept wings. The unswept-wing values of $\frac{C_{l_r}}{C_L}$ used in reference 13 were obtained from reference 5, and are essentially the same (but slightly higher in value) than the values given in reference 16. The net situation therefore, is that the only theoretical values for comparison with the present theory are those of reference 13. Consider now the applicable equation of reference 13, which is

$$\frac{C_{l_r}}{C_L} = \frac{1}{3} + \left[\frac{A + 2\cos\Lambda}{A + 4\cos\Lambda}\right]\left[\frac{\tan^2\Lambda}{24} + \frac{\bar{x}}{c}\frac{\tan\Lambda}{2A}\right] \tag{119}$$

For unswept wings, this results in a constant value of $C_{l_r}/C_L = \frac{1}{3}$, and is independent of wing geometry. The above equation can also be written as

$$\frac{C_{l_r}}{C_L} = \left[1 + \frac{A + 2\cos\Lambda}{A + 4\cos\Lambda}\left(\frac{\tan^2\Lambda}{8} + \frac{3}{2}\frac{\bar{x}}{c}\frac{\tan\Lambda}{2A}\right)\right]\left(\frac{C_{l_r}}{C_L}\right) \tag{120}$$

The values of $\left(\frac{C_{l_r}}{C_L}\right)_{\Lambda=0}$ used in reference 13 were those of reference 5. The values of reference 5 are applicable for aspect ratios greater than 6. The values of reference 5 were extrapolated to lower aspect

ratios in reference 13. Extrapolation of derivatives in the low aspect ratio region can be dangerous in that certain derivatives are very sensitive to this parameter at low aspect ratios.

Equation (119) shows certain trends of interest. First (for $\bar{X} = 0$), the effect of sweep is primarily to add on increment to $\frac{C_{l_r}}{C_L}$ which is very nearly independent of aspect ratio. Because of this, equation (119) indicates that the variation of $\frac{C_{l_r}}{C_L}$ with aspect ratio (for a given sweep angle) is essentially the variation shown by the unswept wing. The curves obtained from reference 5 show very little variation of $\frac{C_{l_r}}{C_L}$ with aspect ratio for unswept wings having aspect ratios greater than 6.0. The extrapolations of reference 13 to low aspect ratios are such that $\frac{C_{l_r}}{C_L}$ remains about constant. The net result is that for any sweep angle, $\frac{C_{l_r}}{C_L}$ is very nearly independent of aspect ratio. This has been pointed out in detail because the theory of this thesis indicates somewhat different trends at low aspect ratios. Equation (99) of this thesis and figure 26 (for untapered wings, in order to be comparable with reference 13) also show little variation of $\frac{C_{l_r}}{C_L}$ with aspect ratio in the high aspect ratio range. However, equation (99) indicates a rapid positive increase in $\frac{C_{l_r}}{C_L}$ as the aspect ratio is reduced below about 3.0.

Which theory, then predicts the proper trends at low aspect ratios? The present theory can be defended to some extent by noting that the vortex system and wind velocity components in yawing flow bear a marked resemblance to the vortex pattern and velocity components

associated with sideslip. It might logically be expected therefore, that the trends in $\frac{C_{l_r}}{C_L}$ would be similar to those of $\frac{C_{l_\beta}}{C_L}$. The trends for $\frac{C_{l_\beta}}{C_L}$ are well substantiated by numerous experimental results. The trends for variation of $\frac{C_{l_r}}{C_L}$ are similar to those of $\frac{C_{l_\beta}}{C_L}$ according to the theory of the present thesis.

The two theories are compared with experimental data in figure 43. The theoretical values of $\frac{C_{l_r}}{C_L}$ are applicable only in the linear range near $C_L = 0$. This form of comparison was chosen to show actual data points (from reference 13) in order to point out a number of facts with regard to experimental determination of the parameter $\frac{C_{l_r}}{C_L}$. First it is pointed out that the present theory appears to be somewhat more consistent in determining $\frac{C_{l_r}}{C_L}$ than the theory of reference 13.

Determination of $\frac{C_{l_r}}{C_L}$ experimentally can be accomplished by several means:

(a) Curving the airflow past the model (Method used in the Stability Tunnel).

(b) Rotating a model on a long boom.

(c) Straight flow past a curved model.

(d) Oscillating a model about its vertical axis (reference 36).

(e) Pure yawing oscillation mechanisms (see reference 37).

Method (b) is not attractive or used because of the turbulence set up during the first circuit of the model and because of boom interference problems. Method (c) has been suggested but the author has never seen results, if any exist. Method (d) yields combinations of derivatives, in particular $(C_{l_r} + C_{l_{\dot\beta}})$, instead of the desired

isolated derivative C_{l_r}. Method (e) requires a special mechanism and data reduction equipment. Method (a) is cumbersome in that curving the airflow requires certain equipment changes so that the primary variable $rb/2V$ cannot be varied conveniently.

Methods (a) and (e), which appear to be the better means of determining C_{l_r} have a common difficulty in that the primary variable $rb/2V$ can be changed over only a very small range. This results in small measured forces and makes accurate determination of yawing derivatives quite difficult. The net result is that data points tend to scatter, and fairing the data points to obtain first C_{l_r} and then $\frac{C_{l_r}}{C_L}$, for example, is by no means an exact process.

The above is pointed out primarily to indicate that the data of figure 43 for the 60° swept wing can be faired to show reasonable agreement with either of the two theories.

3. Rolling wing.- Two derivatives were derived for the rolling wing, and these were C_{Y_p} and C_{n_p}. In general, the derivative C_{Y_p} has no effect on the dynamic lateral stability of an aircraft, and hence is not important per se. However, its value is of some importance in transforming certain of the other derivatives to different systems of reference axes. The only available reference for theoretical values of this parameter is reference 13. The applicable equation of reference 13 is

$$\frac{C_{Y_p}}{C_L} = \frac{A + \cos \Lambda}{A + 4 \cos \Lambda} \tan \Lambda \qquad (120)$$

The equation derived in the present thesis is

$$\frac{C_{Y_p}}{C_L} = \bar{y}^* \tan \Lambda \qquad (83)$$

Both equations indicate that $\frac{C_{Y_p}}{C_L}$ is a linear function of the tangent of the sweep angle, so that for unswept wings C_{Y_p} is theoretically zero. The equations are different in other respects however. For example, equation (120) indicates no effect of taper ratio, and only a sign change if the sweep angle changes sign. Equation (83) shows an effect of all geometric changes (A, Λ, λ) as reflected through changes in $\bar{y}^*$ (see figure 16).

The theory of reference 13 and values from equation (83) are compared with experimental results in figure 44. Both theories generally underestimate the numerical value of C_{Y_p} for any specific lift coefficient, with the values of equation (83) showing the poorer agreement. The lack of good correlation between the theory of reference 13 and available data had been noted previously in reference 38, and an imperical method for improving the correlation was suggested. The suggested modification was to add a term $\frac{1}{A}$ to equation (120) to obtain

$$\frac{C_{Y_p}}{C_L} = \frac{A + \cos \Lambda}{A + 4 \cos \Lambda} \tan \Lambda + \frac{1}{A} \qquad (121)$$

The suggestion was based on a theory developed in reference 39 for low aspect ratio triangular wings. Reference 39 derives an expression

$$\frac{C_{Y_p}}{C_L} = \frac{4}{3A} \qquad (122)$$

for low aspect ratio triangular wings. Reference 38 suggests a value of

$$\left(\frac{C_{Y_p}}{C_L}\right)_{\Lambda=0} = \frac{1}{A}$$

for unswept wings, and assumes that this value is also to be added to the theoretical value of reference 13 for swept wings. It is interesting to see what happens to equation (121) for triangular wings. In this case, equation (118) can be used with equation (121) to obtain

$$\frac{C_{Y_p}}{C_L} = \frac{A + \cos \Lambda}{A + 4 \cos \Lambda} \frac{3}{A} + \frac{1}{A} \tag{123}$$

The cos Λ can be replaced by

$$\cos \Lambda = \frac{A}{\sqrt{A^2 + 9}}$$

so that equation (123) becomes

$$\frac{C_{Y_p}}{C_L} = \frac{1}{A}\left[1 + 3\,\frac{1 + \sqrt{A^2 + 9}}{4 + \sqrt{A^2 + 9}}\right] \tag{124}$$

Here we have an interesting situation. Equation (122) was derived by Ribner for low aspect ratio triangular wings. Reference (38) used the concepts of reference 39 (Ribner) to modify an equation, which becomes equation (124) for triangular wings. A comparison of results from equations (120), (122), and (124) are shown in figure 45. The point to be made here is that equation (120) of reference 13 approaches the value predicted by reference 39 for triangular wings.

Modification of equation (120) as was done to obtain equation (12) yields results which do not agree with the equation for which it was modeled. The point to be made is that adaption of emperical corrections based on a few data points and a theory which is not applicable to the situation may aid the correlation for a specific family of wings, but can give incorrect results when applied to other families of wings. The equation of this thesis (equation (83)) agrees well with equation (122). At present, there appears to be no theory to accurately predict C_{Y_P} for arbitrary wings.

The wing contribution to the yawing moment due to rolling C_{n_p} is quite important with regard to dynamic lateral stability of an aircraft. Here again very little theoretical work exists for prediction of this derivative for wings. One available reference is reference 13, and the applicable equation is

$$\frac{C_{n_p}}{C_L} = \frac{A + 4}{A + 4\cos\Lambda}\left[1 + 6\left(1 + \frac{\cos\Lambda}{A}\right)\left(\frac{\bar{x}}{c}\frac{\tan\Lambda}{A} + \frac{\tan^2\Lambda}{12}\right)\right]\left(\frac{C_{n_p}}{C_L}\right)_{\Lambda=0} \tag{125}$$

A direct comparison of equations (125) and the corresponding equation of this thesis, equation (103), is not possible because of the differences in terms. However, terms involving sweep angle appear in approximately the same form.

Results of the two theories are compared with some experimental data (from reference 13) in figure 46 for several representative wings.

Both theories show fairly good agreement with the data, with the present theory generally showing the better agreement. It might have been expected that the poor agreement noted for C_{Y_p} would effect the C_{n_p} correlation. This did not occur because the centroid of the C_{Y_p} force apparently falls near the wing moment center.

C. Variation of $\frac{C_{l_r}}{C_L}$ and $\frac{C_{n_p}}{C_L}$ with $\bar{X}^*$, the Displacement Between the Wing Aerodynamic Center and the Origin of the Wing Axis System (or Center of Gravity Position in Flight)

Two of the derivatives for which equations have been derived are dependent on $\bar{X}^*$, and these derivatives are C_{l_r} and C_{n_p}. Both parameters vary linearly with $\bar{X}$ as can be seen from equations (99) and (103). The variation of the derivatives with $\bar{X}^*$ can be found by taking the derivatives with respect to $\bar{X}^*$. The results are as follows

$$\frac{\partial(C_{l_r}/C_L)}{\partial \bar{X}^*} = \left[\frac{\tan \Lambda}{2\sqrt{1 - M^2 \cos^2\Lambda}} - \frac{3}{A}\left(\frac{1 - \Lambda}{1 + \Lambda}\right)\right] \bar{y}^* + \frac{3}{2A(1 + \Lambda)} \qquad (126)$$

$$\frac{\partial(C_{n_p}/C_L)}{\partial \bar{X}^*} = - \frac{1}{2\sqrt{1 - M^2 \cos^2\Lambda}} \bar{y}^* \tan \Lambda \qquad (127)$$

Equation (126) can be rewritten in the following form

$$\frac{\partial(C_{l_T}/C_L)}{\partial \bar{Y}^*} = \frac{1}{2}\left\{\frac{3}{A(1+\lambda)} + \bar{y}^*\left[\frac{\tan\Lambda}{\sqrt{1-M^2\cos^2\Lambda}} - \frac{6}{A}\left(\frac{1-\lambda}{1+\lambda}\right)\right]\right\} - .05 + .05$$

Now note that the first two terms on the right are exactly the negative of equation (95) which is the equation for $\frac{C_{l_\beta}}{C_L}$, hence equation (126) can be written as

$$\frac{\partial(C_{l_T}/C_L)}{\partial \bar{Y}^*} = -\frac{C_{l_\beta}}{C_L} + 0.05 \qquad (128)$$

Another form for equation (99) therefore is

$$\frac{C_{l_T}}{C_L} = \left(\frac{C_{l_T}}{C_L}\right)_{\bar{X}^*=0} - \bar{X}^*\left(\frac{C_{l_\beta}}{C_L} - 0.05\right) \qquad (129)$$

This equation permits evaluation of the derivative C_{l_T} for wings having the aerodynamic center displaced from the moment (or axis) center.

Comparison of equations (127) and (103) shows that equation (127) can be written as

$$\frac{\partial(C_{n_P}/C_L)}{\partial \bar{Y}^*} = -\frac{1}{2}\frac{C_{Y_P}}{C_L} \qquad (130)$$

Another form of equation (103) therefore is

$$\frac{C_{n_p}}{C_L} = \left(\frac{C_{n_p}}{C_L}\right)_{\bar{X}^*=0} - \frac{\bar{X}^*}{2}\frac{C_{Y_p}}{C_L} \tag{131}$$

Equations (129) and (131) can be used with the charts presented herein to obtain the various aerodynamic derivatives for wings having the axis system (or center of gravity in flight) displaced from the wing aerodynamic center.

D. Effects of Compressibility on the Aerodynamic Derivatives

Very little theoretical work has been done in determining compressibility effects on the derivatives investigated in this thesis. The Prandtl-Glauert transformation is applicable for symmetric flow, but there are a number of fundamental questions regarding its application if the flow about the wing is not symmetric. As has been mentioned previously, the Prandtl-Glauert transformation can be applied either as a change in section lift curve slope, or as a change in wing geometry in symmetric flow. In unsymmetric flow, a geometric change in accordance with the Prandtl-Glauert transformation results in a somewhat distorted wing shape - that is, the transformed wing semi-spans are different from each other. This basic problem of application can be ignored, as was done in reference 15, by assuming that each wing semi-span is one half of a wing in symmetric flow. The compressibility corrections are then applied to each wing semi-span and the loads of each semi-span are used to obtain the wing characteristics. This

process is illustrated graphically as follows. Assume a swept wing at a sideslip angle β as shown by I.

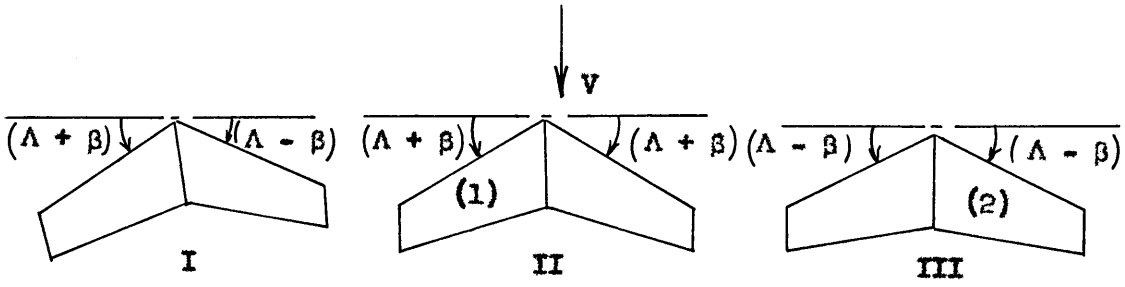

Replace the original wing by two wings (II and III), one having a sweep angle ($\Lambda' = \Lambda + \beta$) and the other a sweep angle ($\Lambda' = \Lambda - \beta$). Apply the Prandtl-Glauert corrections to wings II and III, which are in symmetric flow. Compute the loads on wing panels (1) and (2) of wings II and III respectively. Use these loads to compute the aerodynamic characteristics of wing I at sideslip angle β.

A somewhat simpler approach was used in reference 40. Here the author simply chose to modify the section lift curve slope as if the actual wing were in symmetric flow. The section lift curve slope is increased as indicated by the equation of page

As stated previously there has been very little work done on the effects of compressibility on the aerodynamic derivatives derived herein. The available references are those quoted above, i.e., reference 15 which applies only to C_{l_β}, and reference 40 which attempts to predict compressibility effects on all the common wing derivatives.

1. Sideslipping wing.- The effects of Mach number on the derivative $\frac{C_l}{C_L}$ are shown in figure 47 for a representative wing. The experimental results are from reference 15. The prediction of references 15, 40, and the present theory are shown. Reference 15 and the present thesis correctly predict the effect of Mach number. Reference 40 does not predict proper trends.

2. Yawing wing.- Reference 40 and equation (99) of this thesis both predict an increase in $\frac{C_{l_r}}{C_L}$ with Mach number for a specific wing. Results of the two theories are compared in figure 48 for several untapered wings. Both methods predict about the same effect of Mach number on the derivative.

There is no experimental data available for comparison with the theories with regard to compressibility effects. The reason for the lack of such data is that experimental techniques for obtaining derivatives for yawing wings, mentioned in a previous section are not useable at high speeds. The two techniques which were suited for low speed tests have rather severe restrictions on them. The curved flow technique requires curving the tunnel walls and addition of drag screens to obtain the proper velocity distribution in the tunnel. The screens limit the speeds available in the tunnel, and in the case of the Stability Tunnel (which is the only known facility of its type), the Mach number available was less than 0.2 with curved-flow screens installed. The speeds available for the pure-yawing-oscillation mechanism were not limited in this manner, but were restricted by

the available rotational speed of the oscillation mechanism and a fundamental relationship between wind velocity and model oscillation frequency (see reference 37).

3. Rolling wing.- There is little that can be said with regard to the effects of compressibility on the parameters $\frac{C_{Y_p}}{C_L}$ and $\frac{C_{n_p}}{C_L}$. The present theory predicts an increase of these parameters with increase in Mach number whereas the theory of reference (40) predicts a decrease with increase in Mach number. The author could find no data to substantiate either theory. The experimental techniques for measuring these parameters are by

(a) Rotating the flow past a stationary model as done in the Stability Tunnel (see reference 41)

(b) Rotating the model in a steady, rectilinear flow

(c) Oscillation techniques.

Methods (a) and (b) have been used at low speeds, however the Stability Tunnel is speed limited to Mach numbers below about 0.2 when used with the rolling-flow apparatus. The mechanism required inside a tunnel to use method (b) can result in severe interference effects if not properly designed, and does not appear to have been used at speeds sufficiently high to obtain Mach number effects. Method (c) is quite complex if one attempts to extract individual derivatives rather than combination derivatives (see references 42 and 43). Although the method is valid in theory and should be applicable at high speeds, there appears to be insufficient published data from this technique for use here. Also note that the mechanism used in this technique requires a body for proper shielding of strain gage balance and drive mechanism, so that isolated wing characteristics would probably be unobtainable.

E. Span Load Distributions

The present theory permitted the derivation of equations for the additional span loading due to sideslip and due to yawing. There appear to be no other methods available in the literature to obtain these loadings for plane wings. The additional load due to sideslip was investigated by the author for wings in incompressible flow in reference 23. Experimental determinations of span loadings for sideslipping and for yawing wings also appear to be nonexistant except for the sideslip data given in reference 44. The reason for lack of span load data in general is the very tedious work in measuring span load distributions by use of pressure orifices and the fact that the integrated effects are generally desired and obtainable from force tests.

The span load in sideslip obtained from reference 44 is compared with the present theory in figure 49. The agreement is quite good.

There is no available data for comparing the span loads in yawing flow.

F. Variation of the Various Aerodynamic Derivatives With Sweep Angle and Mach Number

The discussion thus far has been concerned primarily with comparing results of the theory developed herein with results from other theories and with experimental data. It is of interest to examine some of the results of the theory itself to determine the effects of the various geometric parameters and Mach number on the derivatives. These effects could be noted by examination of the design charts (figs. 18 through 37), however, these effects can be shown more clearly by plotting the derivatives as functions of various parameters. The factors having the largest effects on the derivatives developed in this thesis are aspect ratio, sweep angle, and Mach number. Figures 18 through 37 show curves of the derivatives plotted against aspect ratio. In this section a few figures are presented showing typical curves of the derivatives plotted against sweep angle and Mach number. The figures are presented, but will not be discussed since the trends shown are self-evident. The curves in the figures are as follows:

	Figure
Variation of $\frac{C_{l_\beta}}{C_L}$ with sweep angle	50
Variation of $\frac{C_{l_\beta}}{C_L}$ with Mach number	51
Variation of $\frac{C_{l_r}}{C_L}$ with sweep angle	52
Variation of $\frac{C_{l_r}}{C_L}$ with Mach number	53

XI. CONCLUDING REMARKS

A theory and method have been developed, and design charts drawn, for the estimation of certain stability derivatives for wings of arbitrary plan form in subsonic flow. The derivatives obtained are those which are linearly dependent on the wing lift coefficient, and are C_{l_β}, C_{l_r}, C_{Y_p}, and C_{n_p}. The method is generally applicable to wings of any plan form provided the angle-of-attack load distribution is known. Such information is available in the literature for a great variety of wing planforms, hence the requirement for this information should not be a serious limitation on the method. Further, for wings of odd planform, the angle-of-attack load distribution can be determined by straightforward methods, after which the present method is applicable for determining the above-mentioned derivatives.

The theory developed herein is based on a vortex representation of the wing. The vortex strength distribution in sideslip and yawing is justified as being the same as for the wing at angle of attack, and zero sideslip and yawing velocity. The velocity components associated with sideslip and yawing are then used with the vortex system to obtain the desired derivatives. A similar method is used for the rolling wing, however, in this case the circulation strength must be altered because rolling velocity causes an incremental change in angle of attack across the wing span.

The derivatives estimated by the methods developed in this thesis are compared with results from other theories (where available) and

also with experimental data. In general, the various theories are in agreement with regard to trends, at least for wings in incompressible flow. The present method generally appears to provide better correlation with data than other theories. The derivative which does not show very good correlation with experiment is C_{Y_p}, but fortunately this derivative is not particularly important with regard to the dynamic stability of aircraft.

Compressibility effects were also included in the method. Comparisons with data for the derivative $\frac{C_{l_\beta}}{C_L}$ show that the method predicts the proper trends with regard to Mach Number effects. There were no data available for verification of the theory with regard to the other derivatives.

Equations have been derived for the additional span loading associated with sideslip and yawing. There appear to be no other theories available in the literature for comparison with the present theory, and the available span load data appear to be limited to one source for loads in sideslip. In this case the present theory showed very good agreement with experiment.

In general, the methods developed herein agree well with experimental results. The method is, however, subject to certain limitation by the nature of the assumptions made in the development, as follows:

(1) It will probably decrease in validity as wing thickness-to-chord ratio increases.

(2) It should not be used at Mach numbers for which the Mach number component normal to the wing quarter-chord-line approaches 1.0.

(3) It should be used with caution if the wing tips have much rounding (planform), since the methods were developed for straight wing tips.

XII. SUMMARY

A theory and method have been developed, and design charts drawn, for the estimation of certain stability derivatives for wings of arbitrary plan form in subsonic flow. The derivatives obtained are those which are linearly dependent on the wing lift coefficient, and are C_{l_β}, C_{l_r}, C_{Y_p}, and C_{n_p}. The method is generally applicable to wings of any plan form provided the angle-of-attack load distribution is known. Such information is available in the literature for a great variety of wing planforms, hence the requirement for this information should not be a serious limitation on the method. Further, for wings of odd planform, the angle-of-attack load distribution can be determined by straightforward methods, after which the present method is applicable for determining the above-mentioned derivatives.

The theory developed herein is based on a vortex representation of the wing. The vortex strength distribution in sideslip and yawing is justified as being the same as for the wing at angle of attack, and zero sideslip and yawing velocity. The velocity components associated with sideslip and yawing are then used with the vortex system to obtain the desired derivatives. A similar method is used for the rolling wing, however, in this case the circulation strength must be altered because rolling velocity causes an incremental change in angle of attack across the wing span.

The derivatives estimated by the methods developed in this thesis are compared with results from other theories (where available) and

also with experimental data. In general, the various theories are in agreement with regard to trends, at least for wings in incompressible flow. The present method generally appears to provide better correlation with data than other theories. The derivative which does not show very good correlation with experiment is C_{Y_p}, but fortunately this derivative is not particularly important with regard to the dynamic stability of aircraft.

Compressibility effects were also included in the method. Comparisons with data for the derivative $\frac{C_{l_\beta}}{C_L}$ show that the method predicts the proper trends with regard to Mach number. There were no data available for verification of the theory with regard to the other derivatives.

Equations have been derived for the additional span loading associated with sideslip and yawing. There appear to be no other theories available in the literature for comparison with the present theory, and the available span load data appear to be limited to one source for loads in sideslip. In this case the present theory showed very good agreement with experiment.

XIII. ACKNOWLEDGEMENTS

The author wishes to express appreciation to the National Aeronautics and Space Administration for permission to use this material as a doctoral dissertation. The author is indebted to

for the stimulating discussions which led to the concepts of the vortex systems used in the theory, and to

for checking the many mathematical steps involved in developing the theory.

REFERENCES

1. Jones, A. L., and Alksne, A.: A Summary of Lateral Stability Derivatives Calculated for Wing Planforms in Supersonic Flow. NACA Rep. 1052, 1951.

2. Margolis, K.: Theoretical Lift and Damping-in-Roll of Thin Sweptback Tapered Wings with Raked-In and Cross-Stream Wing Tips at Supersonic Speeds. Subsonic Leading Edges. NACA TN 2048, 1950.

3. Harmon, S. M.: Stability Derivatives at Supersonic Speeds of Thin Rectangular Wings With Diagonals Ahead of the Tip Mach Lines. NACA Rep. 925, 1949.

4. Margolis, K., et al.: Theoretical Calculation of the Pressure Distribution, Span Loading, and Rolling Moment Due to Sideslip at Supersonic Speeds for Thin Sweptback Tapered Wings With Supersonic Trailing Edges and Wing Tips Parallel to the Axis of Wing Symmetry. NACA TN 2698, 1953.

5. Pearson, Henry A., and Jones, Robert T.: Theoretical Stability and Control Characteristics of Wings With Various Amounts of Taper and Twist. NACA Rep. 635, 1938.

6. Weissinger, J.: Der schiebende Tragflügel bei gesunder Strömung. Bericht S 2 der Lilienthal-Gesellschaft für Luftfahrtforschung, 1938-1939, pp. 13-31.

7. Jones, Robert T.: Properties of Low Aspect Ratio Pointed Wings at Speeds Below and Above the Speed of Sound. NACA Rep. 835, 1946.

8. De Young, John, and Harper, Charles W.: Theoretical Symmetric Span Loading at Subsonic Speeds for Wings Having Arbitrary Plan Form. NACA Rep. 921, 1948.

9. De Young, John: Theoretical Antisymmetric Span Loading for Wings of Arbitrary Plan Form at Subsonic Speeds. NACA TN 2140, 1950.

10. Falkner, V. M.: The Calculation of Aerodynamic Loading on Surfaces of Any Shape. R. and M. no. 1910, British A.R.C., 1943.

11. Mutterperl, William: The Calculation of Span Load Distributions on Swept-Back Wings. NACA TN 834, 1941.

12. Weissinger, J.: The Lift Distribution of Swept-Back Wings. NACA TM no. 1126, 1947.

13. Toll, Thomas A., and Queijo, M. J.: Approximate Relations and Charts for Low-Speed Stability Derivatives of Swept Wings. NACA TN 1581, 1948.

14. Queijo, M. J., and Jaquet, B[illegible]n M.: Calculated Effects of Geometric Dihedral on the Low-Speed Rolling Derivatives of Swept Wings. NACA TN 1732, 1948.

15. Polhamus, Edward C., and Sleeman, William C., Jr.: The Rolling Moment Due to Sideslip of Swept Wings at Subsonic and Transonic Speeds. NASA TN D-209, 1960.

16. Anon: Data Sheets. Aerodynamics Vols. I, II, III, Royal Aeronautical Society.

17. Campbell, John P., and Goodman, Alex: A Semiemperical Method for Estimating the Rolling Moment Due to Yawing of Airplanes. NACA TN 1984, 1949.

18. Anon: Dynamics of the Airframe. CalAer Report AE-61-4, Vol. II.

19. Thomas, H. H. B. M.: State of the Art of Estimation of Derivatives. AGARD Report 339, 1961.

20. Van Dorn, Nicholas, and De Young, John: A Comparison of Three Theoretical Methods of Calculating Span Load Distributions on Swept Wings. NACA TN 1476, 1947.

21. Bird, John D.: Some Theoretical Low-Speed Span Loading Characteristics of Swept Wings in Roll and Sideslip. NACA Rep. 969, 1950.

22. Jaquet, Byron M.: Effect of Linear Spanwise Variation of Twist and Circular-Arc Camber on Low-Speed Static Stability, Rolling, and Yawing Characteristics of a 45° Sweptback Wing of Aspect Ratio 4 and Taper Ratio 0.6. NACA TN 2775, 1952.

23. Queijo, M. J.: Theoretical Span Load Distributions and Rolling Moments for Sideslipping Wings of Arbitrary Plan Form in Incompressible Flow. NACA Rep. 1269, 1956.

24. Blenk, Herman: The Monoplane As a Lifting Vortex Surface. NACA TM 1111, 1947.

25. Millikan, Clark B.: Aerodynamics of the Aeroplane. John Wiley and Sons, Inc., New York, 1941.

26. Campbell, George S.: A Finite-Step Method for the Calculation of Span Loadings of Unusual Plan Forms. NACA RM L50L13, 1951.

27. Gray, W. L., and Schenk, K. M.: A Method for Calculating the Subsonic Steady-State Loading on an Airplane With a Wing of Arbitrary Plan Form and Stiffness. NACA TN 3030, 1953.

28. Diederich, Franklin W., and Zlotnick, Martin: Calculated Spanwise Lift Distributions and Aerodynamic Influence Coefficients for Unswept Wings in Subsonic Flow. NACA TN 3014, 1953.

29. Diederich, Franklin W., and Letham, W. Owen: Calculated Aerodynamic Loadings of M, W, and A Wings in Incompressible Flow. NACA RM L51E29, 1951.

30. Goodman, Alex, and Brewer, Jack D.: Investigation at Low Speeds of the Effect of Aspect Ratio and Sweep on Static and Yawing Stability Derivatives of Untapered Wings. NACA TN 1809, 1949.

31. Letko, William, and Cowan, John W.: Effect of Taper Ratio on Low-Speed Static and Yawing Stability Derivatives of 45° Sweptback Wings With Aspect Ratio of 2.01. NACA TN 1871, 1949.

32. Jaquet, Byron M., and Brewer, Jack D.: Low-Speed Static Stability and Rolling Characteristics of Low-Aspect-Ratio Wings of Triangular and Modified Triangular Plan Forms. NACA RM L8L29, 1949.

33. Goodman, Alex, and Thomas, David F., Jr.: Effects of Wing Position and Fuselage Size on the Low Speed Static and Rolling Stability Characteristics of a Delta-Wing Model. NACA Rep. 1224, 1955.

34. Falkner, V. M.: The Calculation of l_r and l_p by Lifting Plane Theory. ARC 11,607 and 12,671 (unpublished), 1949.

35. Bryant, L. W., and Garner, H. C.: Note on Rotary Derivatives Due To Yawing of a Wing. ARC 12,672 (unpublished), 1949.

36. Fisher, Louis R.: Experimental Determination of Effects of Frequency and Amplitude on the Lateral Stability Derivatives for a Delta, a Swept, and an Unswept Wing Oscillating in Yaw. NACA TR 1357, 1958.

37. Queijo, M. J., Fletcher, H. S., Marple, C. G., and Hughes, F. M.: Preliminary Measurements of the Aerodynamic Yawing Derivatives of a Triangular, a Swept, and an Unswept Wing Performing Pure Yawing Oscillations, With a Description of the Instrumentation Employed. NACA RM L9514, 1950.

38. Goodman, Alex, and Fisher, Lewis R.: Investigation at Low Speeds of the Effects of Aspect Ratio and Sweep on Rolling Stability Derivatives of Untapered Wings. NACA Rep. 968, 1950.

39. Ribner, Herbert S.: The Stability Derivatives of Low-Aspect-Ratio Triangular Wings at Subsonic and Supersonic Speeds. NACA TN 1423, 1947.

40. Fisher, Lewis R.: Approximate Corrections for the Effects of Compressibility on the Subsonic Stability Derivatives of Swept Wings. NACA TN 1854, 1949.

41. MacLachlan, Robert, and Letko, William: Correlation of Two Experimental Methods of Determining the Rolling Characteristics of Unswept Wings. NACA TN 1309, 1947.

42. Lessing, Henry C., Freyer, Thomas B., and Reed, Marvill H.: A System for Measuring Dynamic Lateral Stability Derivatives in High-Speed Wind Tunnels. NACA TN 3348, 1954.

43. Beam, Benjamin H.: A Wind-Tunnel Test Technique for Measuring the Dynamic Rotary Stability Derivatives Including the Cross Derivatives at High Mach Numbers. NACA TN 3347, 1955.

44. Jacobs, W.: Systematische Druckverteilungsmessungen an Pfeilflügen Konstanter Tiefe bei symmetrischer und unsymmetrischer Anströmung. Bericht 44/28 Aerodynamisches Institut der T. H. Braunschweig. Nov. 8, 1944.

The two page vita has been removed from the scanned document. Page 1 of 2

The two page vita has been removed from the scanned document. Page 2 of 2

TABLE I. SUMMARY OF GENERAL EQUATIONS FOR AERODYNAMIC DERIVATIVES

Sideslipping wing:

$$\frac{C_{l_\beta}}{C_L} = -\frac{1}{2}\int_0^1 \left[\left(\frac{cc_l}{\bar{c}C_L}\right)_0 \frac{\tan \Lambda}{\sqrt{1 - M^2 \cos^2 \Lambda}} - \frac{3}{4} \frac{d\left(\frac{cc_l}{\bar{c}C_L}\right)_0}{dy^*} \right] y^* dy^* + 0.05$$

Yawing wing:

$$\frac{C_{l_r}}{C_L} = \frac{1}{2}\int_0^1 \left\{ \left[y^* - (x^*)_{\frac{c}{4}} \tan \Lambda \right] \left(\frac{1}{\sqrt{1 - M^2 \cos^2 \Lambda}} \right) \left(\frac{cc_l}{\bar{c}C_L}\right)_0 + \frac{1}{2}\left[(x^*)^2_{\frac{c}{4}} - (x^*)^2_c \right] \frac{d\left(\frac{cc_l}{\bar{c}C_L}\right)_0}{dy^*} \right\} y^* dy^*$$

Rolling wing:

$$\frac{C_{Y_p}}{C_L} = \int_0^1 \left(\frac{cc_l}{\bar{c}C_L}\right)_0 \frac{\tan \Lambda}{\sqrt{1 - M^2 \cos^2 \Lambda}} \, y^* dy^*$$

$$\frac{C_{n_p}}{C_L} = \frac{1}{2}\int_0^1 \left(\frac{cc_l}{\bar{c}C_L}\right)_0 \left[(x^*)_{\frac{c}{4}} \tan \Lambda - y^* \right] \frac{y^*}{\sqrt{1 - M^2 \cos^2 \Lambda}} \, dy^*$$

TABLE II. SUMMARY OF EQUATIONS FOR AERODYNAMIC DERIVATIVES OF SWEPT WINGS

Sideslipping wing:

$$\frac{C_{l_\beta}}{C_L} = -\frac{1}{2}\left\{\frac{3}{A(1+\lambda)} + \bar{y}^*\left[\frac{\tan\Lambda}{\sqrt{1 - M^2\cos^2\Lambda}} - \frac{6}{A}\left(\frac{1-\lambda}{1+\lambda}\right)\right]\right\} + 0.05$$

Yawing wing:

$$\frac{C_{l_r}}{C_L} = \left[\frac{1}{2}\left(\frac{1+\tan^2\Lambda}{\sqrt{1 - M^2\cos^2\Lambda}}\right) - \frac{9}{2A}\left(\frac{1-\lambda}{1+\lambda}\right)\tan\Lambda + \frac{27}{4A^2}\left(\frac{1-\lambda}{1+\lambda}\right)^2\right](\tilde{y}^*)^2$$

$$+\left[\frac{3}{A}\left(\frac{1-\lambda}{1+\lambda}\right)\tan\Lambda - \frac{\tan^2\Lambda}{2\sqrt{1 - M^2\cos^2\Lambda}}\right](\bar{y}^*)^2 + \left[\frac{3\tan\Lambda}{2A(1+\lambda)} - \frac{9(1-\lambda)}{A^2(1+\lambda)^2}\right]\bar{y}^*$$

$$+\left[\frac{\tan\Lambda}{2\sqrt{1 - M^2\cos^2\Lambda}} - \frac{3}{A}\left(\frac{1-\lambda}{1+\lambda}\right)\right]\bar{x}^*\bar{y}^* + \frac{3\bar{x}^*}{2A(1+\lambda)} + \frac{9}{4A^2(1+\lambda)^2}$$

Rolling wing:

$$\frac{C_{Y_p}}{C_L} = \frac{\bar{y}^*\tan\Lambda}{\sqrt{1 - M^2\cos^2\Lambda}}$$

$$\frac{C_{n_p}}{C_L} = -\frac{1}{2\sqrt{1 - M^2\cos^2\Lambda}}\left\{(\tilde{y}^*)^2 + \left[(\tilde{y}^*)^2 - (\bar{y}^*)^2\right]\tan^2\Lambda + \bar{x}^*\bar{y}^*\tan\Lambda\right\}$$

TABLE III. SUMMARY OF GENERAL EQUATIONS FOR ADDITIONAL LOCAL SPAN LOADING

Sideslipping wing:

$$\frac{\left(\frac{cc_l}{\bar{c}C_L}\right)_\beta}{\beta} = \left(\frac{cc_l}{\bar{c}C_L}\right)_0 \frac{\tan \Lambda}{\sqrt{1 - M^2 \cos^2 \Lambda}} - \frac{3}{4} c^* \frac{d\left(\frac{cc_l}{\bar{c}C_L}\right)_0}{dy^*}$$

Yawing wing:

$$\frac{\left(\frac{cc_l}{\bar{c}C_L}\right)_r}{\frac{rb}{2V}} = - \left[y^* - (x^*)_{\frac{c}{4}} \tan \Lambda \right] \frac{\left(\frac{cc_l}{\bar{c}C_L}\right)_0}{\sqrt{1 - M^2 \cos^2 \Lambda}} - \frac{1}{2} \left[(x^*)^2_{\frac{c}{4}} - (x^*)^2_c \right] \frac{d\left(\frac{cc_l}{\bar{c}C_L}\right)_0}{dy^*}$$

TABLE IV. SUMMARY OF EQUATIONS FOR ADDITIONAL LOCAL SPAN LOADING FOR SWEPT WINGS

Sideslipping wing:

$$\frac{\left(\frac{cc_l}{\bar{c}C_L}\right)_\beta}{\beta} = \left(\frac{cc_l}{\bar{c}C_L}\right)_0 \frac{\tan \Lambda}{\sqrt{1 - M^2 \cos^2 \Lambda}} - \frac{3}{A(1 + \lambda)} \left[1 - (1 - \lambda)\, \bar{y}^*\right] \frac{d\left(\frac{cc_l}{\bar{c}C_L}\right)_0}{dy^*}$$

Yawing wing:

$$\frac{\left(\frac{cc_l}{\bar{c}C_L}\right)_r}{\frac{rb}{2V_0}} = -\left\{y^* - \left[(\bar{y}^* - y^*) \tan \Lambda - \bar{x}^*\right] \tan \Lambda\right\} \frac{\left(\frac{cc_l}{\bar{c}C_L}\right)_0}{\sqrt{1 - M^2 \cos^2 \Lambda}}$$

$$- \frac{2}{A(1 + \lambda)} \left[1 - (1 - \lambda)\, y^*\right] \left\{\frac{3}{2} (\bar{y}^* - y^*) \tan \Lambda - \frac{3}{2} \bar{x}^* - \frac{9}{4A(1 + \lambda)} \left[1 - (1 - \lambda)\, y^*\right]\right\} \left\{\frac{d\left(\frac{cc_l}{\bar{c}C_L}\right)}{dy^*}\right\}$$

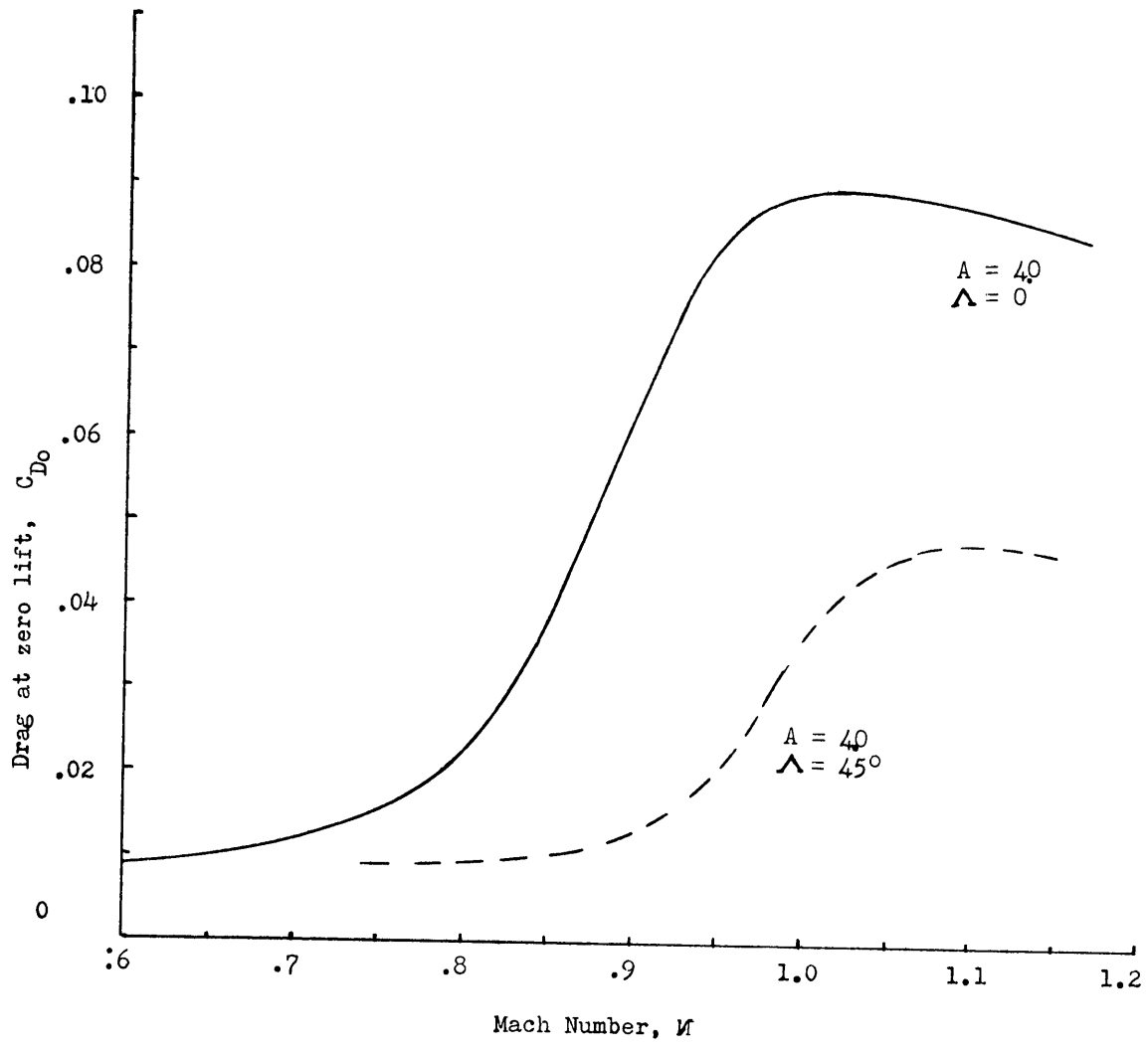

Figure 1.- Illustration of the transonic drag rise. Data taken from NACA TN 3469.

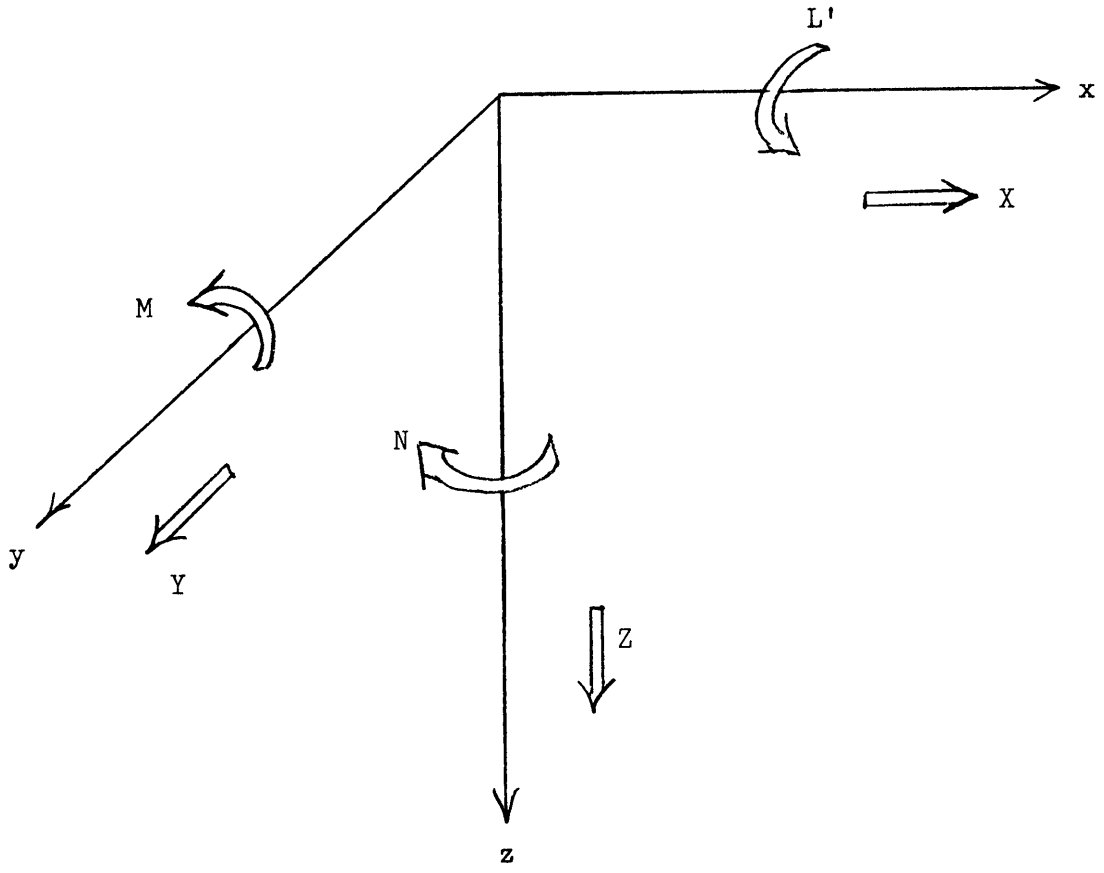

Figure 2.- Force and moment nomenclature and convention. Arrows indicate positive directions of forces, moments, and displacements.

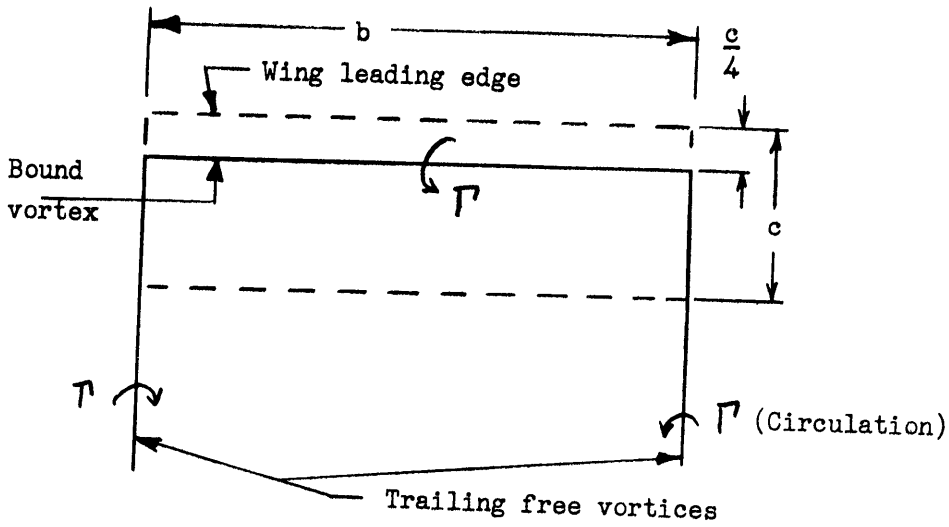

(a) Vortex pattern.

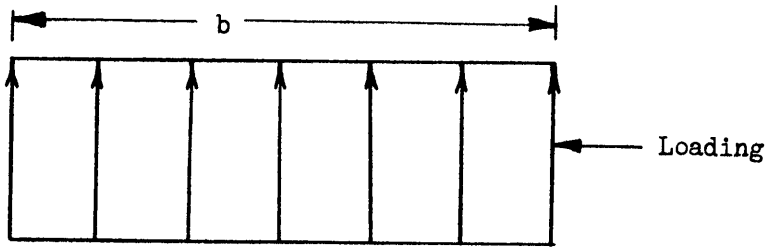

(b) Span-load distribution.

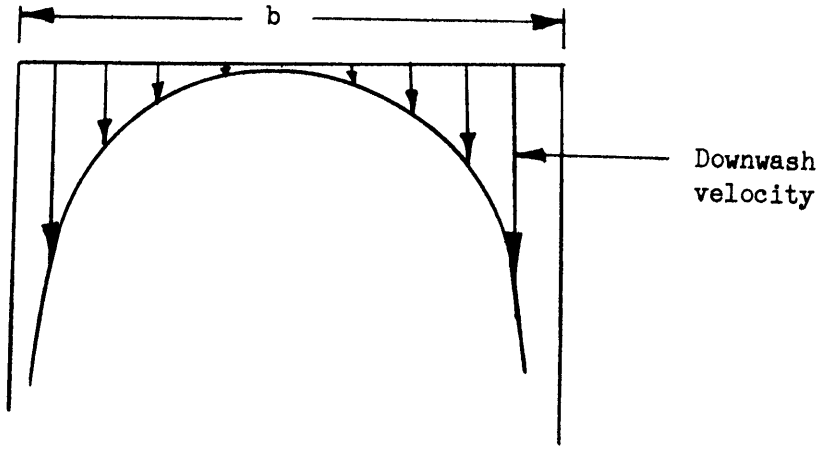

(c) Downwash distribution.

Figure 3.- Pertinent characteristics of a single horseshoe vortex.

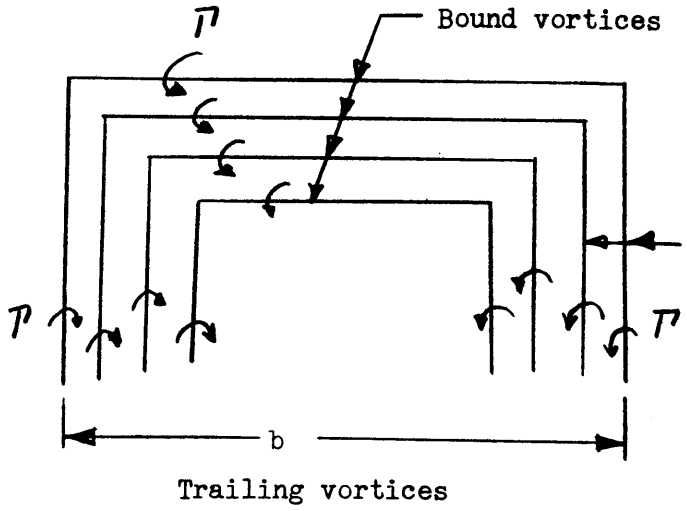

(a) Vortex distribution. Bound vortices should be coincident.

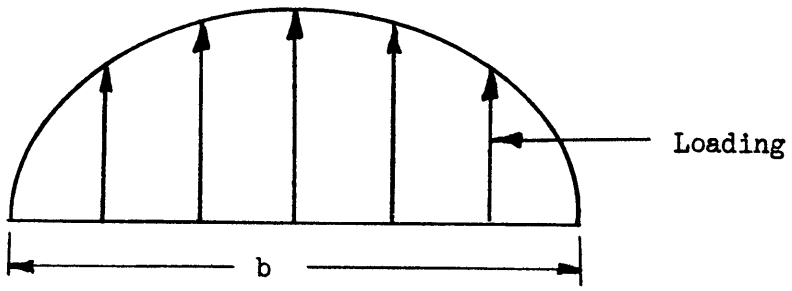

(b) Span load distribution.

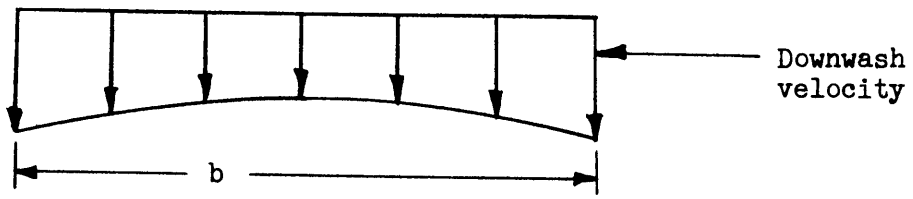

(c) Approximate downwash pattern.

Figure 4.- Pertinent characteristics of the vortex system used in the Prandtl lifting-line theory.

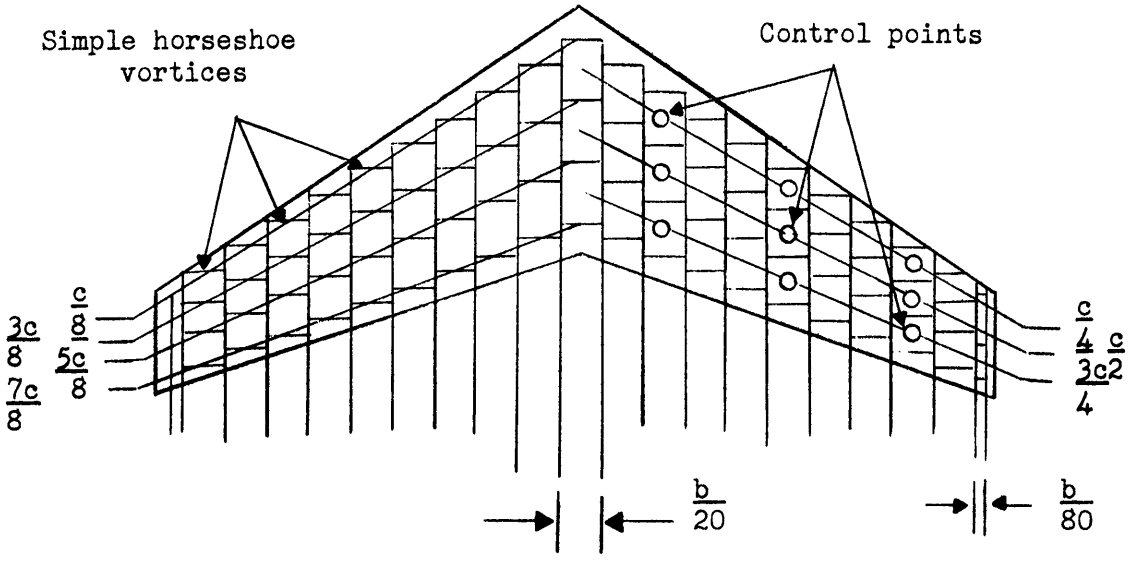

Figure 5.- Vortex distribution and control points used in Falkner method of determining span loads.

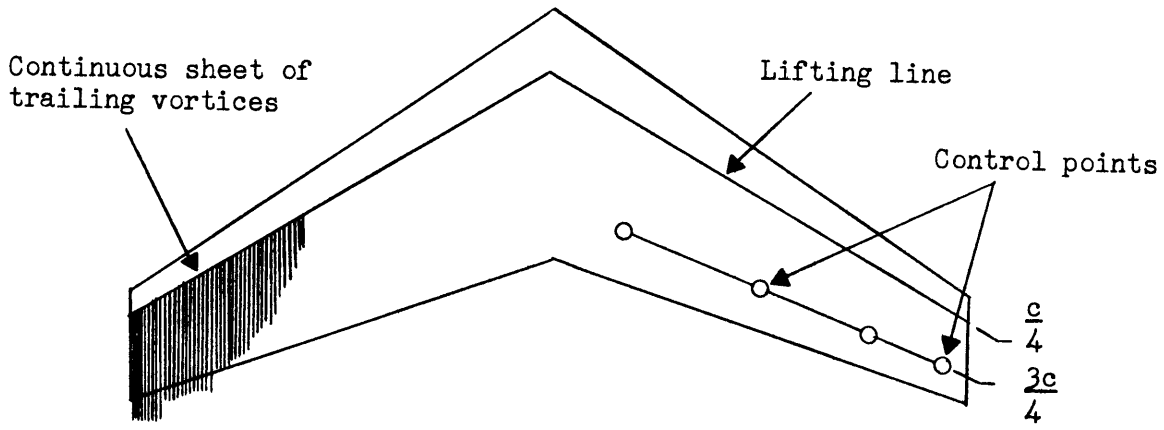

Figure 6.- Vortex distribution and control points used in Mutterperl method of determining span loads.

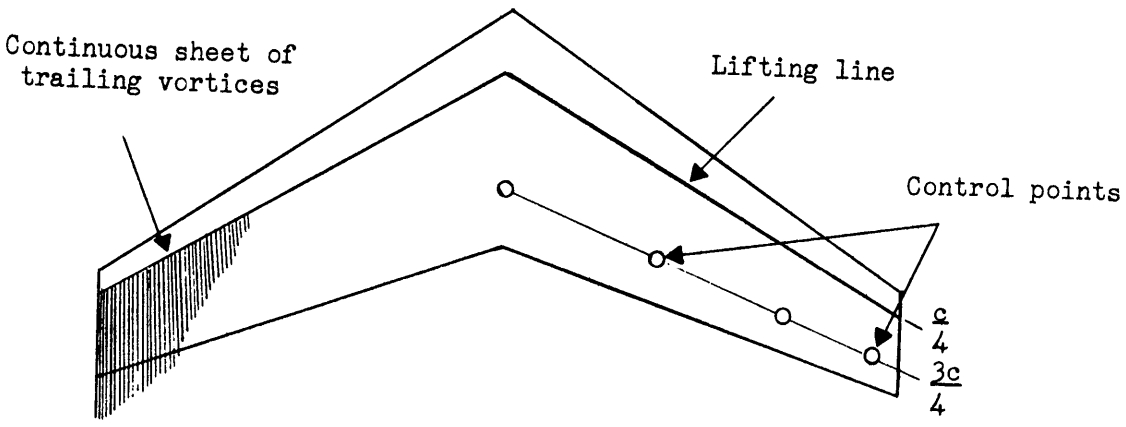

Figure 7.- Vortex distribution and control points used in Weissinger method of determining span loads.

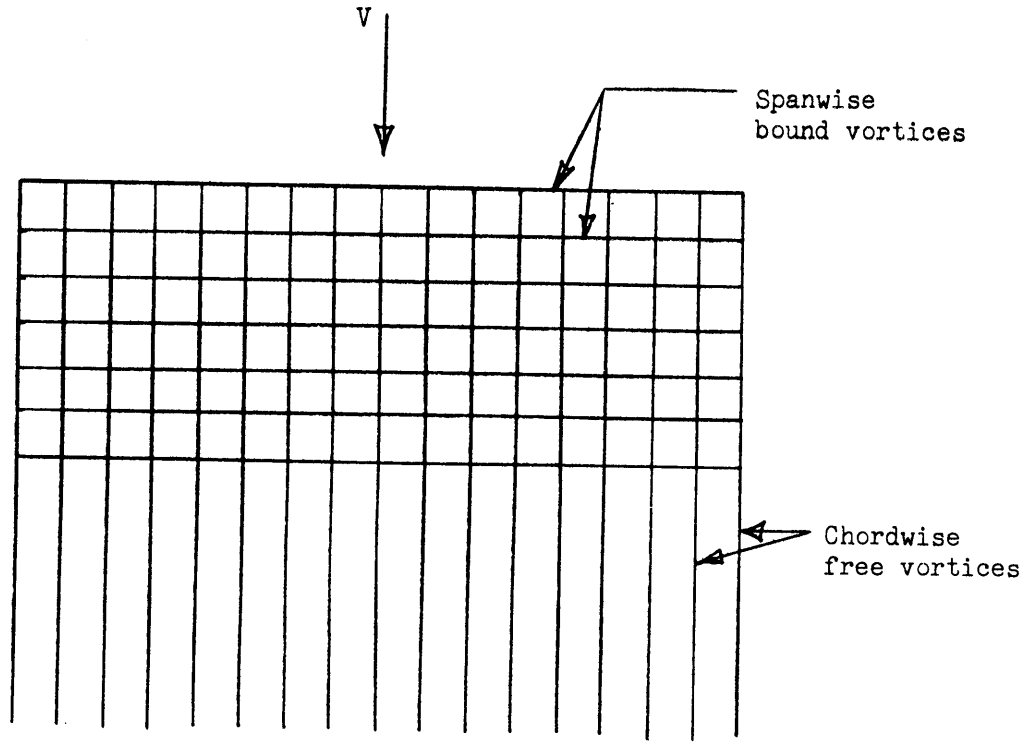

(a) General arrangement for zero sideslip.

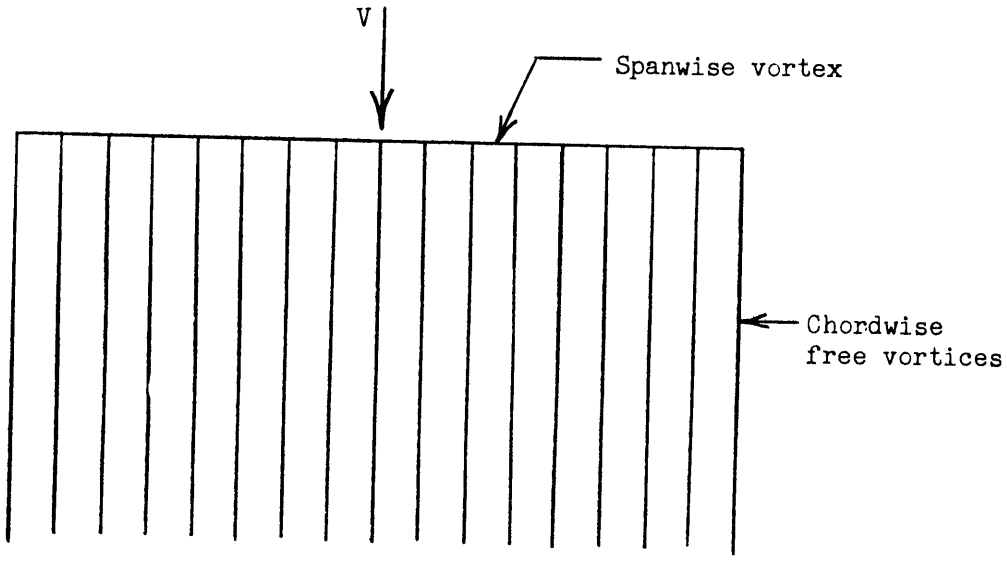

(b) Lifting-line theory arrangement for zero sideslip.

Figure 8.- Vortex systems used for representing unswept wings.

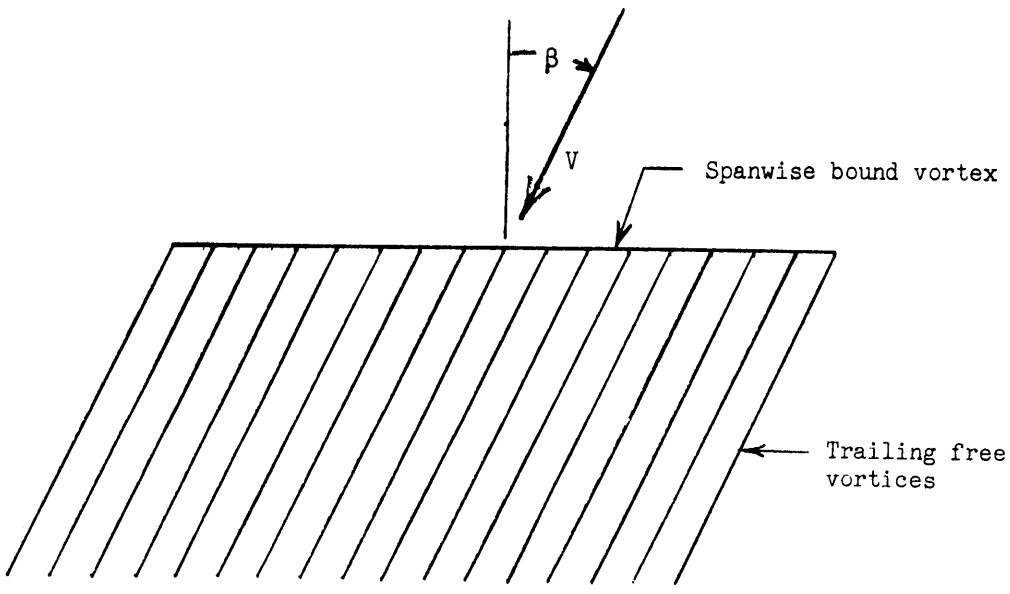

(c) Blenk's arrangement (ref. 24) for sideslip.

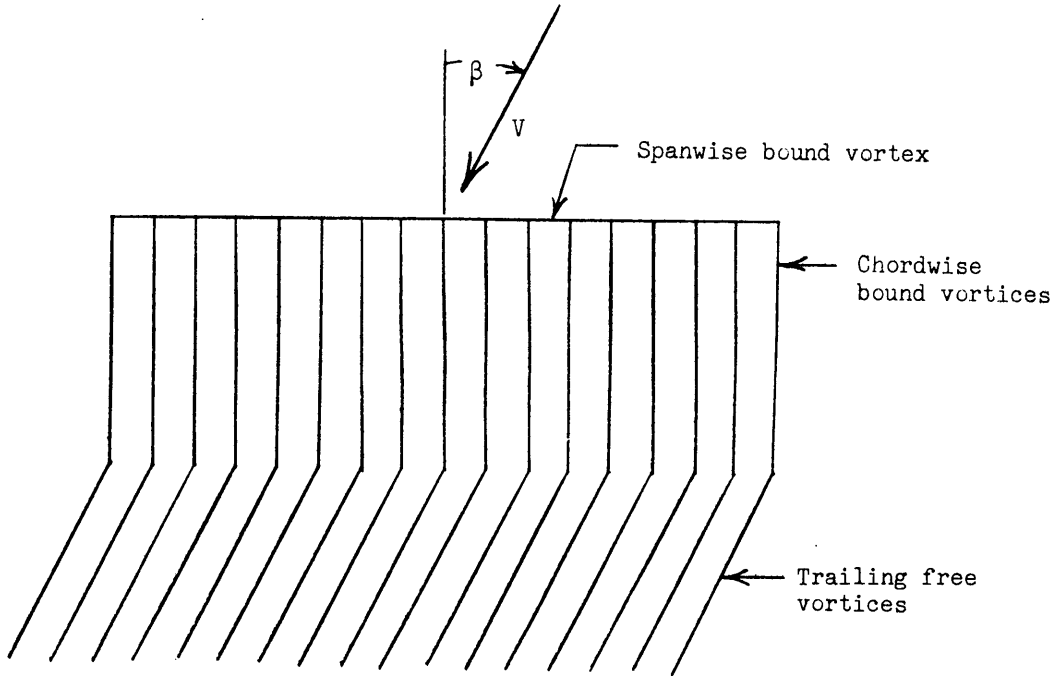

(d) Weissinger's arrangement (ref. 6) for sideslip.

Figure 8.- Concluded.

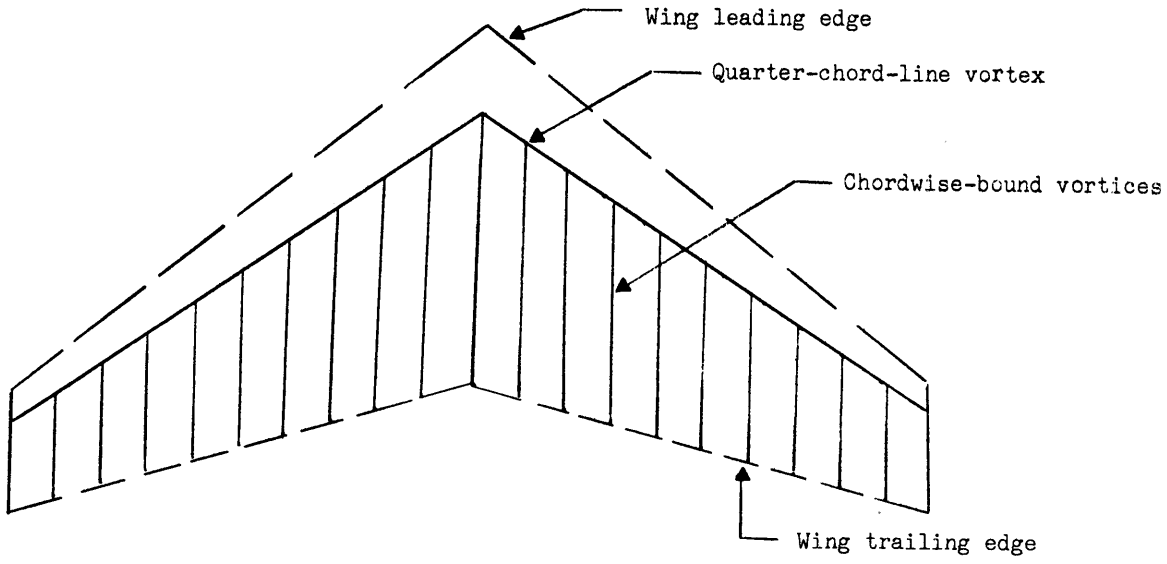

Figure 9.- Bound vortex system used to represent a wing in all types of flow.

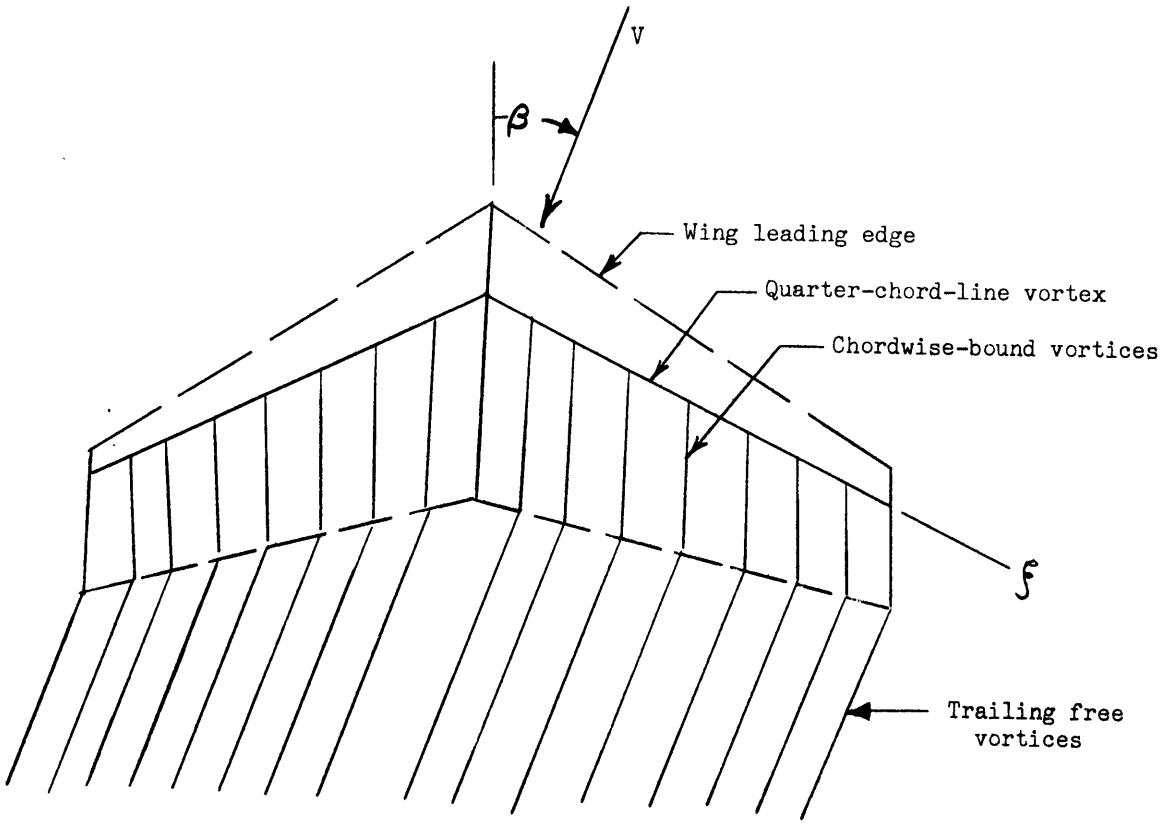

Figure 10.- Complete vortex system for a wing in sideslip.

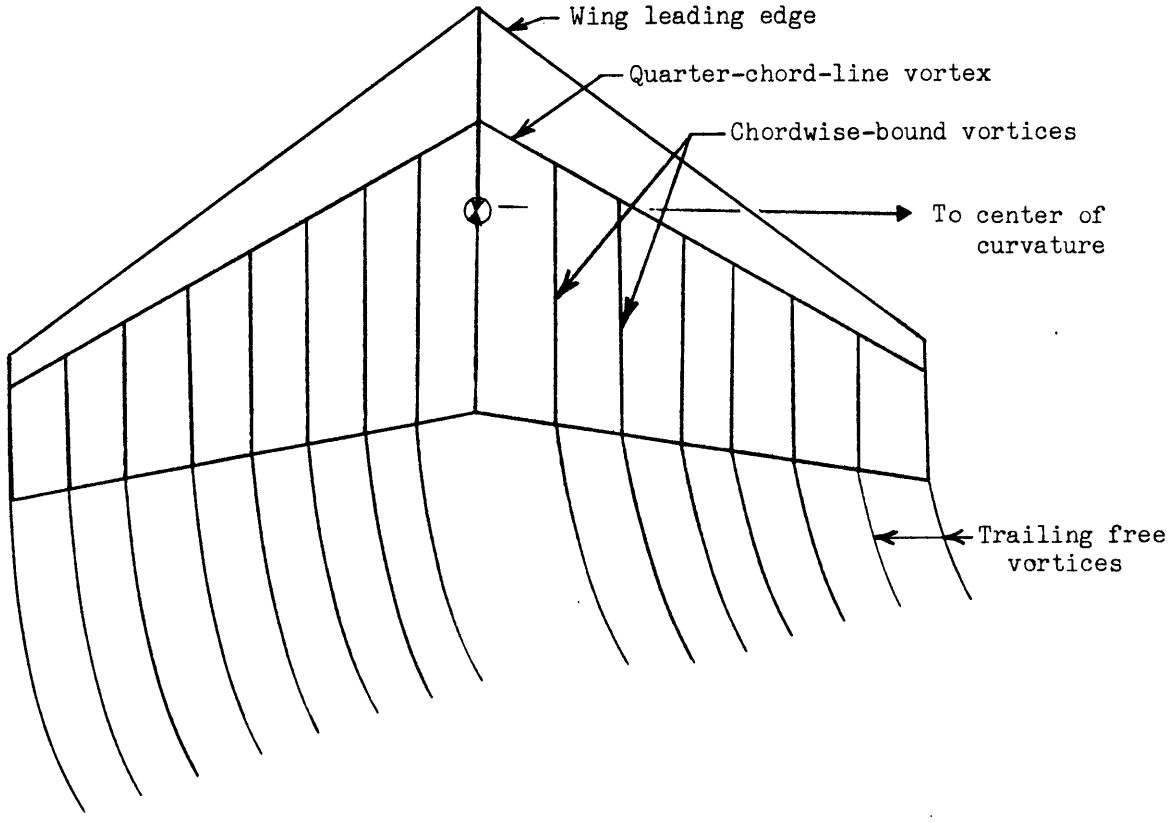

Figure 11.- Complete vortex system for the yawing wing.

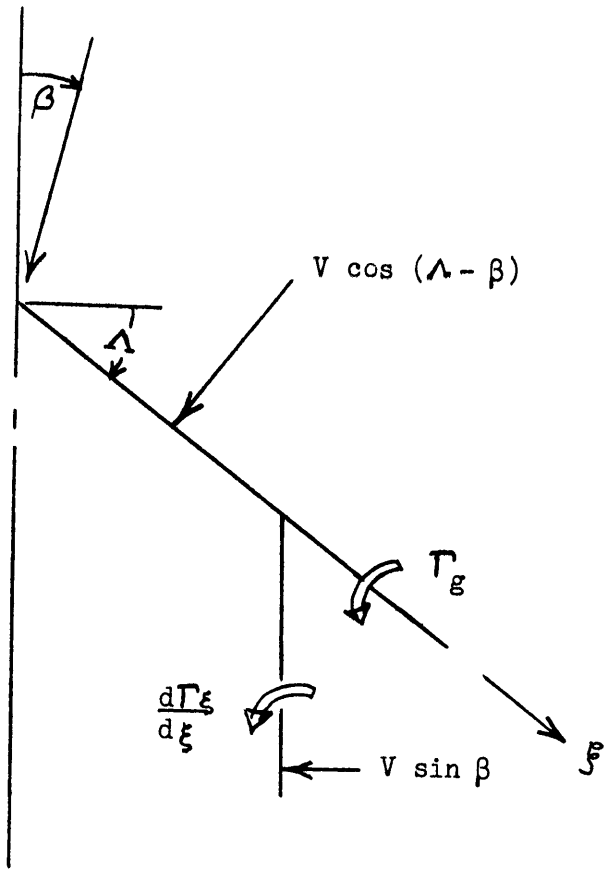

Figure 12.- Details of bound vortices and velocity components for wing in sideslip.

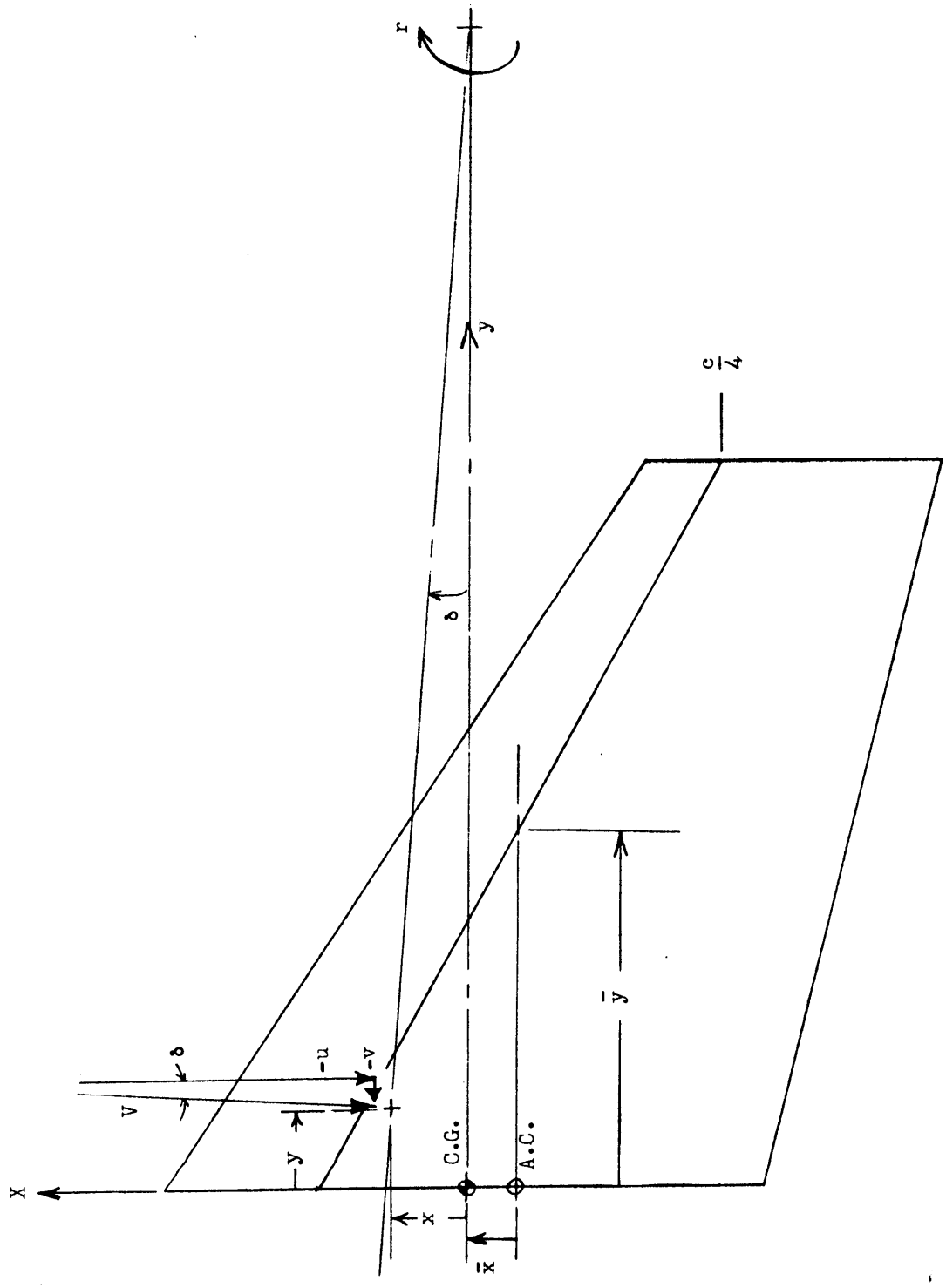

Figure 13.- Details of wing geometry and wind velocity components for yawing wing.

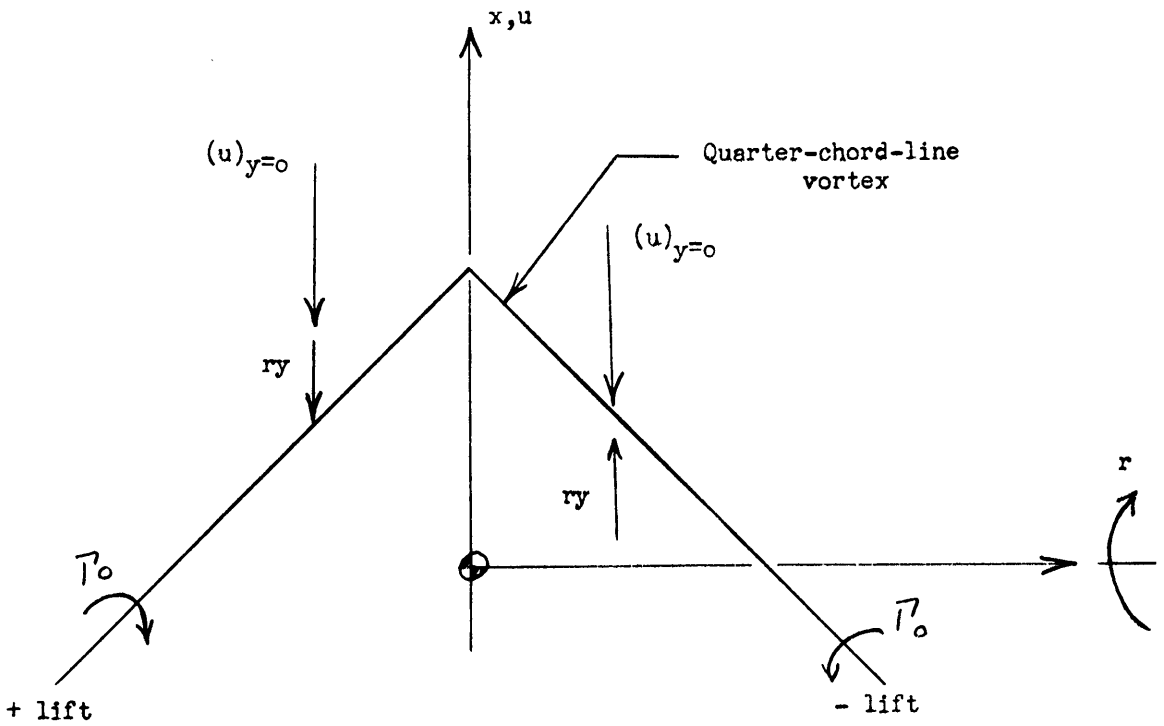

$u = -r(d-y)$ (see equation 45)

$u = (u)_{y=o} + ry$

(a) Geometry involved in term $\int \frac{ry}{V_o}\left(\frac{cc_l}{\bar{c}}\right)_o y^* dy^*$.

Figure 14.- Geometric considerations involved in determining directions of forces on a yawing wing. Note that Γ_o is proportional to $\left(\frac{cc_l}{\bar{c}}\right)_o$

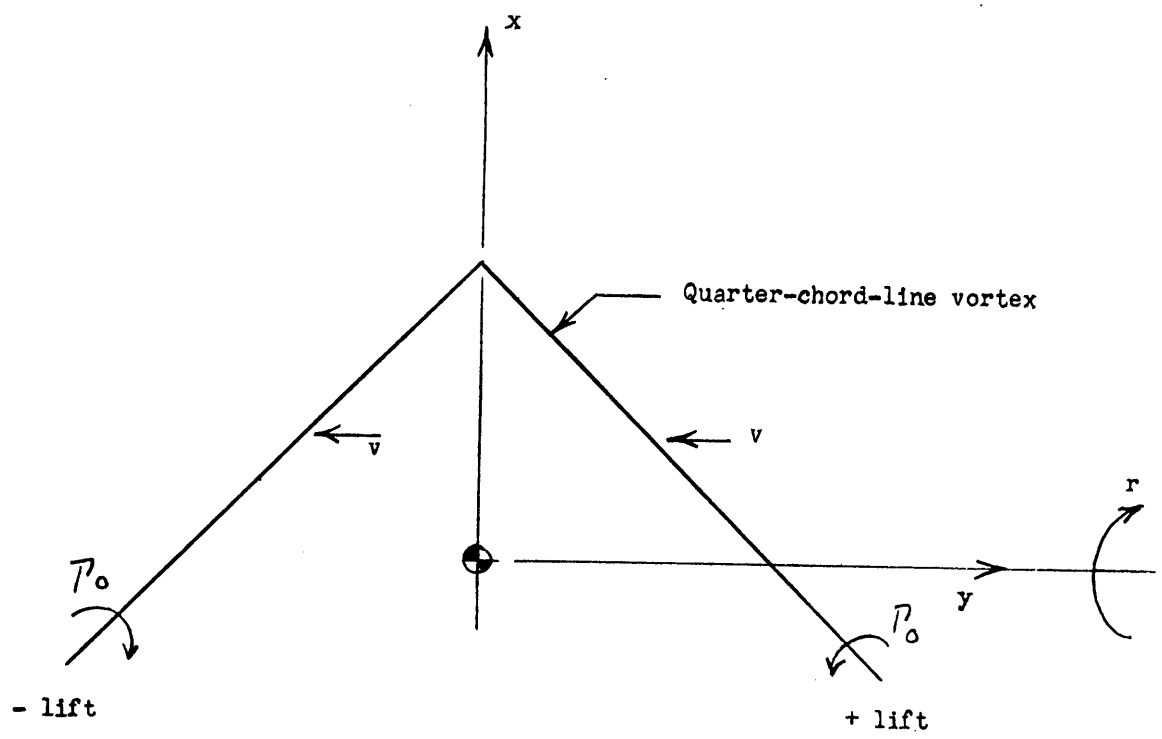

$v = -rx$ (see equation 46)

(b) Geometry involved in term $\int \left[\frac{r(x)_{c/4}}{V_o} \tan \Lambda\right] \left(\frac{cc_l}{\bar{c}}\right)_o y^* dy^*$.

Figure 14.- Continued.

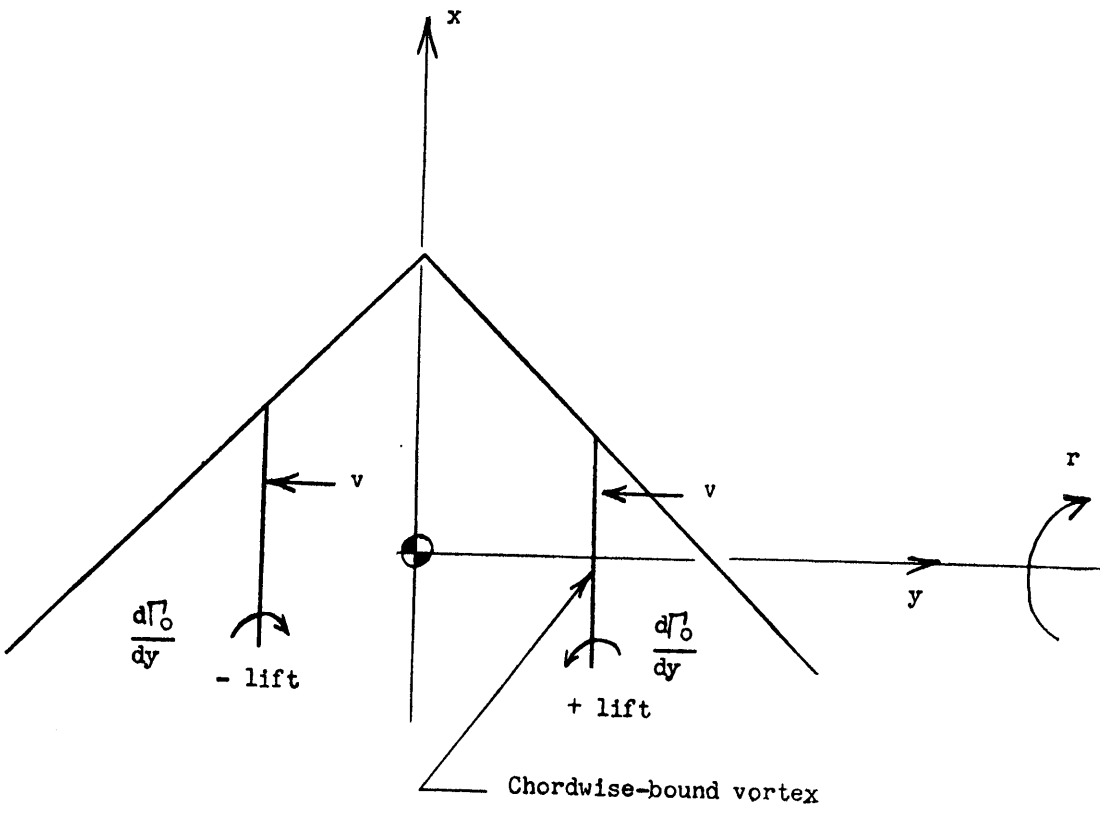

$v = -rx$ (see equation 46)

(c) Geometry involved in term $\int \frac{r}{2V_o} \frac{d\left(\frac{cc_l}{\bar{c}}\right)_o}{dy} \left[(x)^2_{c/4} - (x)^2_c\right] y^* dy^*$.

Figure 14.- Concluded.

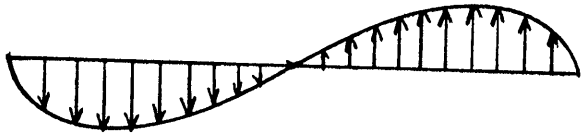

1. Additional loading due to rolling

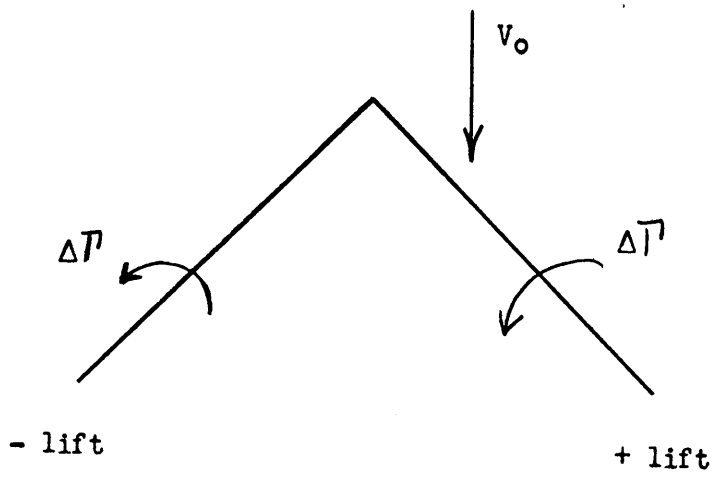

2. Geometric details

(a) Interaction of free-stream velocity with the additional circulation (loading) due to rolling velocity.

Figure 15.- Concepts involved in analysis of the rolling wing.

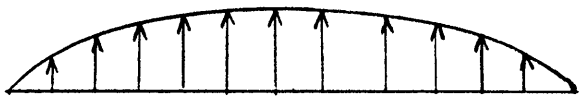

1. Angle-of-attack load distribution

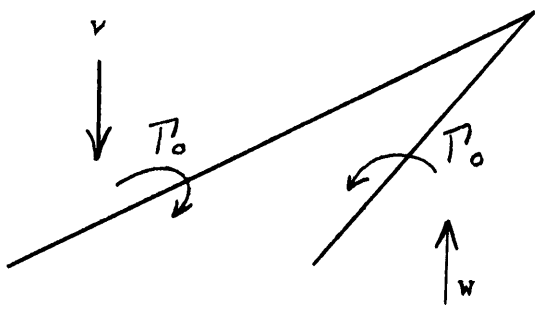

$w = py$

2. Geometric details

(b) Interaction of rolling velocity component with angle-of-attack circulation.

Figure 15.- Concluded.

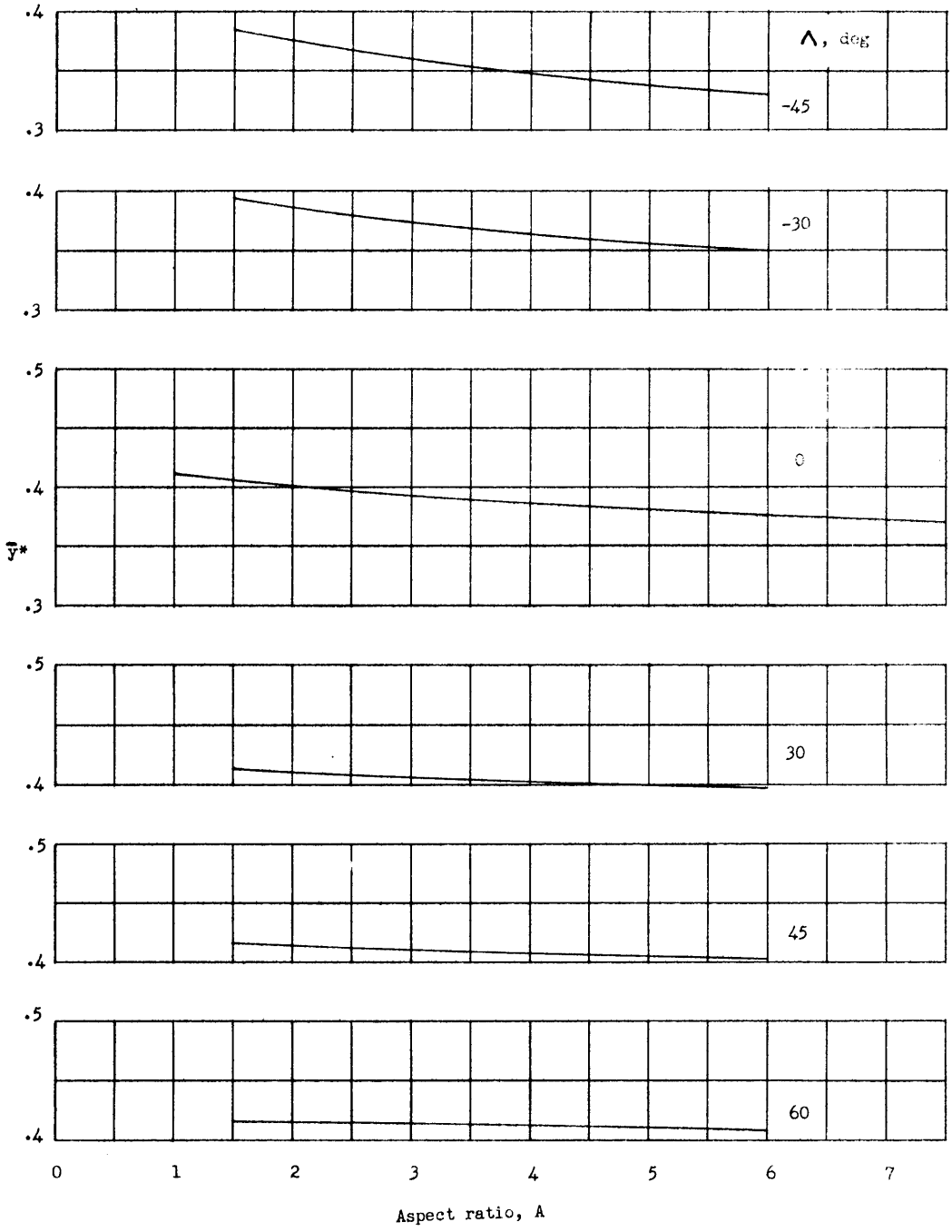

(a) $\lambda = 0.$

Figure 16.- Spanwise location of centroid angle-of-attack loading on a wing semispan.

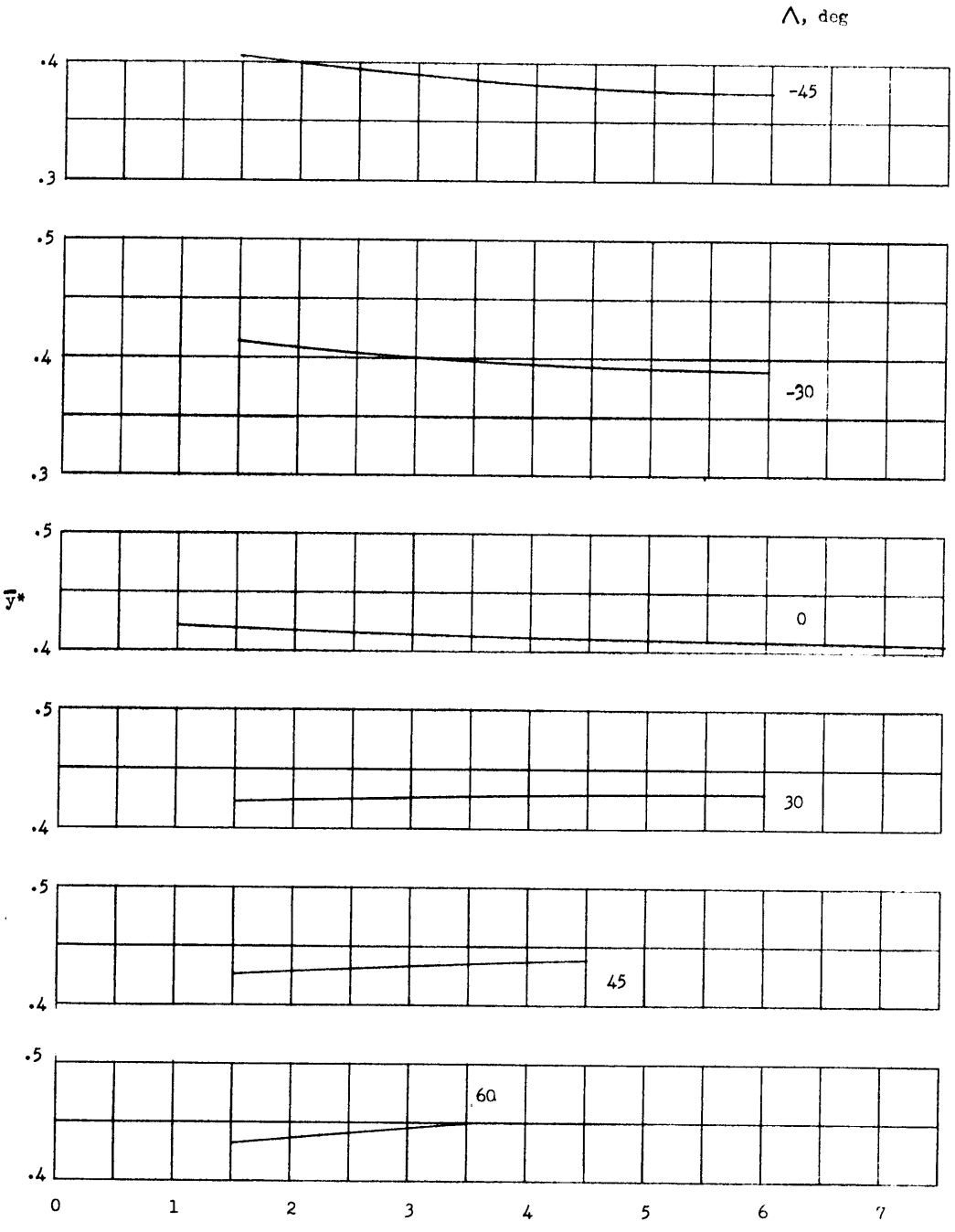

(b) $\lambda = 0.25$.

Figure 16.- Continued.

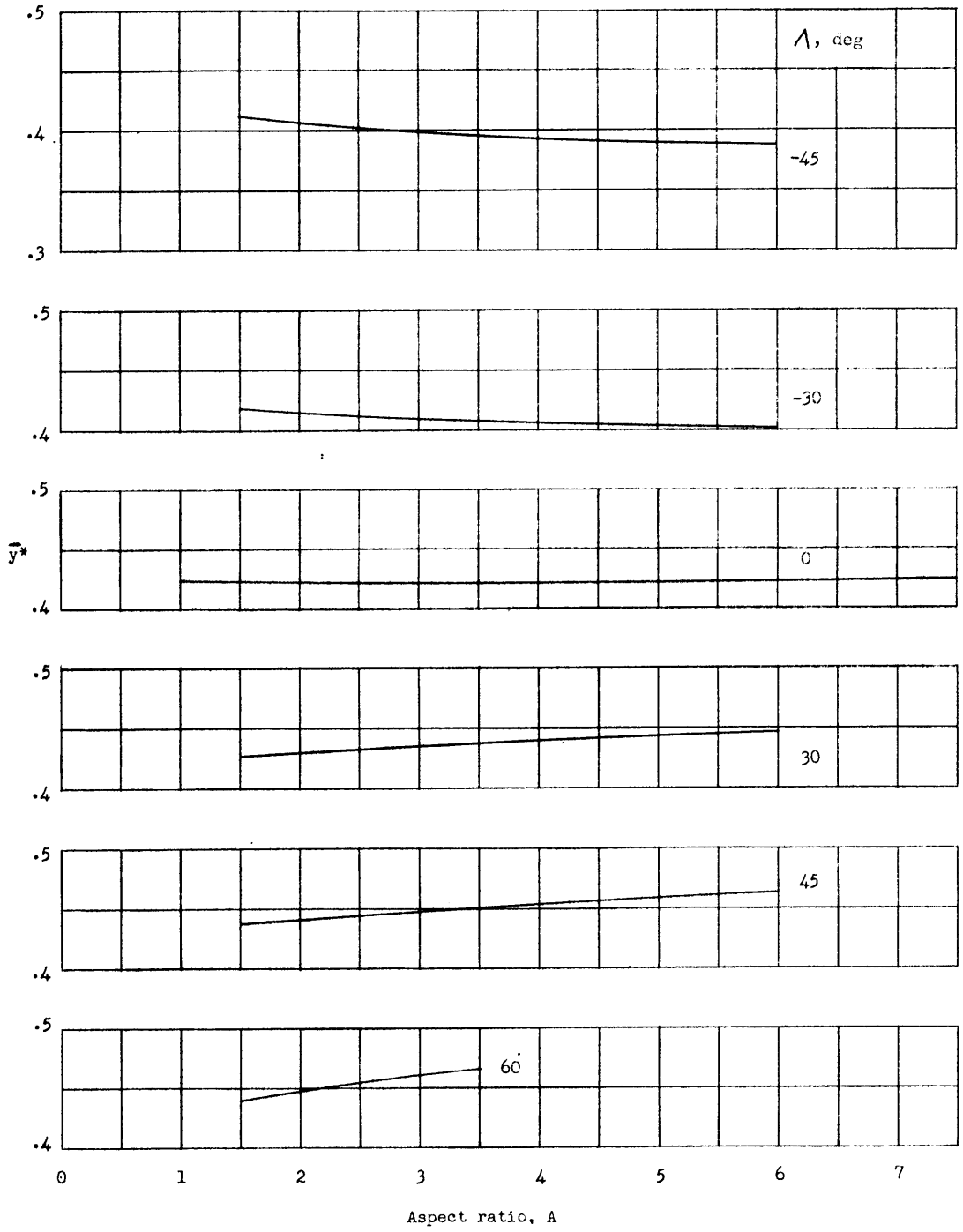

(c) $\lambda = 0.5$.

Figure 16.- Continued.

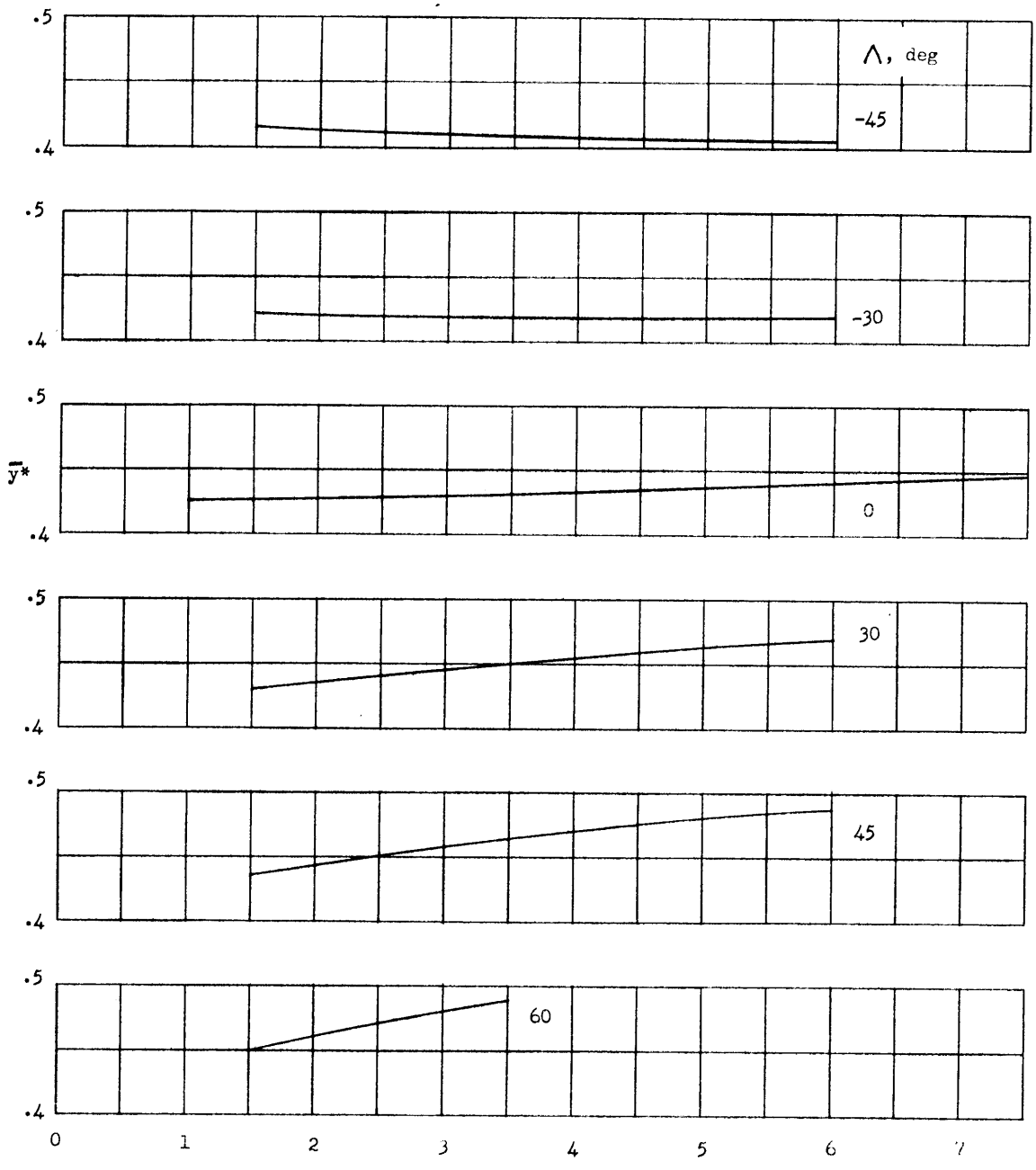

(d) $\lambda = 1.0$.

Figure 16.- Continued.

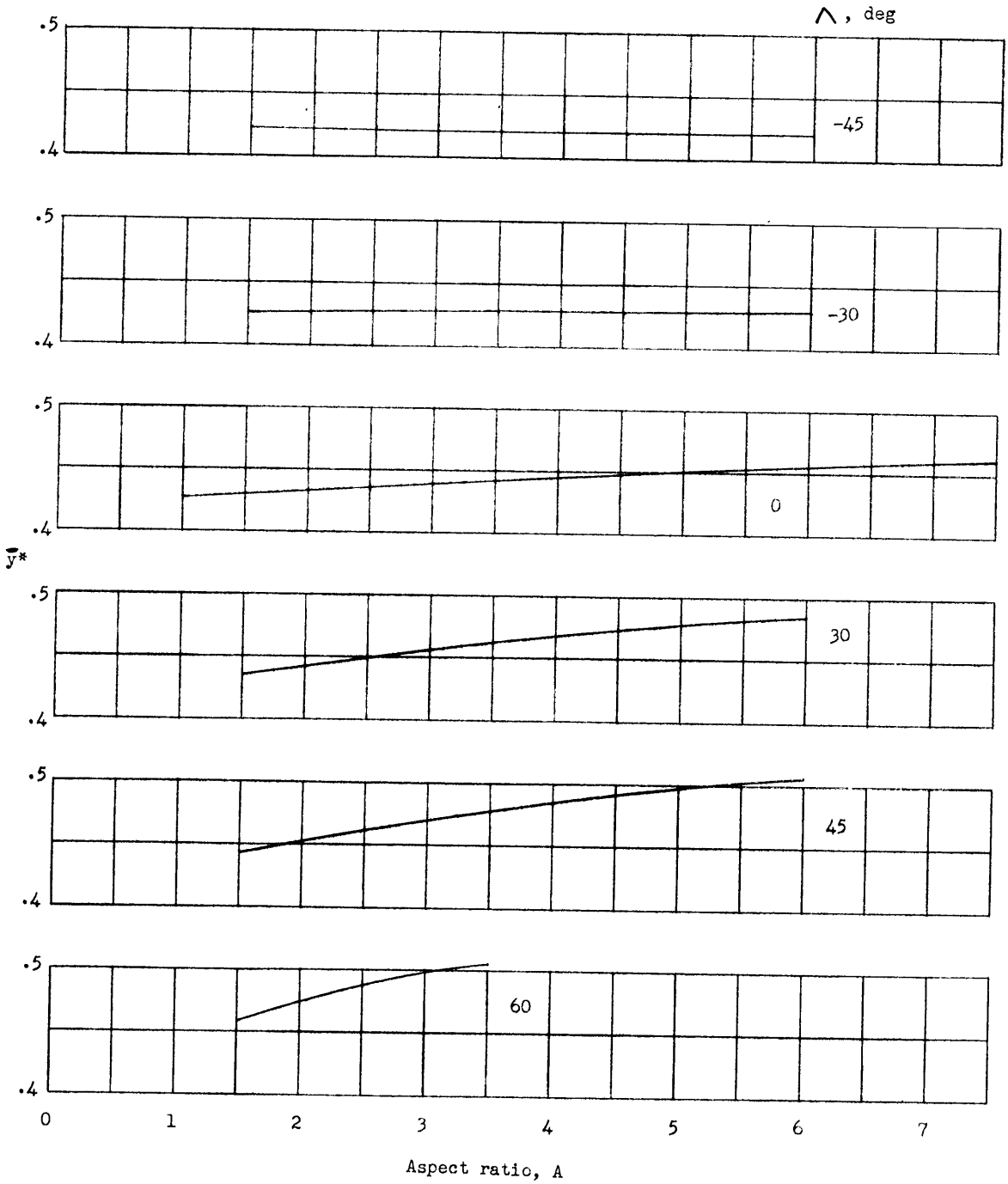

(e) $\lambda = 1.5$.

Figure 16.- Concluded.

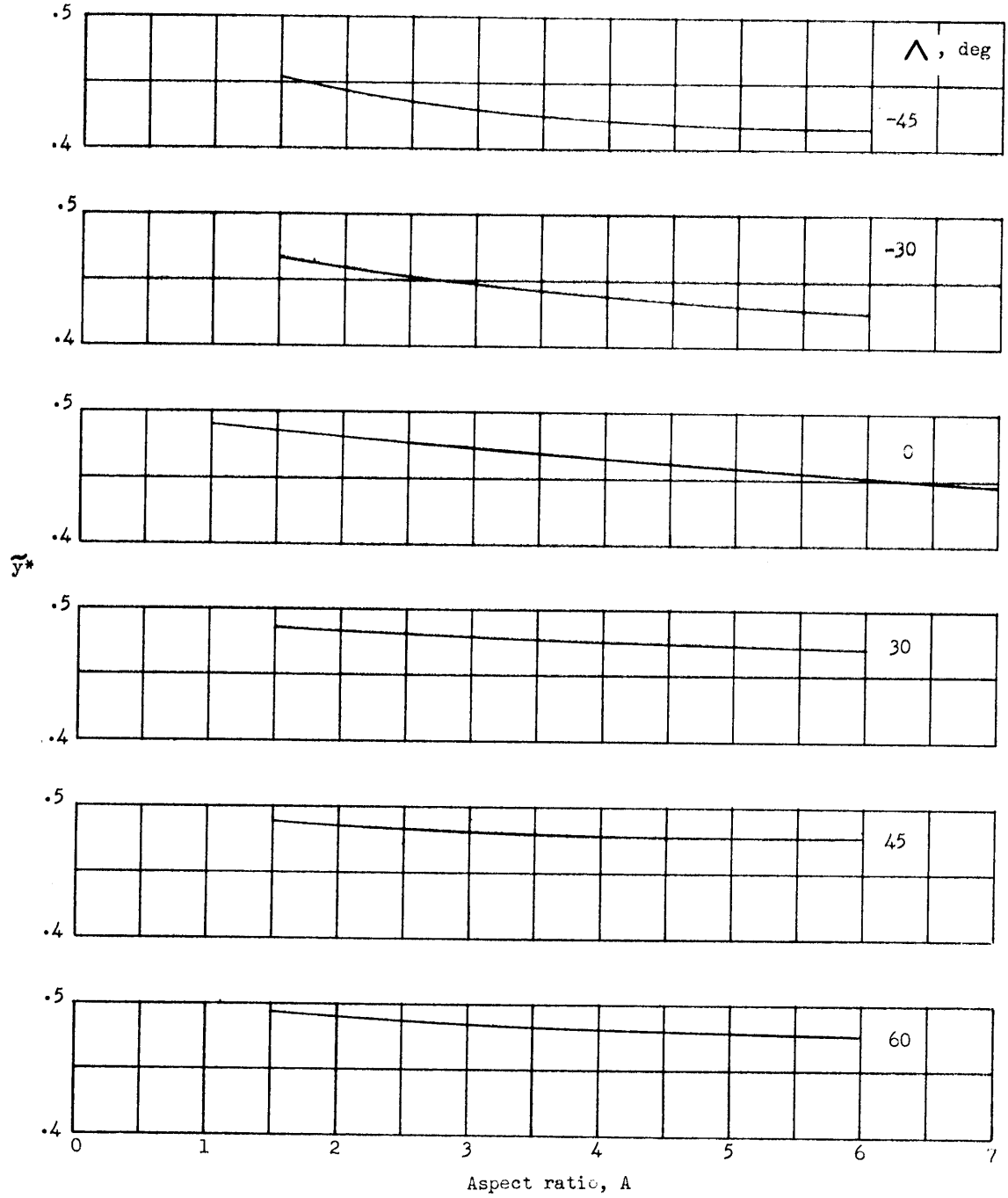

(a) $\lambda = 0$.

Figure 17.- Location of radius of gyration of angle-of-attack span load.

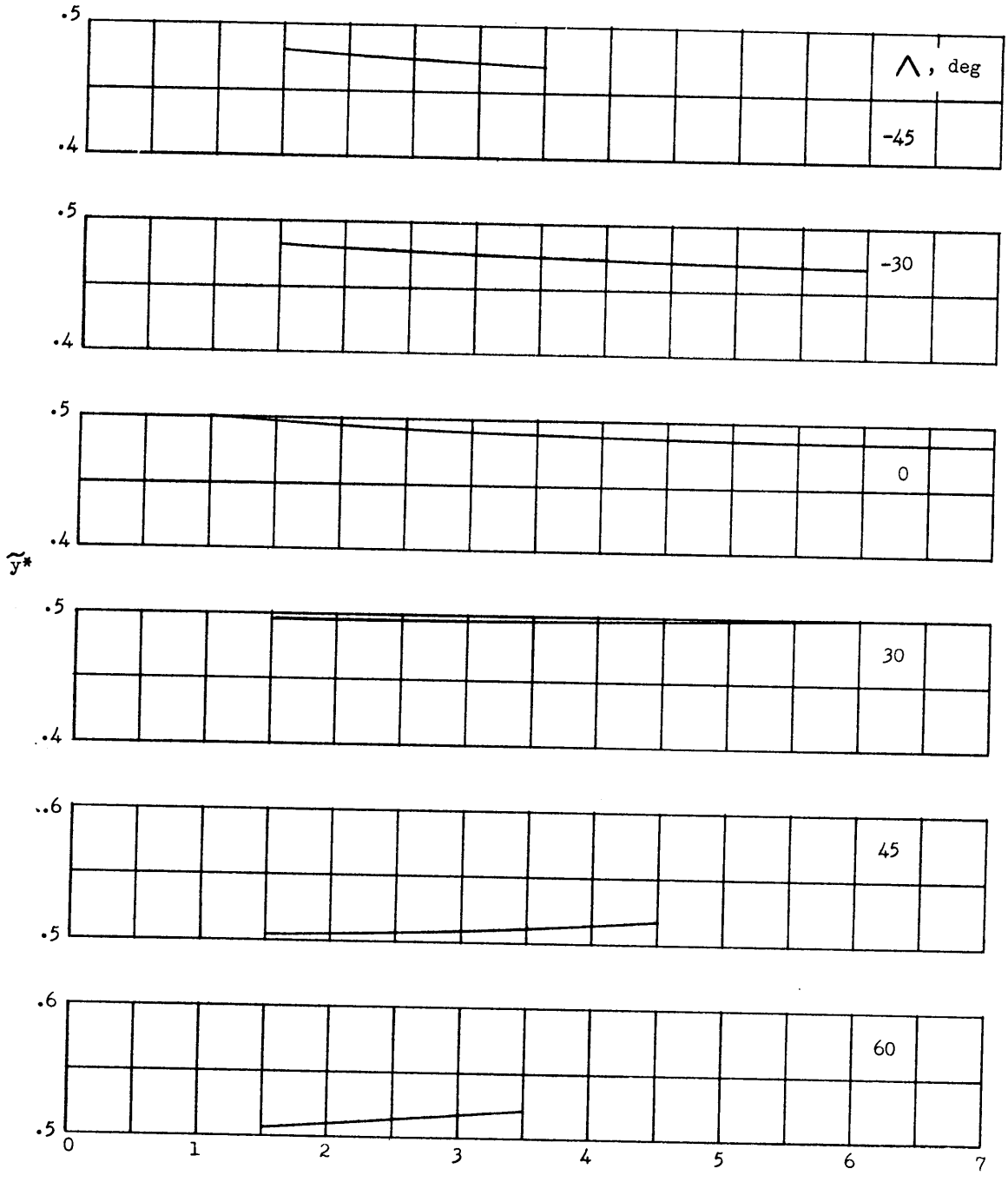

(b) $\lambda = 0.25$.

Figure 17.- Continued.

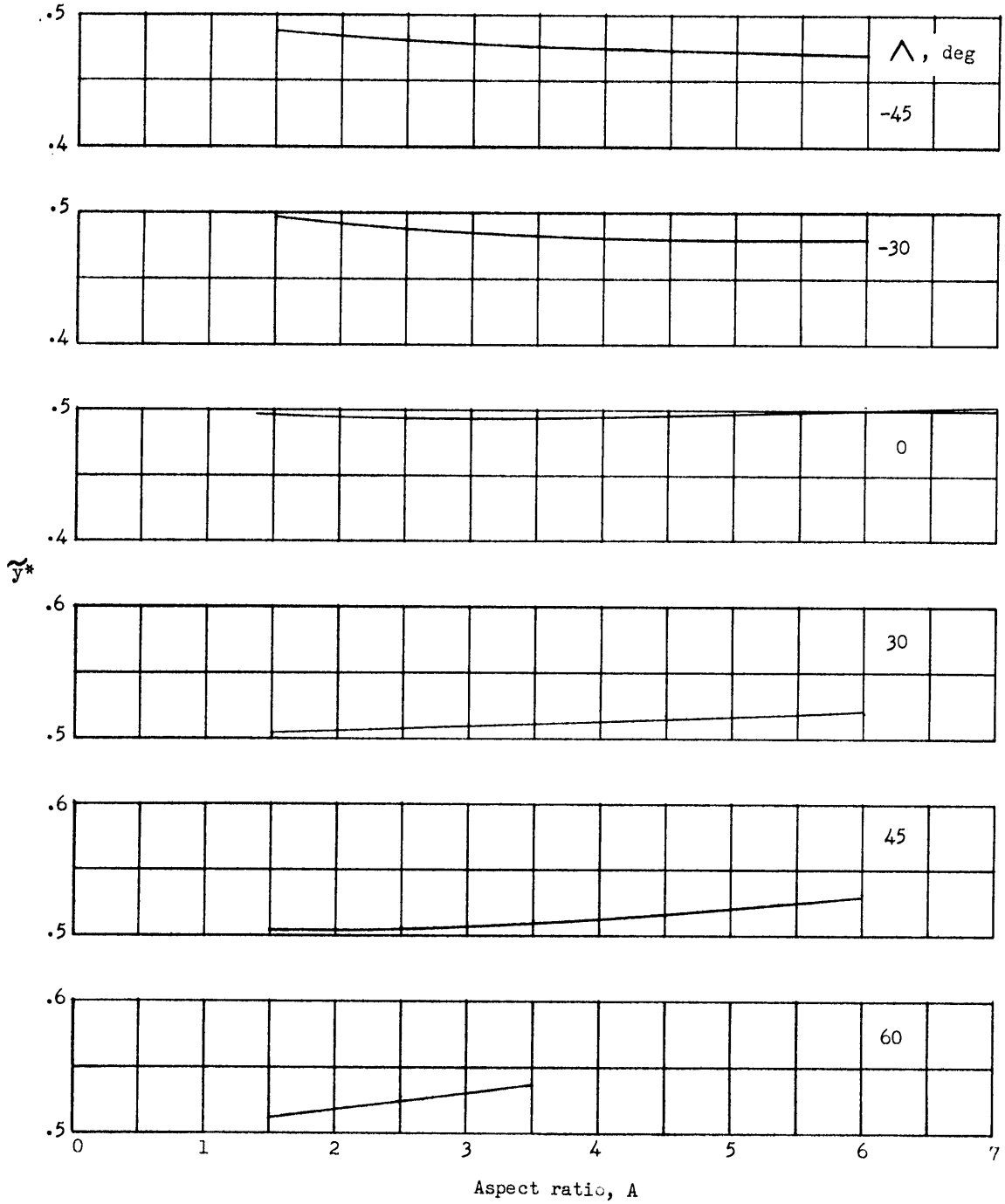

(c) $\lambda = 0.5$.

Figure 17.- Continued.

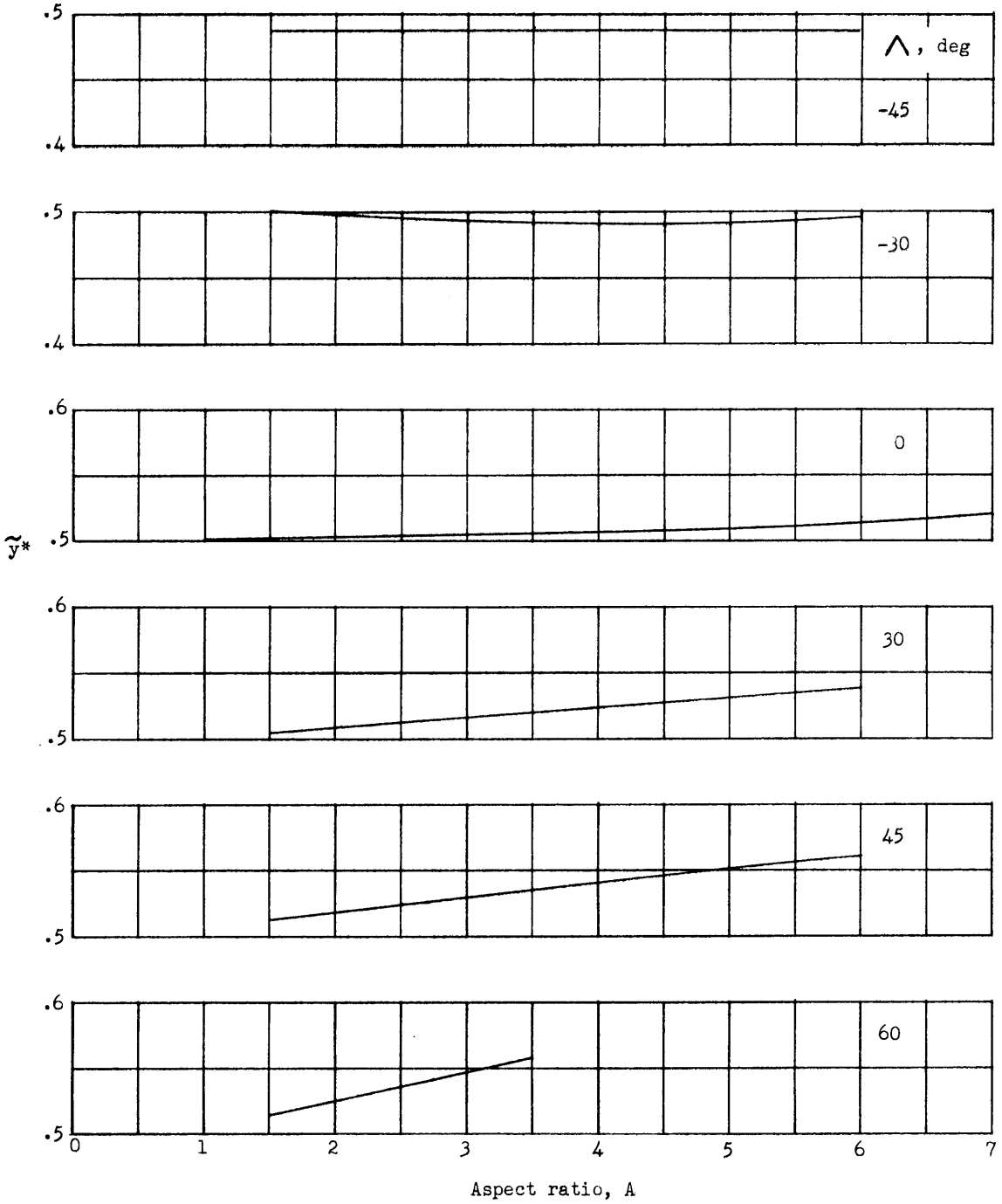

(d) $\lambda = 1.0$.

Figure 17.- Continued.

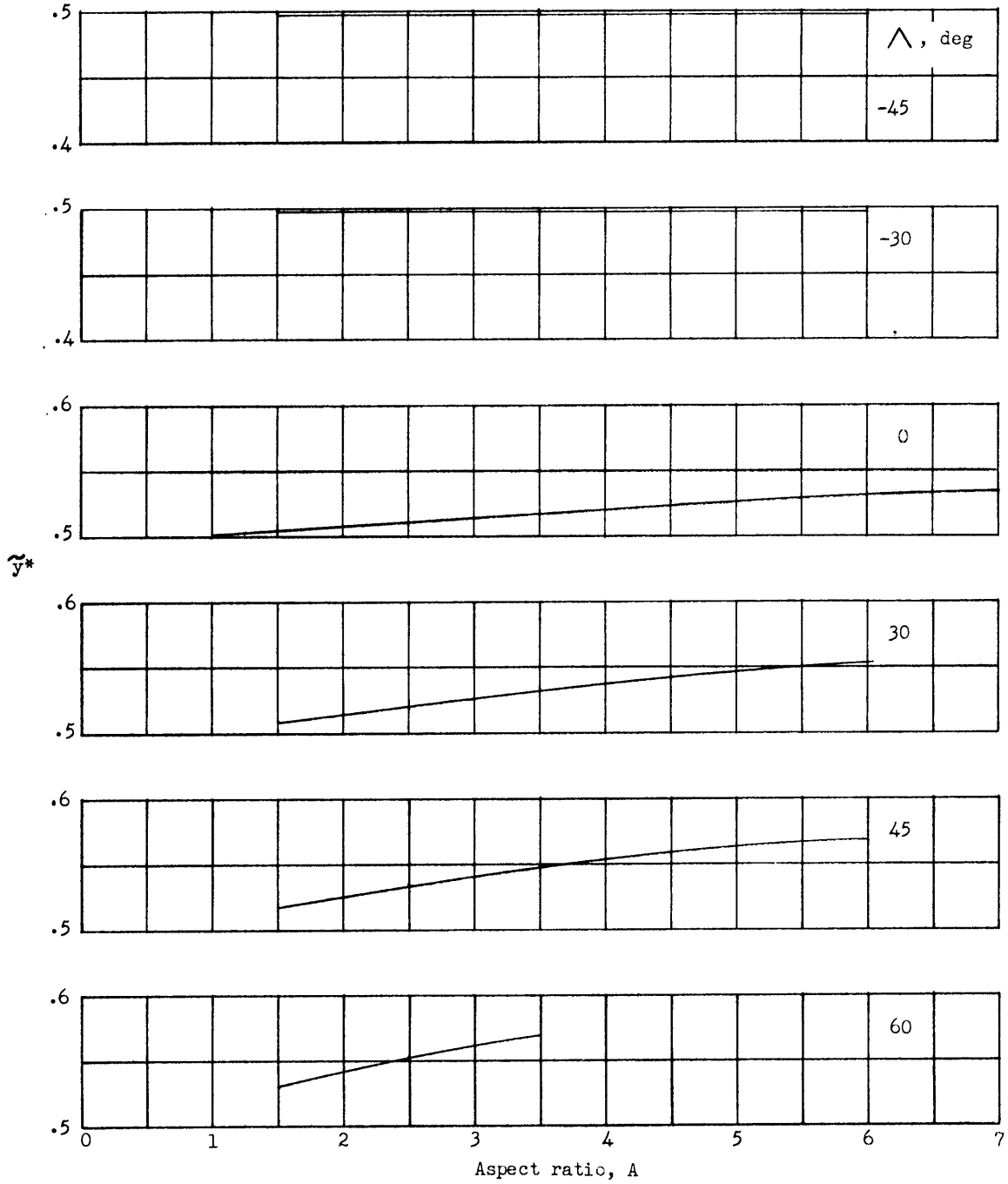

(e) $\lambda = 1.5$.

Figure 17.- Concluded.

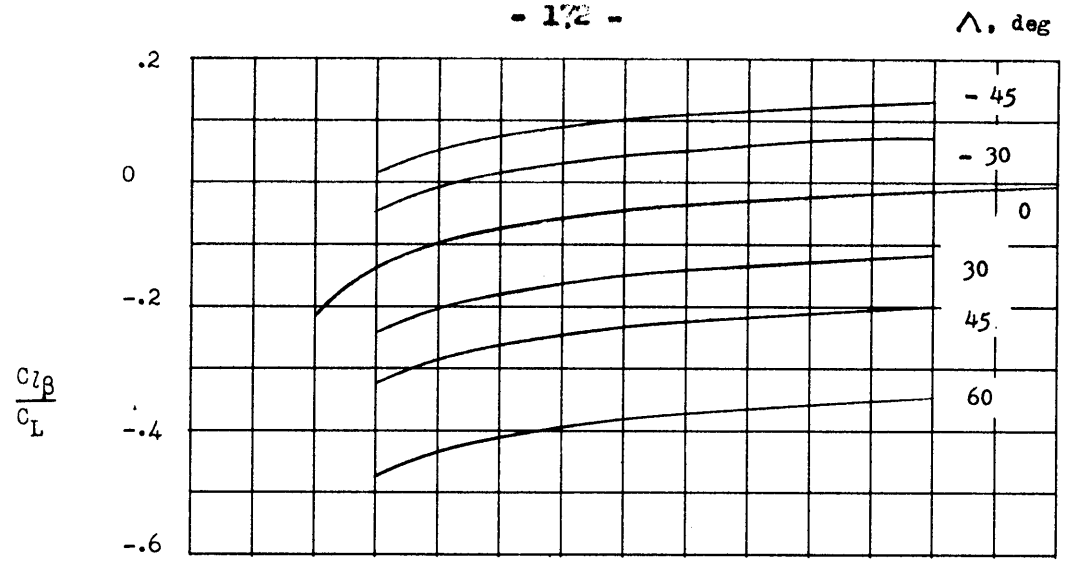

(a) M = 0.

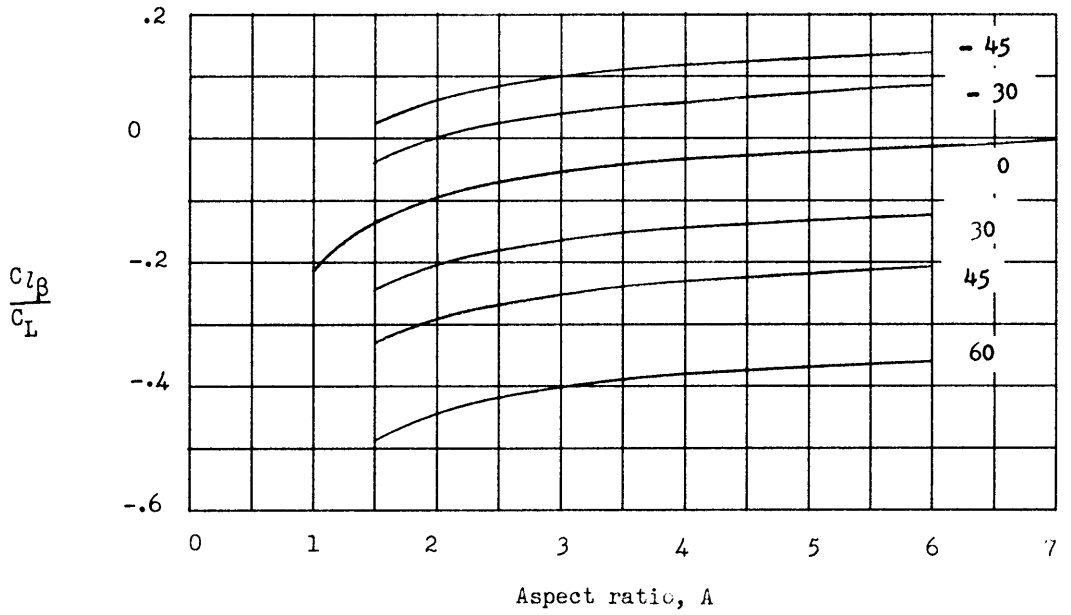

(b) M = 0.4.

Figure 18.- Variation of $\frac{C_{l_\beta}}{C_L}$ with aspect ratio, sweep, and Mach number. $\lambda = 0$.

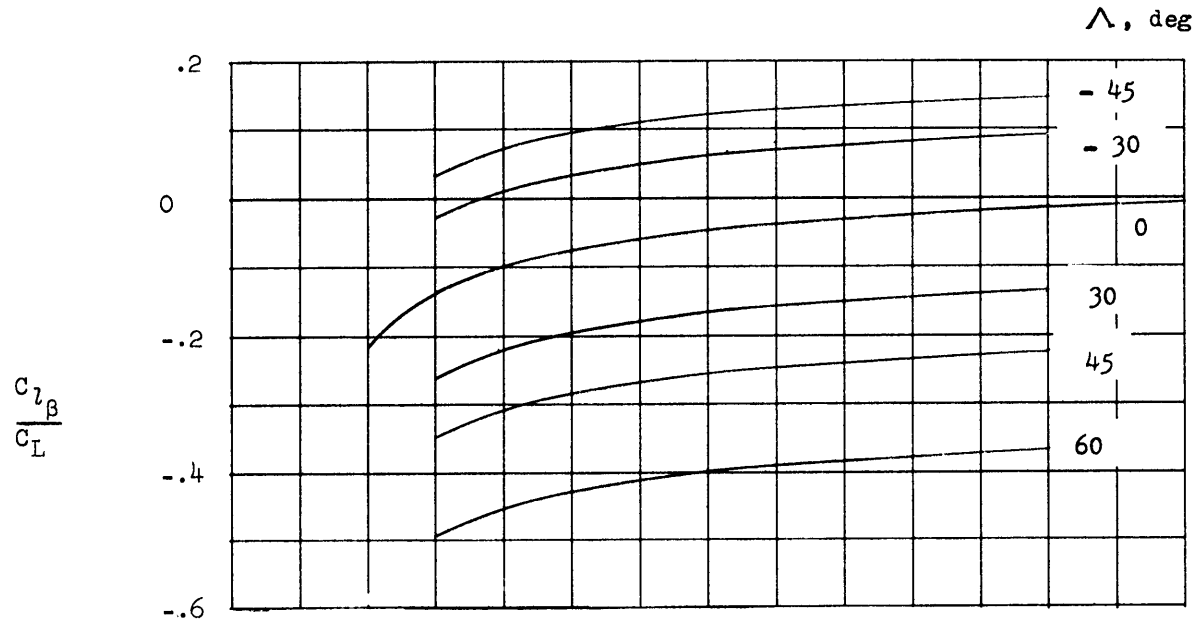

(c) M = 0.6.

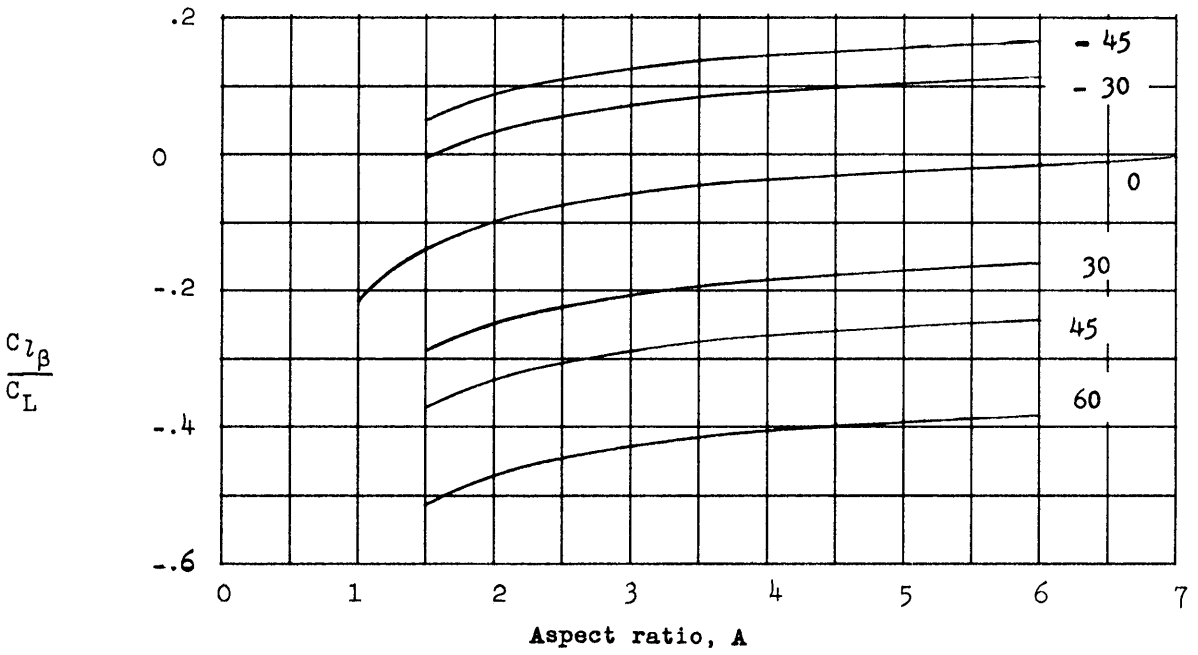

(d) M = 0.8.

Figure 18.- λ = 0. Continued.

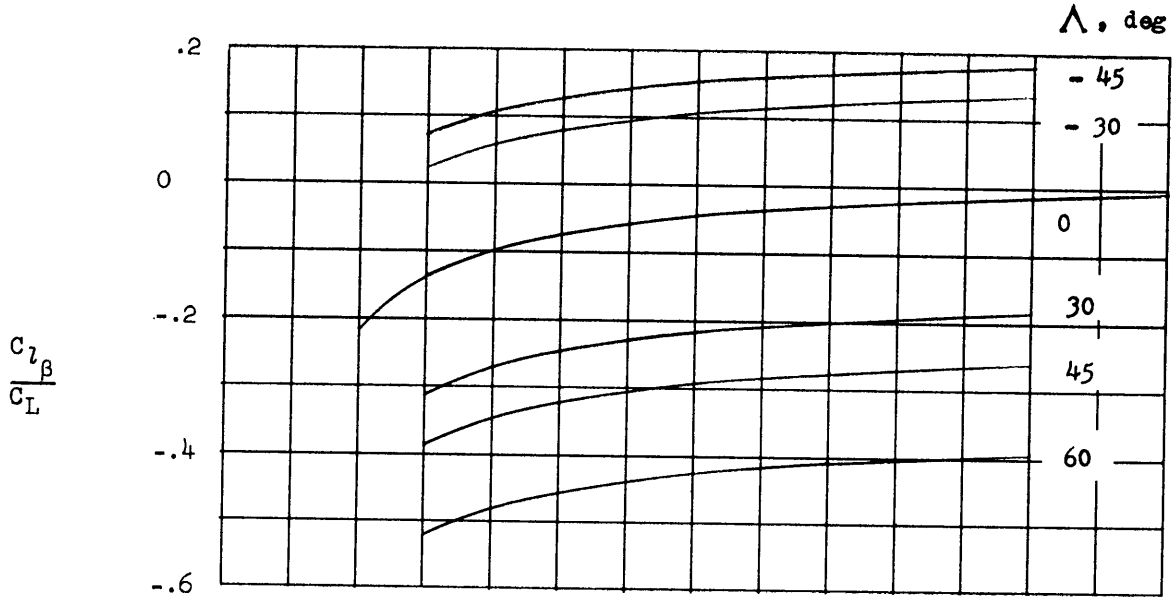

(e) M = 0.9.

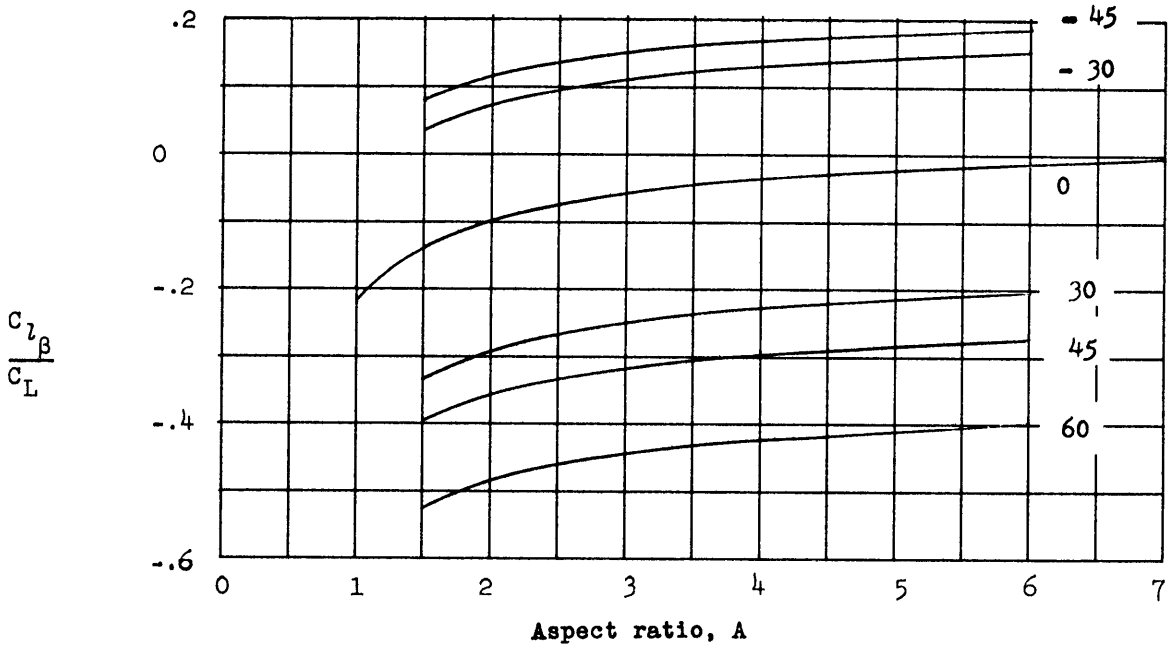

(f) M = 0.95.

Figure 18.- λ = 0. Concluded.

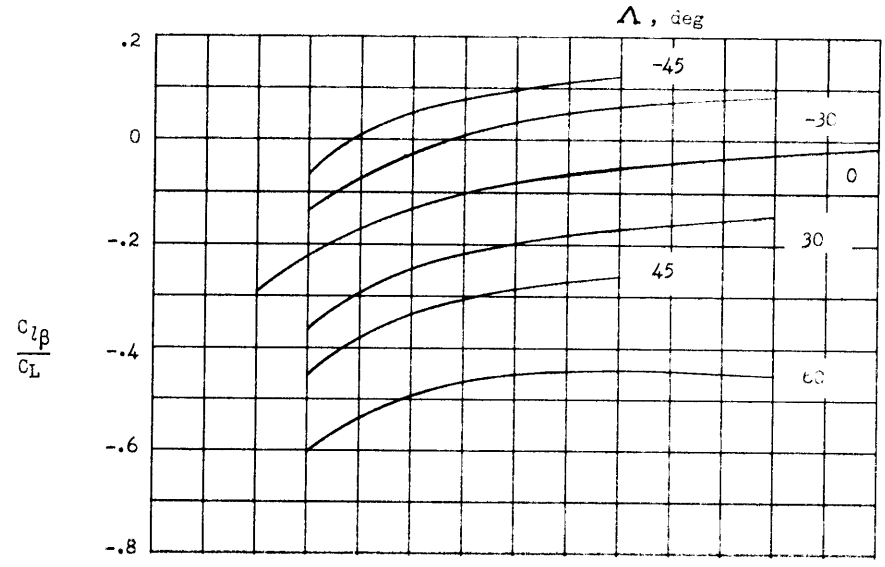

(a) M = 0.

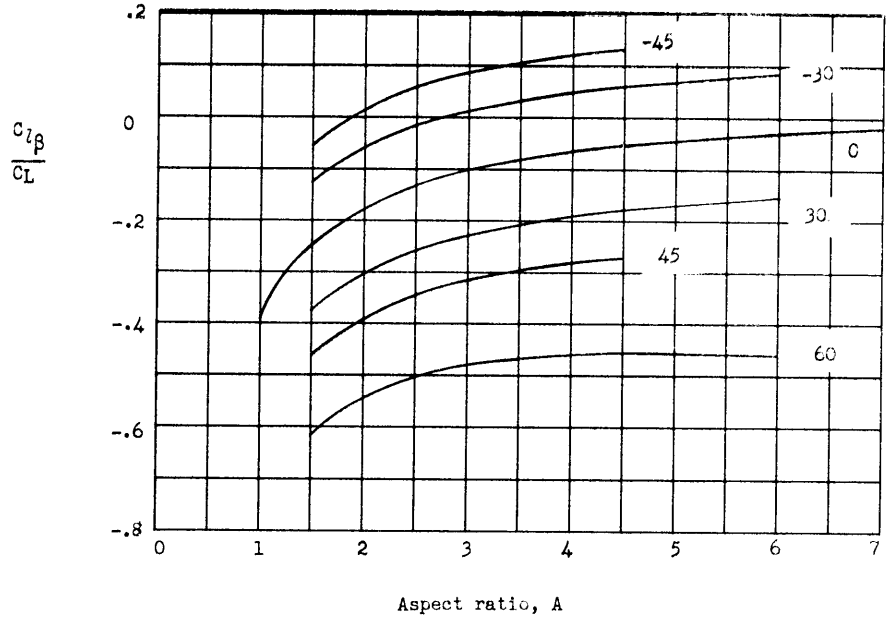

(b) M = 0.4.

Figure 19.- Variation of $\frac{C_{l_\beta}}{C_L}$ with aspect ratio, sweep, and Mach number. $\lambda = 0.25$.

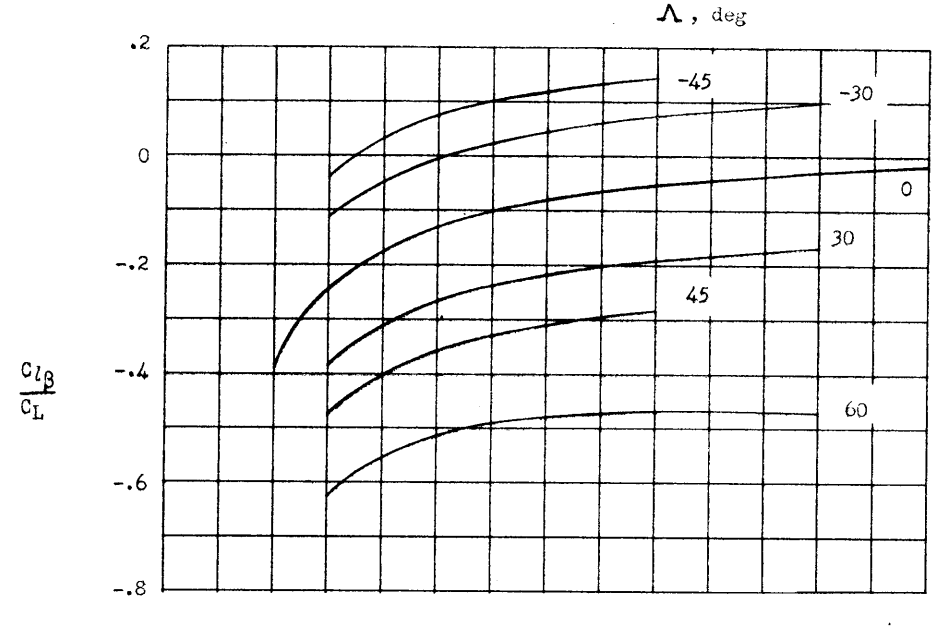

(c) M = 0.6.

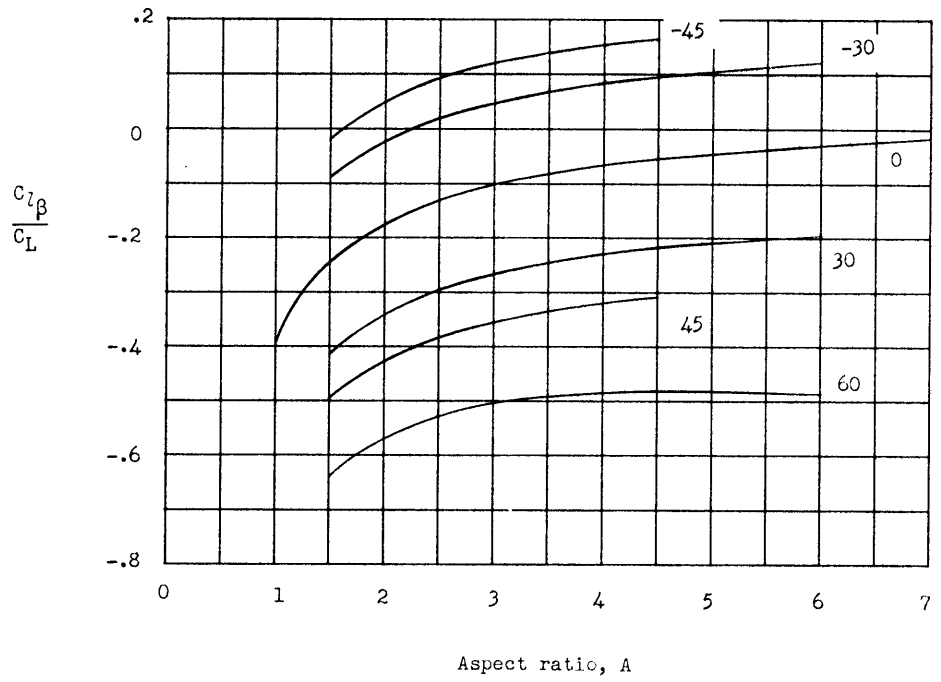

(d) M = 0.8.

Figure 19.- λ = 0.25. Continued.

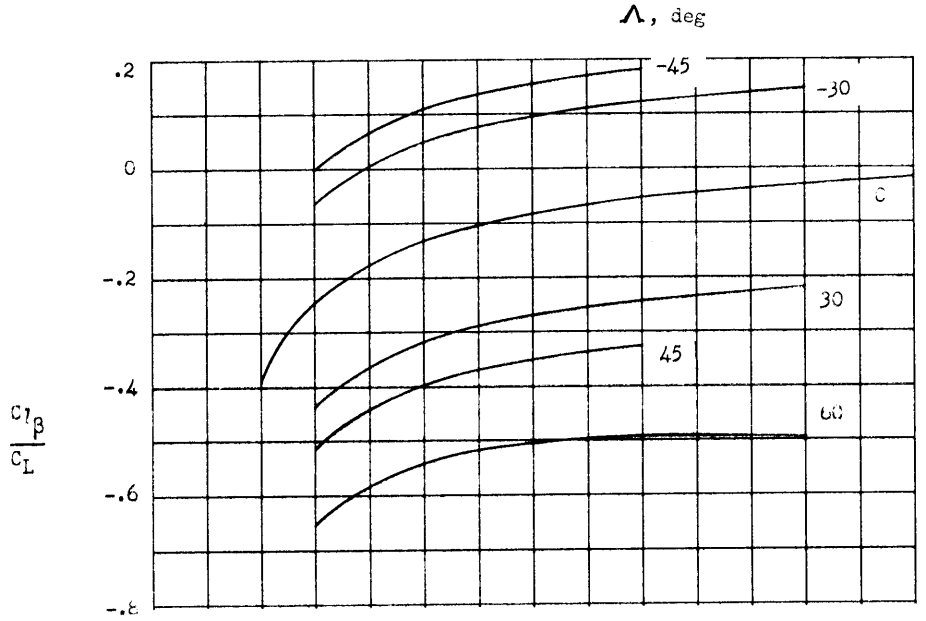

(e) M = 0.9.

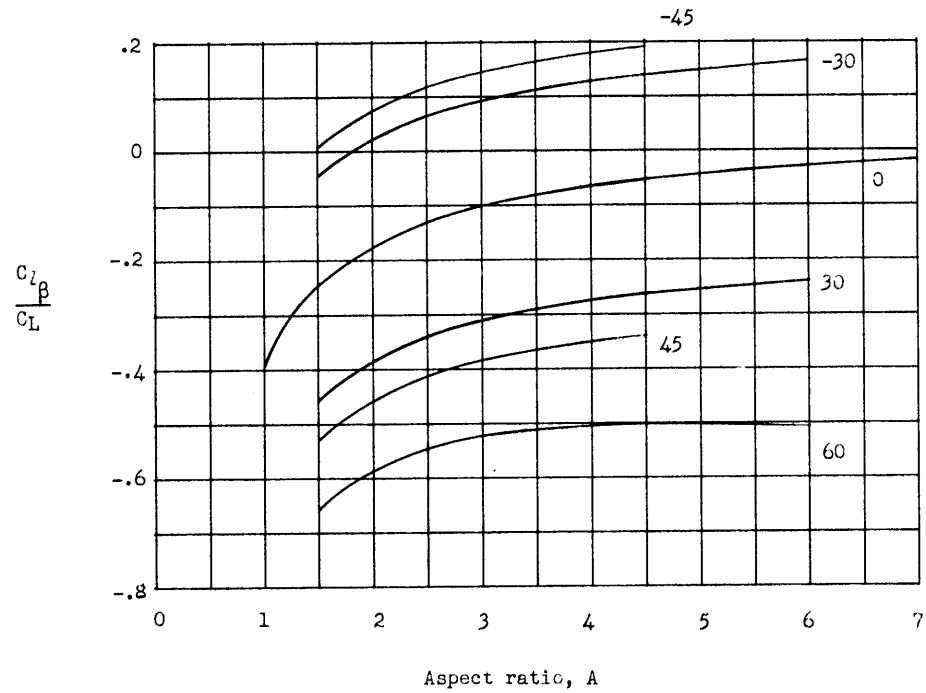

(f) M = 0.95.

Figure 19.- λ = 0.25. Concluded.

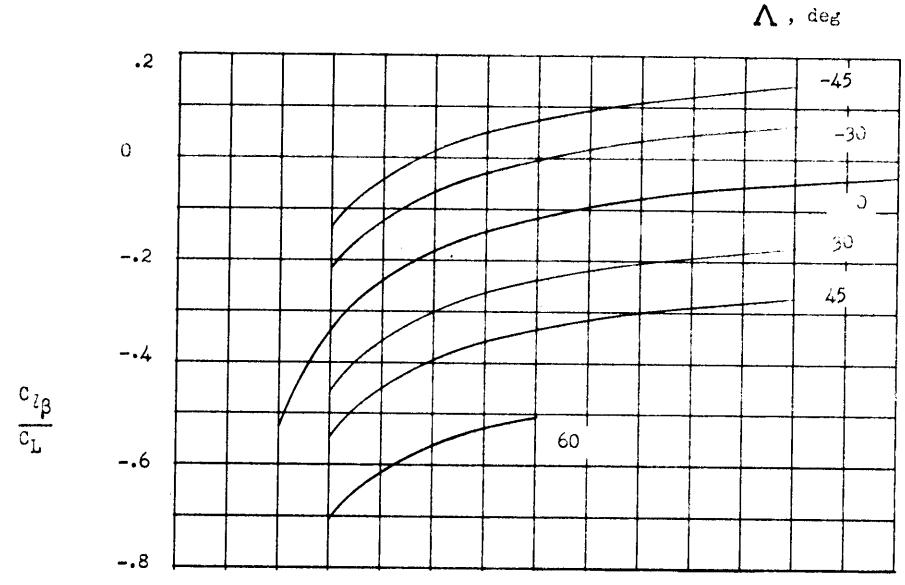

(a) M = 0.

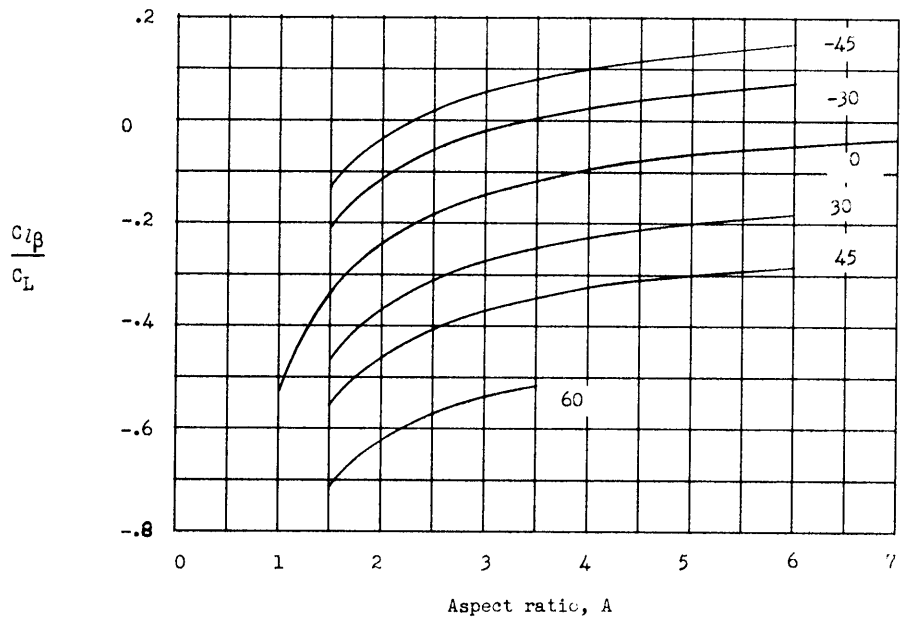

(b) M = 0.4.

Figure 20.- Variation of $\frac{C_{l_\beta}}{C_L}$ with aspect ratio, sweep, and Mach number. $\lambda = 0.50$.

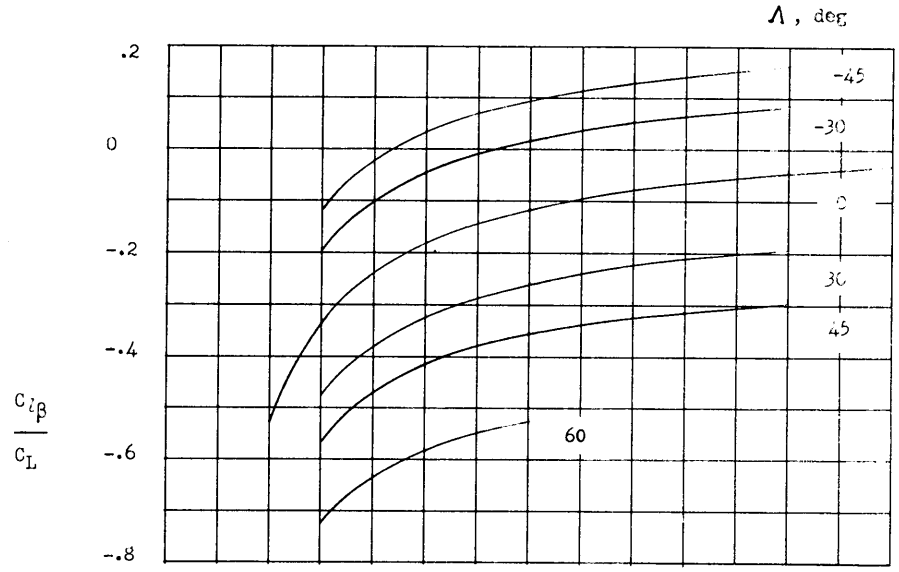

(c) M = 0.6.

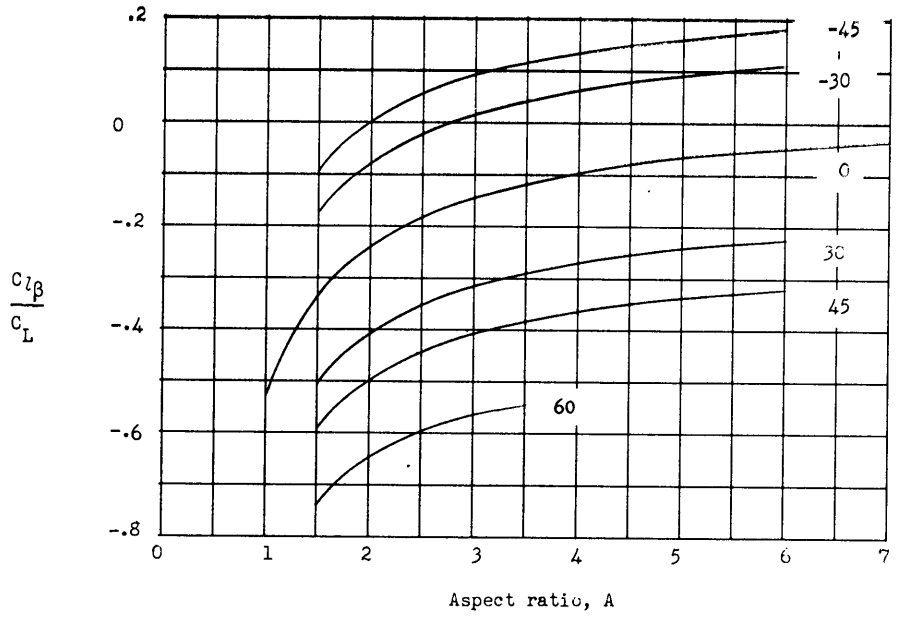

(d) M = 0.8.

Figure 20.- λ = 0.5. Continued.

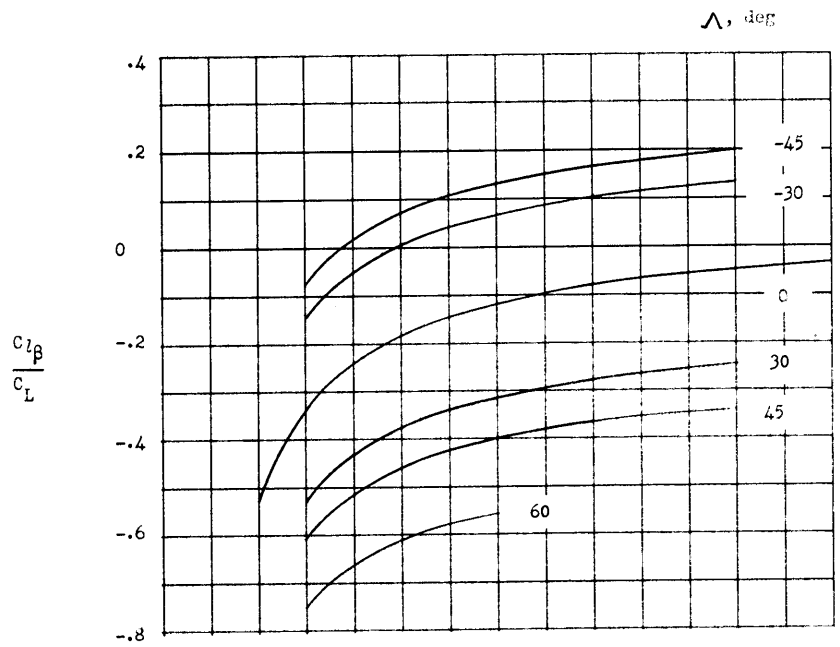

(e) M = 0.9.

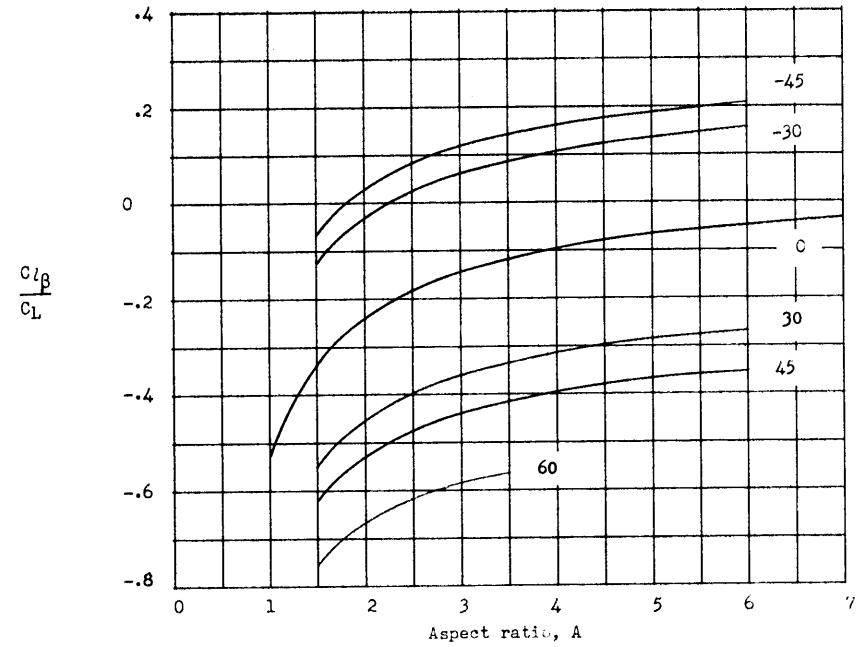

(f) M = 0.95.

Figure 20.- λ = 0.5. Concluded.

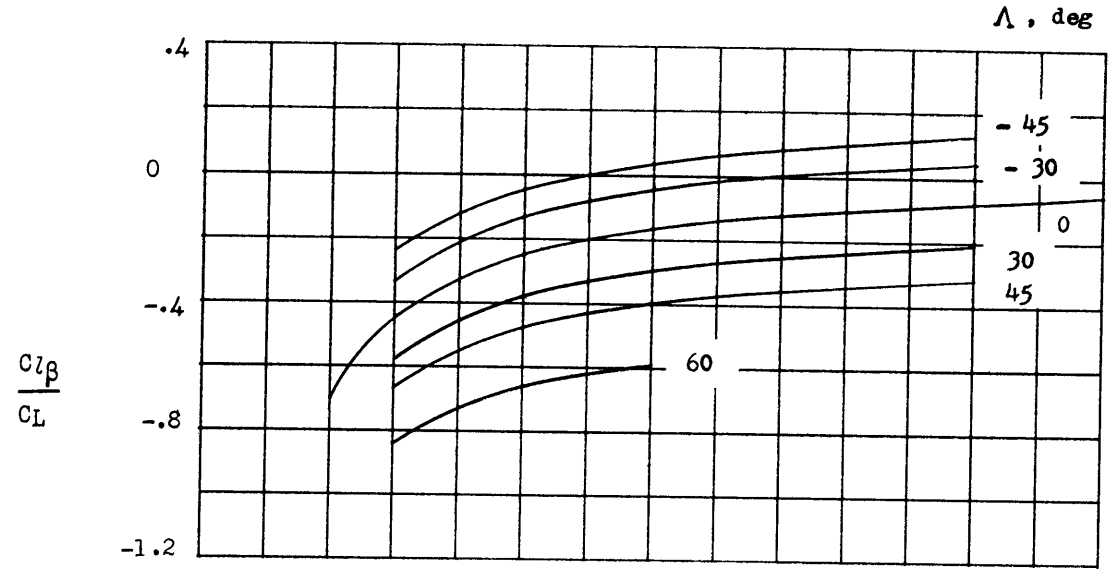

(a) M = 0.

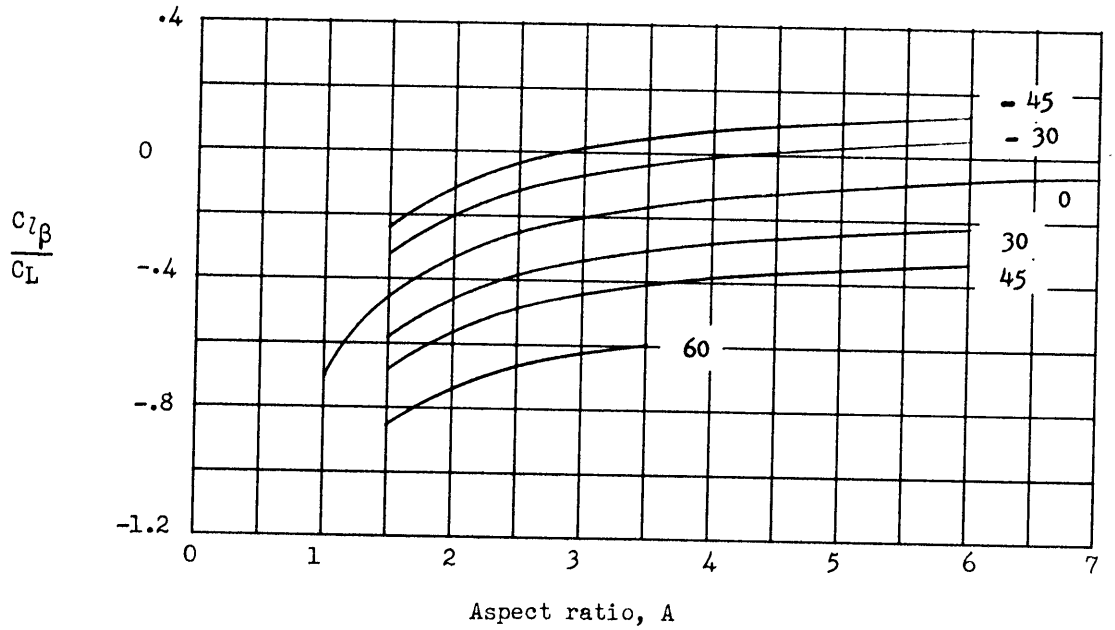

(b) M = 0.4.

Figure 21.- Variation of $\frac{C_{l_\beta}}{C_L}$ with aspect ratio, sweep, and Mach number. $\lambda = 1.0$.

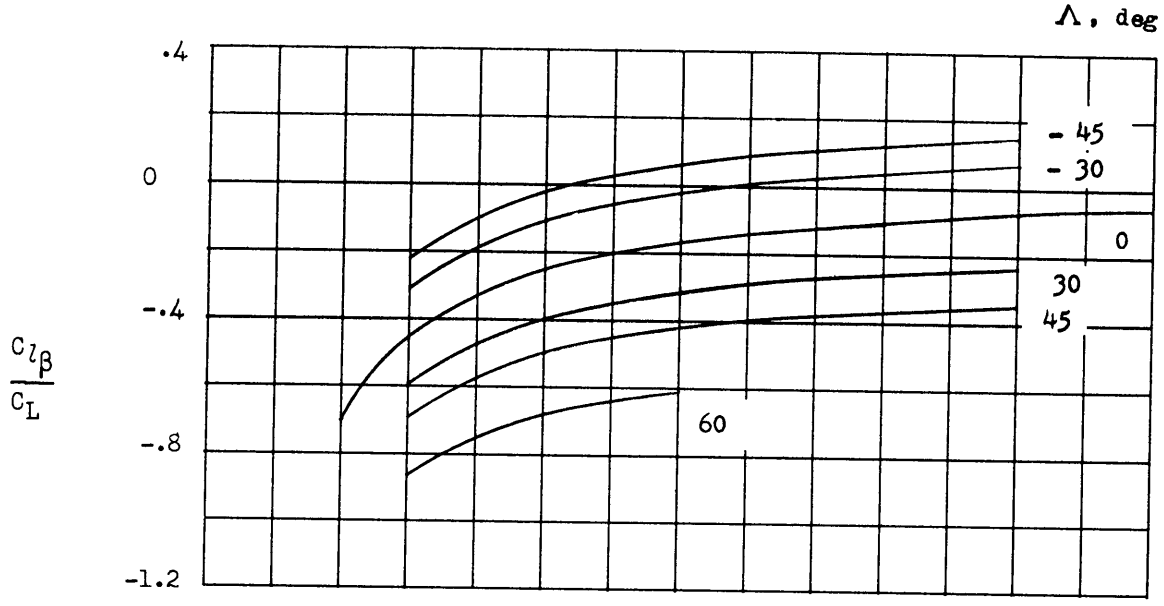

(c) M = 0.6.

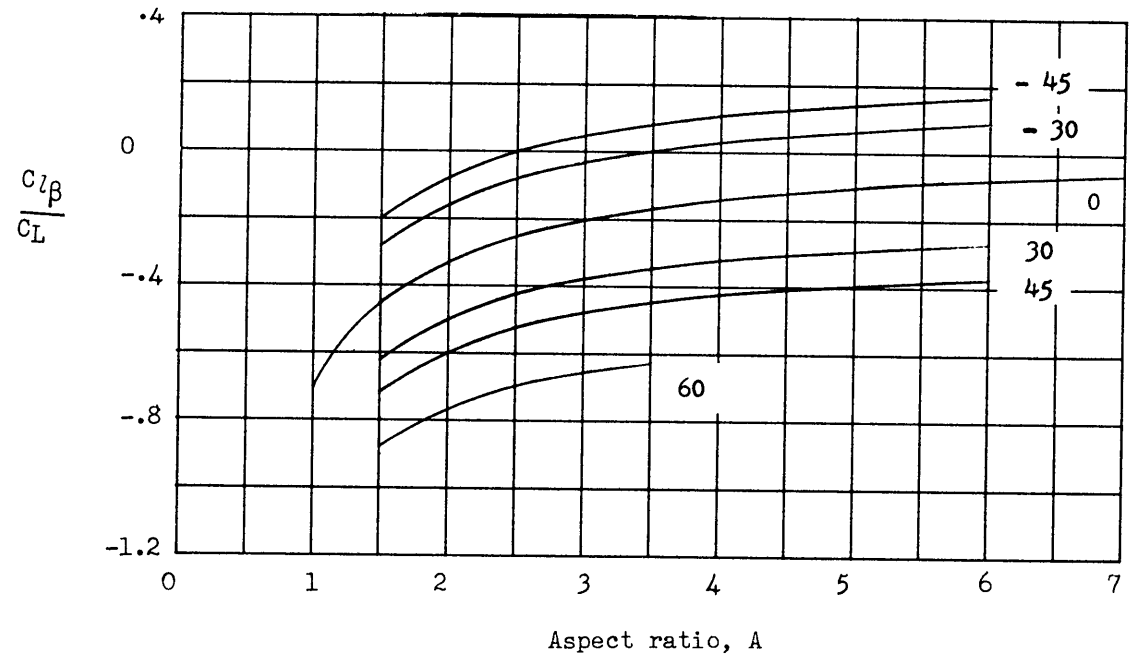

(d) M = 0.8.

Figure 21.- λ = 1.0. Continued.

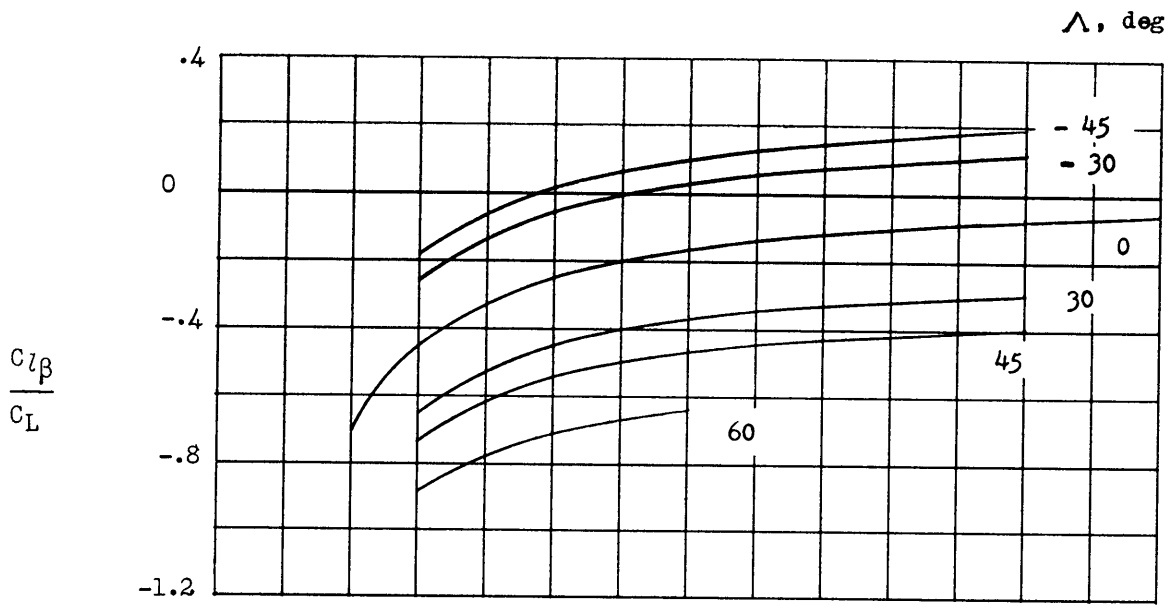

(e) M = 0.9.

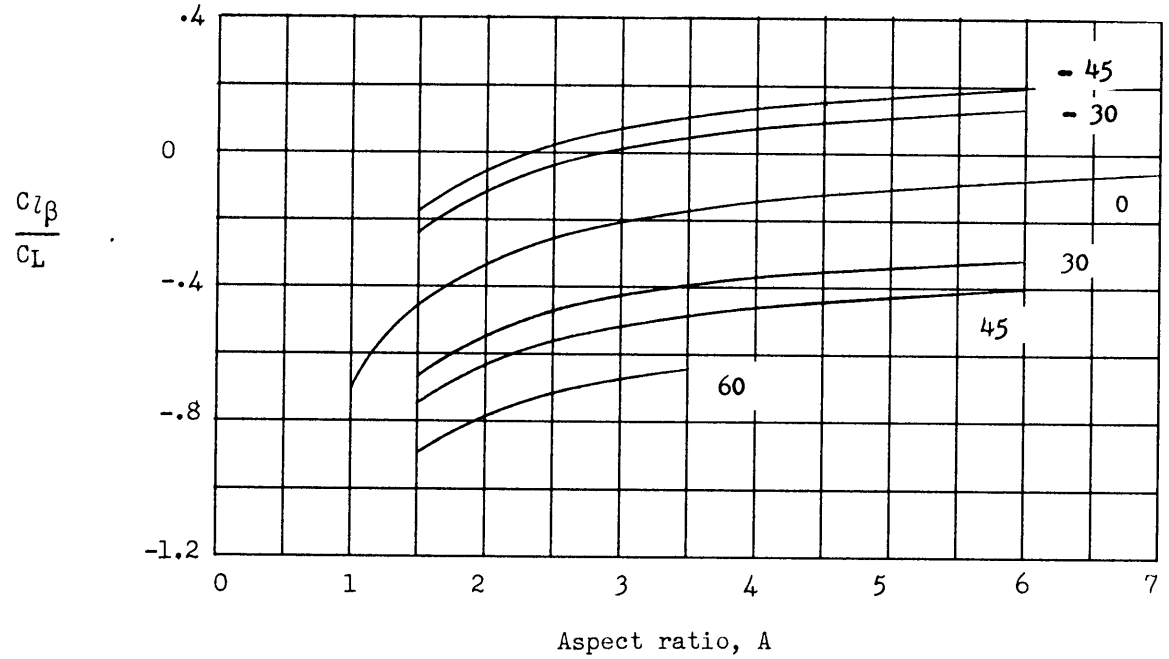

(f) M = 0.95.

Figure 21.- λ = 1.0. Concluded.

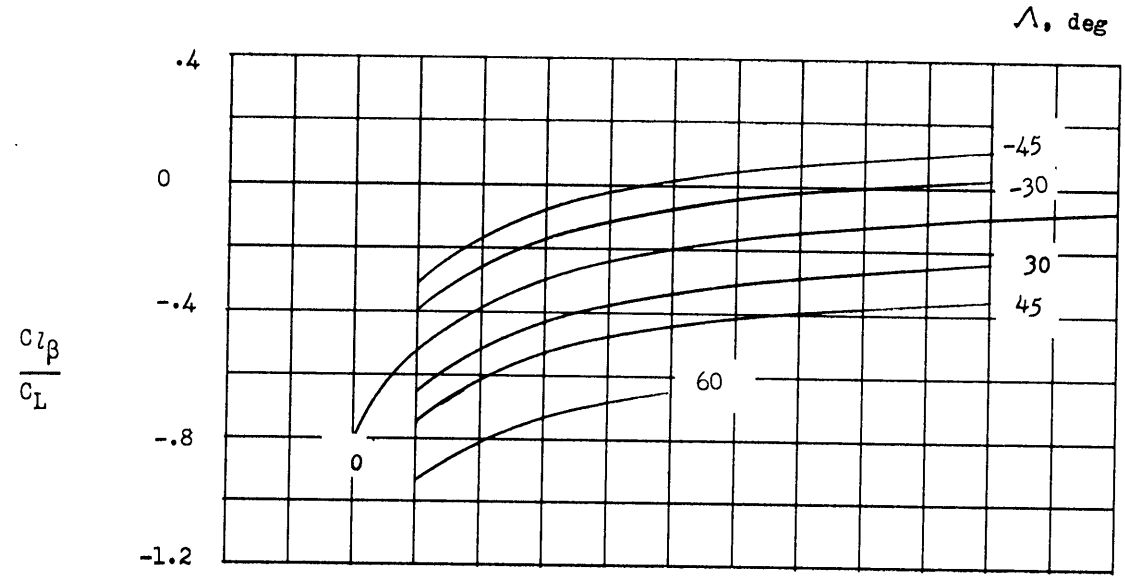

(a) M = 0.

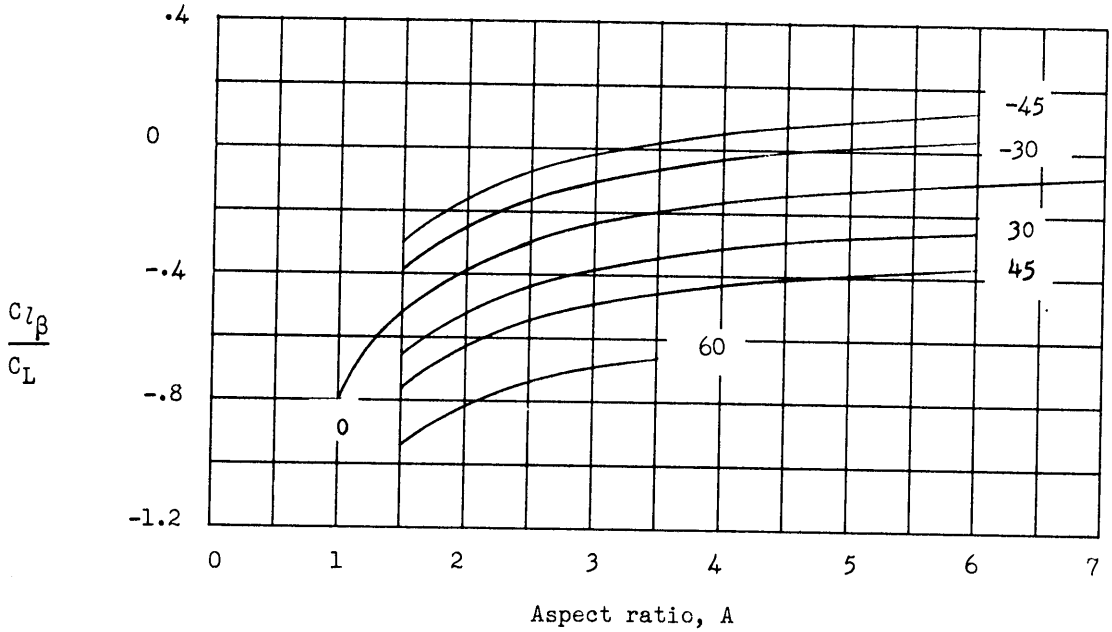

(b) M = 0.4.

Figure 22.- Variation of $\frac{C_{l_\beta}}{C_L}$ with aspect ratio, sweep, and Mach number. $\lambda = 1.5$.

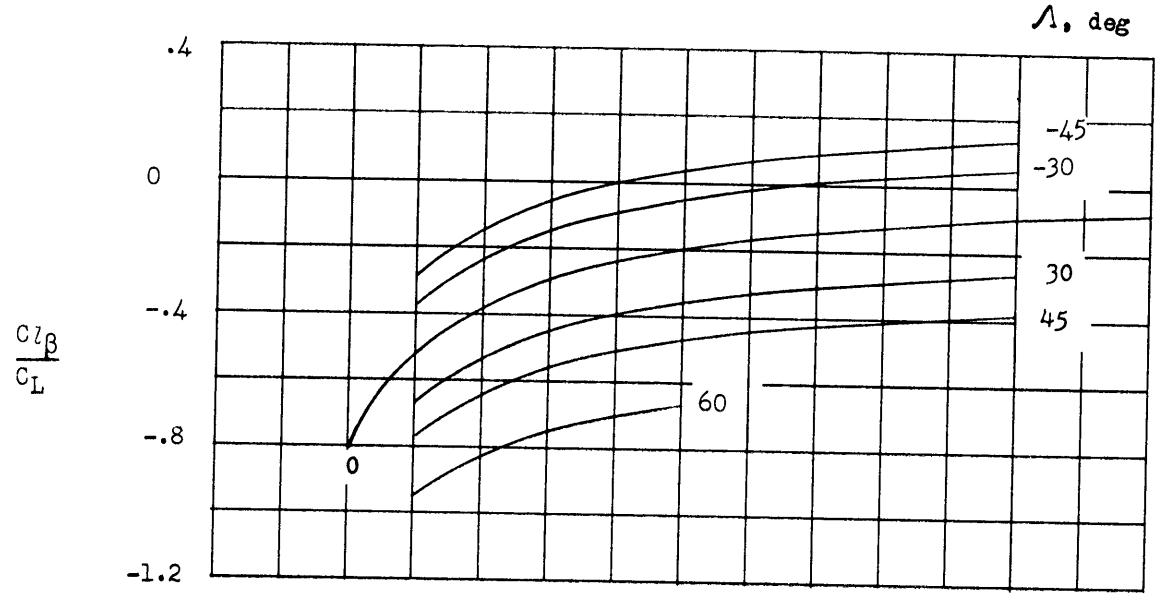

(c) M = 0.6.

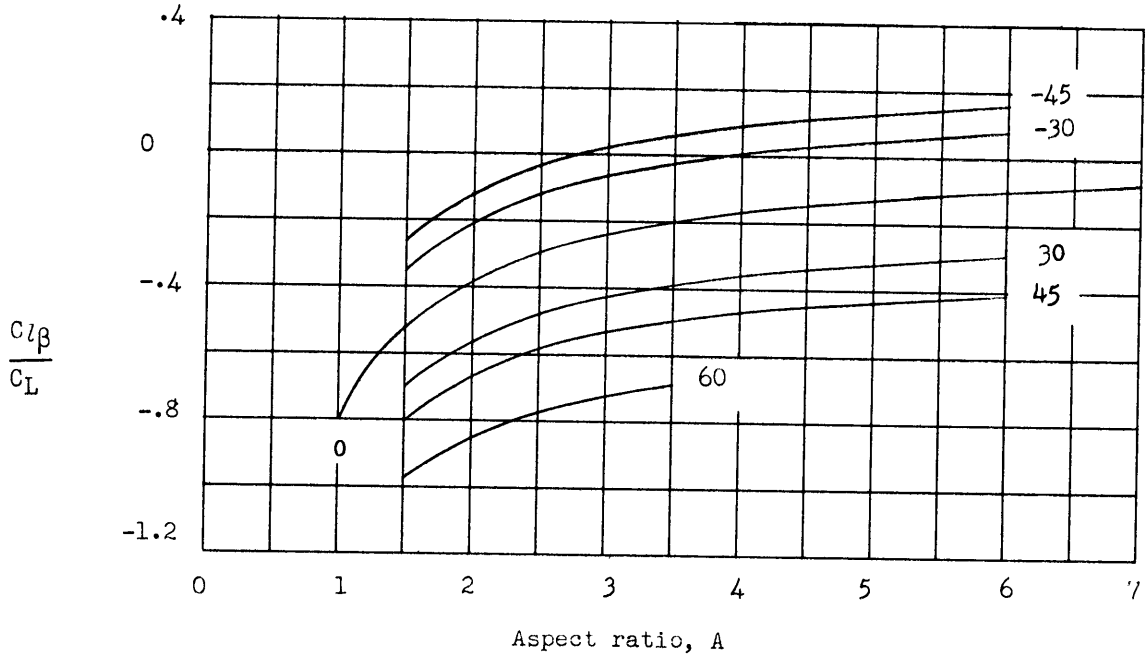

(d) M = 0.8.

Figure 22.- λ = 1.5. Continued.

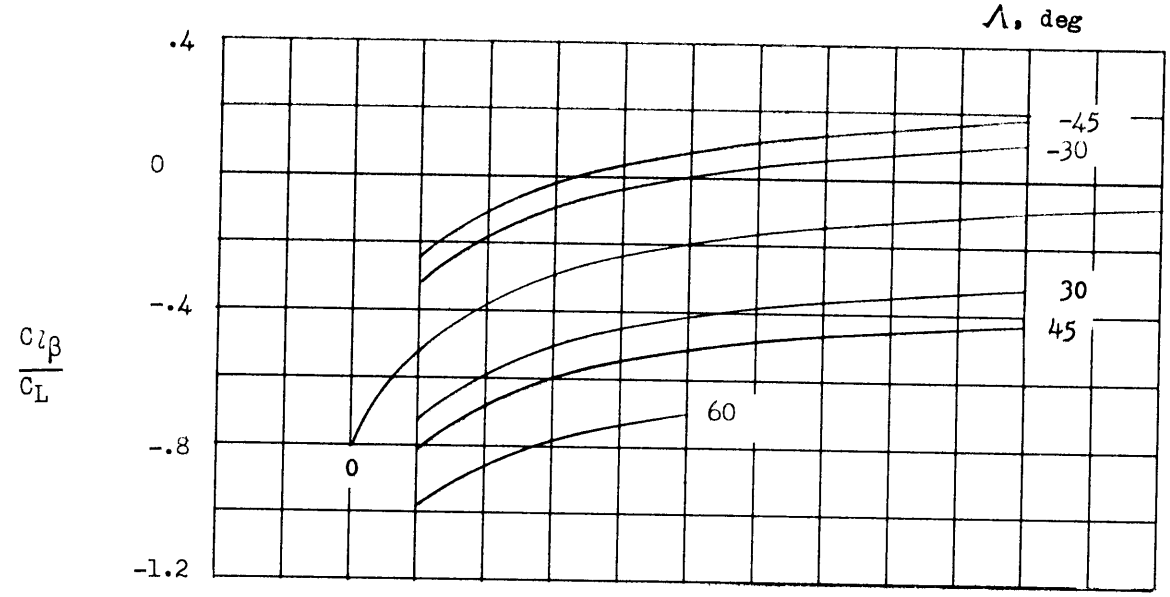

(e) M = 0.9.

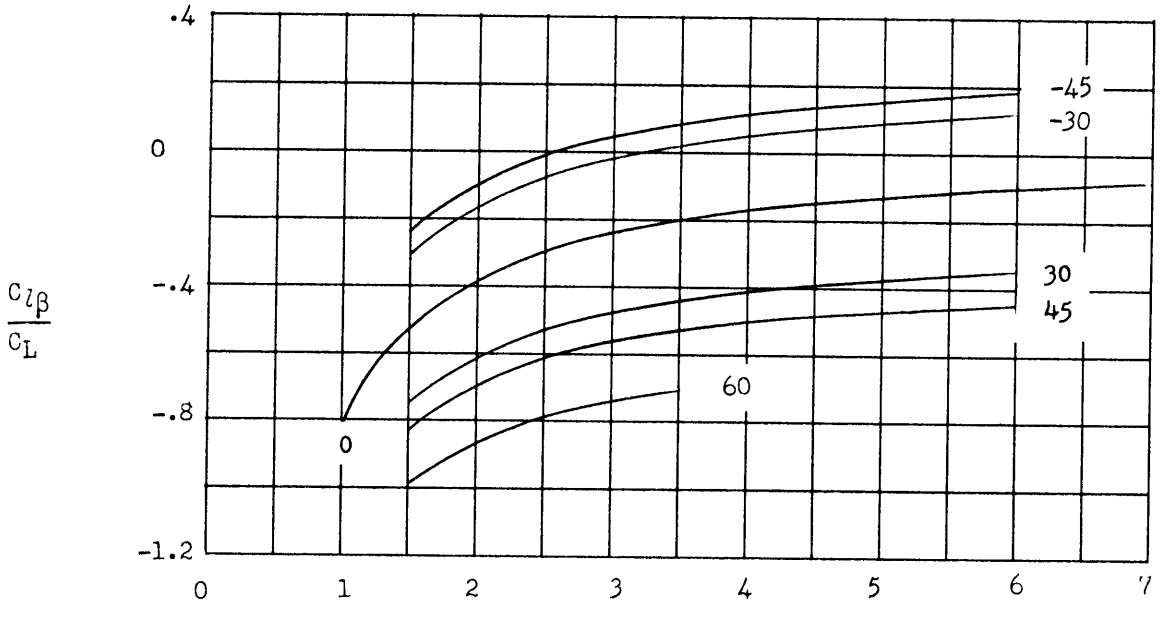

(f) M = 0.95.

Figure 22.- λ = 1.5. Concluded.

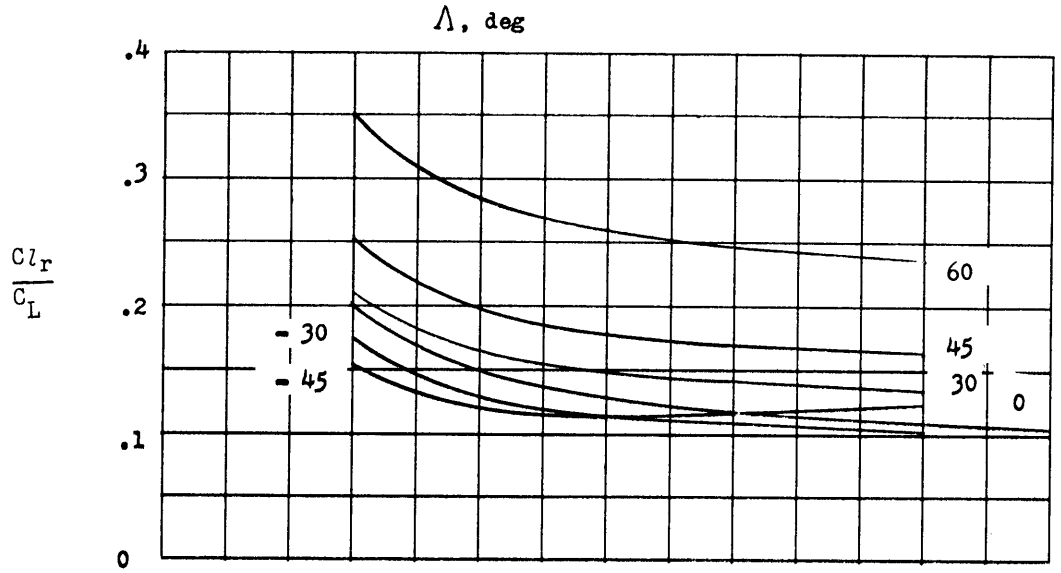

(a) M = 0.

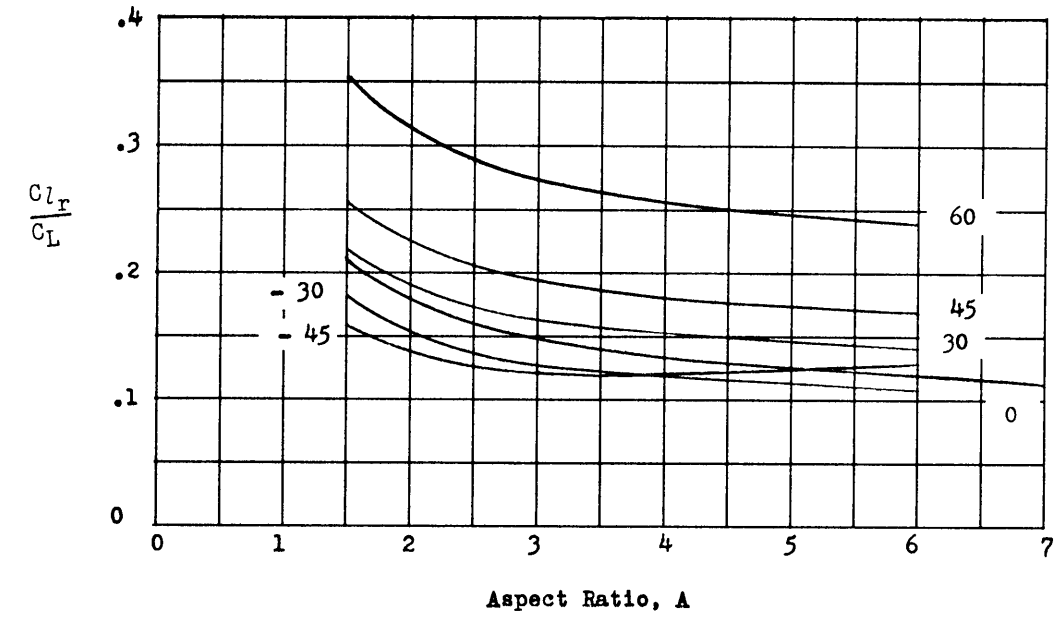

(b) M = 0.4.

Figure 23.- Variation of $\frac{Cl_r}{C_L}$ with aspect ratio, sweep, and Mach number. $\bar{X}^* = 0$, $\lambda = 0$.

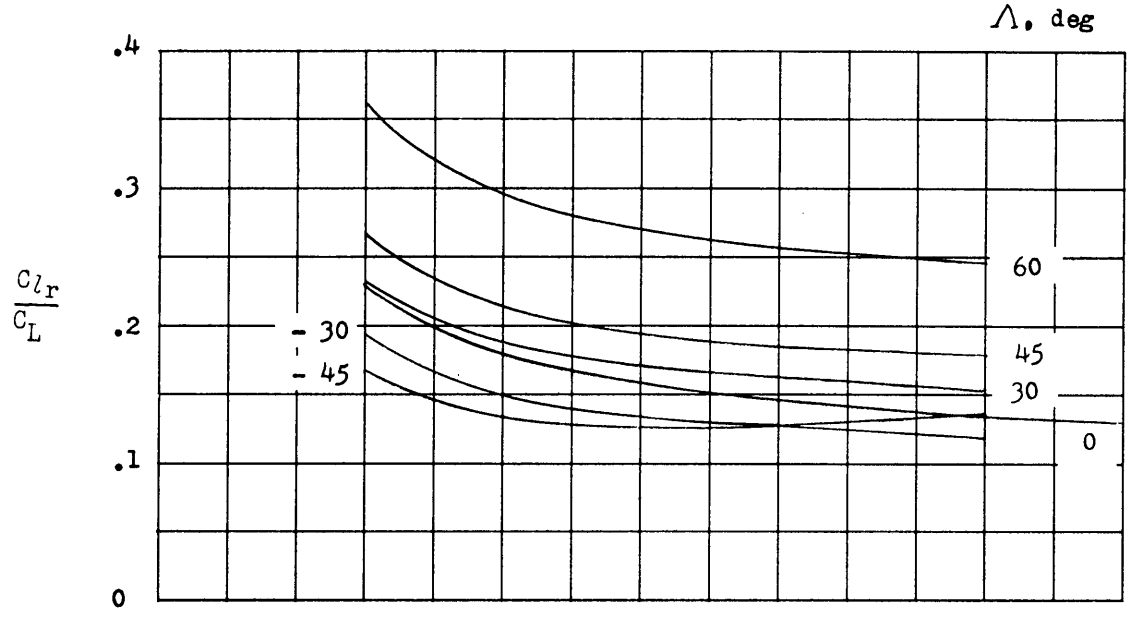

(c) M = 0.6.

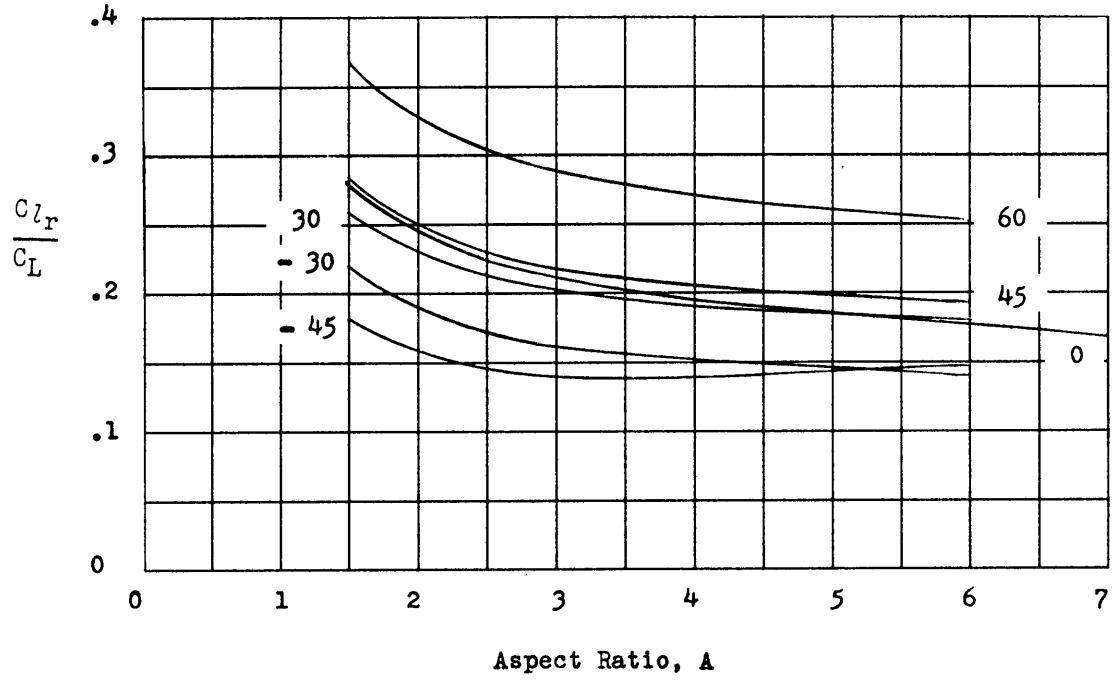

(d) M = 0.8.

Figure 23.- λ = 0. Continued.

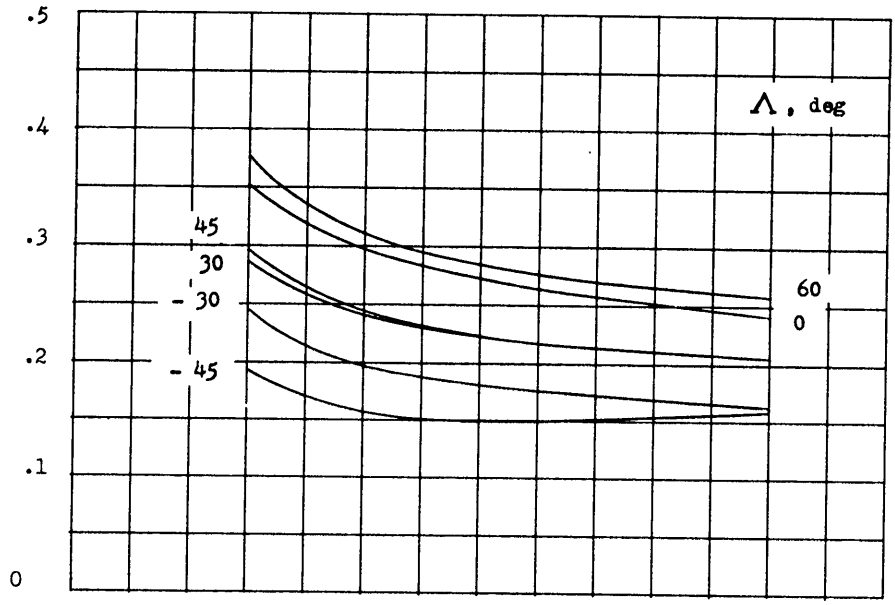

$\frac{C_{l_r}}{C_L}$

(e) M = 0.9.

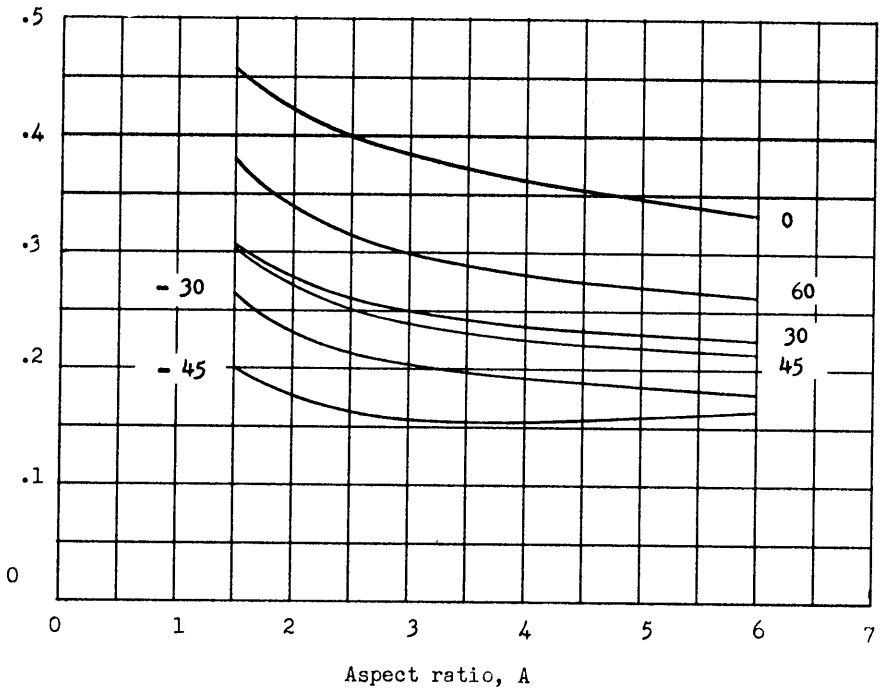

$\frac{C_{l_r}}{C_L}$

(f) M = 0.95.

Figure 23.- λ = 0. Concluded.

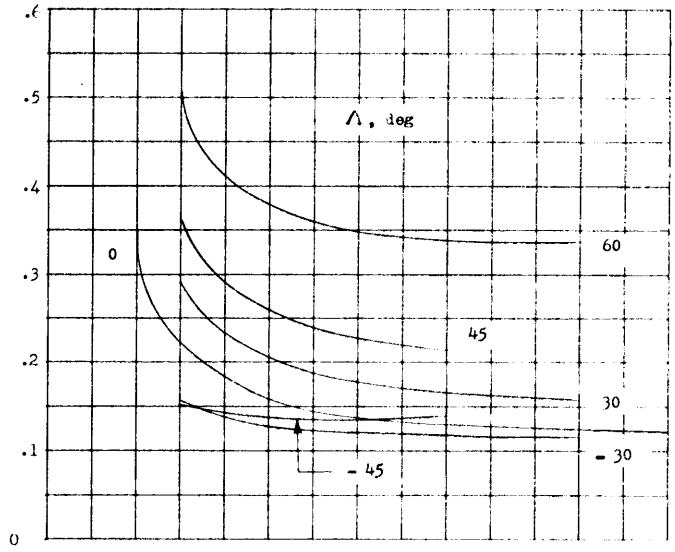

(a) M = 0.

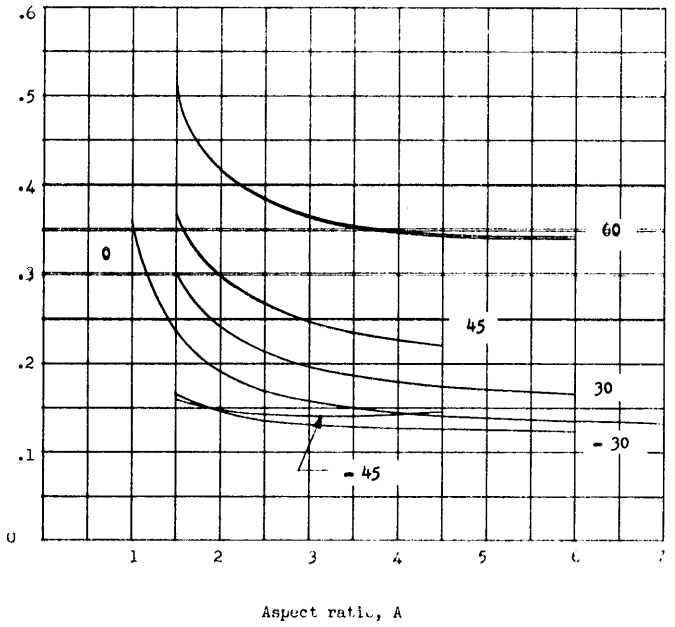

(b) M = 0.4.

Figure 24.- Variation of $\frac{C_{l_r}}{C_L}$ with aspect ratio, sweep, and Mach number. $\bar{X}^* = 0$, $\lambda = 0.25$.

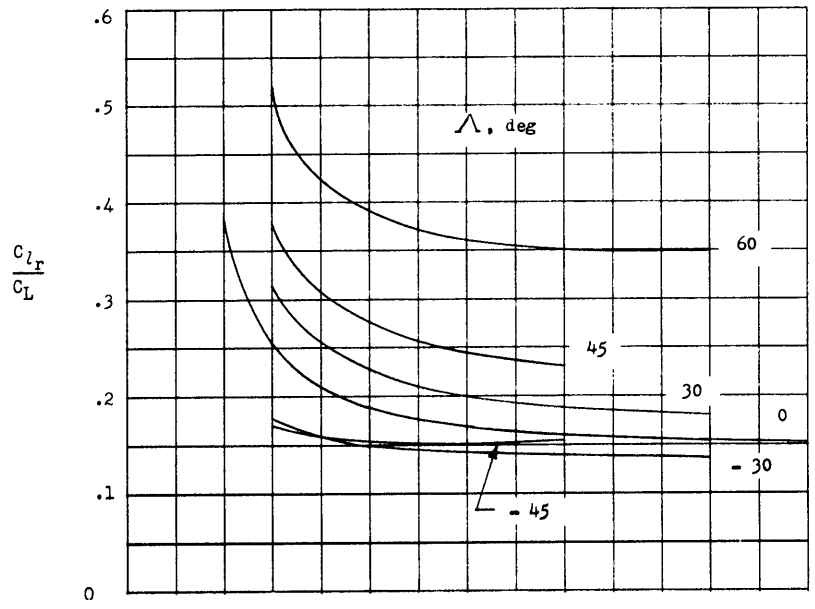

(c) M = 0.6.

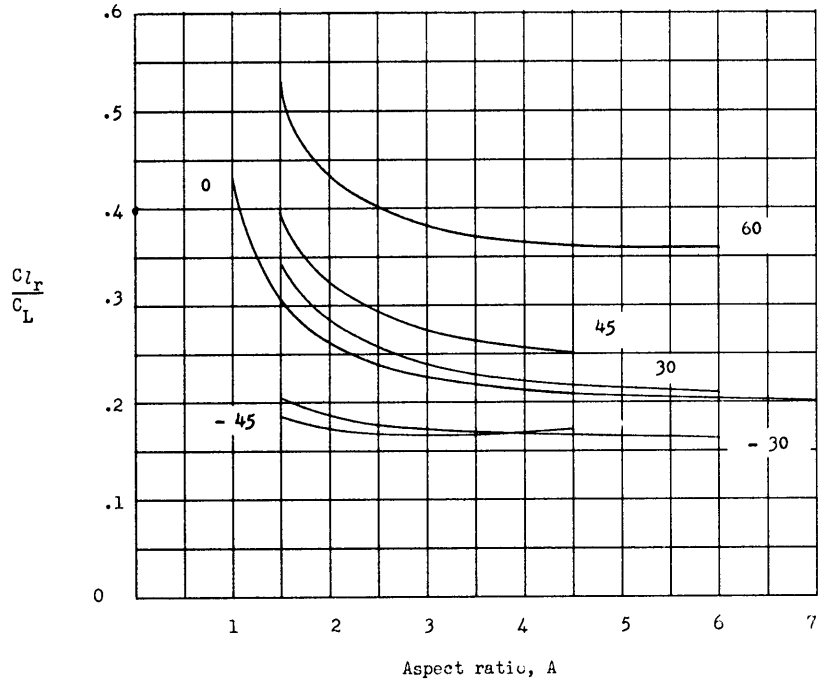

(d) M = 0.8.

Figure 24.- λ = 0.25. Continued.

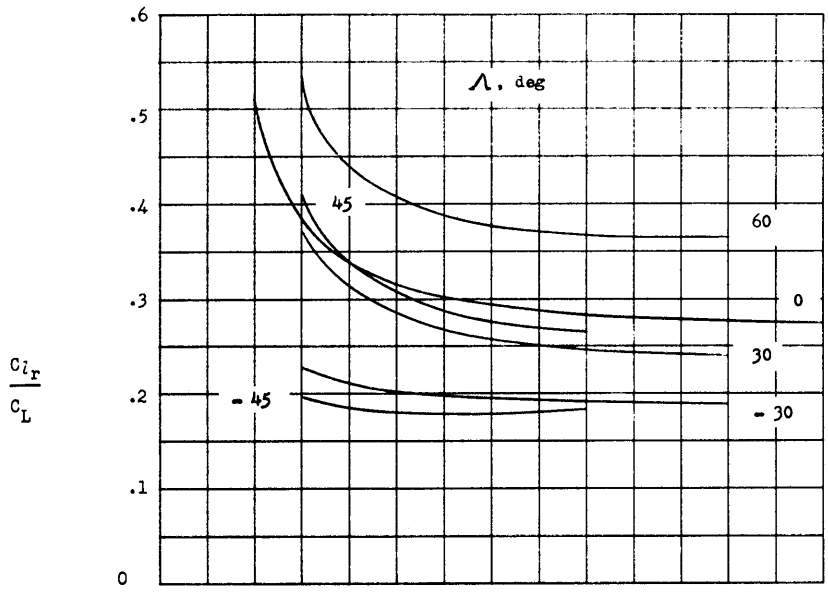

(e) M = 0.9.

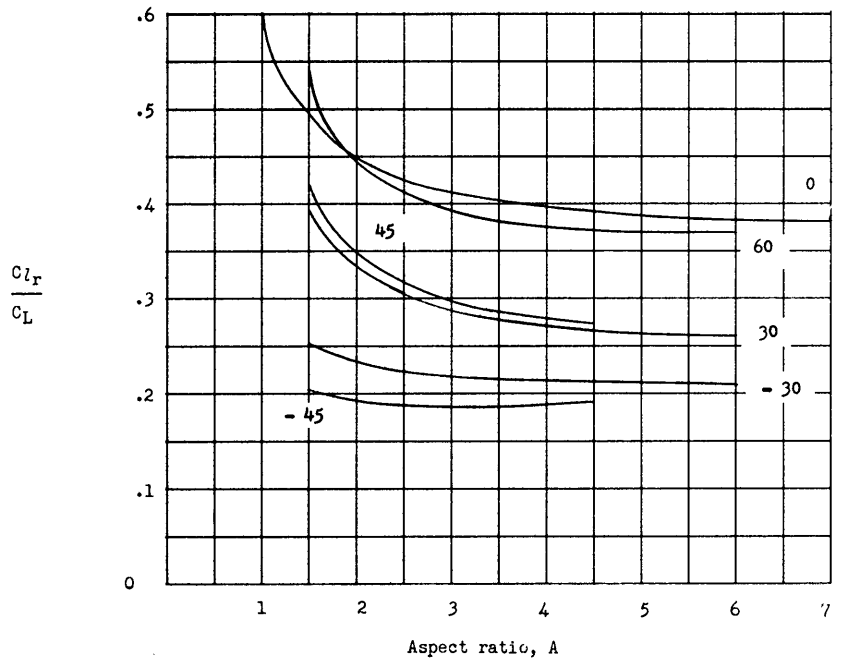

(f) M = 0.95.

Figure 24.- λ = 0.25. Concluded.

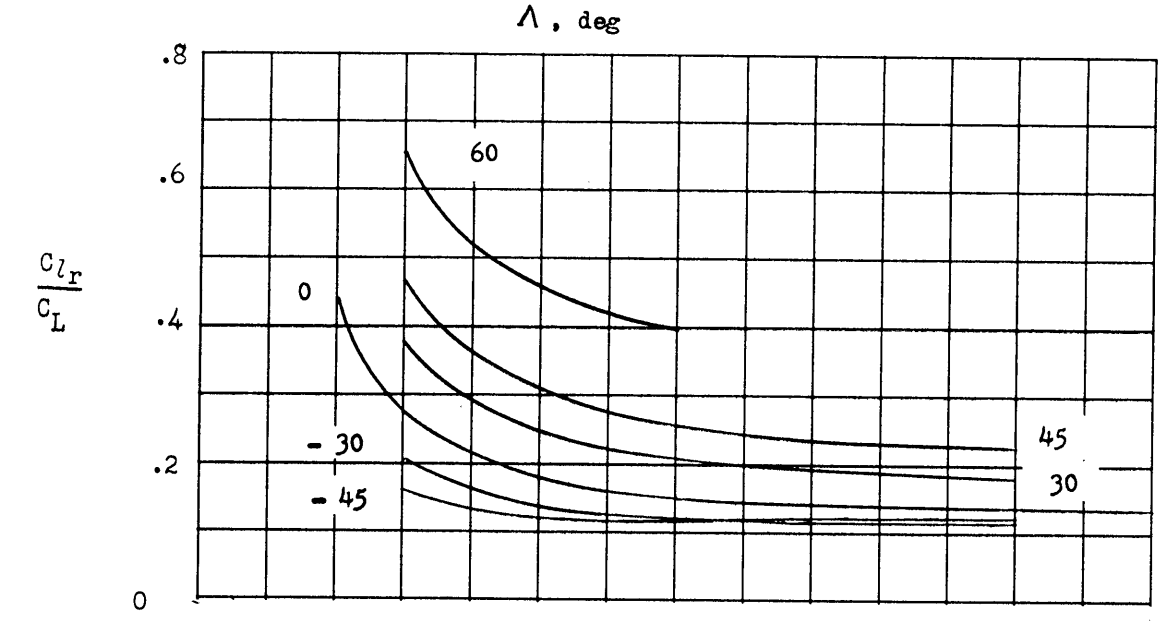

(a) M = 0.

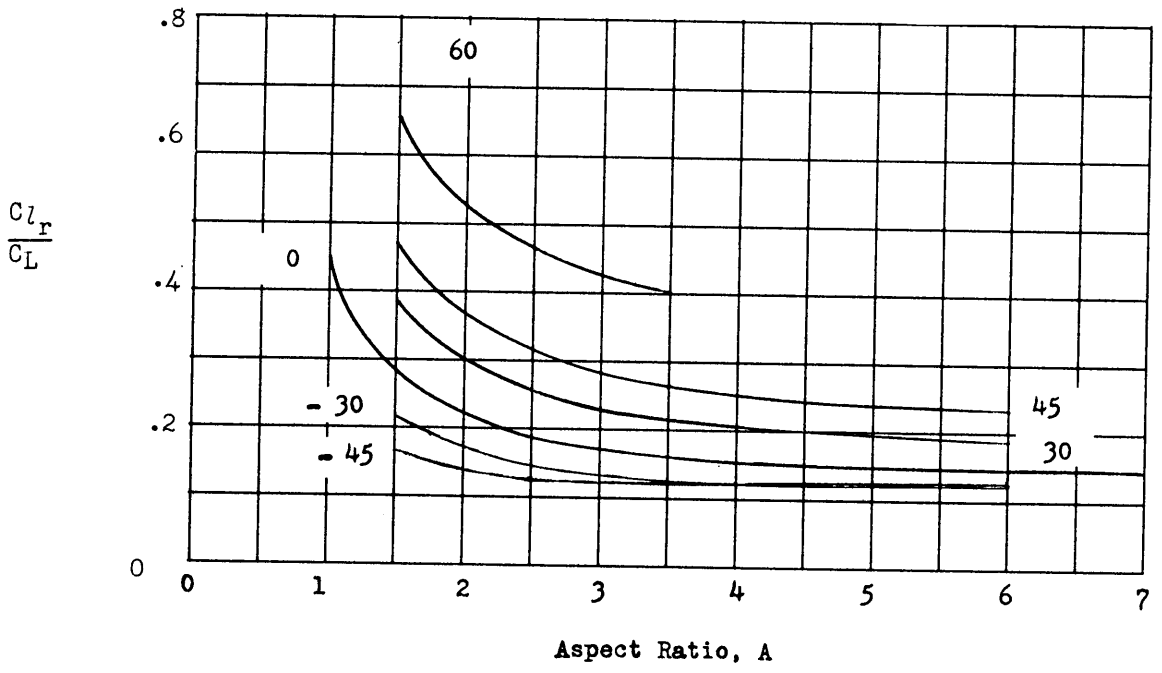

(b) M = 0.4.

Figure 25.- Variation of $\frac{C_{l_r}}{C_L}$ with aspect ratio, sweep, and Mach number. $\bar{X}^* = 0$, $\lambda = 0.50$.

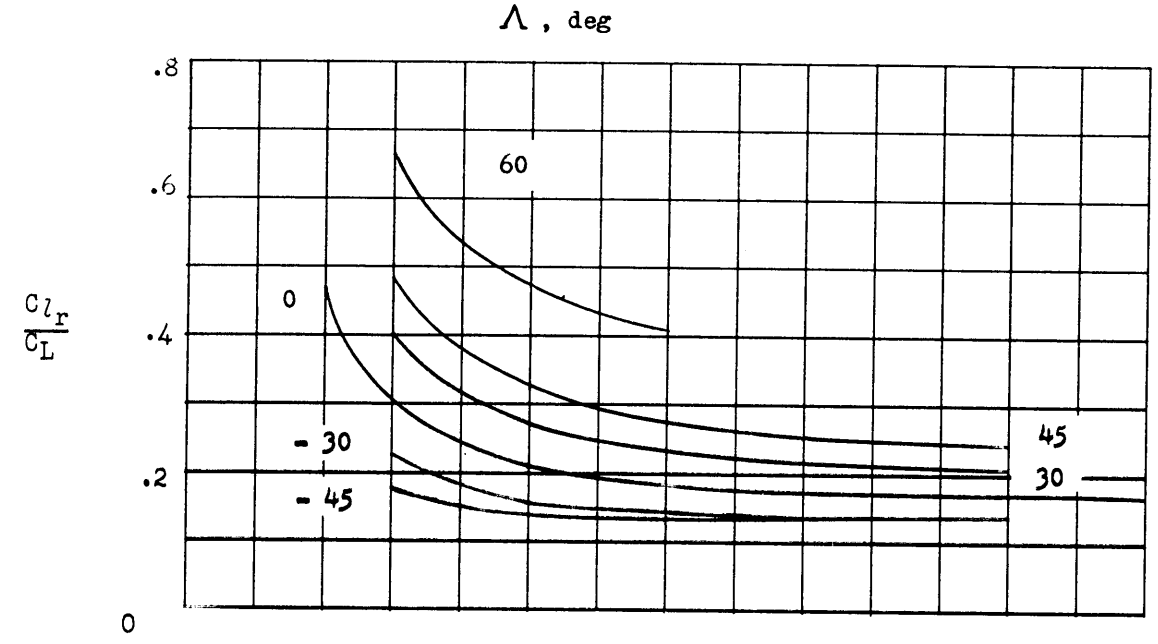

(c) M = 0.6.

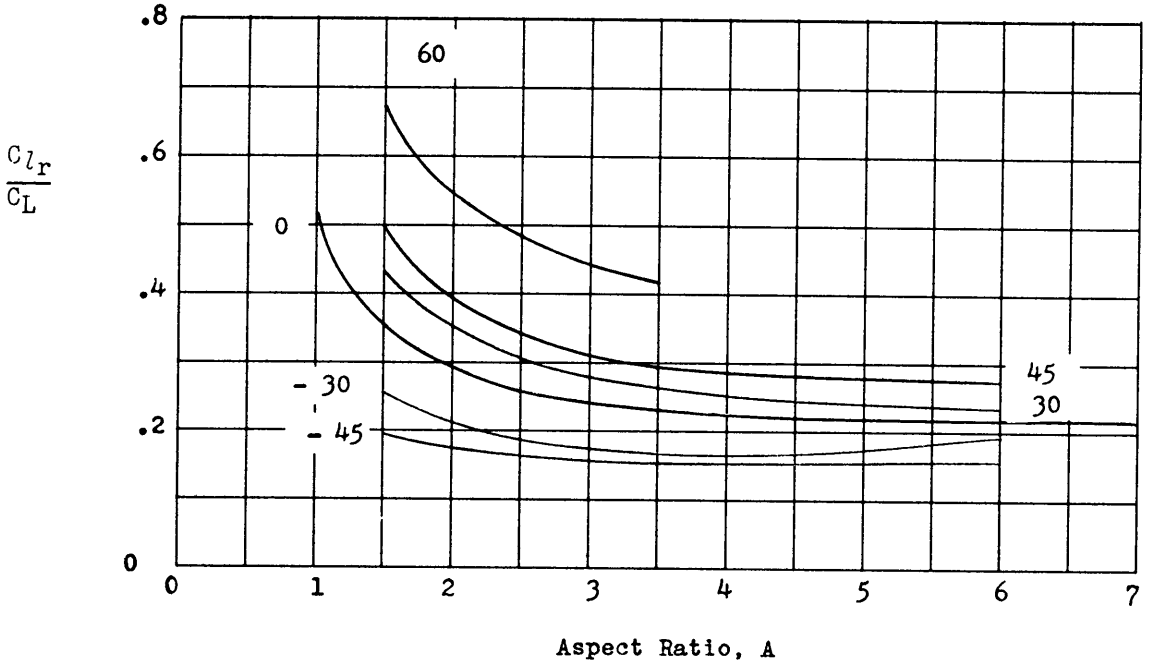

(d) M = 0.8.

Figure 25.- λ = 0.50. Continued.

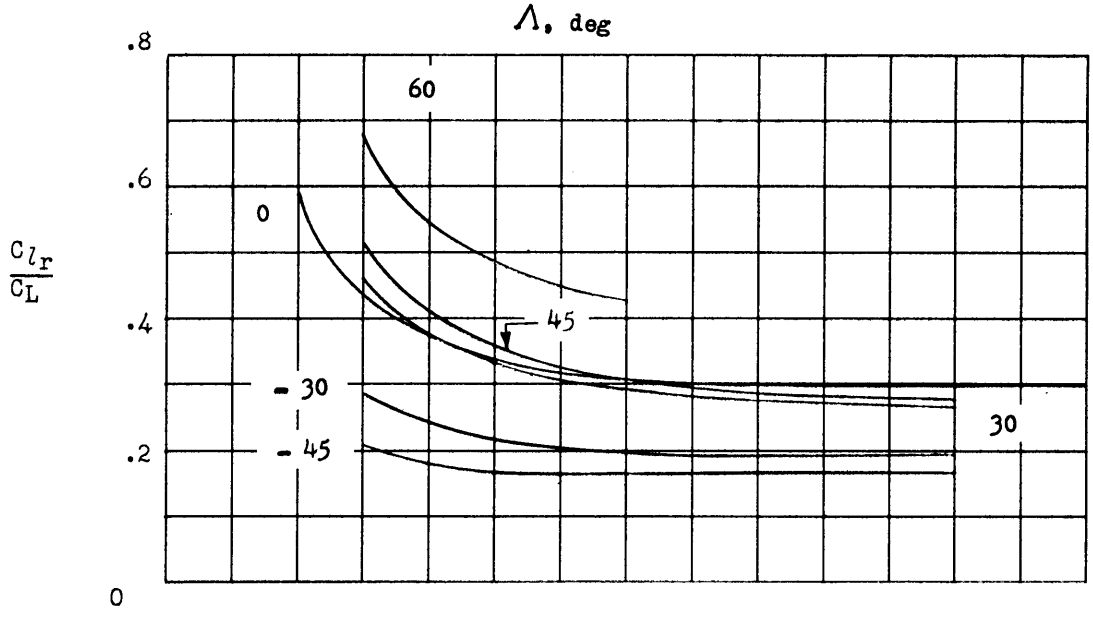

(e) M = 0.9.

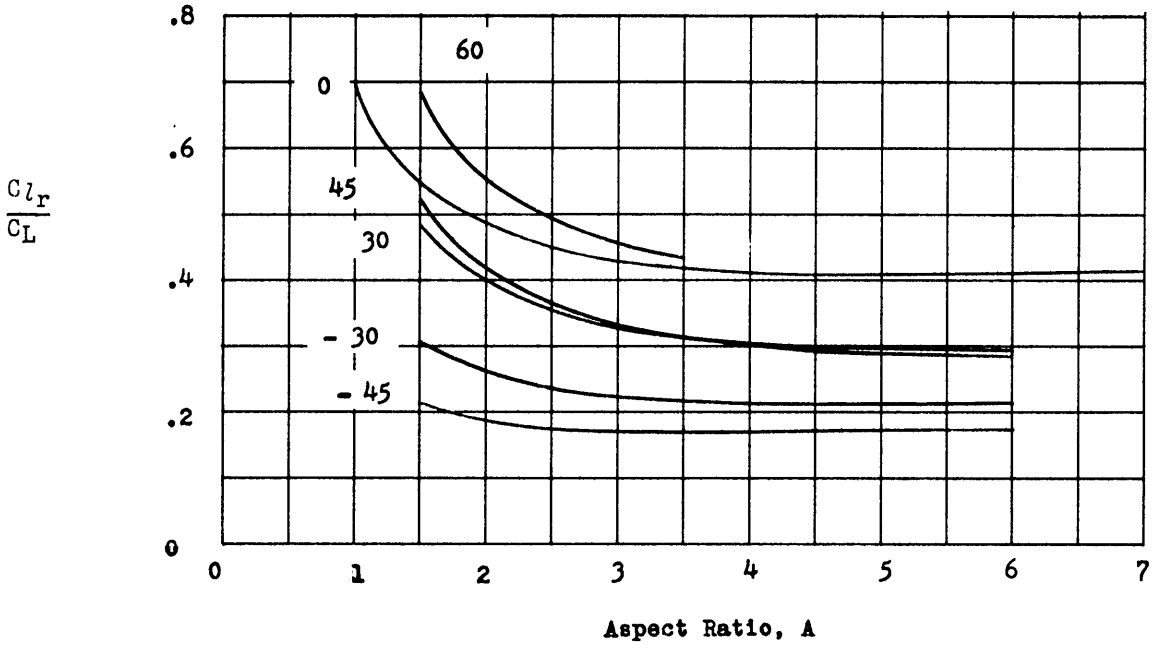

(f) M = 0.95.

Figure 25.- λ = 0.50. Concluded.

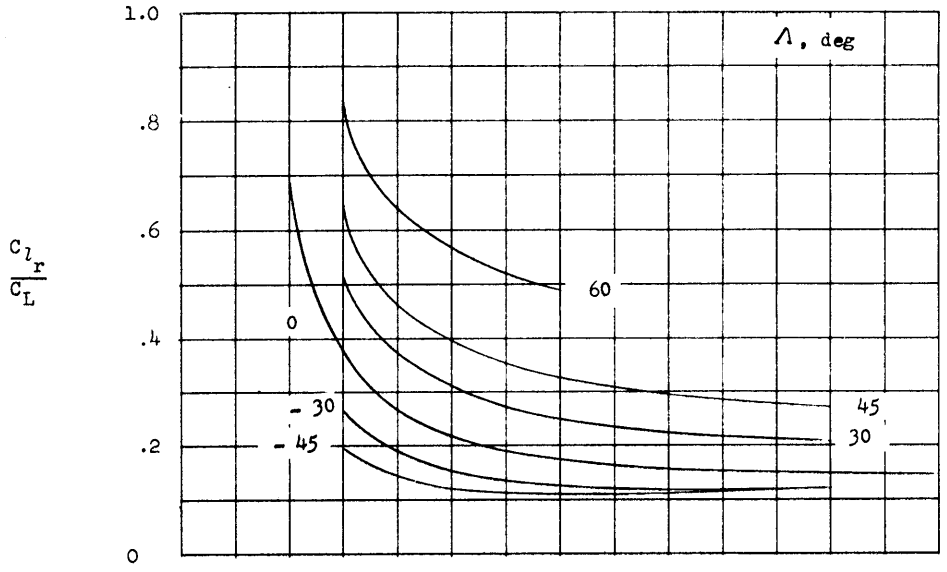

(a) M = 0.

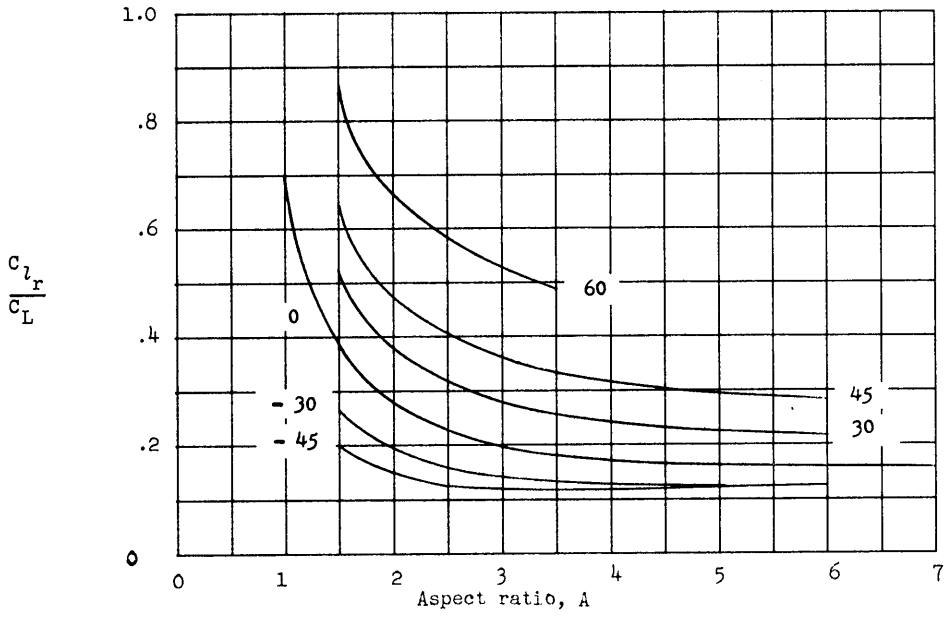

(b) M = 0.4.

Figure 26.- Variation of $\frac{C_{l_r}}{C_L}$ with aspect ratio, sweep, and Mach number. $\bar{X}^* = 0$, $\lambda = 1.0$.

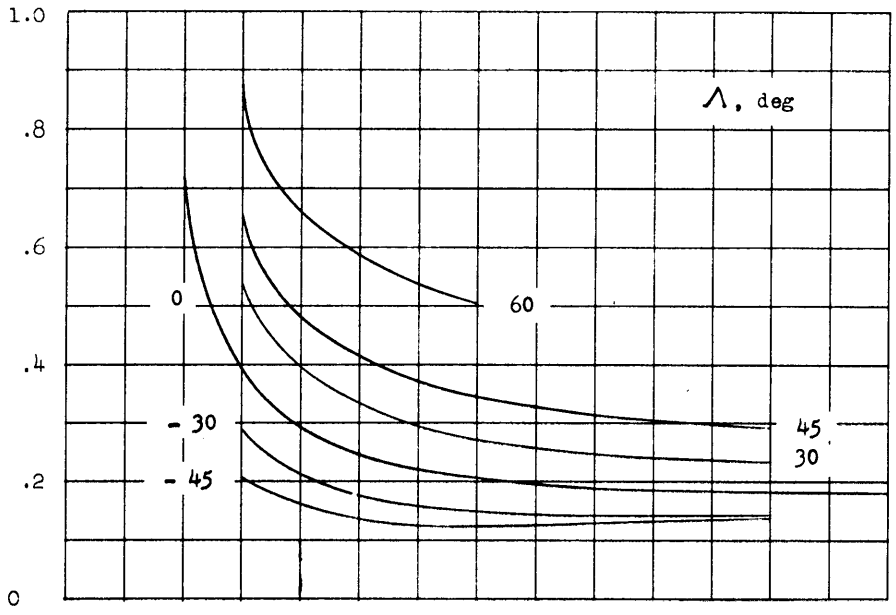

(c) M = 0.6.

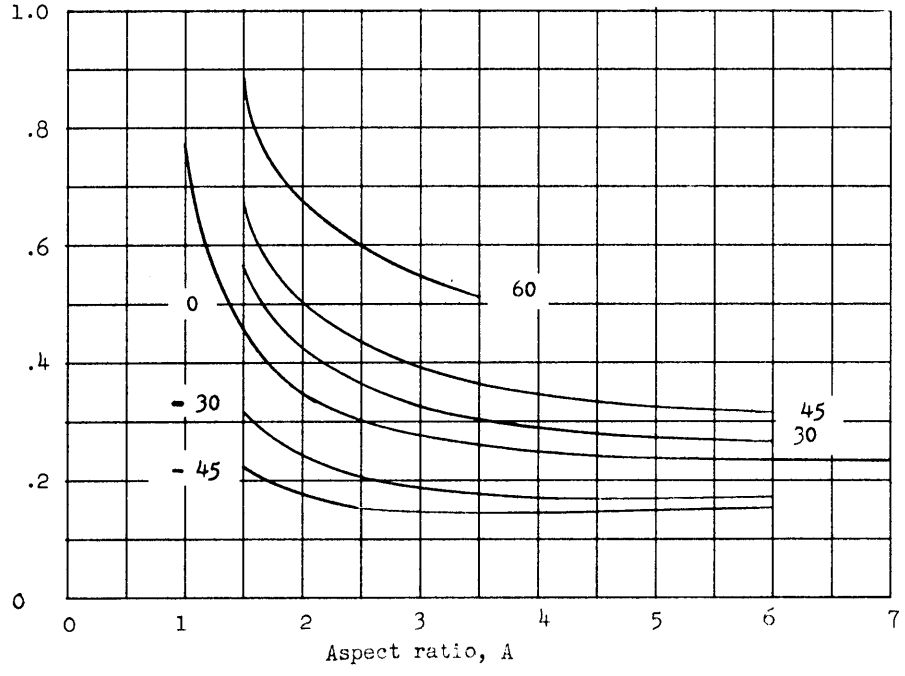

(d) M = 0.8.

Figure 26.- λ = 1.0. Continued.

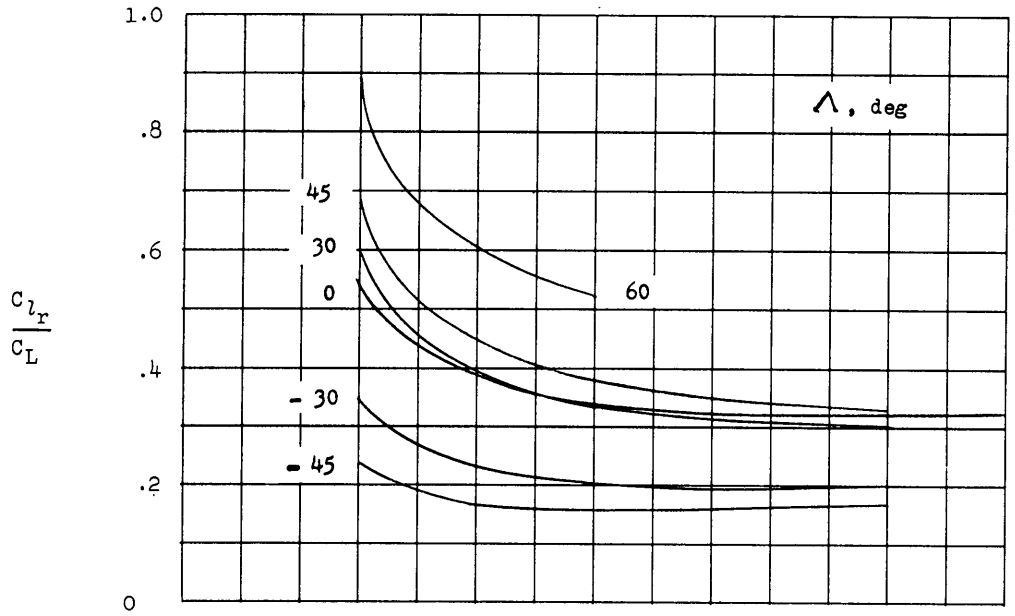

(e) M = 0.9.

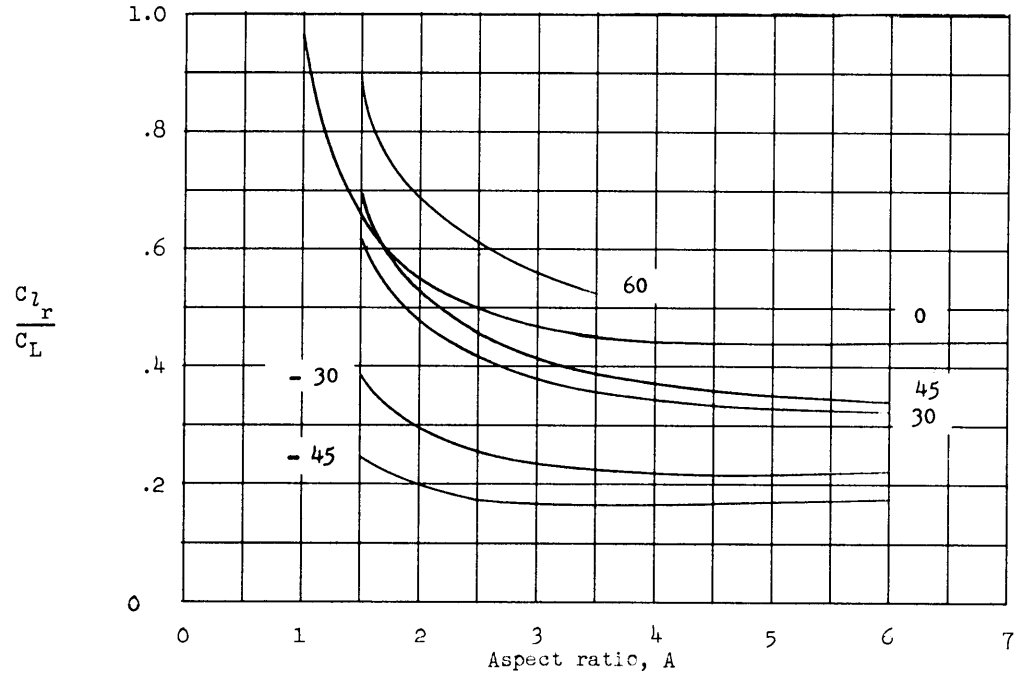

(f) M = 0.95.

Figure 26.- λ = 1.0. Concluded.

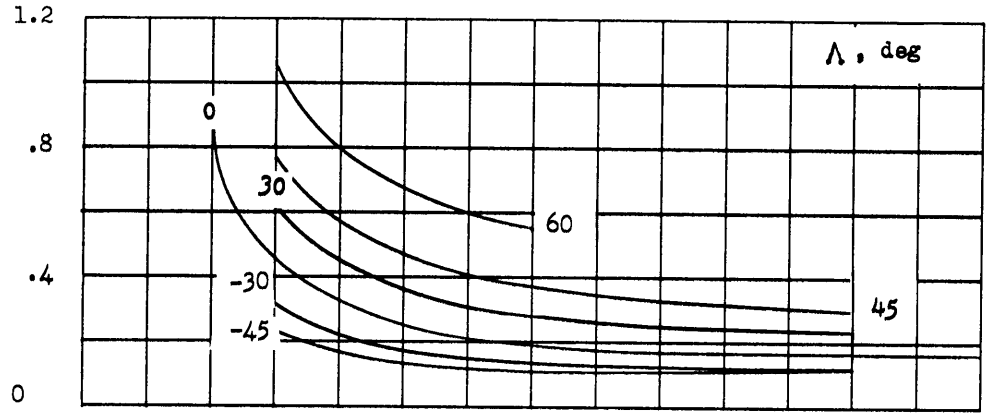

(a) M = 0.

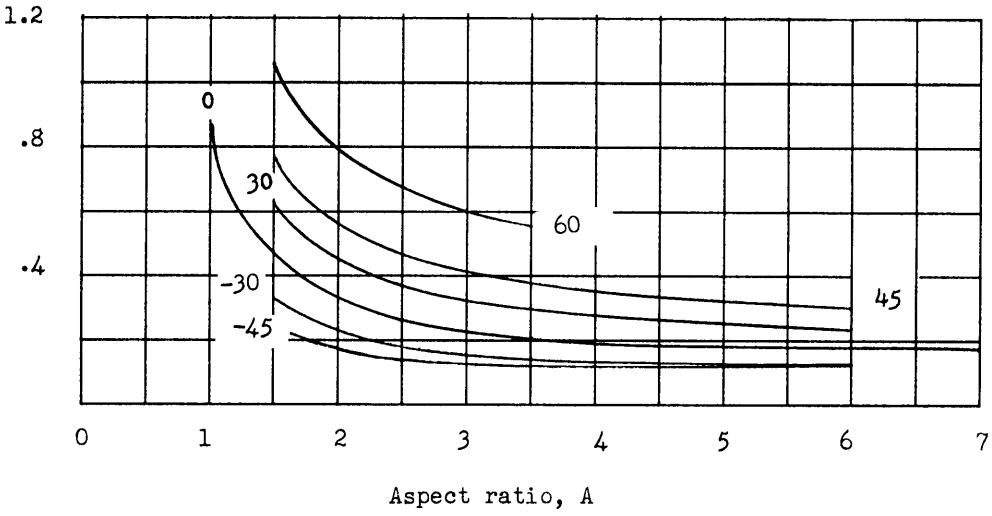

(b) M = 0.4.

Figure 27.- Variation of $\frac{C_{l_r}}{C_L}$ with aspect ratio, sweep, and Mach number. $\bar{X}^* = 0$, $\lambda = 1.5$.

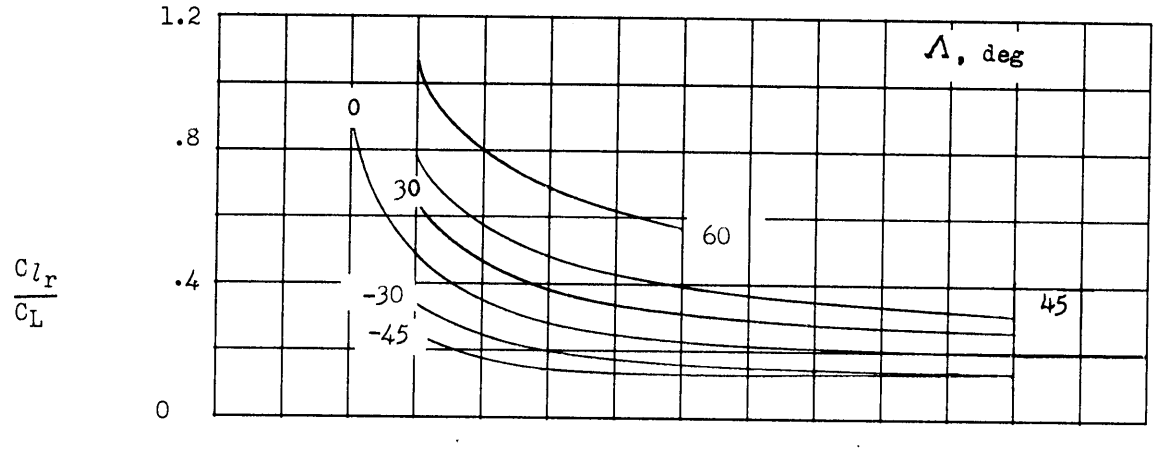

(c) M = 0.6.

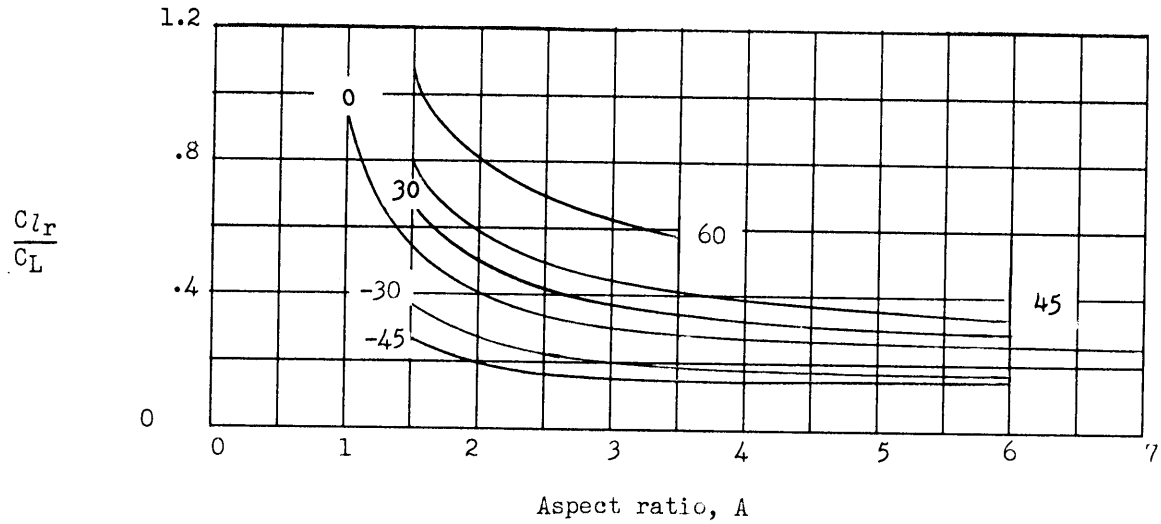

(d) M = 0.8.

Figure 27.- λ = 1.5. Continued.

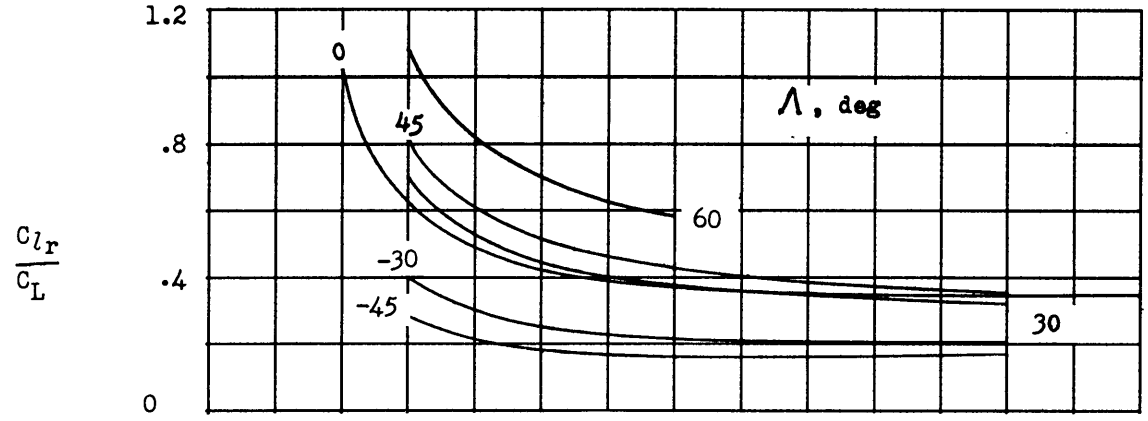

(e) M = 0.9.

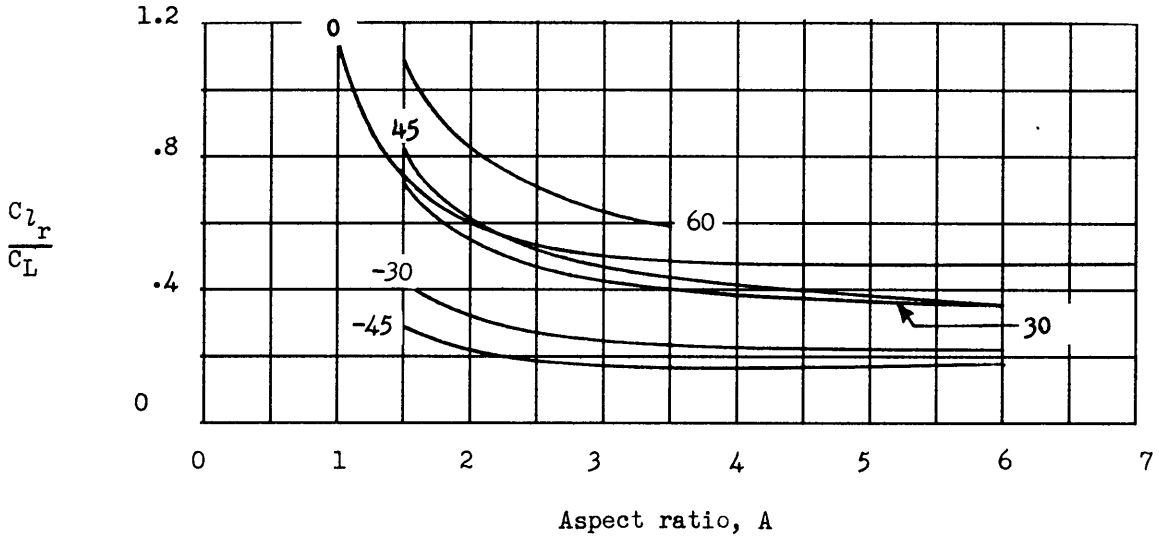

(f) M = 0.95.

Figure 27.- λ = 1.5. Concluded.

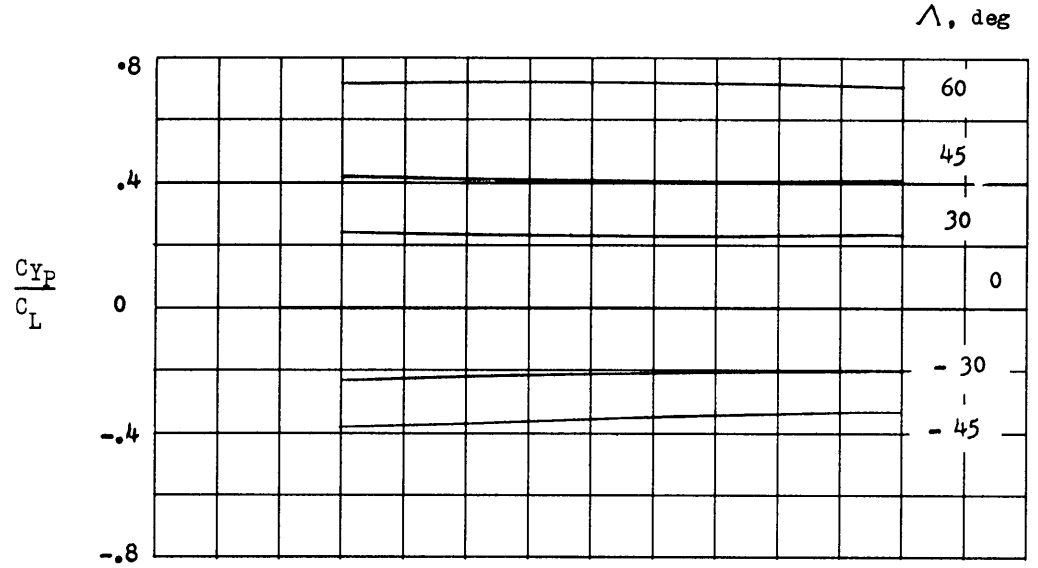

(a) M = 0.

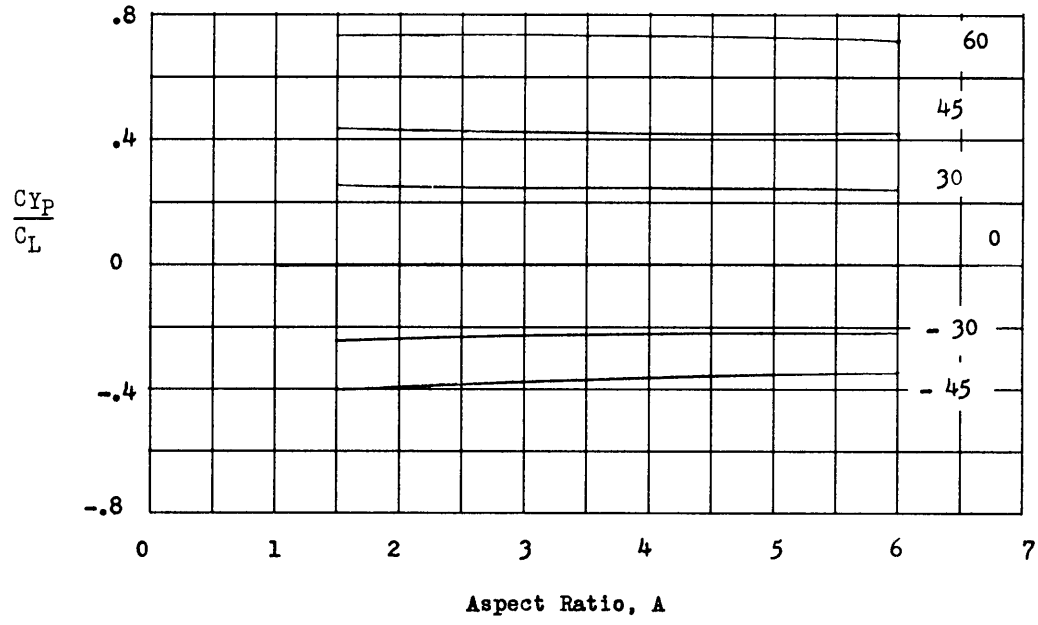

(b) M = 0.4.

Figure 28.- Variation of $\frac{C_{Y_P}}{C_L}$ with aspect ratio, sweep, and Mach number. $\lambda = 0$.

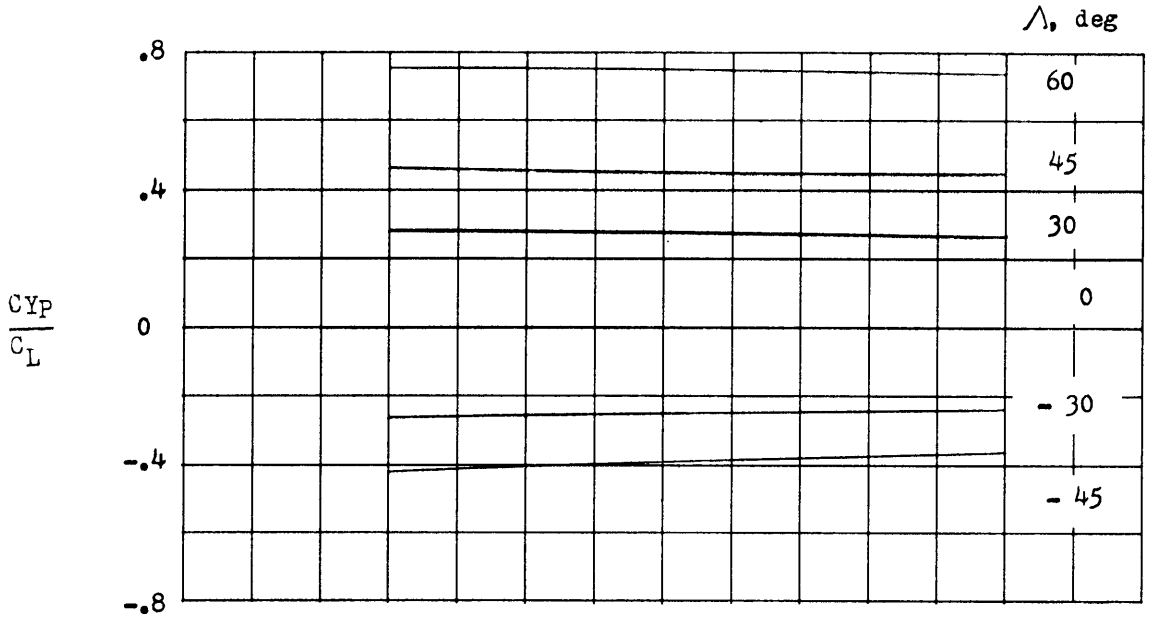

(c) M = 0.6.

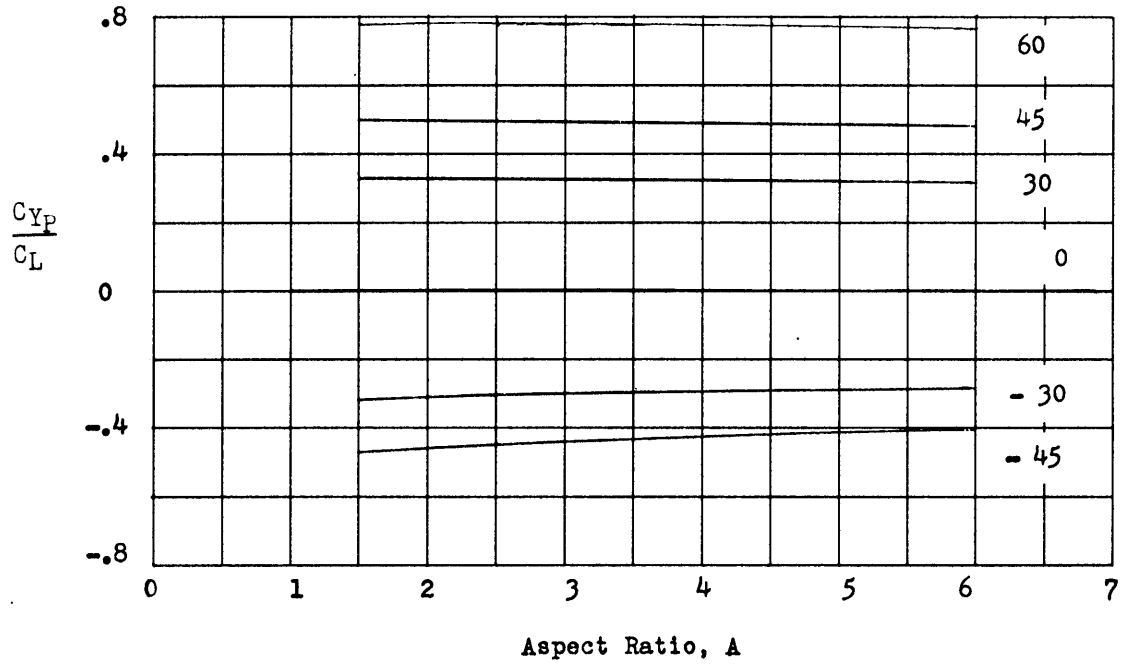

(d) M = 0.8.

Figure 28.- λ = 0. Continued.

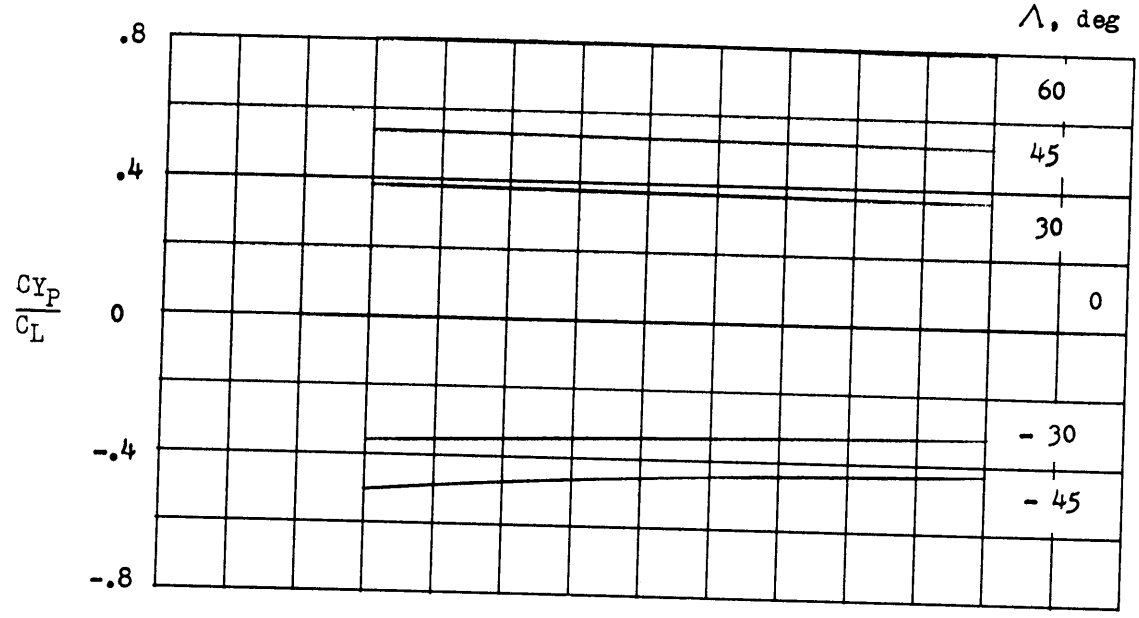

(e) M = 0.9.

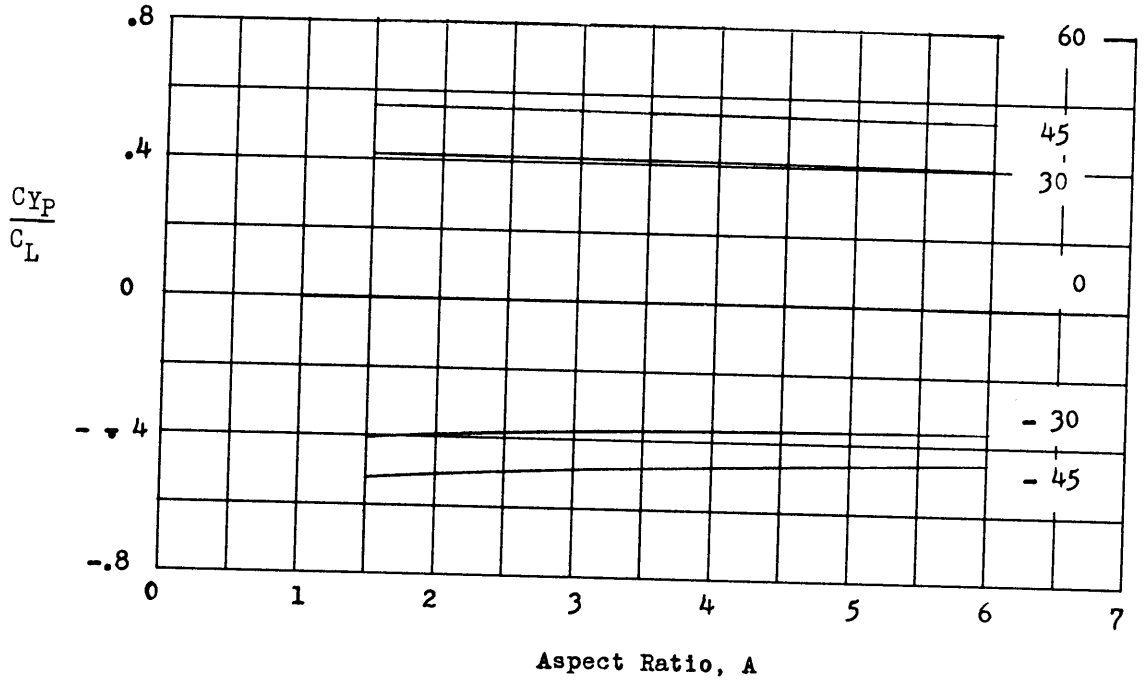

(f) M = 0.95.

Figure 28.- λ = 0. Concluded.

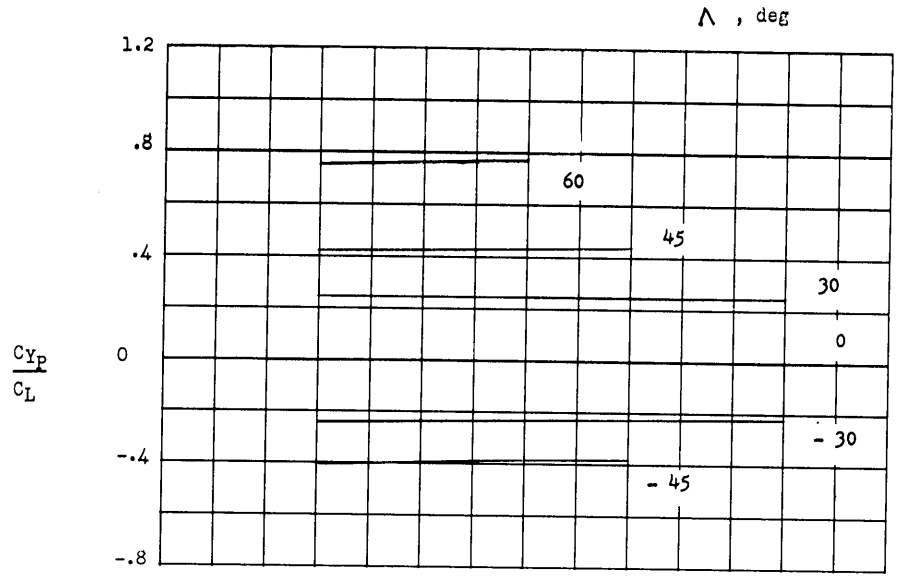

(a) M = 0.

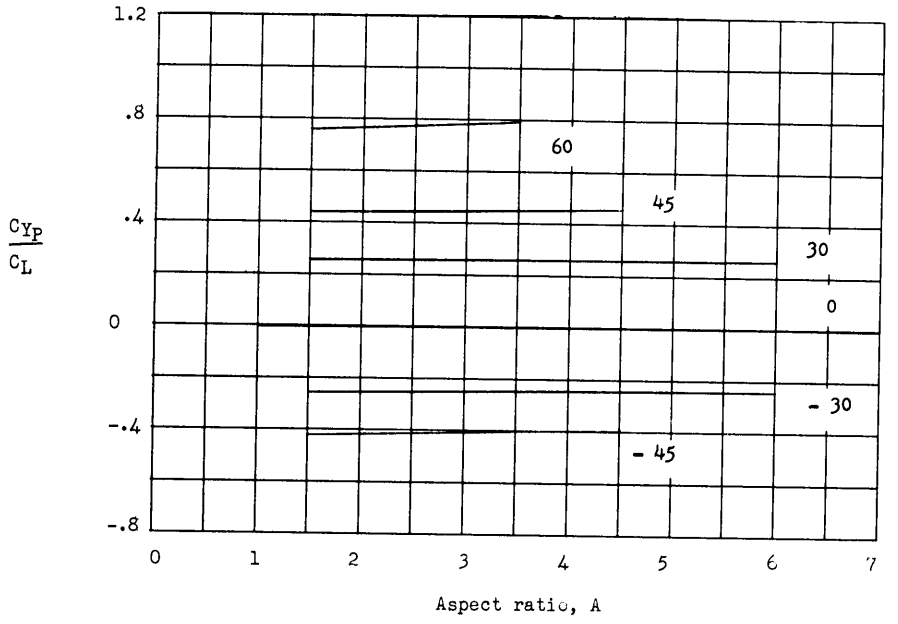

(b) M = 0.4.

Figure 29.- Variation of $\frac{C_{Y_P}}{C_L}$ with aspect ratio, sweep, and Mach number. $\lambda = 0.25$.

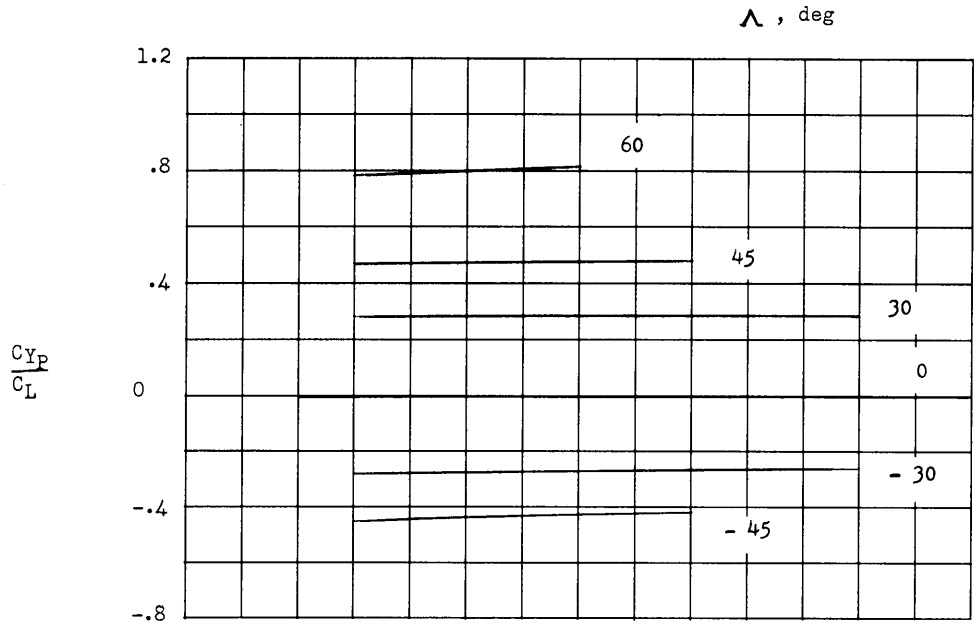

(c) M = 0.6.

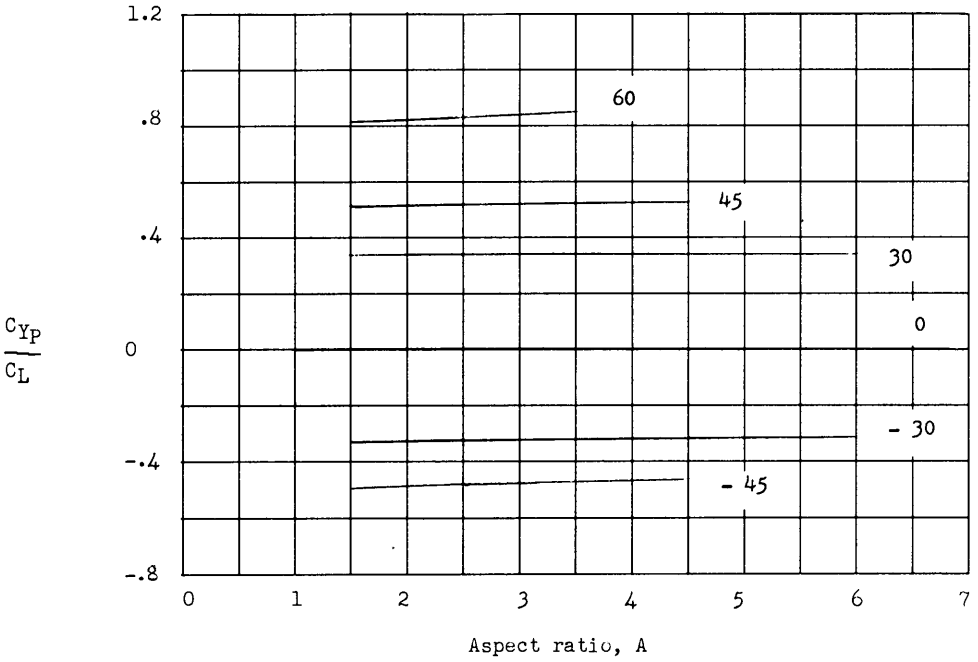

(d) M = 0.8.

Figure 29.- λ = 0.25. Continued.

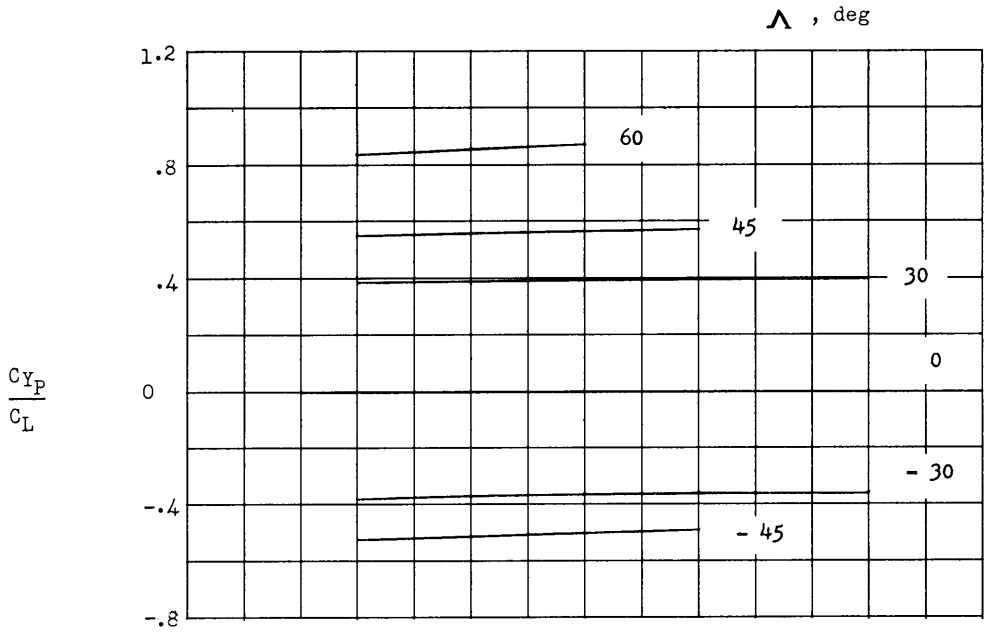

(e) M = 0.9.

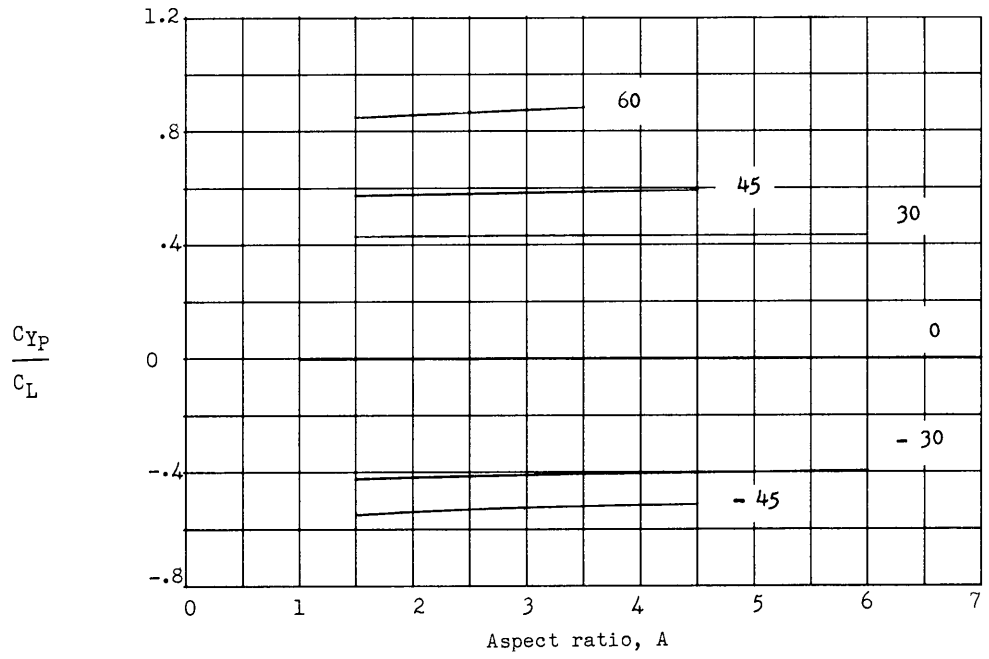

(f) M = 0.95.

Figure 29.- λ = 0.25. Concluded.

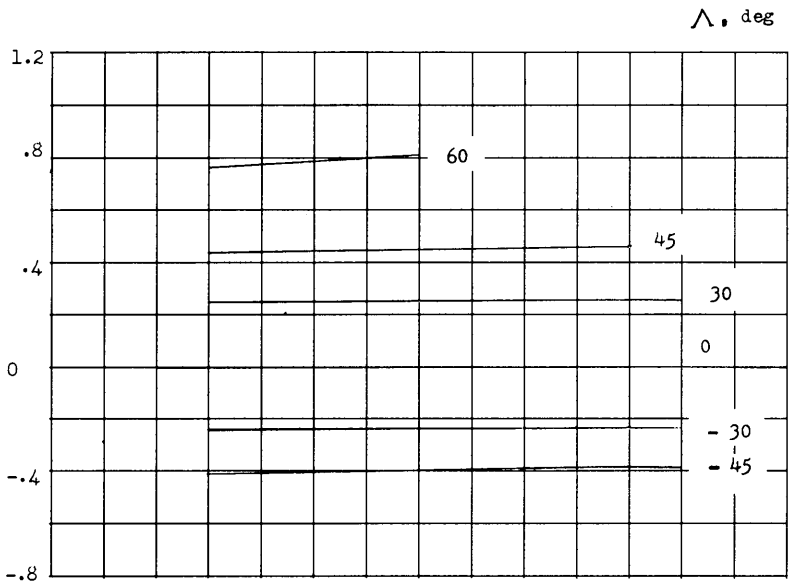

(a) M = 0.

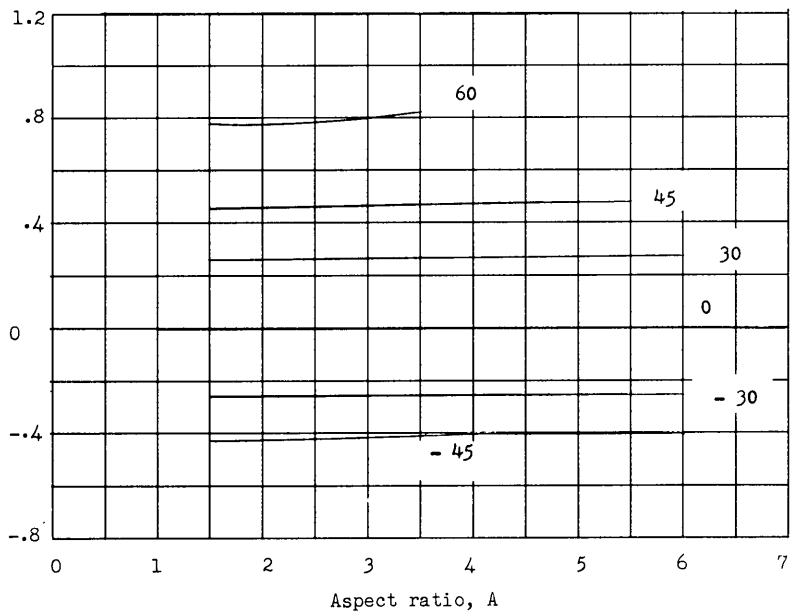

(b) M = 0.4.

Figure 30.- Variation of $\frac{C_{Y_P}}{C_L}$ with aspect ratio, sweep, and Mach number. $\lambda = 0.50$.

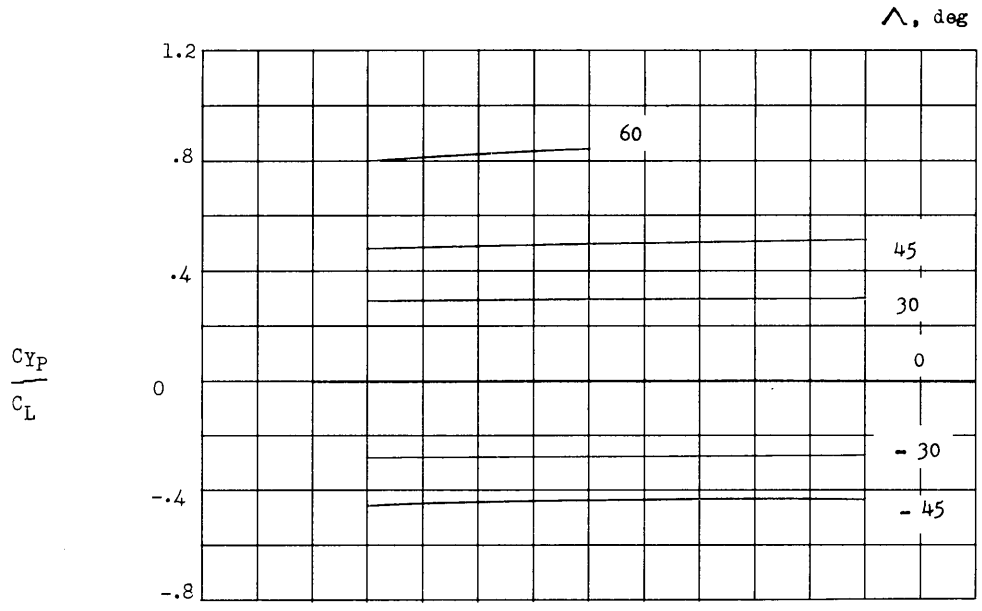

(c) M = 0.6.

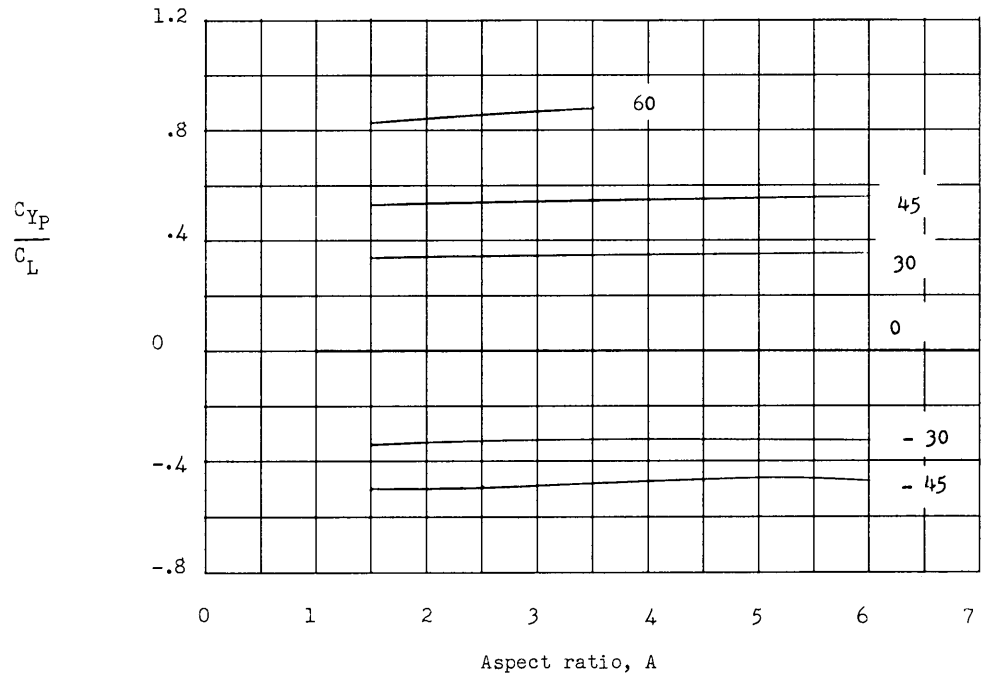

(d) M = 0.8.

Figure 30.- λ = 0.50. Continued.

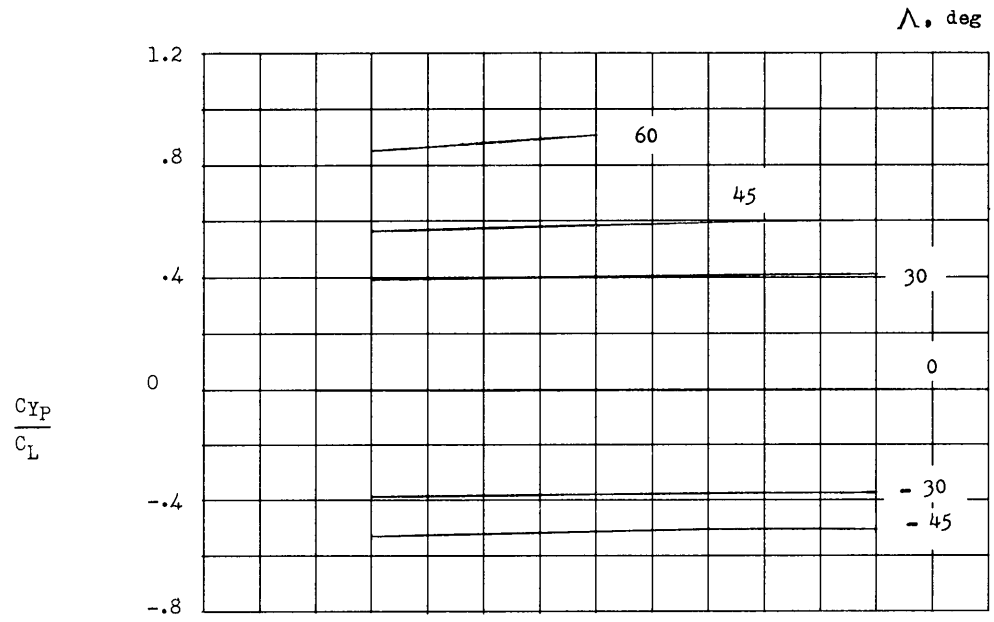

(e) M = 0.9.

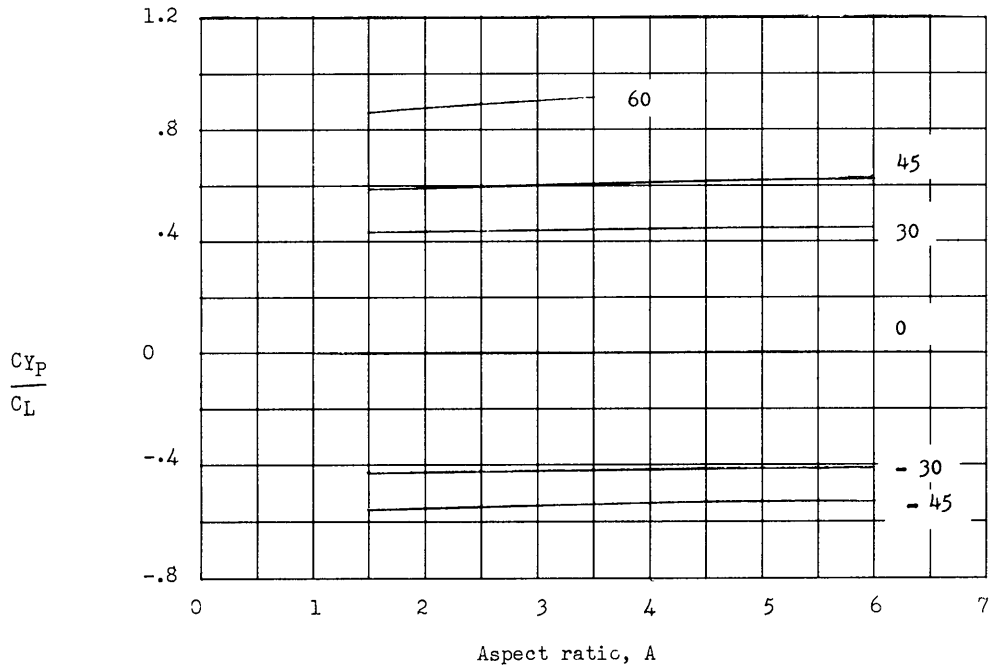

(f) M = 0.95.

Figure 30.- λ = 0.50. Concluded.

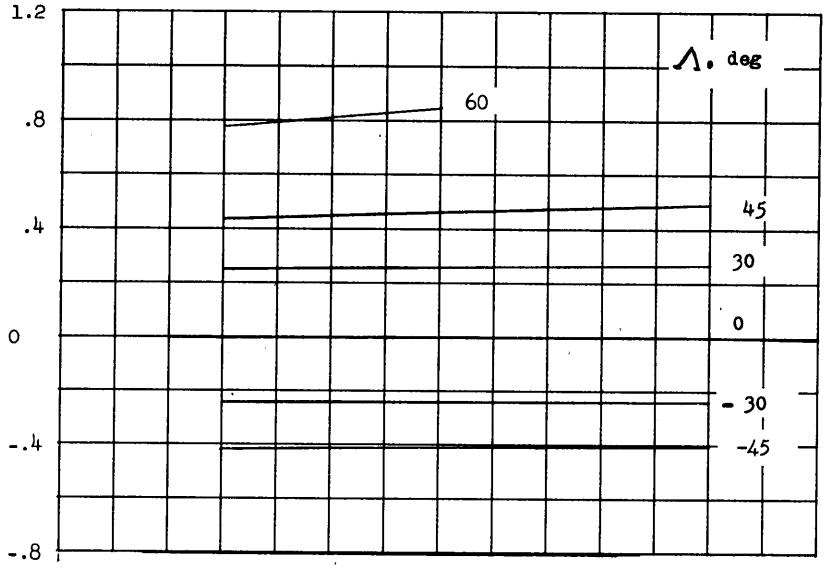

(a) M = 0.

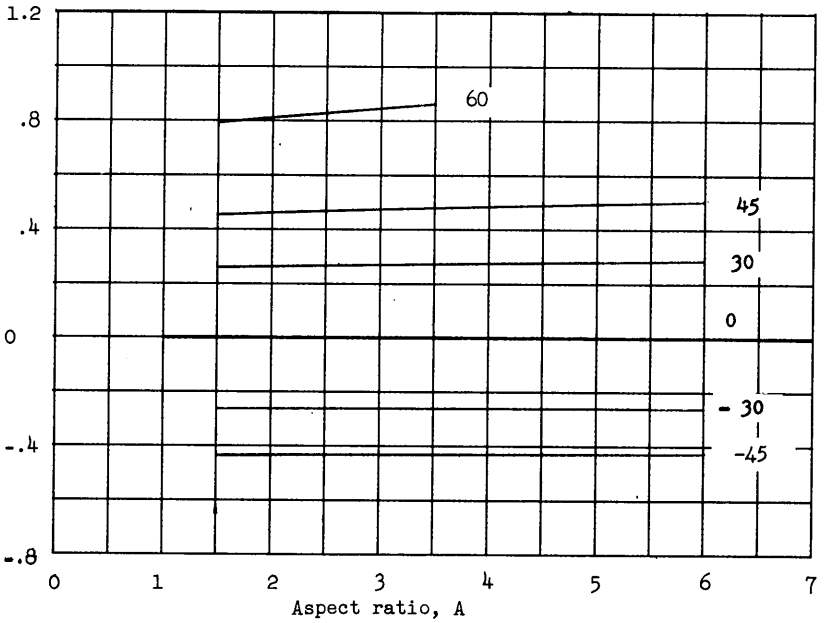

(b) M = 0.4.

Figure 31.- Variation of $\frac{C_{Y_P}}{C_L}$ with aspect ratio, sweep, and Mach number. $\lambda = 1.0$.

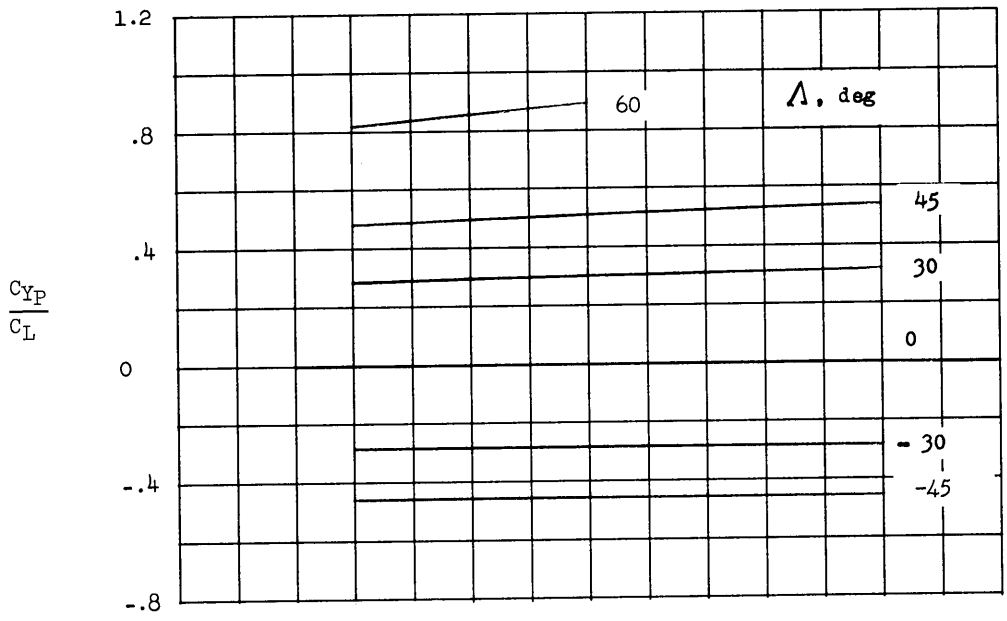

(c) M = 0.6.

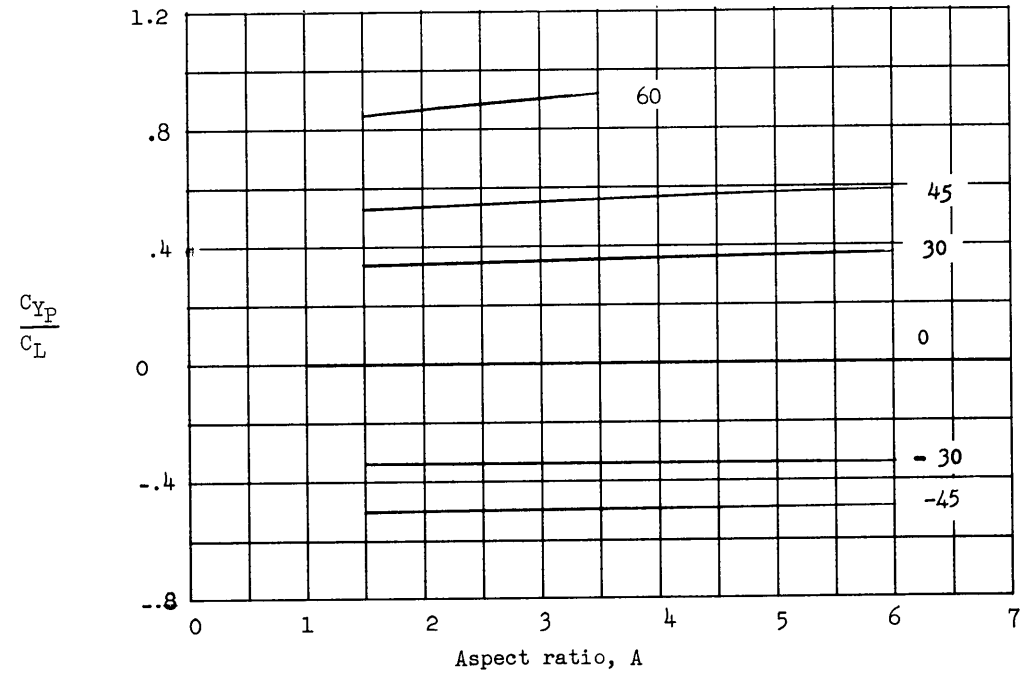

(d) M = 0.8.

Figure 31.- λ = 1.0. Continued.

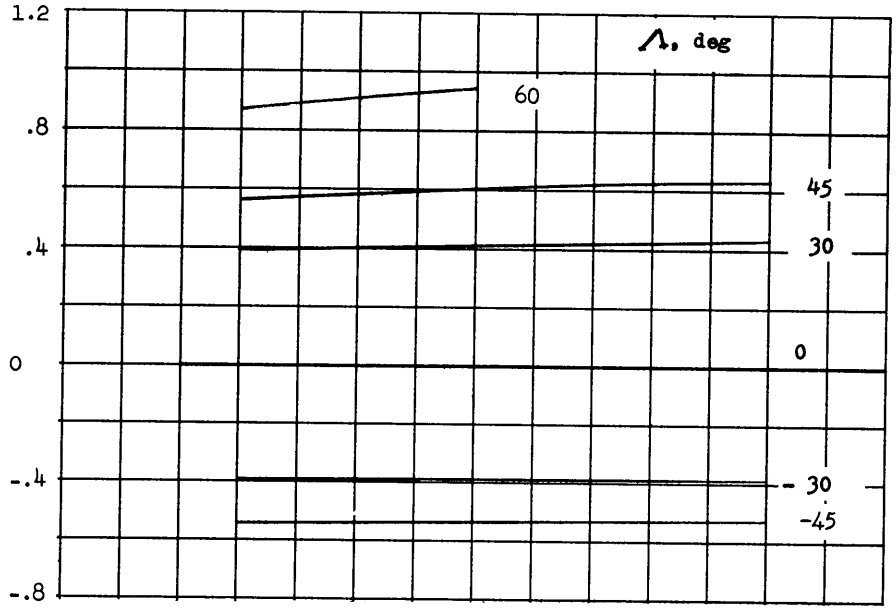

$\frac{C_{Y_P}}{C_L}$

(e) M = 0.9.

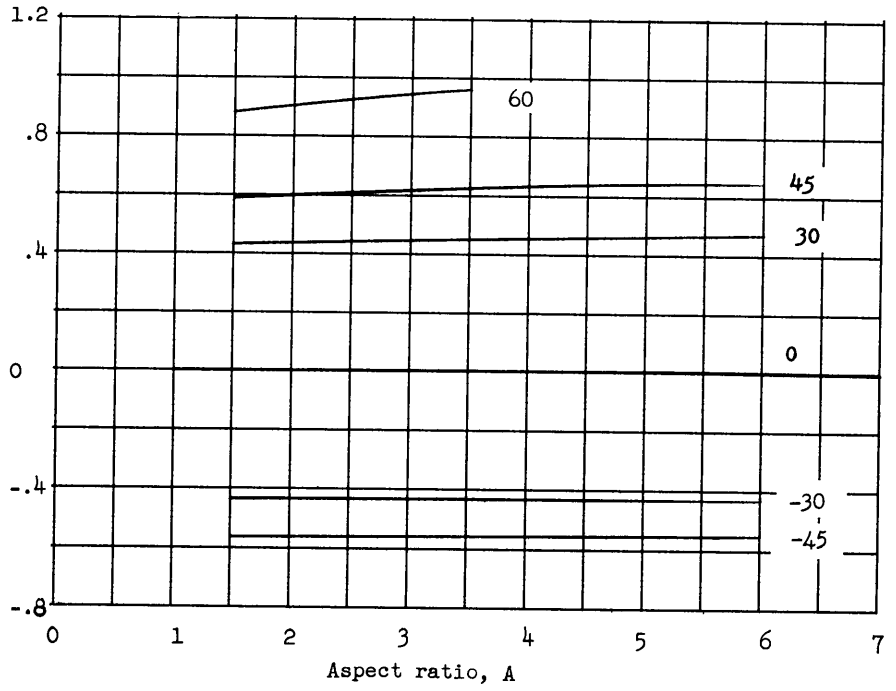

$\frac{C_{Y_P}}{C_L}$

(f) M = 0.95.

Figure 31.- λ = 1.0. Concluded.

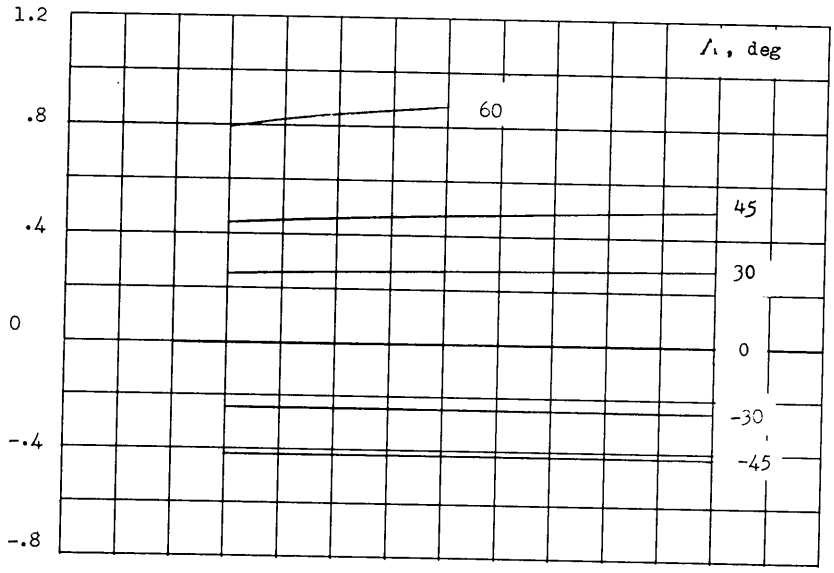

(a) M = 0.

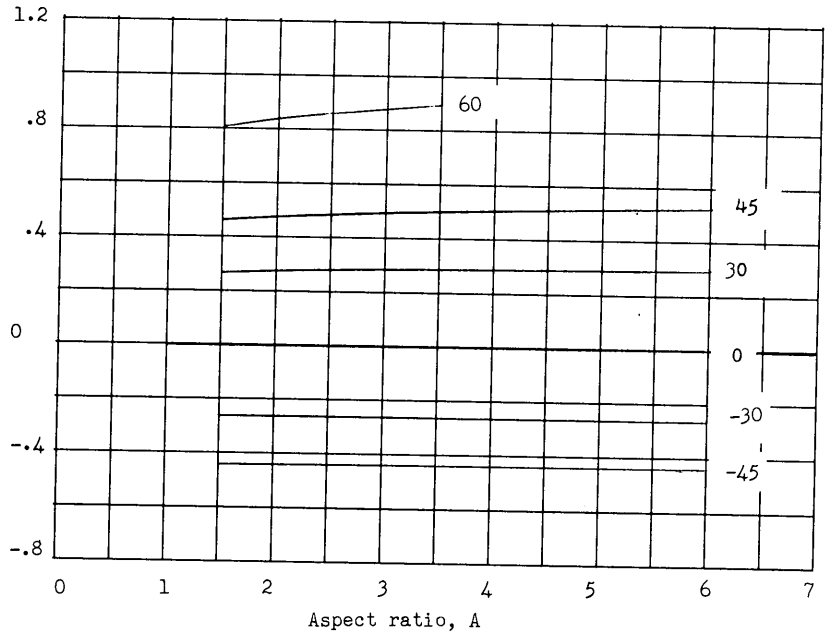

(b) M = 0.4.

Figure 32.- Variation of $\frac{C_{Y_P}}{C_L}$ with aspect ratio, sweep, and Mach number. $\lambda = 1.5$.

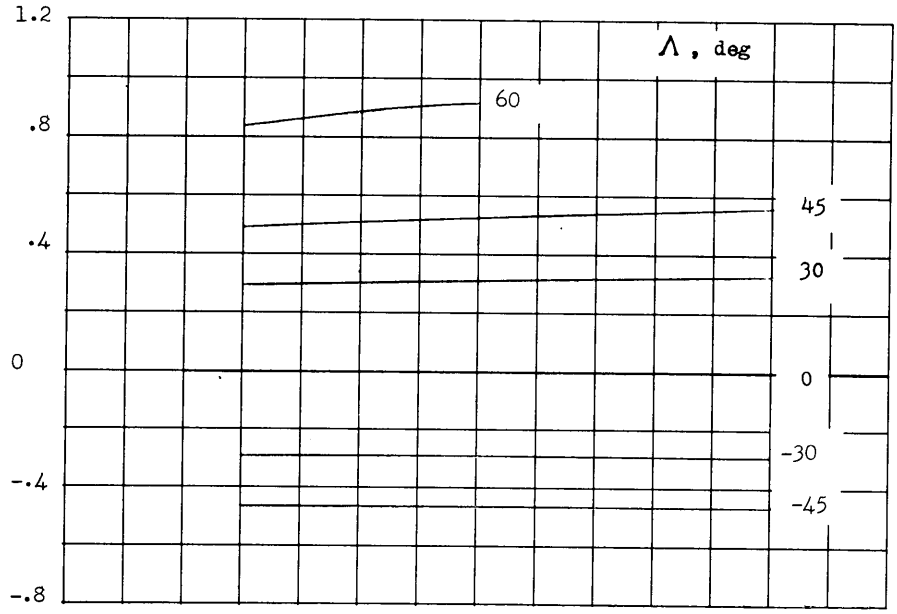

$\frac{C_{Y_P}}{C_L}$

(c) M = 0.6.

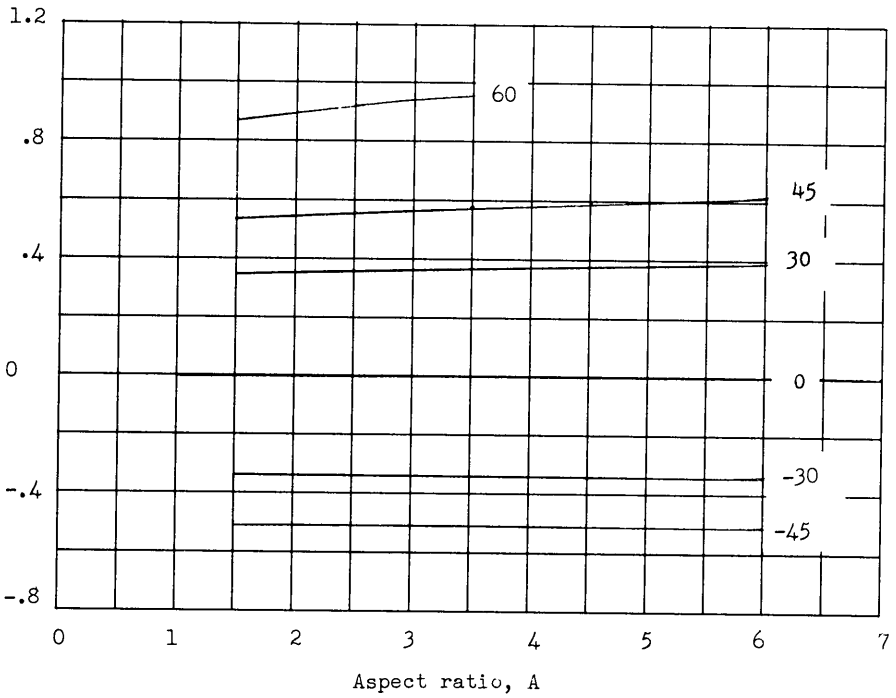

$\frac{C_{Y_P}}{C_L}$

(d) M = 0.8.

Figure 32.- λ = 1.5. Continued.

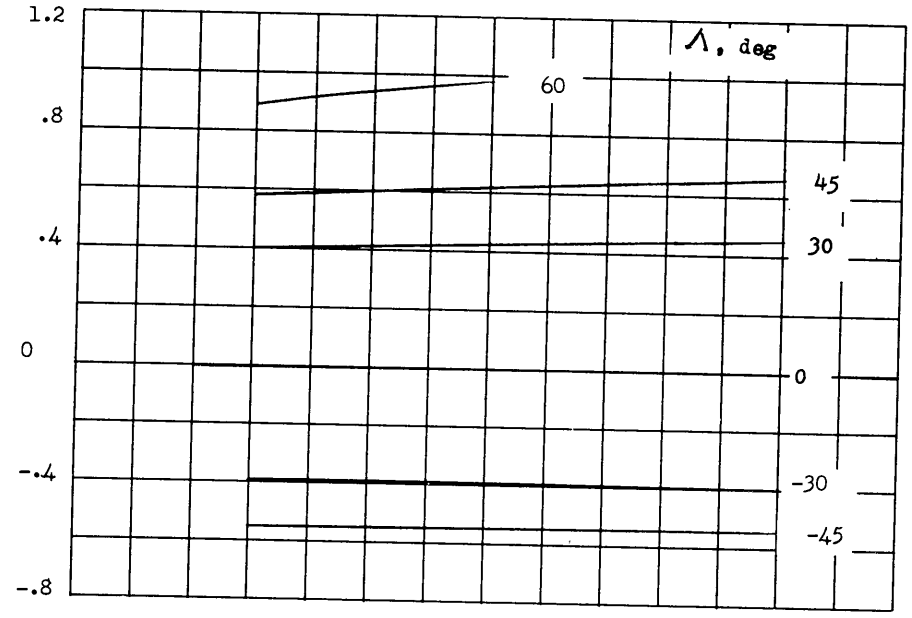

$\frac{C_{Y_P}}{C_L}$

(e) M = 0.9.

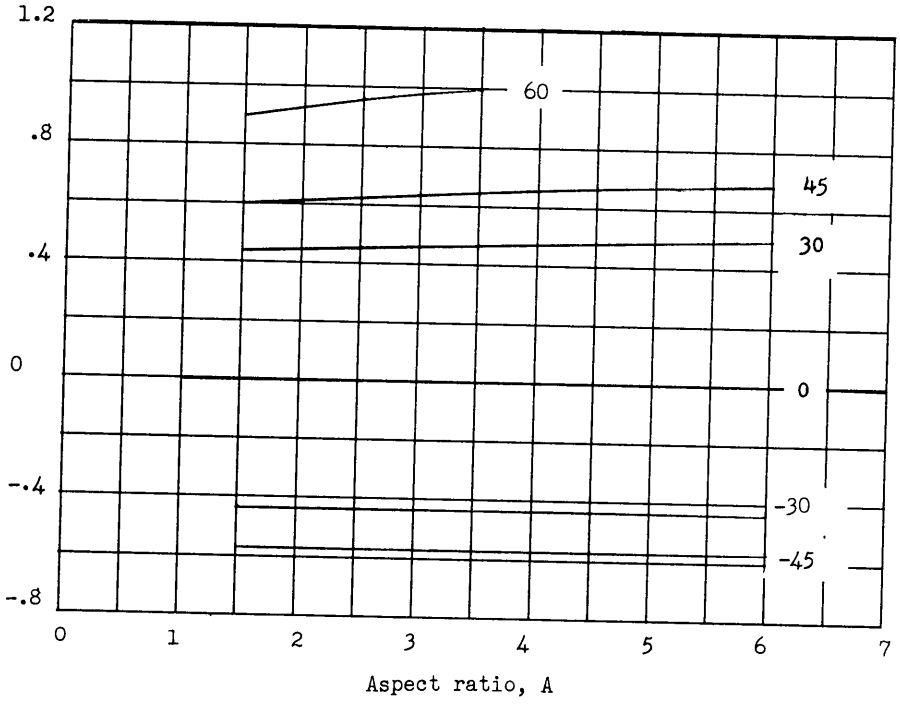

$\frac{C_{Y_P}}{C_L}$

(f) M = 0.95.

Figure 32.- λ = 1.5. Concluded.

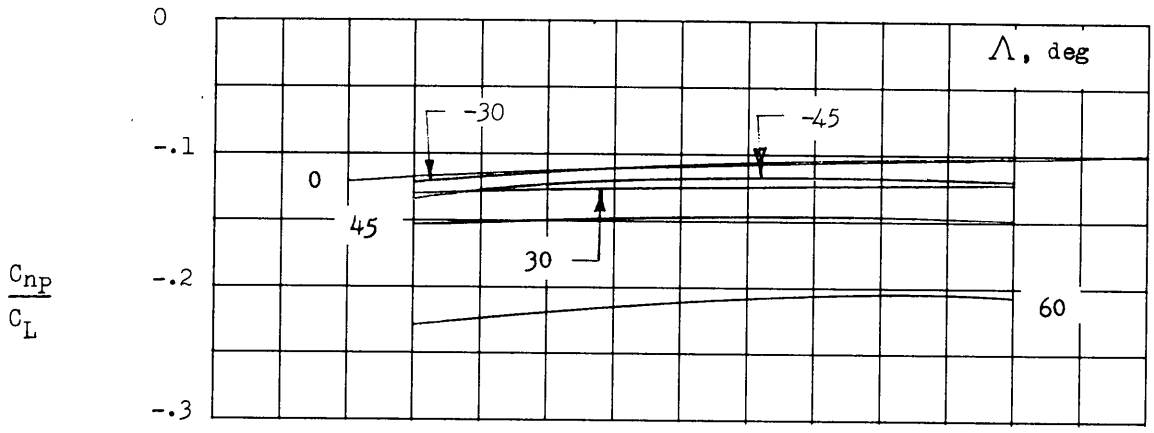

(a) M = 0.

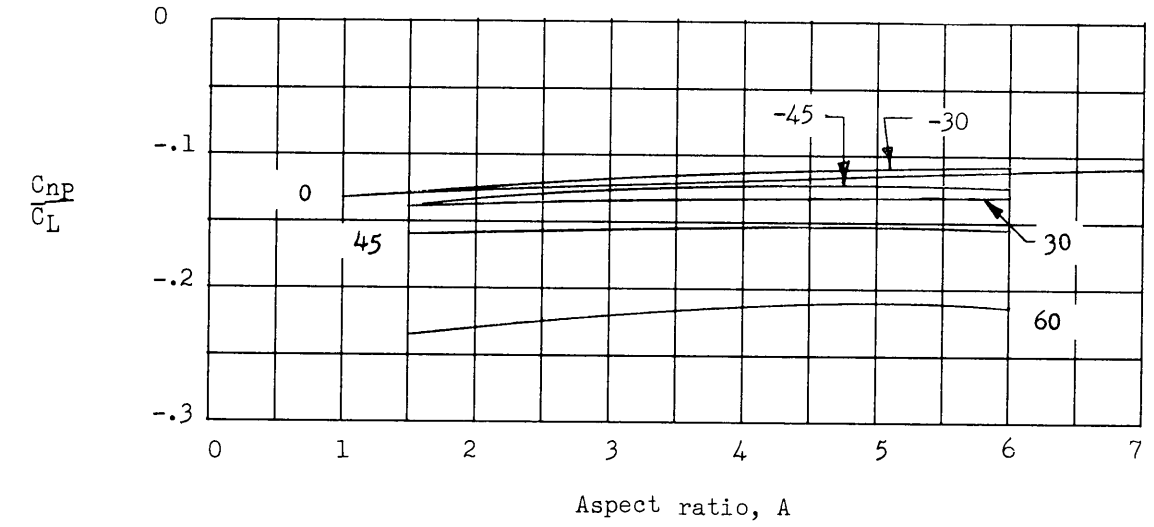

(b) M = 0.4.

Figure 33.- Variation of $\frac{C_{n_P}}{C_L}$ with aspect ratio, sweep, and Mach number. $\bar{X}^* = 0$, $\lambda = 0$.

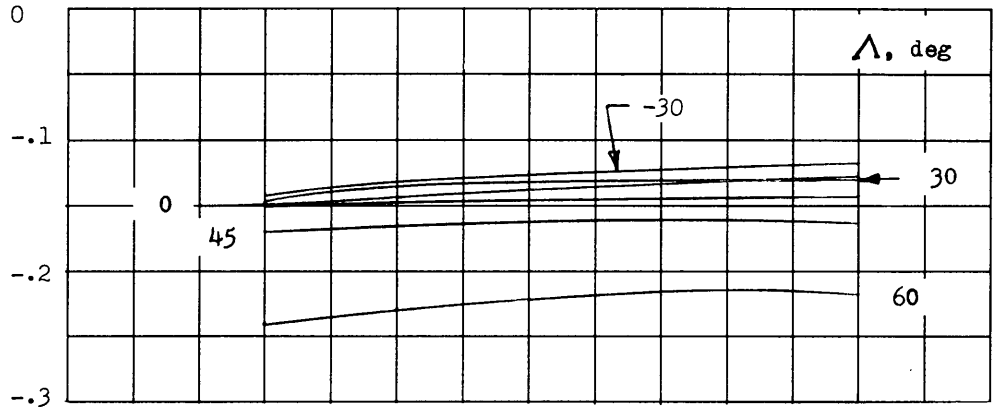

$\frac{C_{n_p}}{C_L}$

(c) M = 0.6.

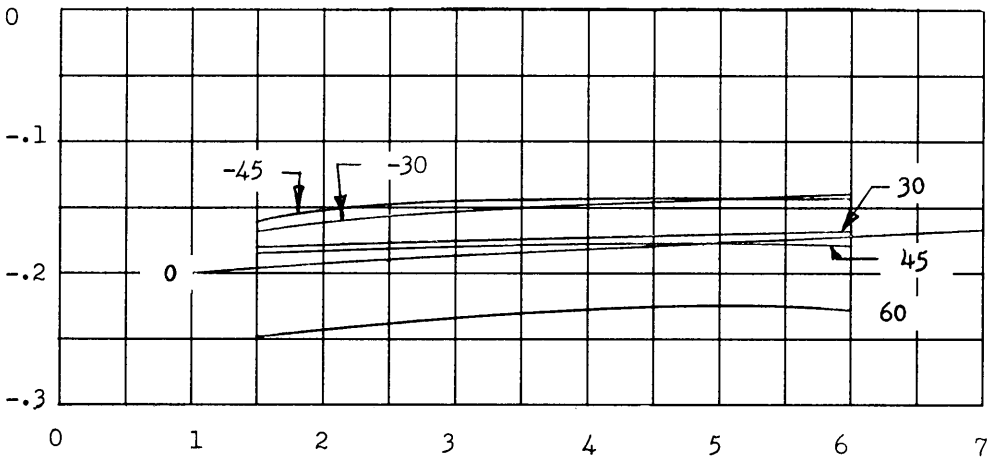

$\frac{C_{n_p}}{C_L}$

(d) M = 0.8.

Figure 33.- λ = 0. Continued.

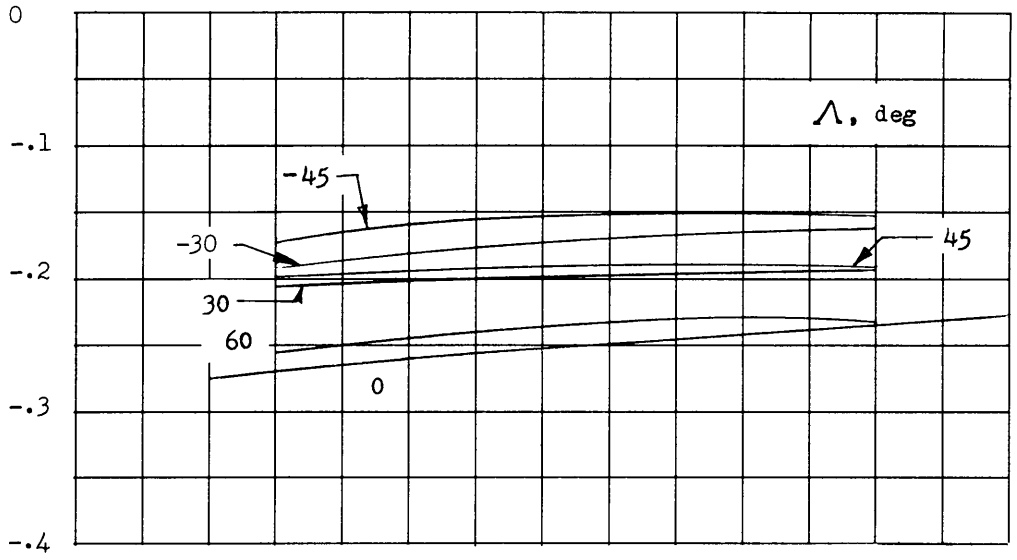

(e) M = 0.9.

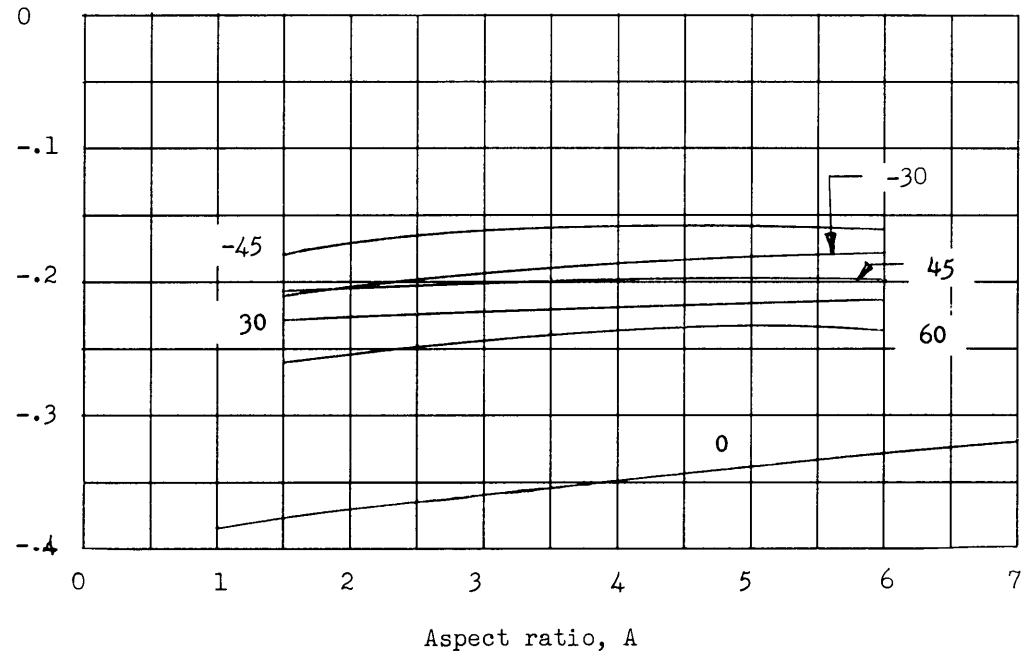

(f) M = 0.95.

Figure 33.- λ = 0. Concluded.

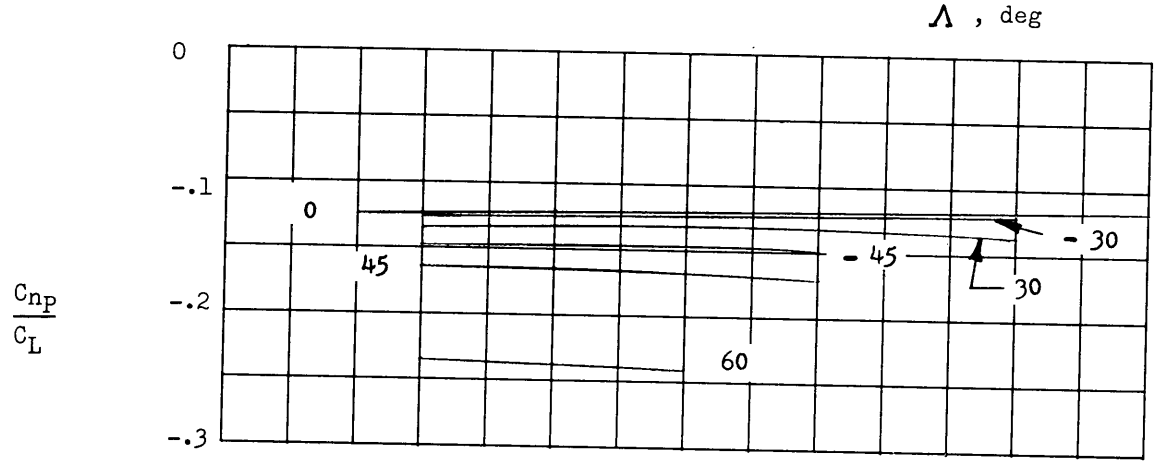

(a) M = 0.

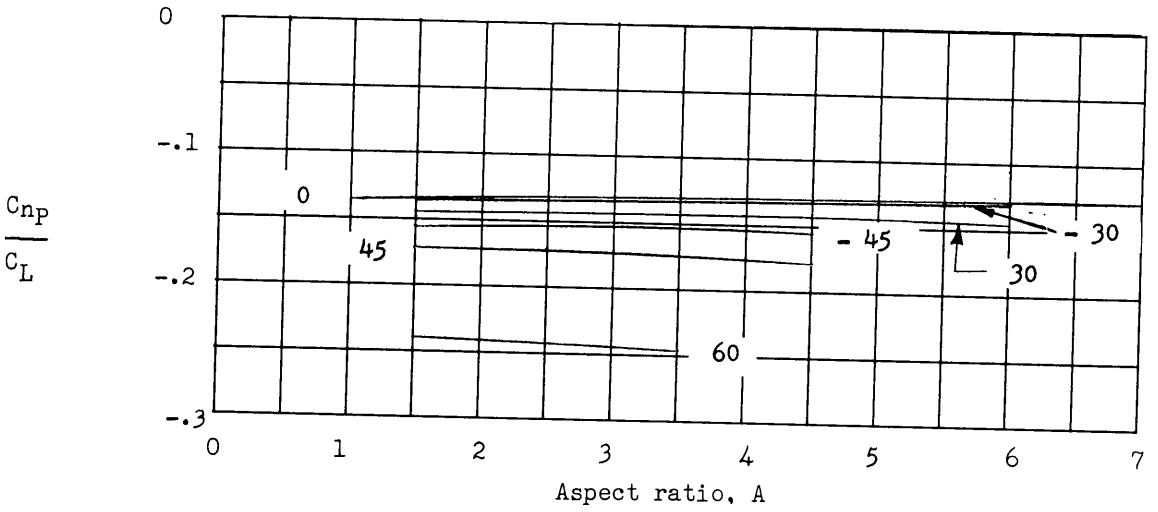

(b) M = 0.4.

Figure 34.- Variation of $\frac{C_{n_P}}{C_L}$ with aspect ratio, sweep, and Mach number. $\bar{X}^* = 0$, $\lambda = 0.25$.

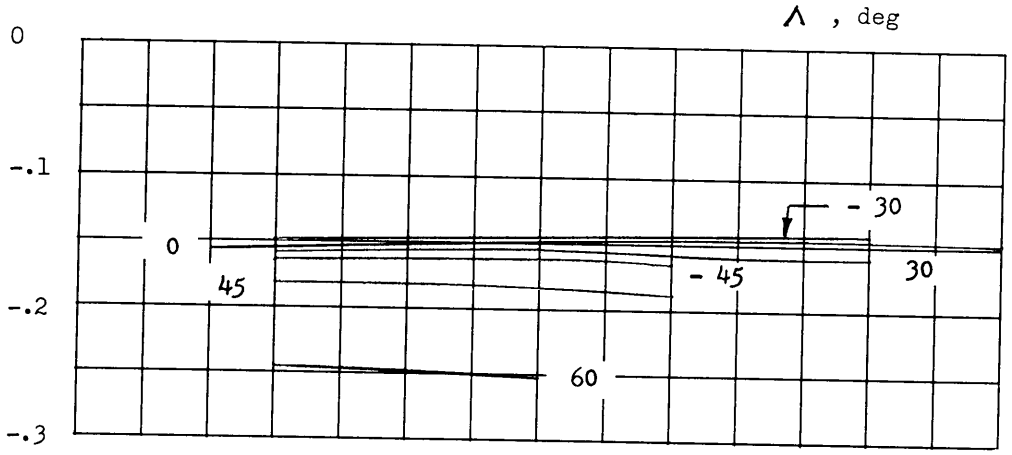

(c) M = 0.6.

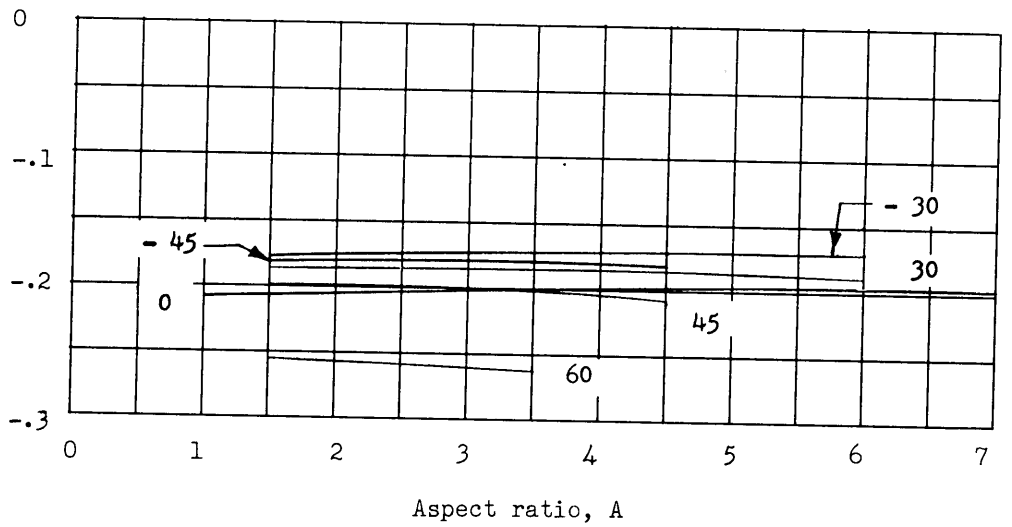

(d) M = 0.8.

Figure 34.- λ = 0.25. Continued.

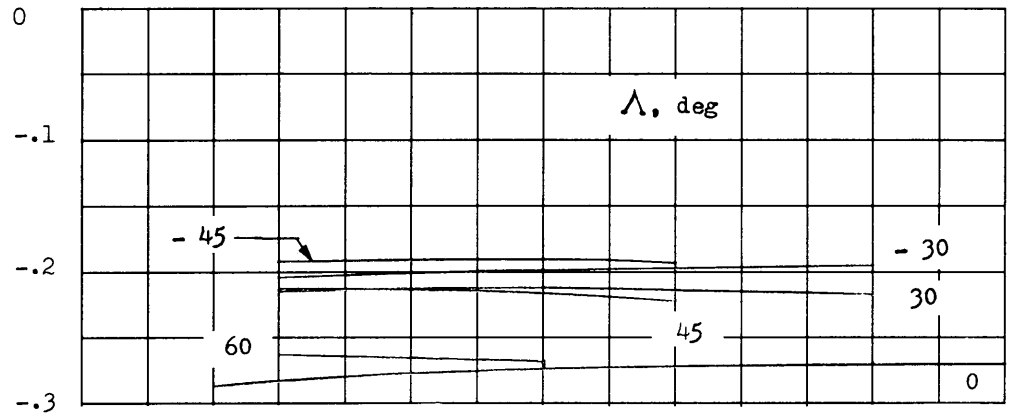

$\frac{C_{n_p}}{C_L}$

(e) M = 0.9.

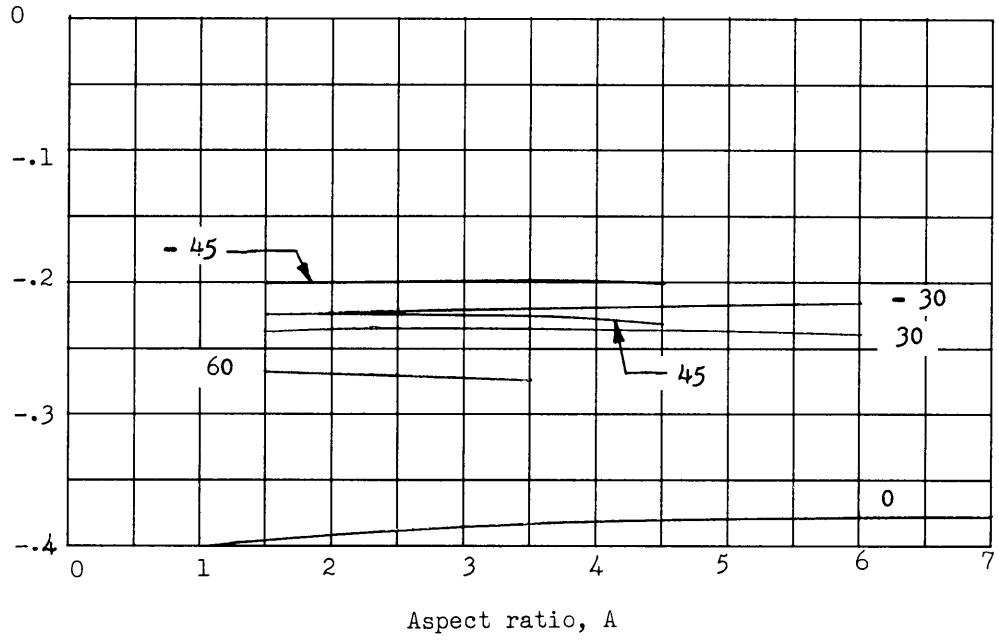

$\frac{C_{n_p}}{C_L}$

(f) M = 0.95.

Figure 34.- λ = 0.25. Concluded.

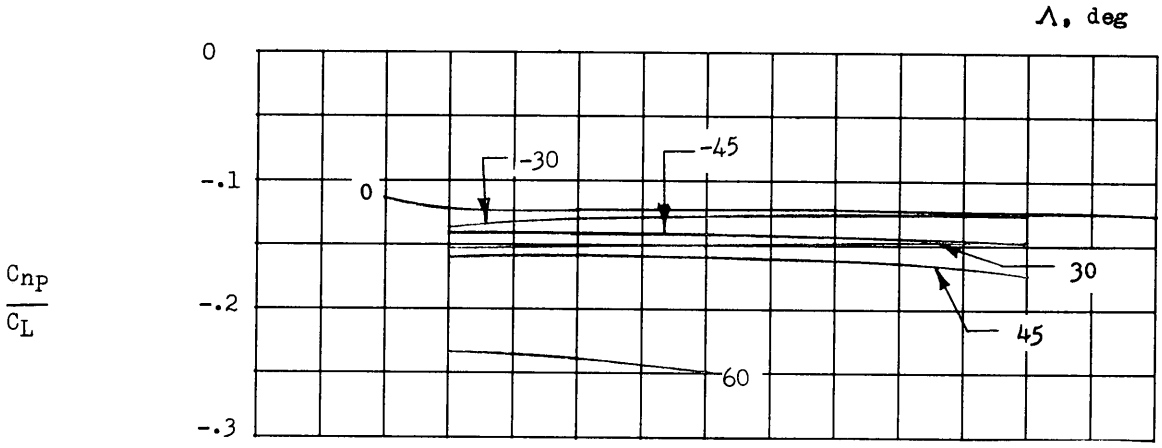

(a) M = 0.

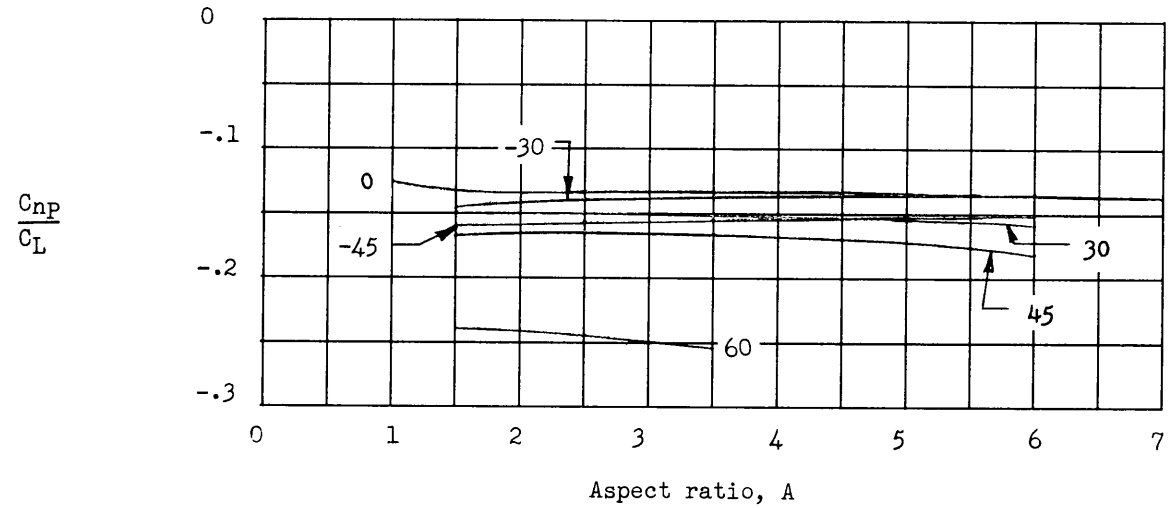

(b) M = 0.4.

Figure 35.- Variation of $\frac{C_{n_P}}{C_L}$ with aspect ratio, sweep, and Mach number. $\bar{X}^* = 0$, $\lambda = 0.50$.

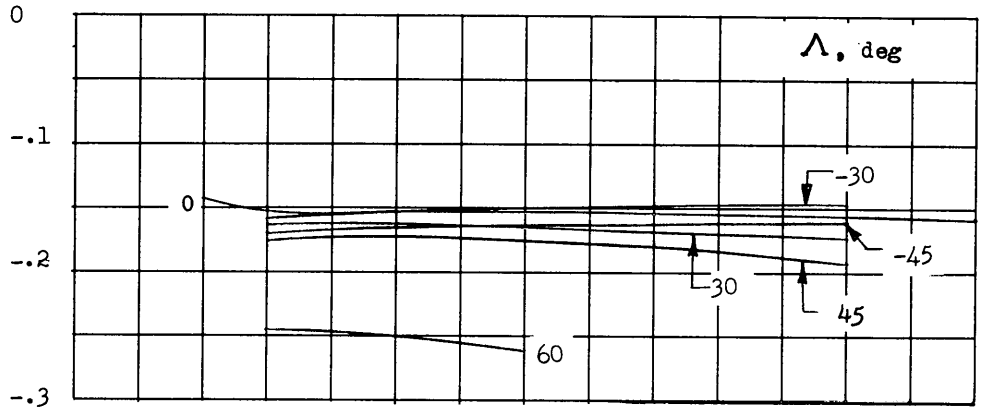

(c) M = 0.6.

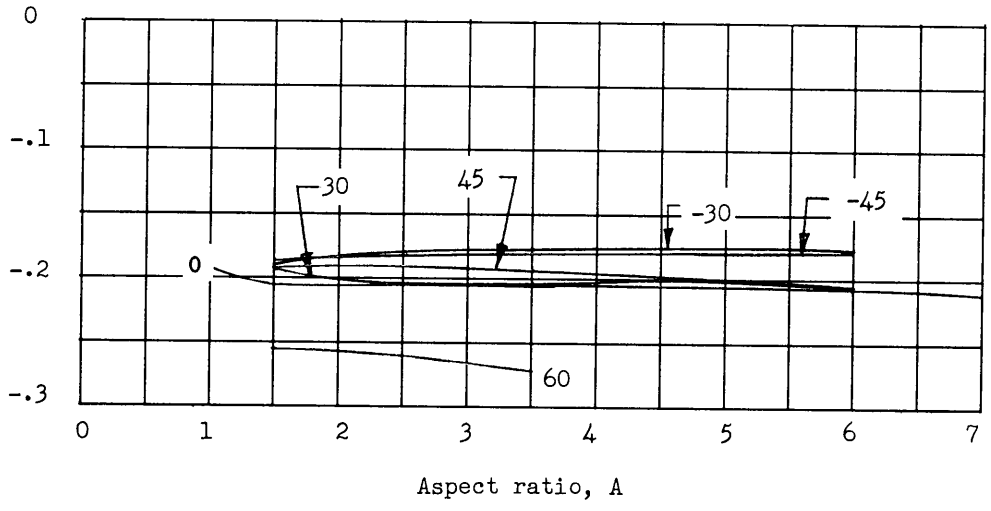

(d) M = 0.8.

Figure 35.- λ = 0.50. Continued.

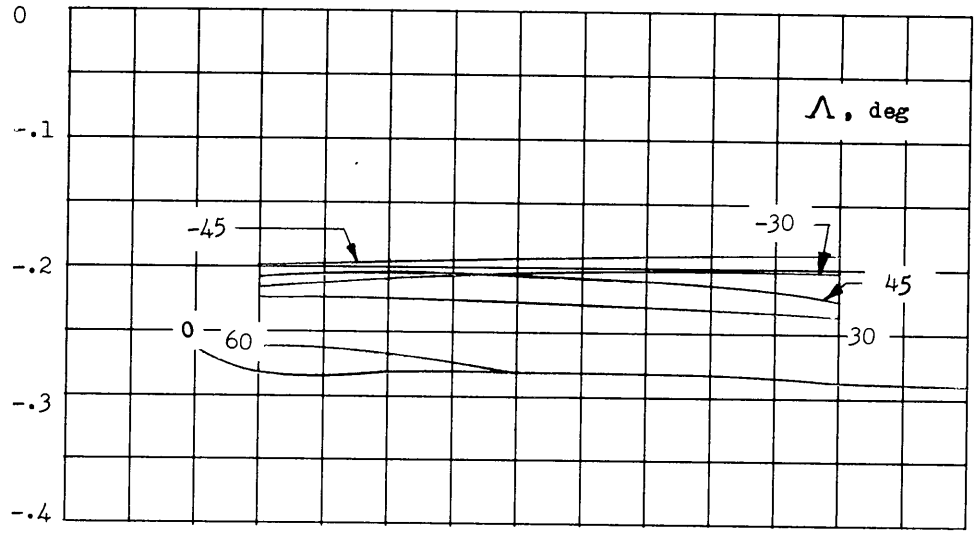

$\frac{C_{n_P}}{C_L}$

(e) M = 0.9.

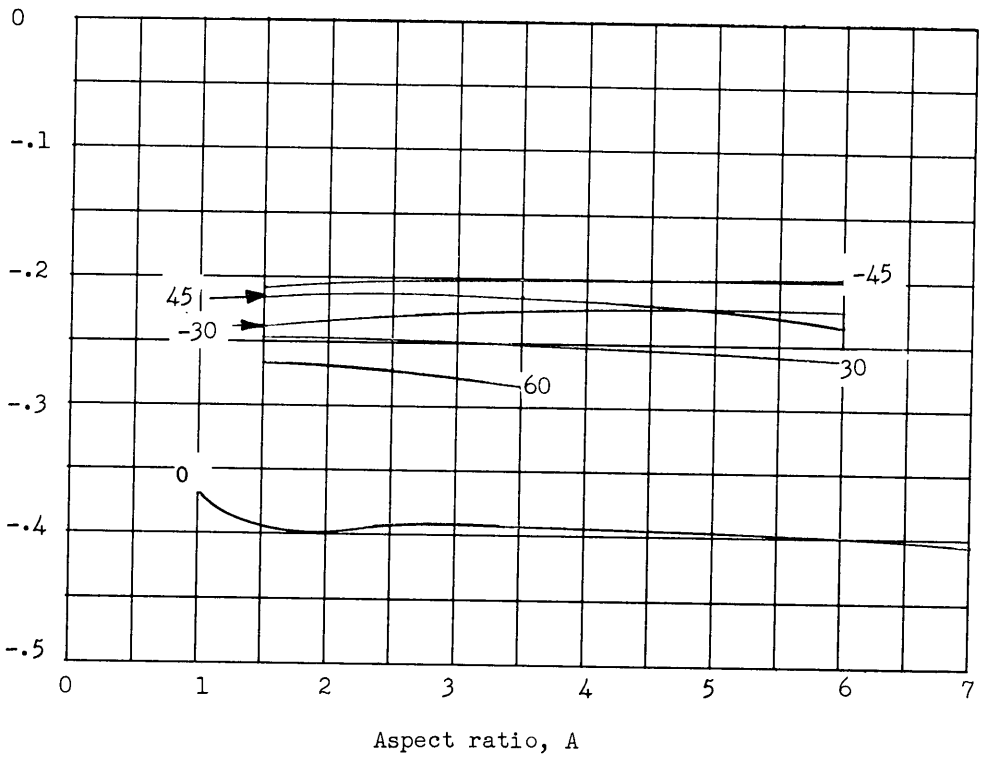

$\frac{C_{n_P}}{C_L}$

(f) M = 0.95.

Figure 35.- λ = 0.50. Concluded.

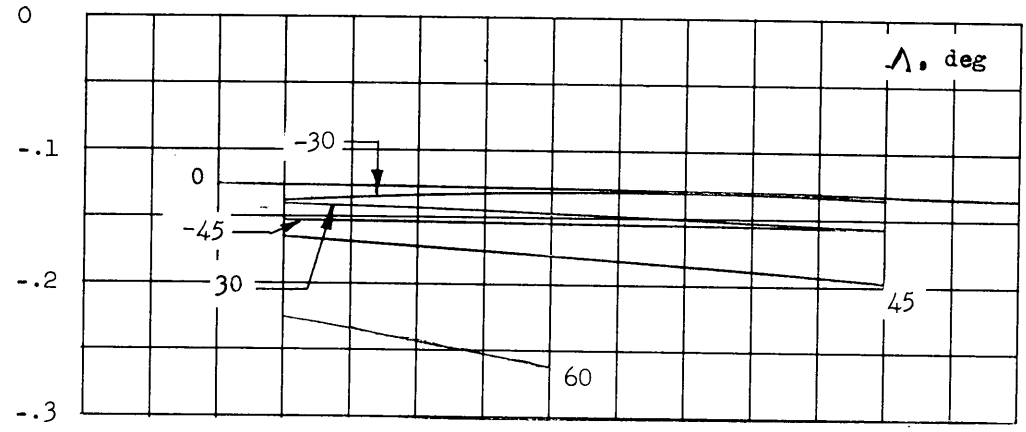

$\frac{C_{n_p}}{C_L}$

(a) M = 0.

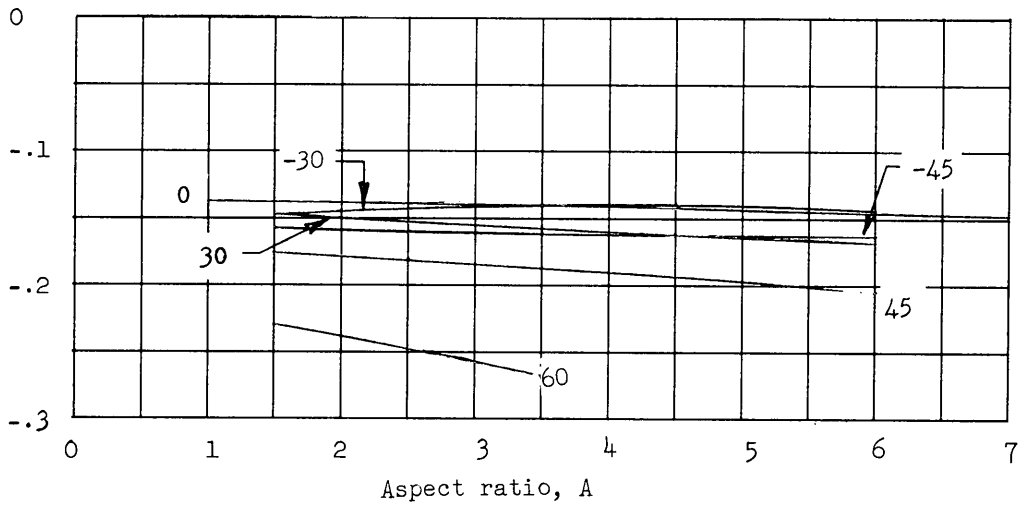

$\frac{C_{n_p}}{C_L}$

(b) M = 0.4.

Figure 36.- Variation of $\frac{C_{n_P}}{C_L}$ with aspect ratio, sweep, and Mach number. $\bar{X}^* = 0$, $\lambda = 1.0$

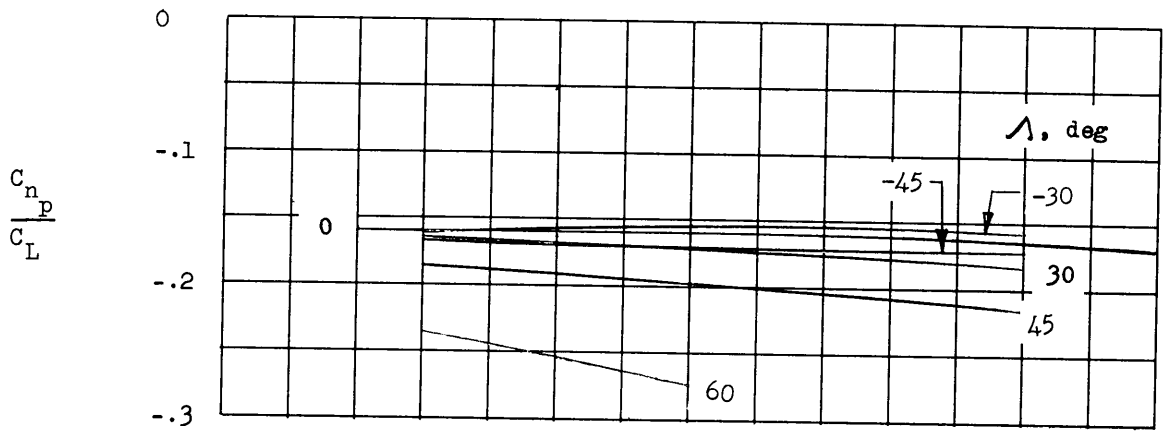

(c) M = 0.6.

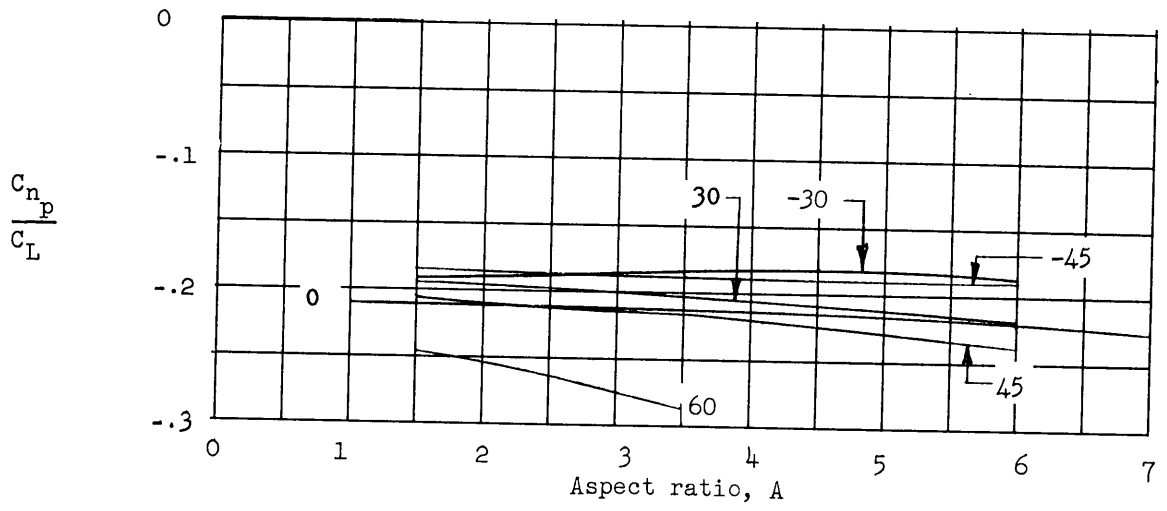

(d) M = 0.8.

Figure 36.- λ = 1.0. Continued.

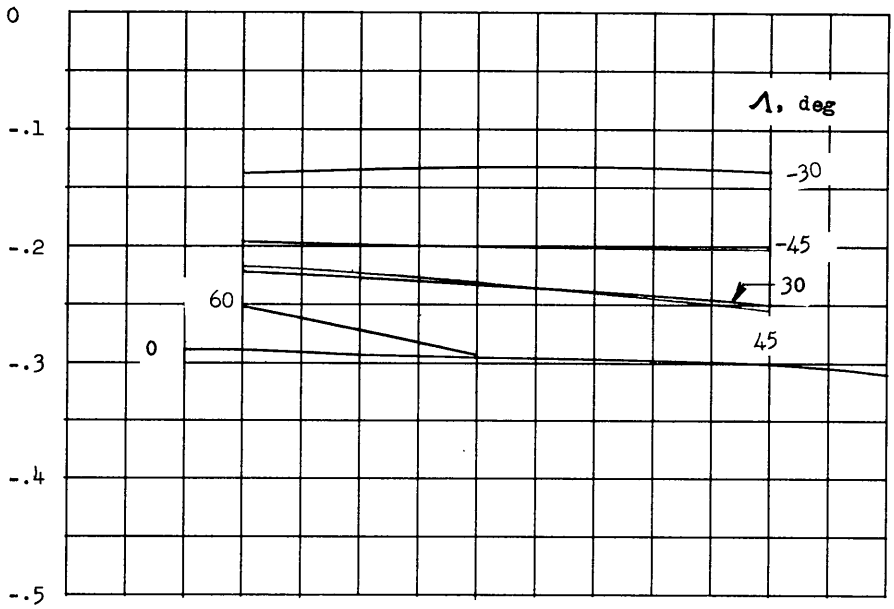

$\frac{C_{n_p}}{C_L}$

(e) M = 0.9.

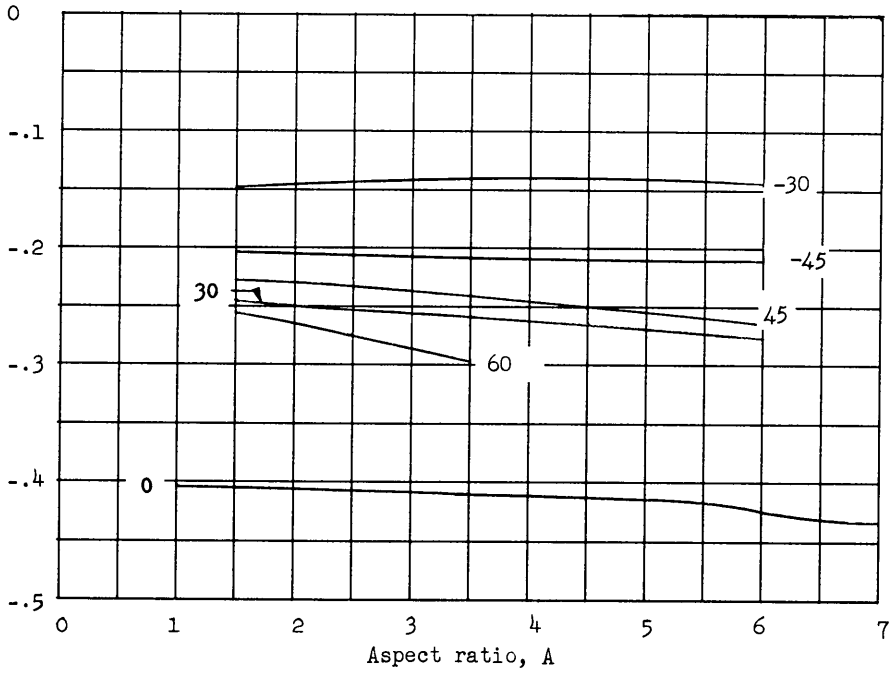

$\frac{C_{n_p}}{C_L}$

(f) M = 0.95.

Figure 36.- λ = 1.0. Concluded.

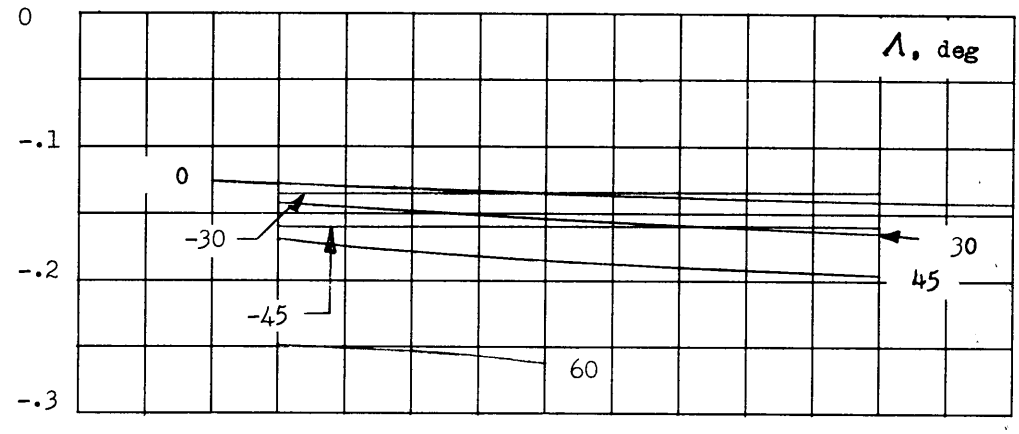

$\frac{C_{nP}}{C_L}$

(a) M = 0.

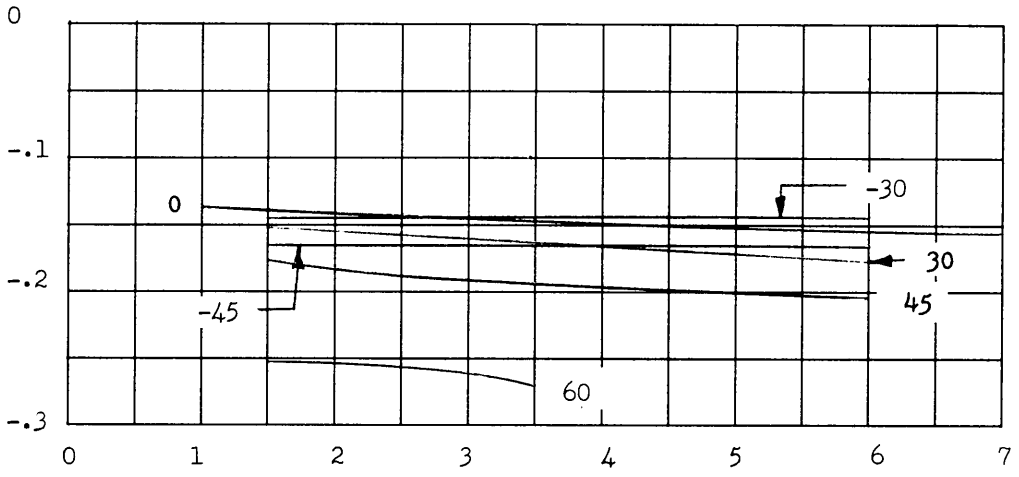

$\frac{C_{nP}}{C_L}$

(b) M = 0.4.

Figure 37.- Variation of $\frac{C_{nP}}{C_L}$ with aspect ratio, sweep, and Mach number. $\bar{X}^* = 0$, $\lambda = 1.5$.

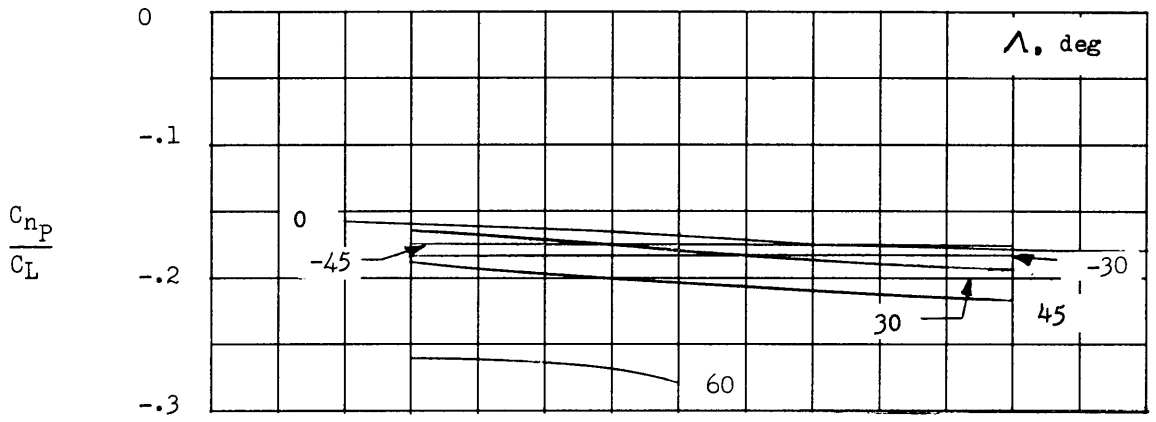

(c) M = 0.6.

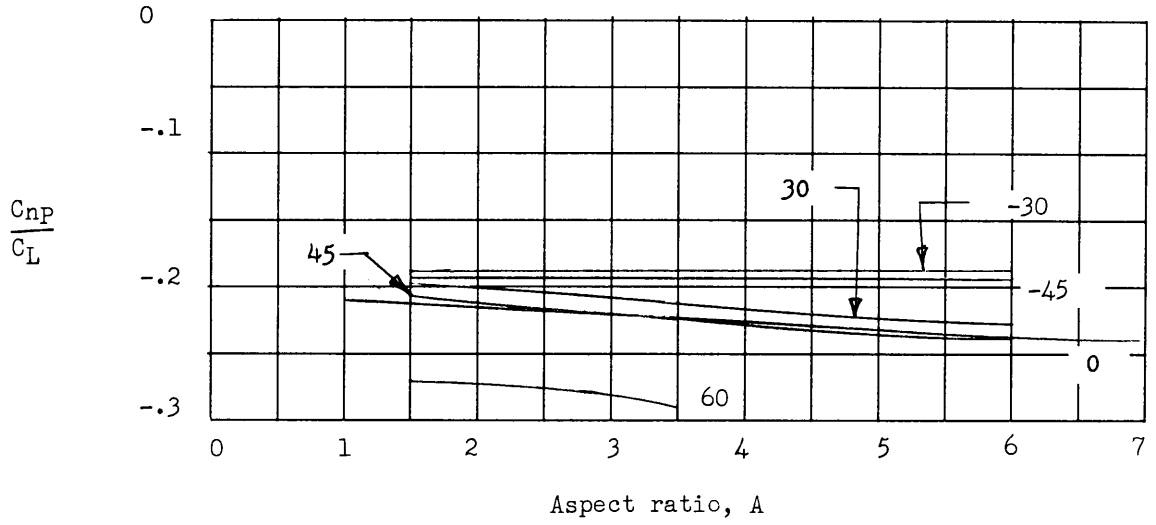

(d) M = 0.8.

Figure 37.- λ = 1.5. Continued.

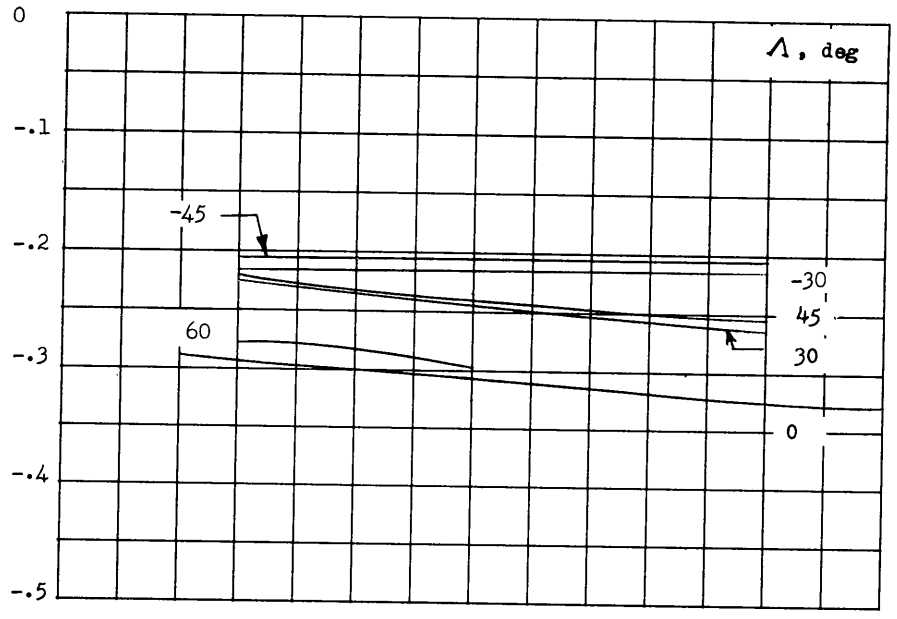

(e) M = 0.9.

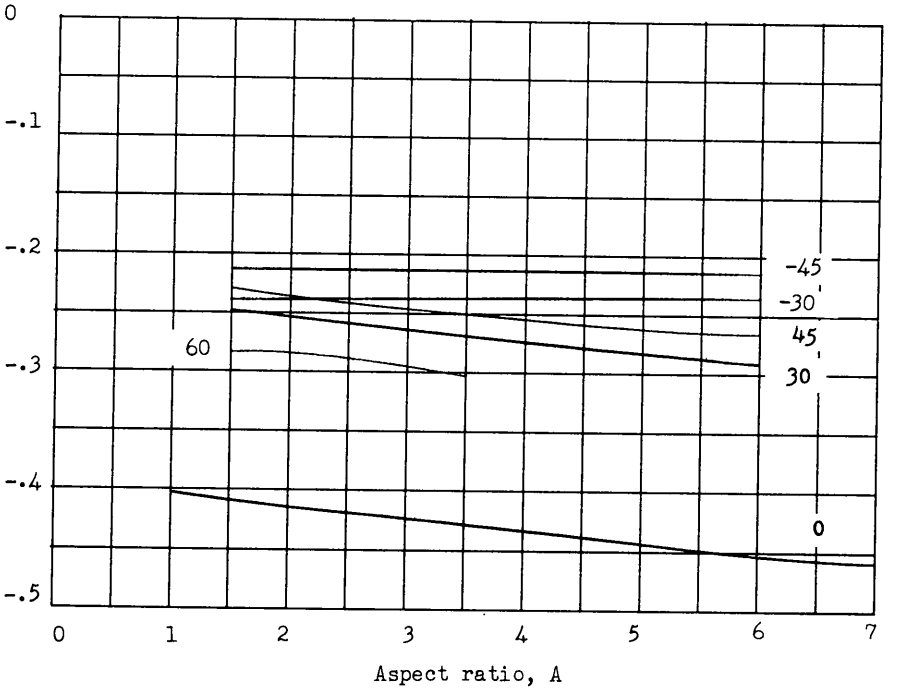

(f) M = 0.95.

Figure 37.- λ = 1.5. Concluded.

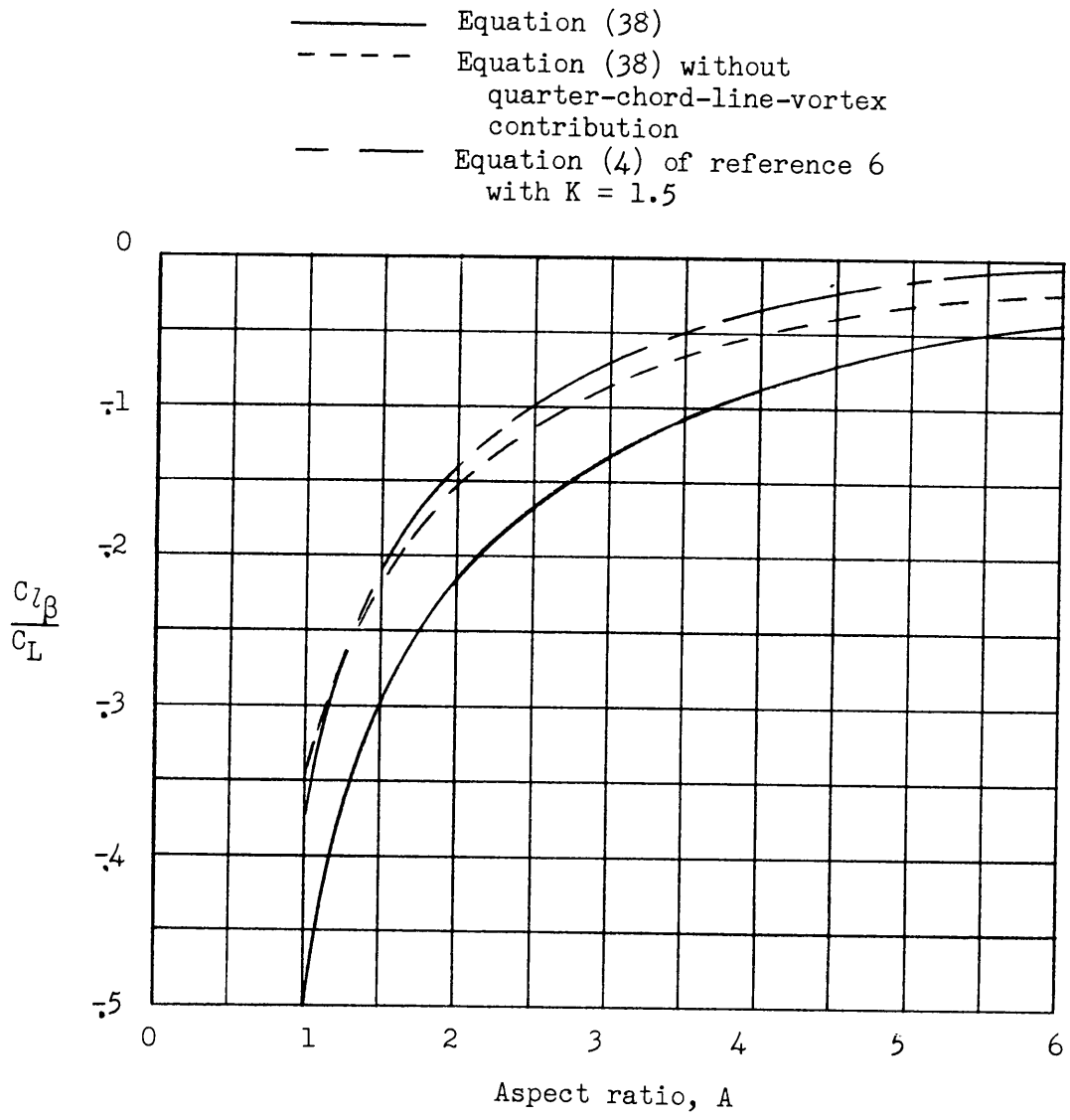

Figure 38.- Coefficient of rolling moment due to sideslip for elliptic wings in incompressible flow.

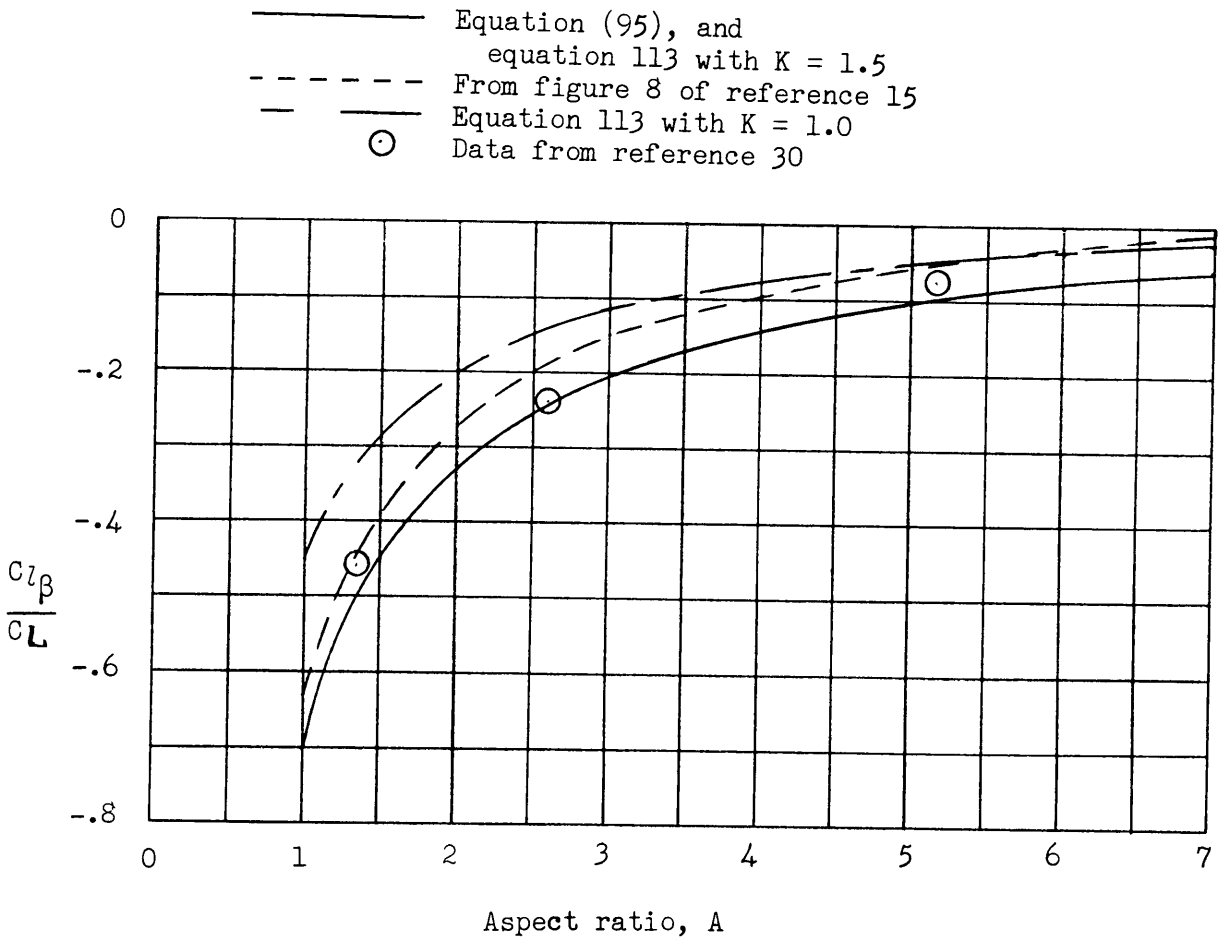

Figure 39.- Comparison of experimental and theoretical values of $\frac{C_{l_\beta}}{C_L}$ for untapered, unswept wings in incompressible flow.

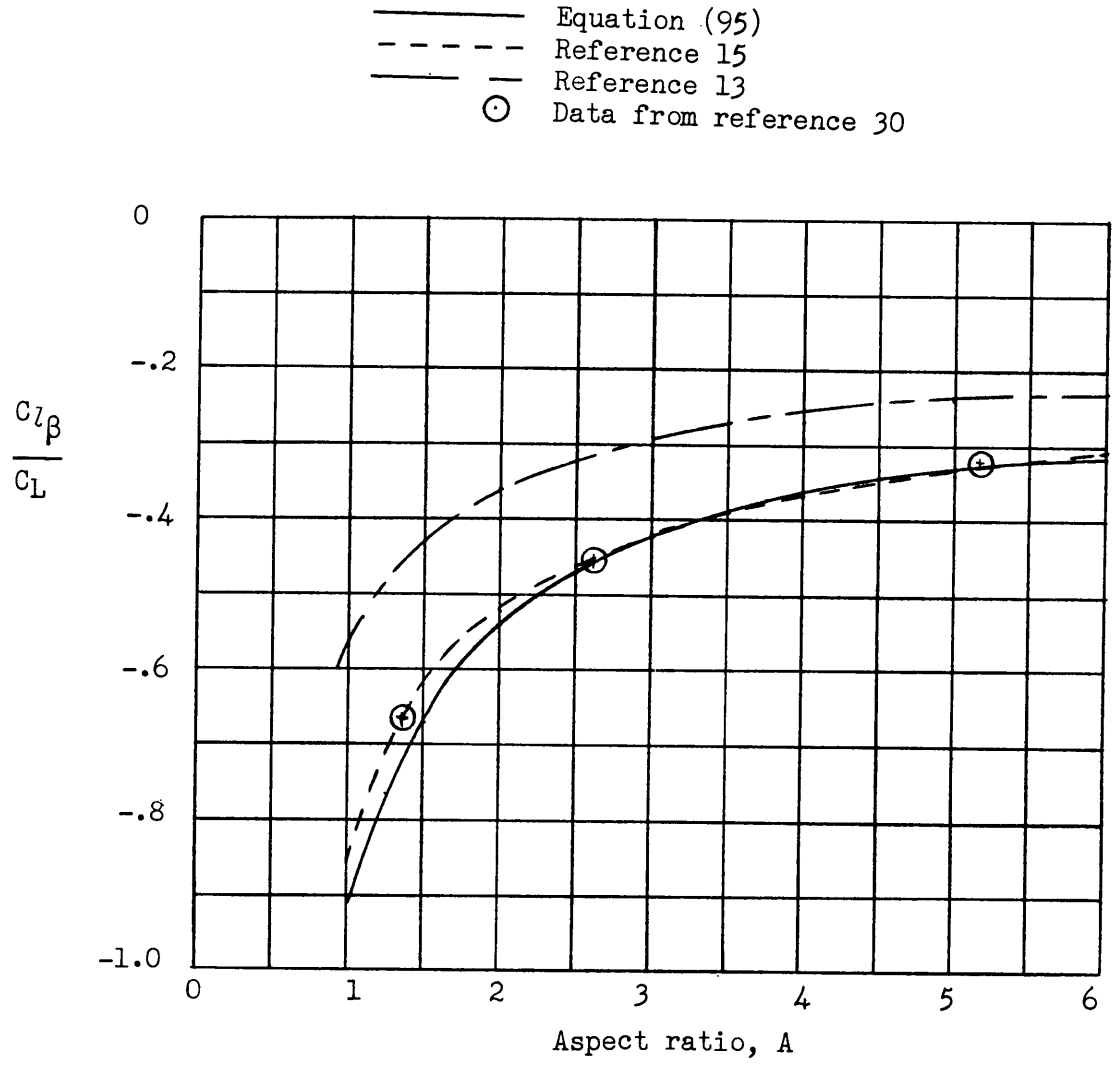

(a) $\Lambda = 45^\circ$.

Figure 40.- Comparison of experimental and theoretical values of $\frac{C_{l_\beta}}{C_L}$ for untapered, swept wings in incompressible flow.

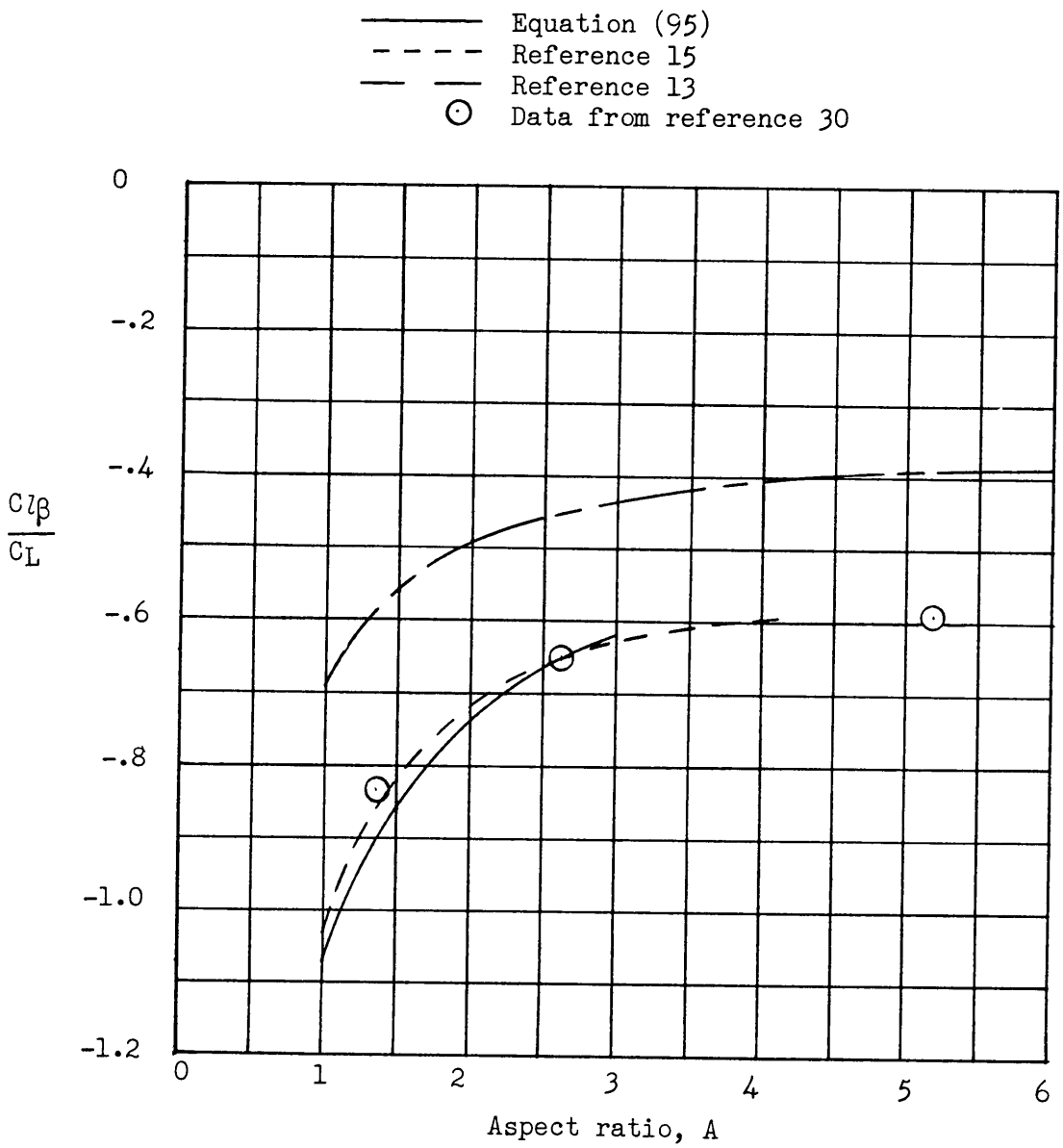

(b) $\Lambda = 60^\circ$.

Figure 40.- Concluded.

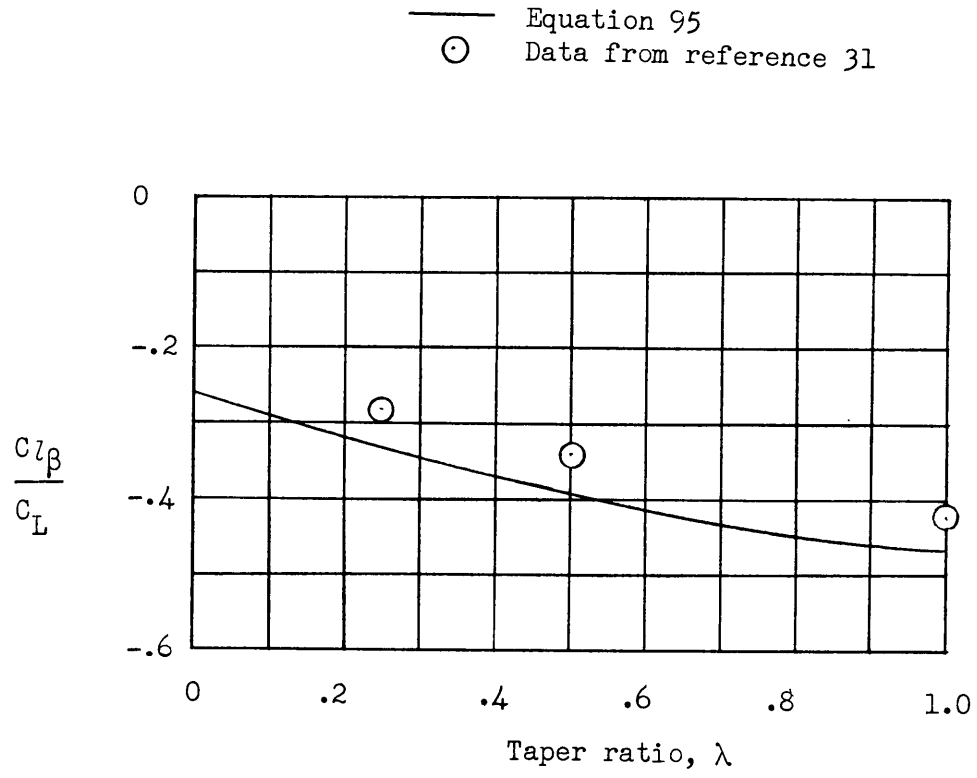

Figure 41.- Comparison of theoretical and experimental effect of taper ratio on values of $\frac{C_{l_\beta}}{C_L}$ for wings in incompressible flow. A = 2.61, $\Lambda = 45^\circ$.

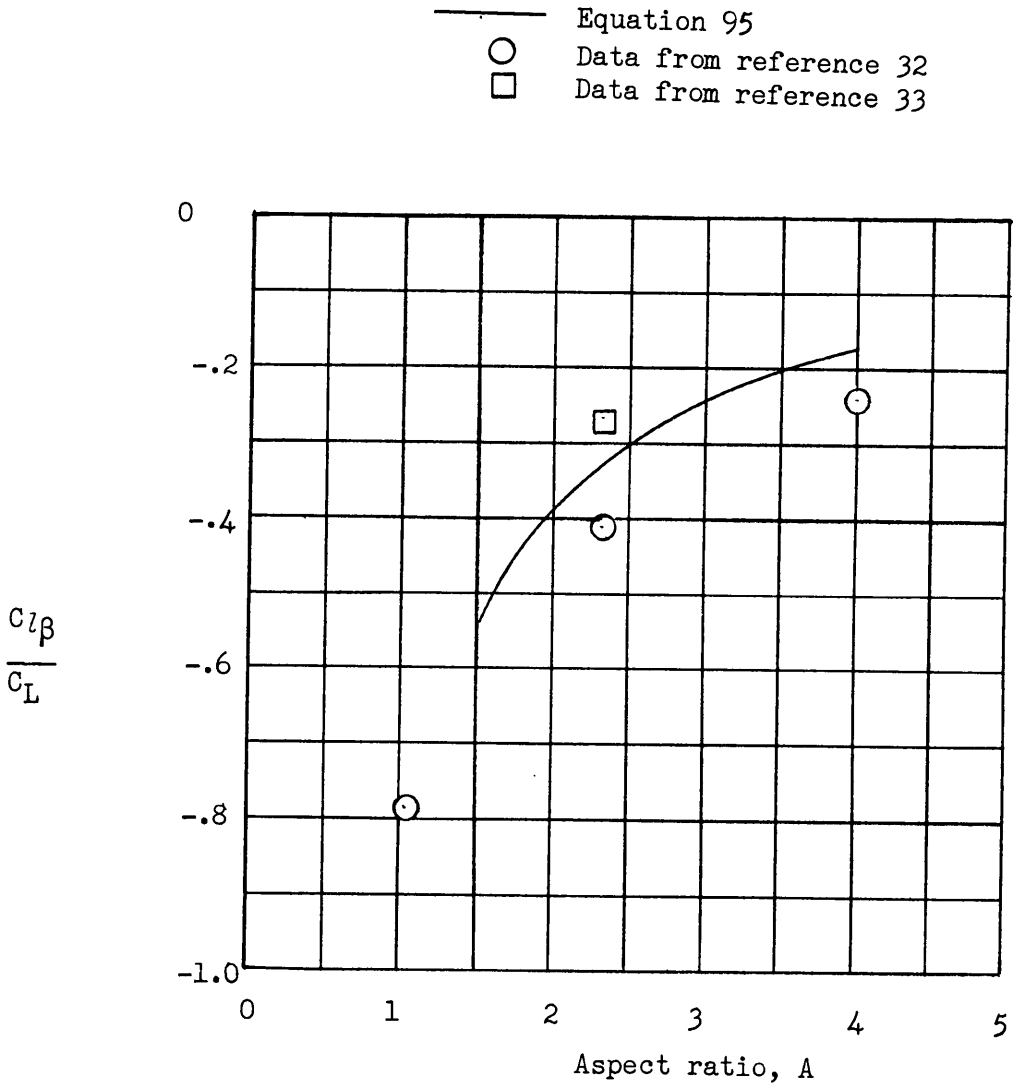

Figure 42.- Comparison of theoretical and experimental values of $\frac{c_{l_\beta}}{C_L}$ for triangular planform wings in incompressible flow.

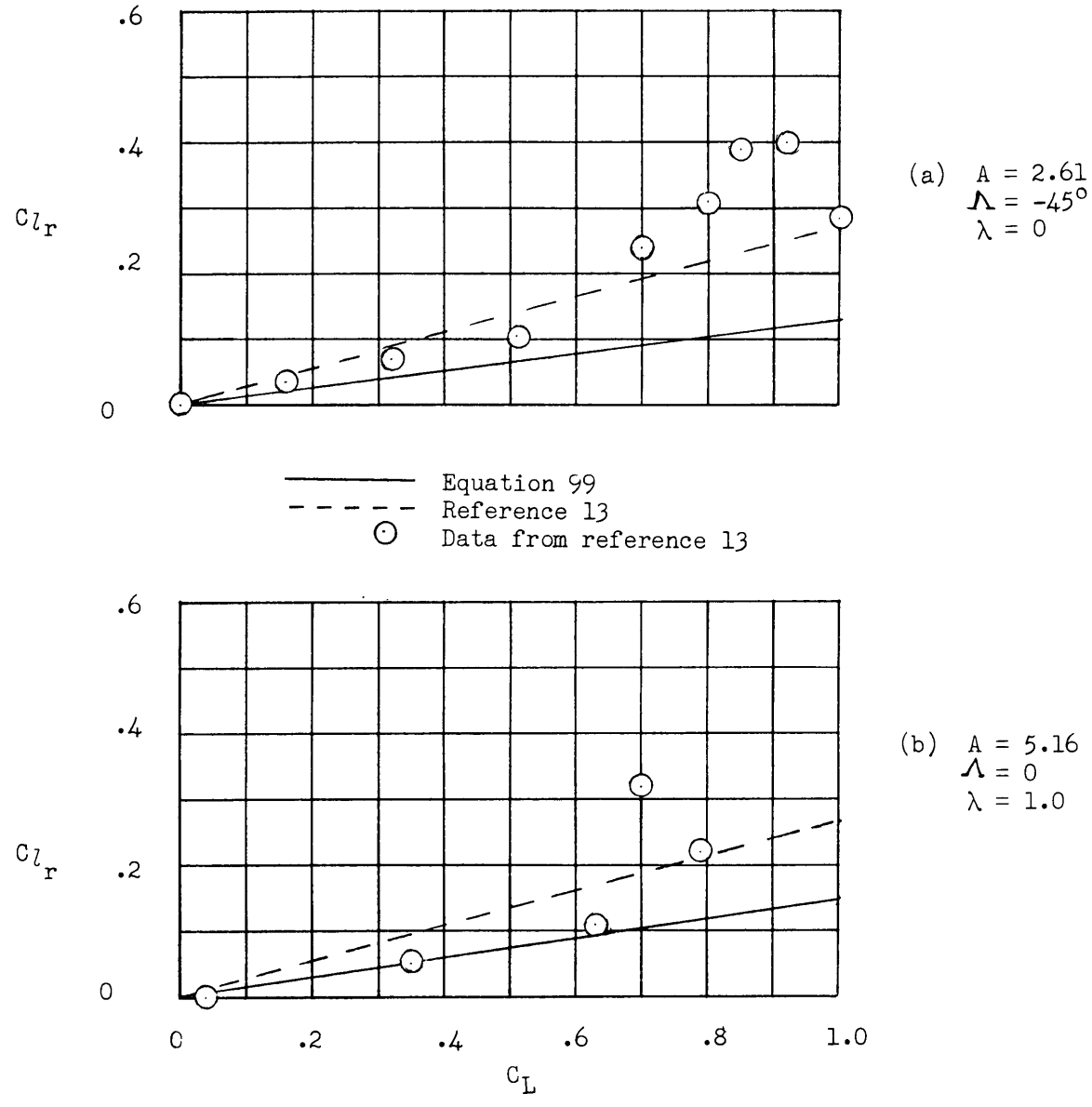

Figure 43.- Comparison of theoretical and experimental values of the variation of C_{l_r} with C_L for several representative wings in incompressible flow.

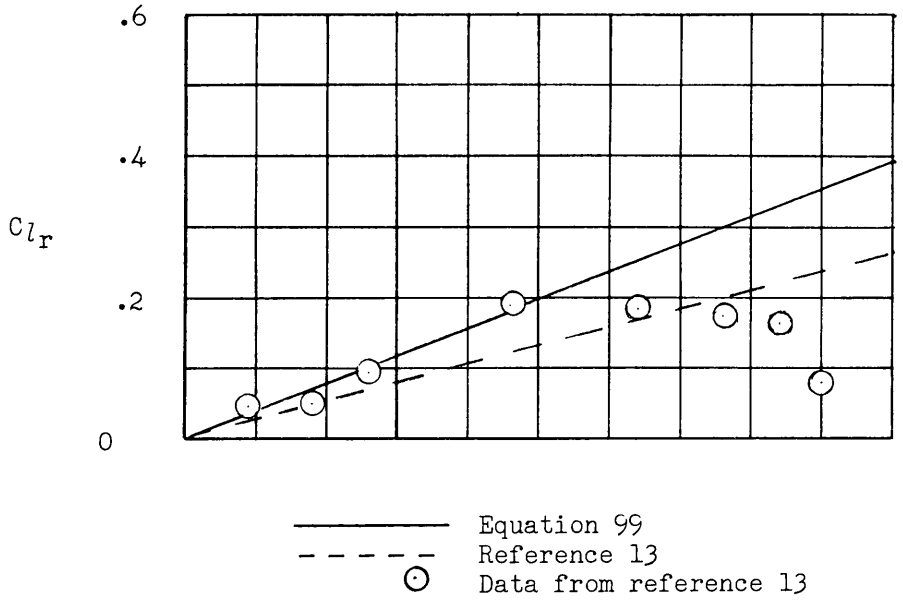

(c) A = 2.61
Λ = 45°
λ = 1.0

Equation 99
Reference 13
Data from reference 13

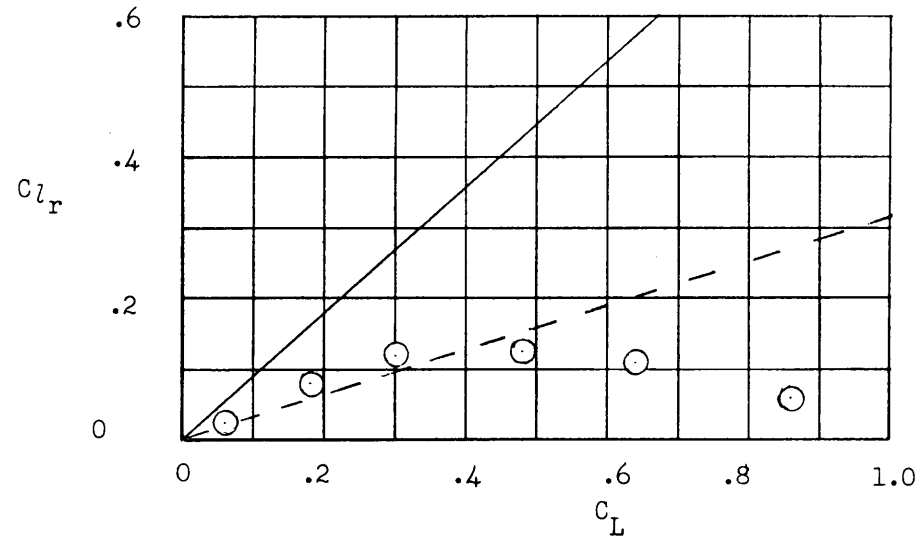

(d) A = 1.34
Λ = 60°
λ = 1.0

Figure 43.- Concluded.

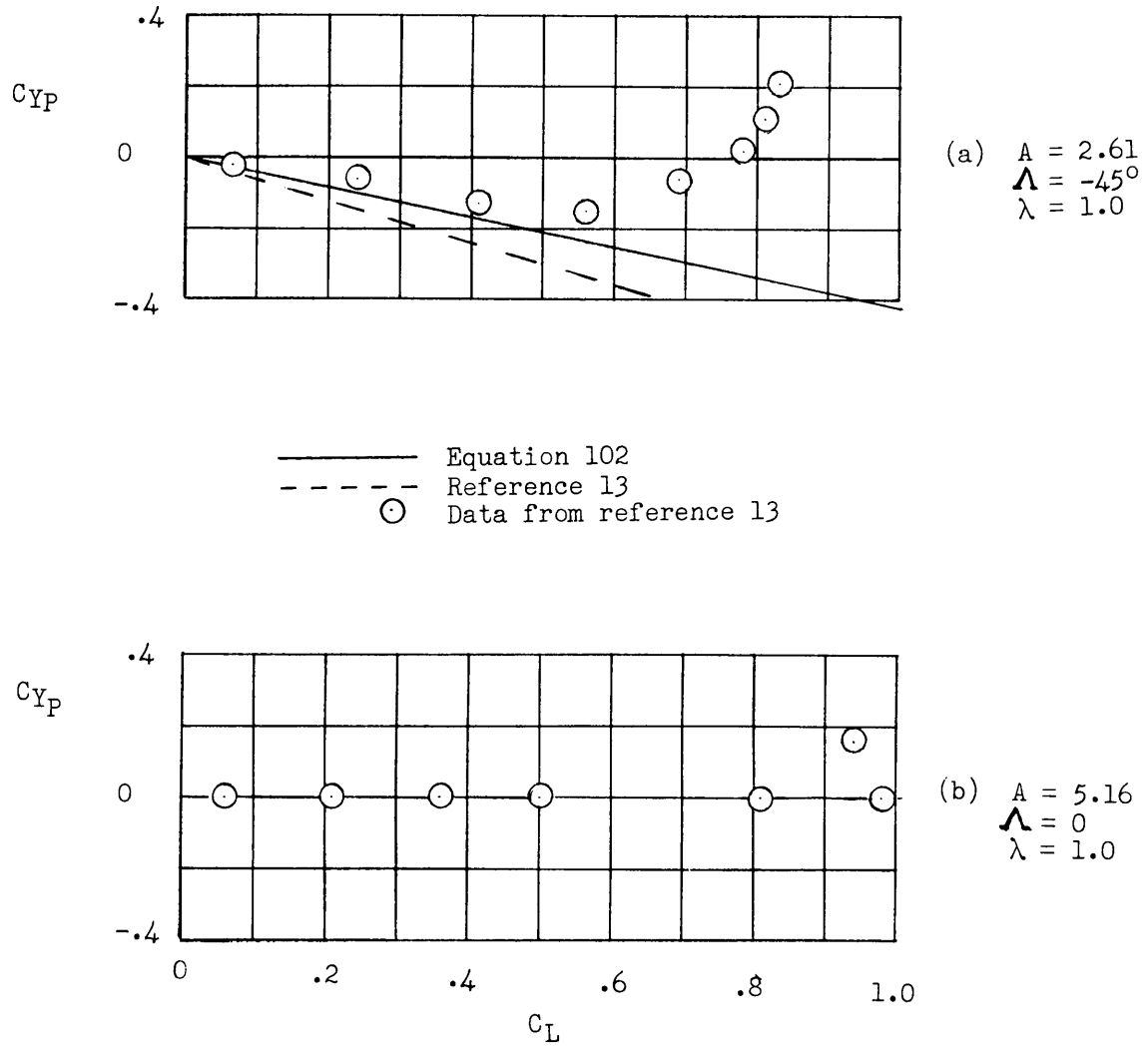

Figure 44.- Comparison of theoretical and experimental values of the variation of C_{Y_P} with C_L for several representative wings in incompressible flow.

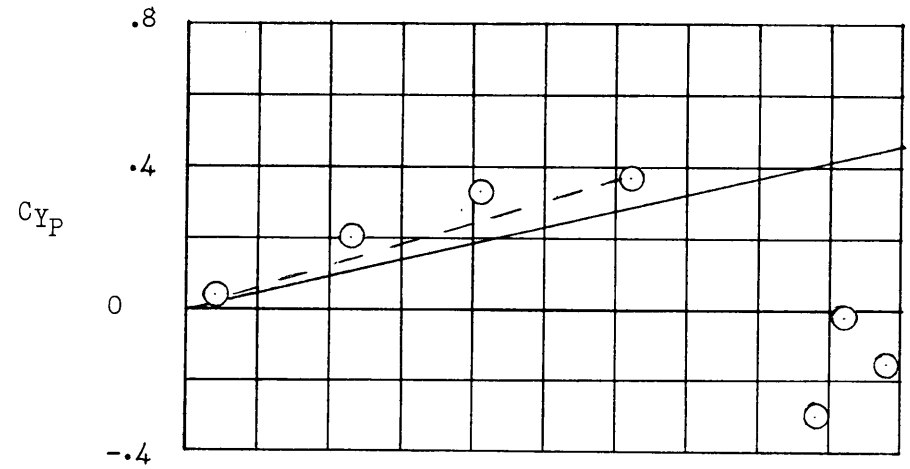

(c) A = 2.61
$\Lambda = 45^\circ$
$\lambda = 1.0$

——— Equation 102
- - - - - Reference 13
⊙ Data from reference 13

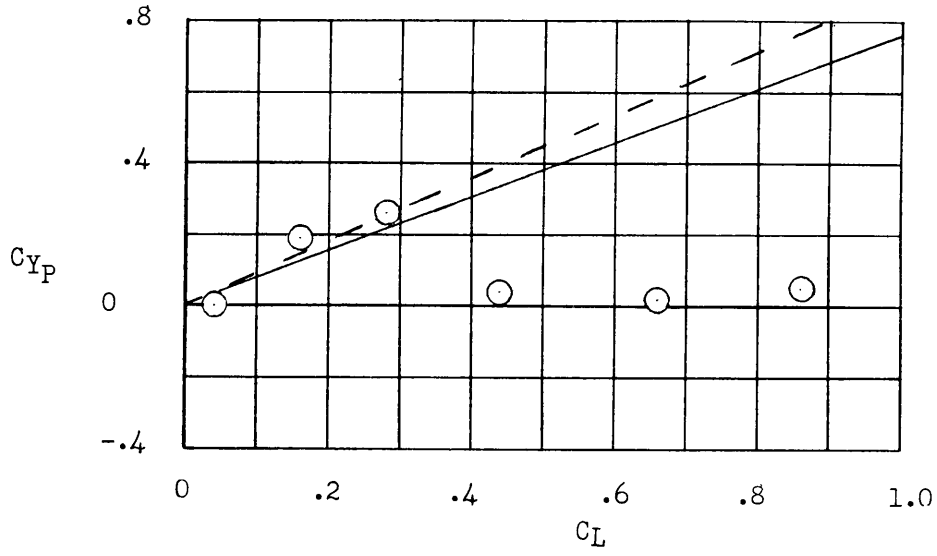

(d) A = 1.34
$\Lambda = 60^\circ$
$\lambda = 1.0$

Figure 44.- Concluded.

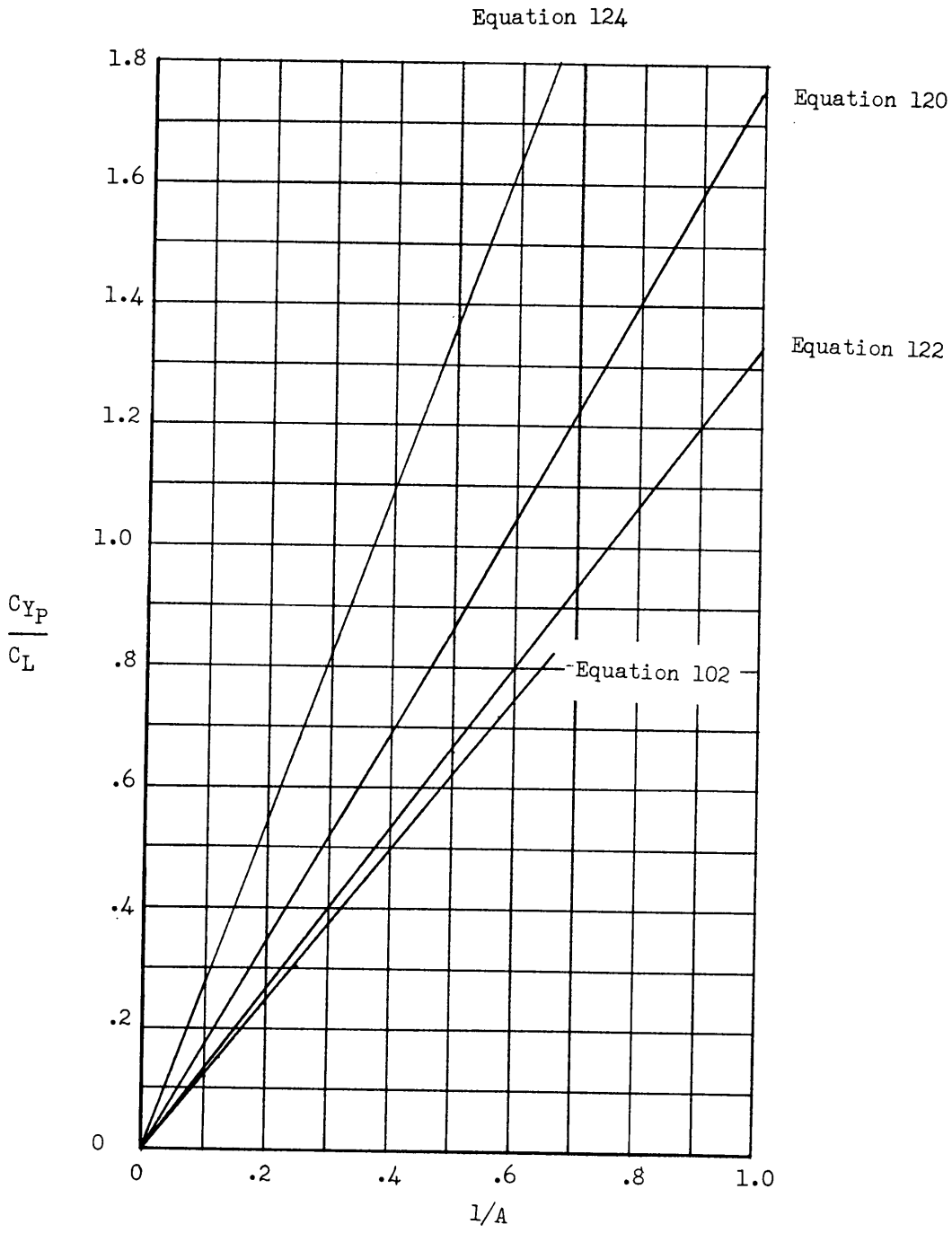

Figure 45.- Variation of $\frac{C_{Y_P}}{C_L}$ with $\frac{1}{A}$ for triangular planform wings in incompressible flow as predicted by several theories.

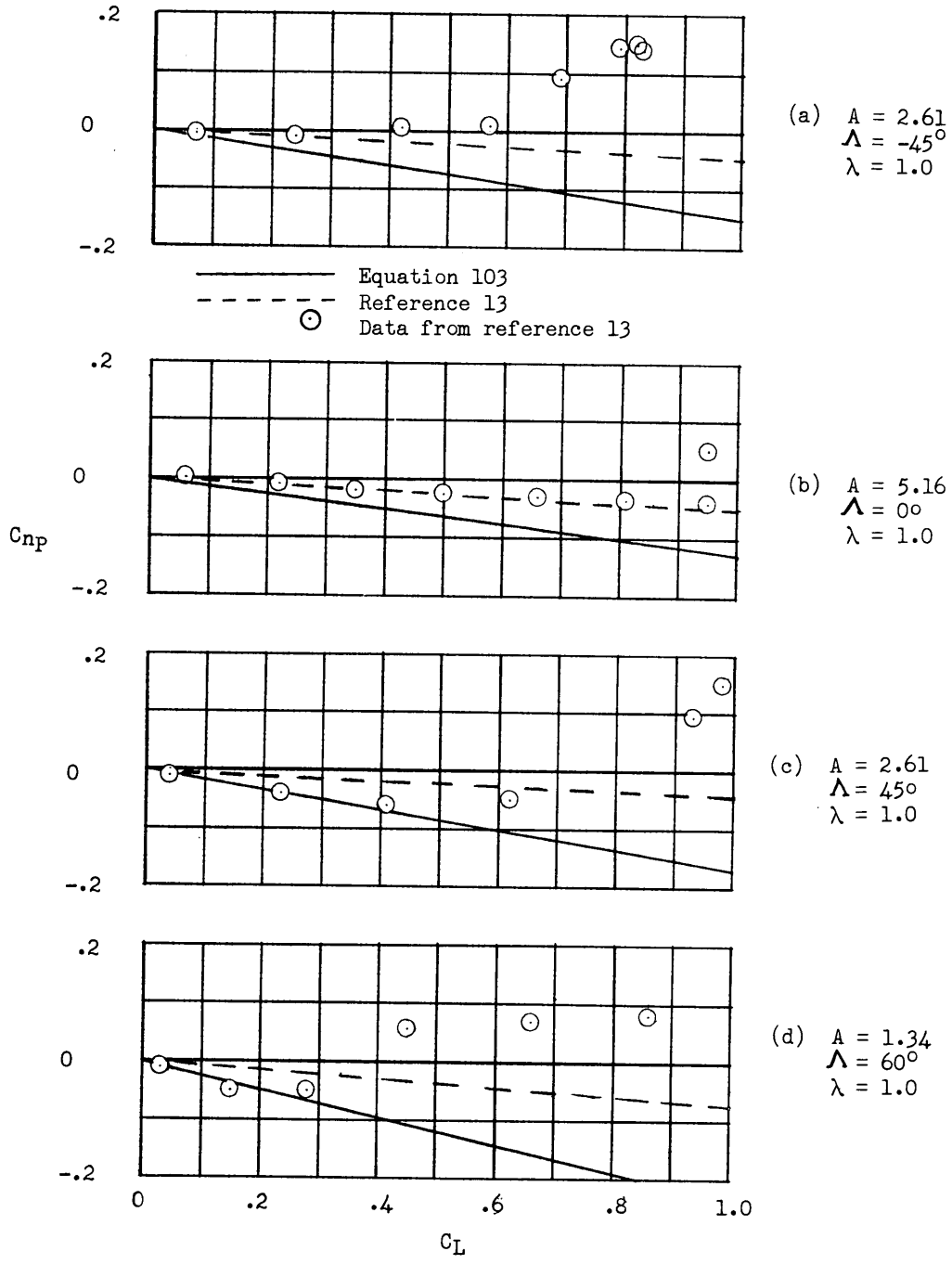

Figure 46.- Comparison of theoretical and experimental values of the variation of C_{n_P} with C_L for several representative wings in incompressible flow.

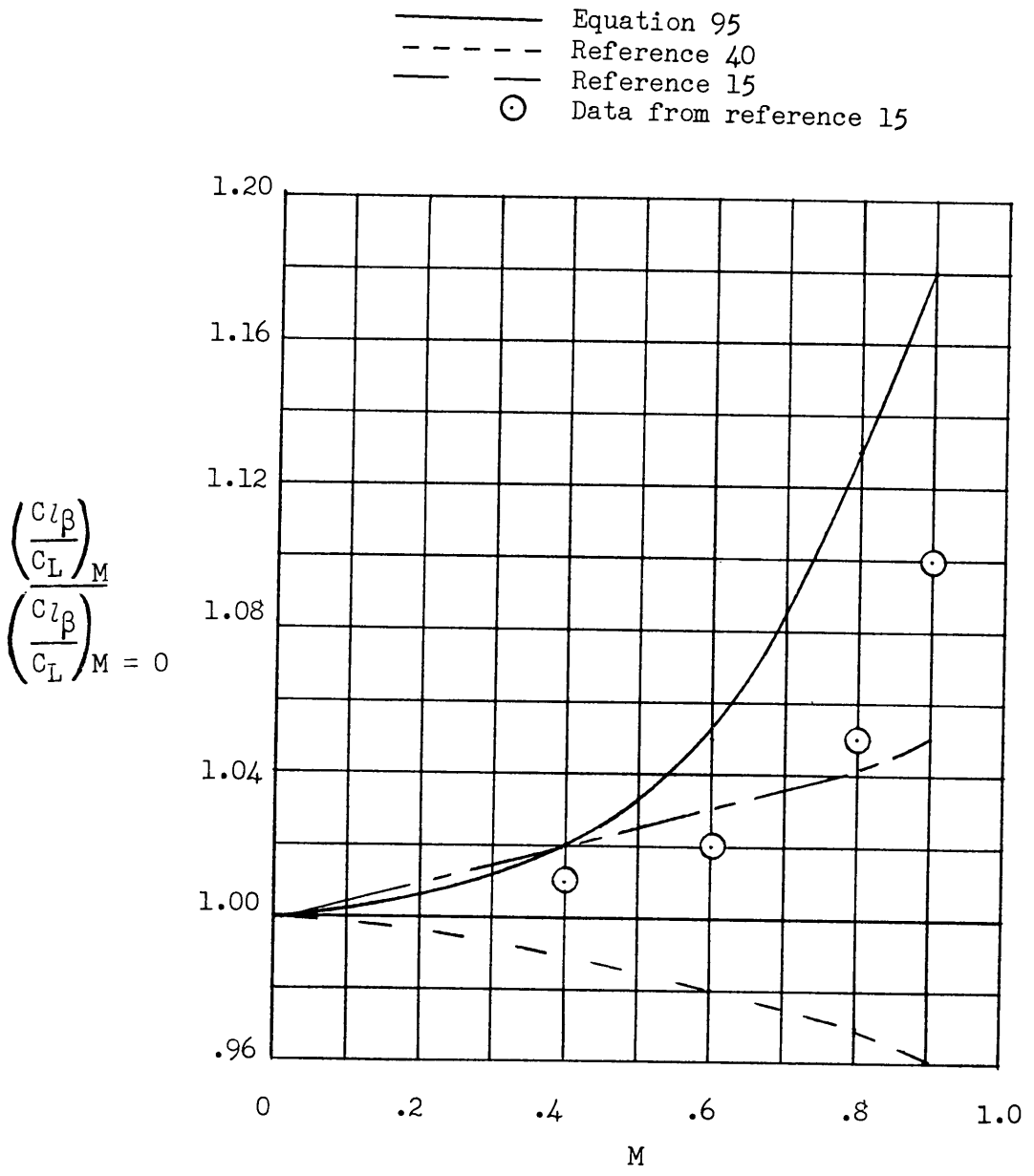

Figure 47.- Comparison of theoretical and experimental values of the effect of Mach number on $\frac{C_{l_\beta}}{C_L}$.

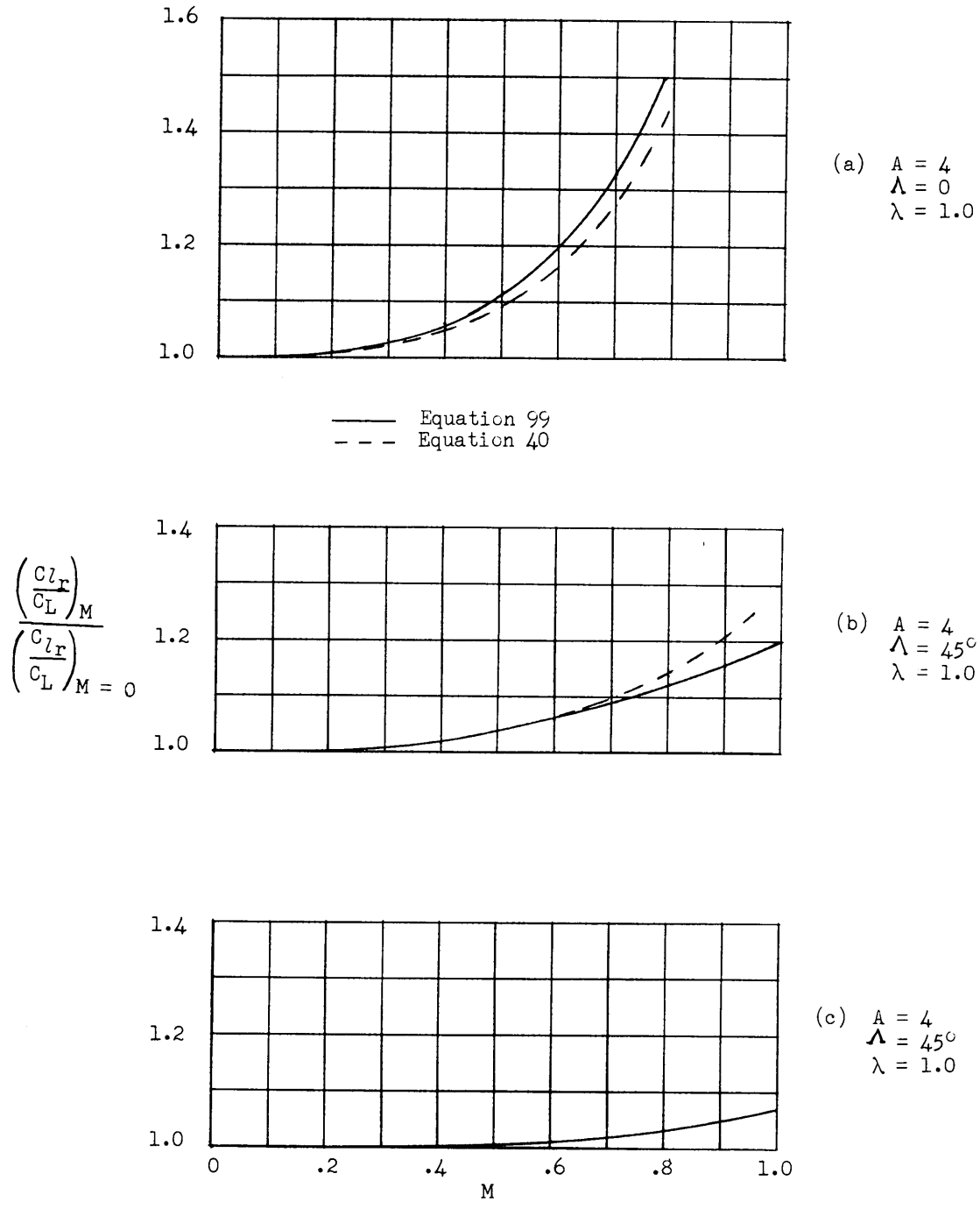

Figure 48.- Comparison of two theories for predicting the effects of Mach number on $\frac{C_{l_r}}{C_L}$ for several representative wings.

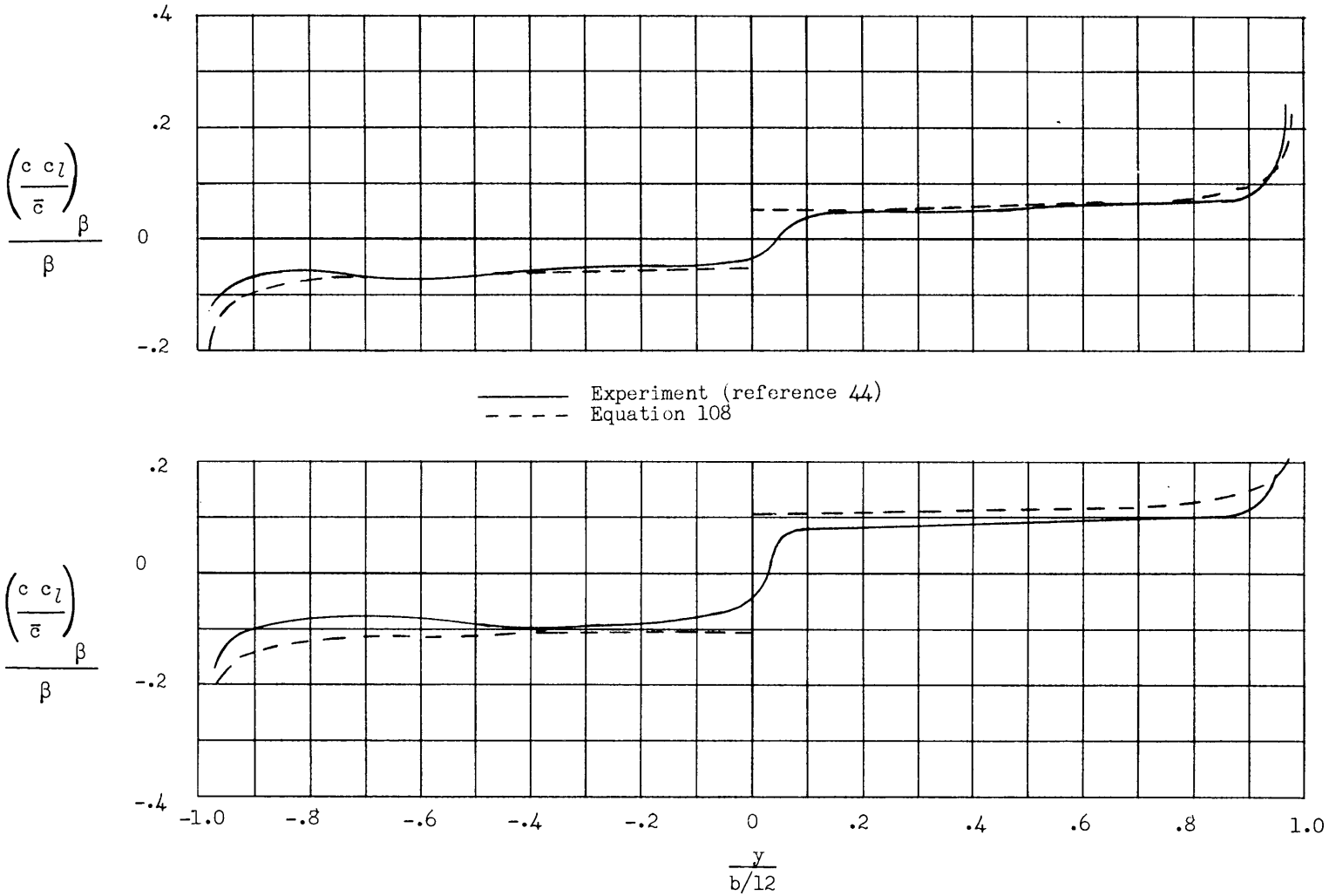

(a) A = 5.16; Λ = 45°; λ = 1.0; α = 5.7; β = 10°.

(b) A = 5.16; Λ = 45°; λ = 1.00; α = 11.5°; and β = 10°.

Figure 49.- Comparison of experimental and theoretical span loads due to sideslip for a wing in incompressible flow.

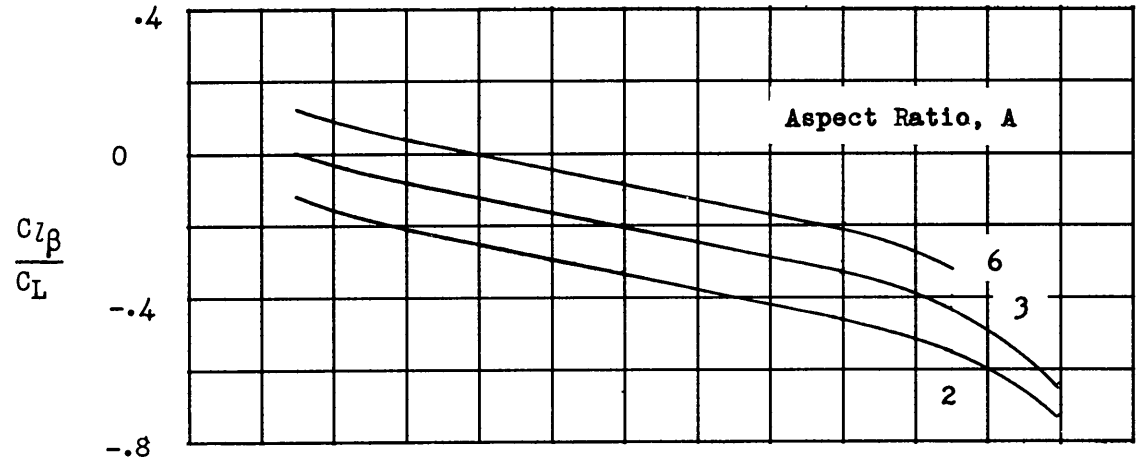

(a) M = 0

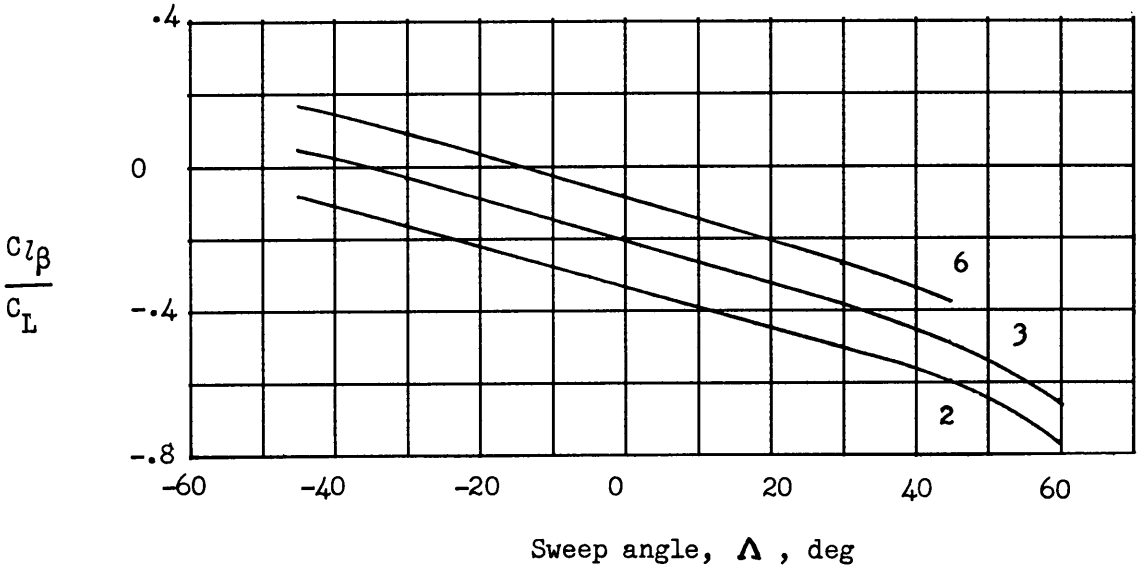

(b) M = 0.8.

Figure 50.- Variation of $\frac{C_{l_\beta}}{C_L}$ with sweep angle as predicted by equation (95). $\lambda = 1.0$.

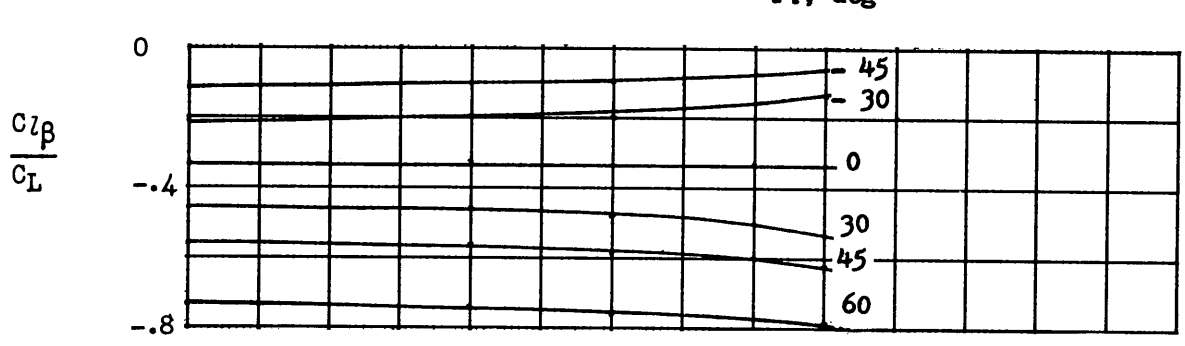

$\frac{C_{l_\beta}}{C_L}$

(a) A = 2.

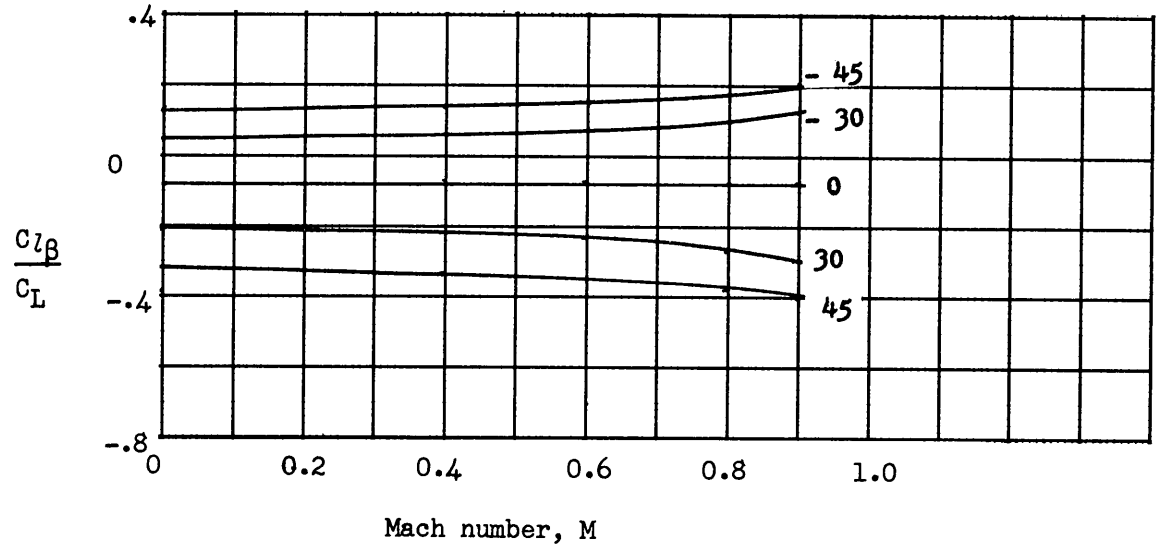

$\frac{C_{l_\beta}}{C_L}$

(b) A = 6.

Figure 51.- Variation of $\frac{C_{l_\beta}}{C_L}$ with Mach number as predicted by equation (95). $\lambda = 1.0$.

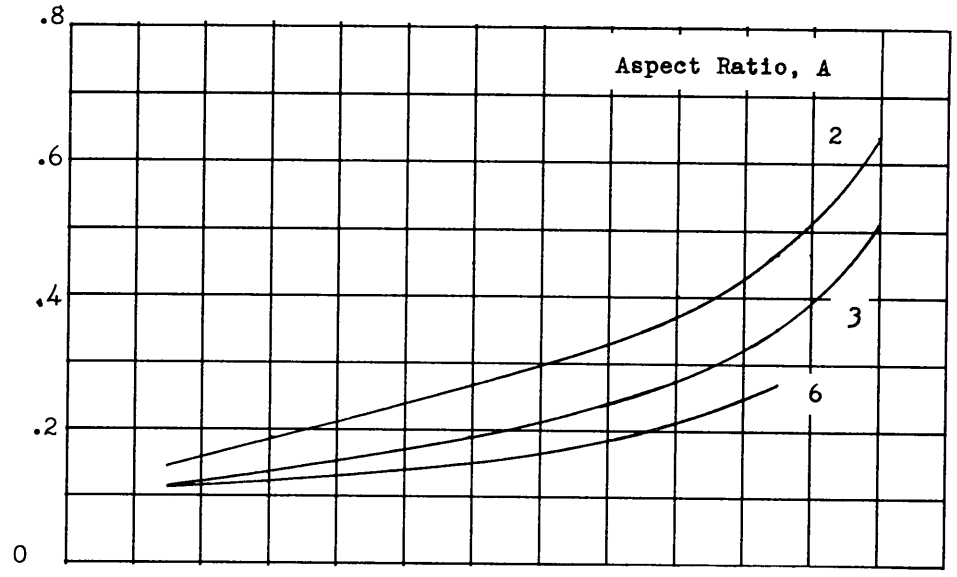

(a) M = 0.

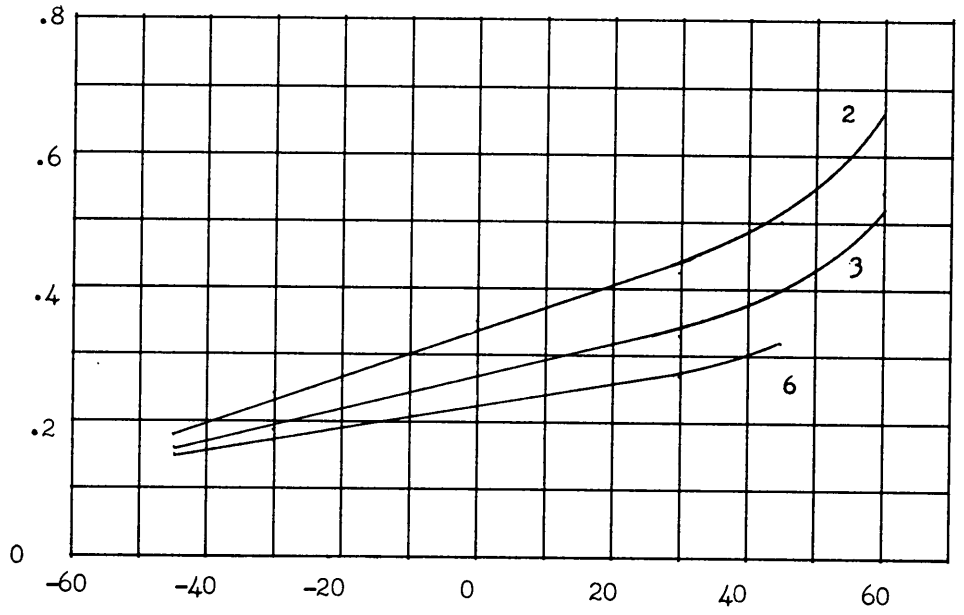

(b) M = 0.8.

Figure 52.- Variation of $\frac{Cl_r}{C_L}$ with sweep angle as predicted by equation (99). $\bar{X}^* = 0$; $\lambda = 1.0$.

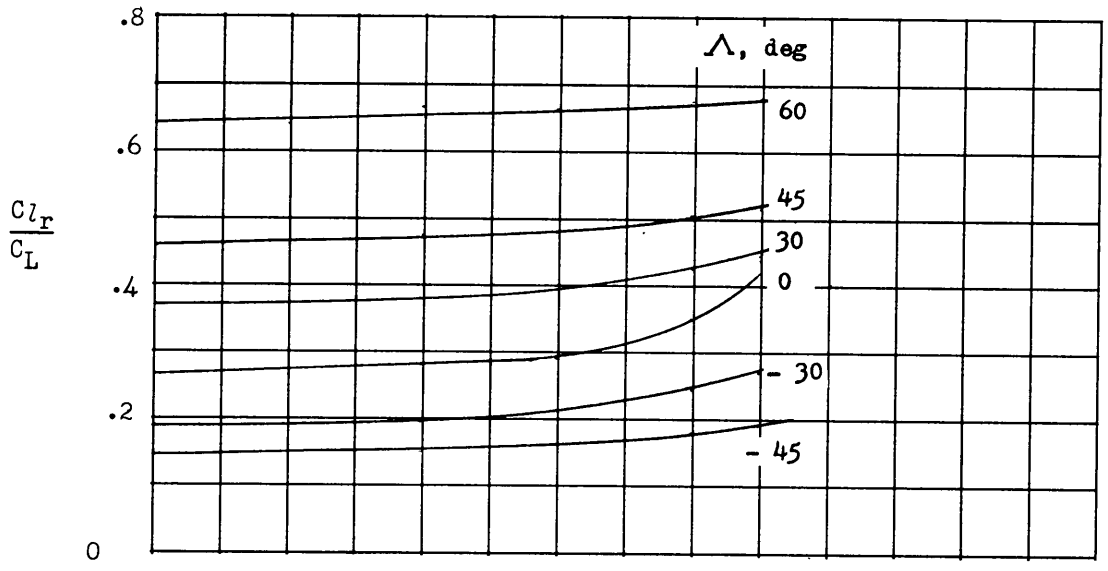

(a) A = 2.

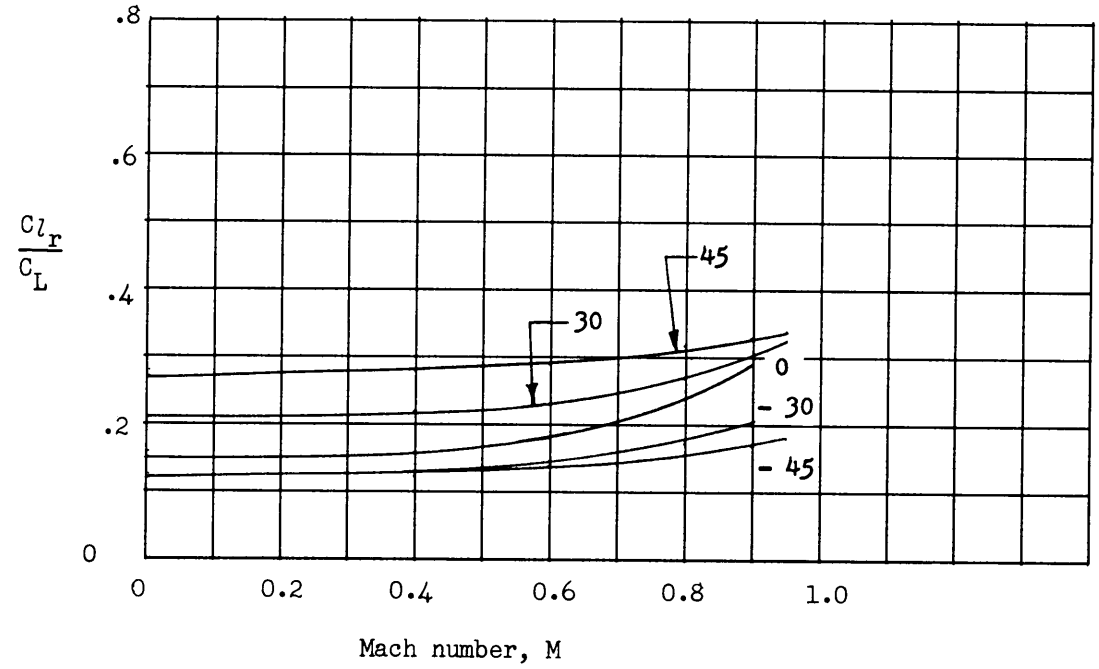

(b) A = 6.

Figure 53.- Variation of $\frac{Cl_r}{C_L}$ with Mach number as predicted by equation (99). $\bar{X}^* = 0$; $\lambda = 1.0$.

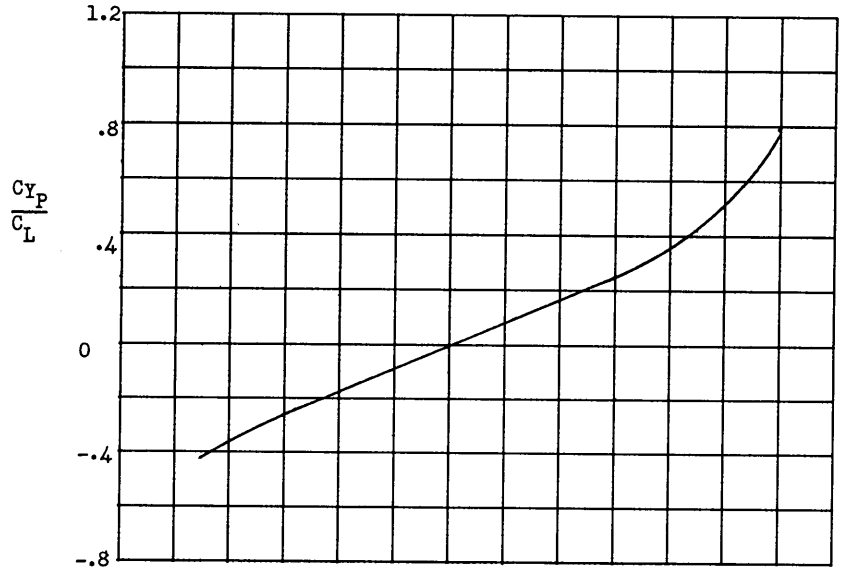

(a) M = 0.

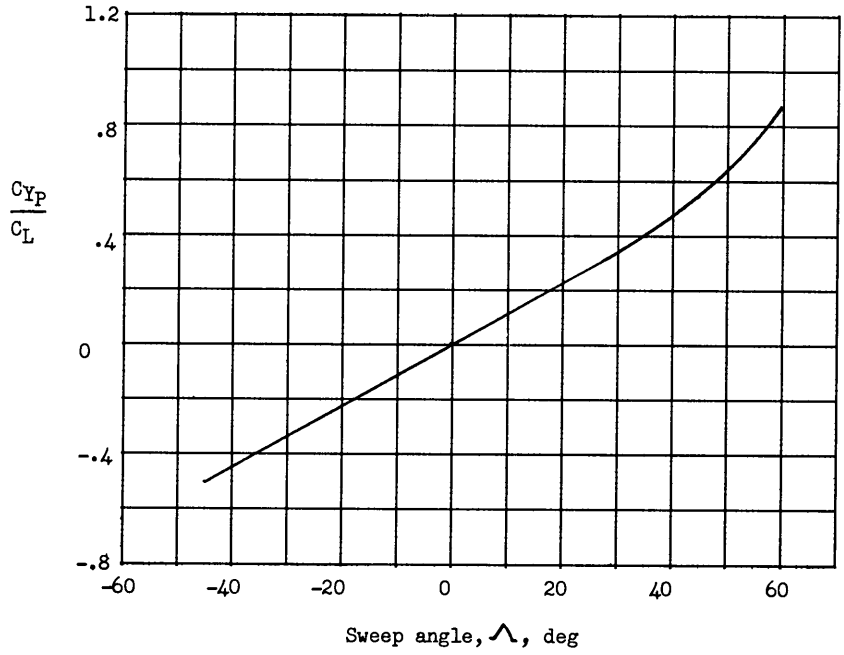

(b) M = 0.8.

Figure 54.- Variation of $\frac{C_{Y_P}}{C_L}$ with sweep angle as predicted by equation (102). Results are shown only for aspect ratio 2 since $\frac{C_{Y_P}}{C_L}$ is very nearly independent of aspect ratio. $\lambda = 1.0$.

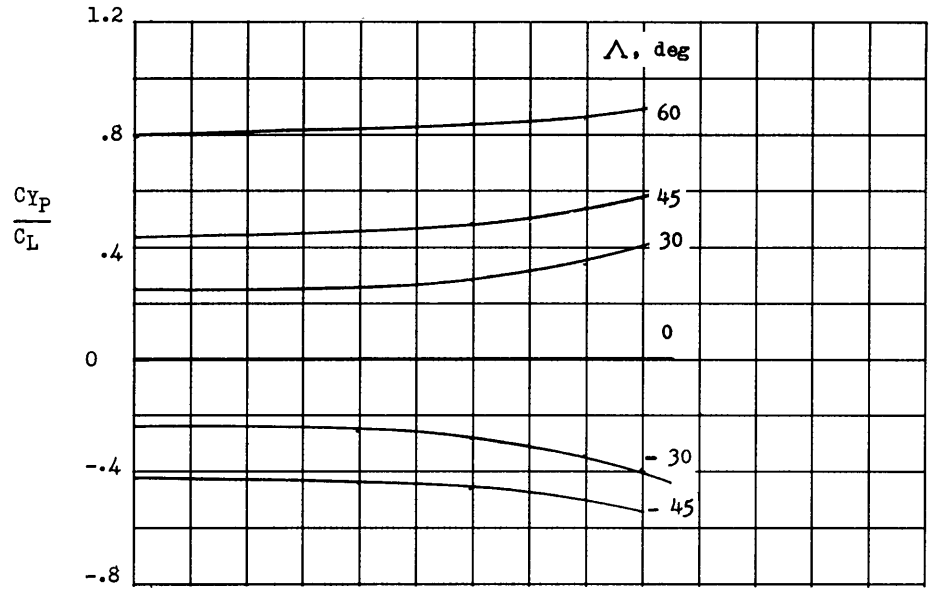

(a) A = 2.

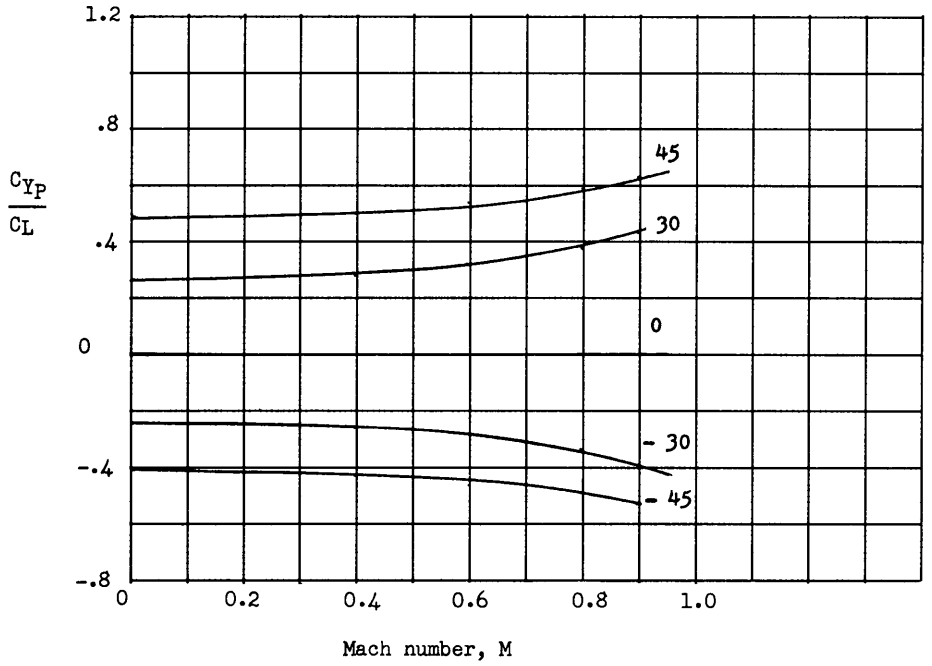

(b) A = 6.

Figure 55.- Variation of $\frac{C_{Y_P}}{C_L}$ with Mach number as predicted by equation (102). $\lambda = 1.0$.

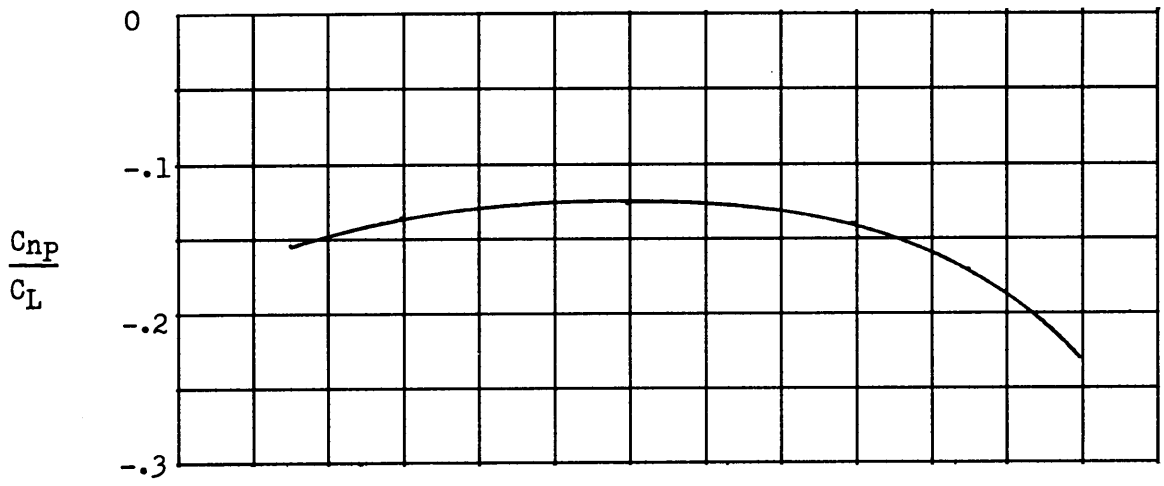

(a) M = 0.

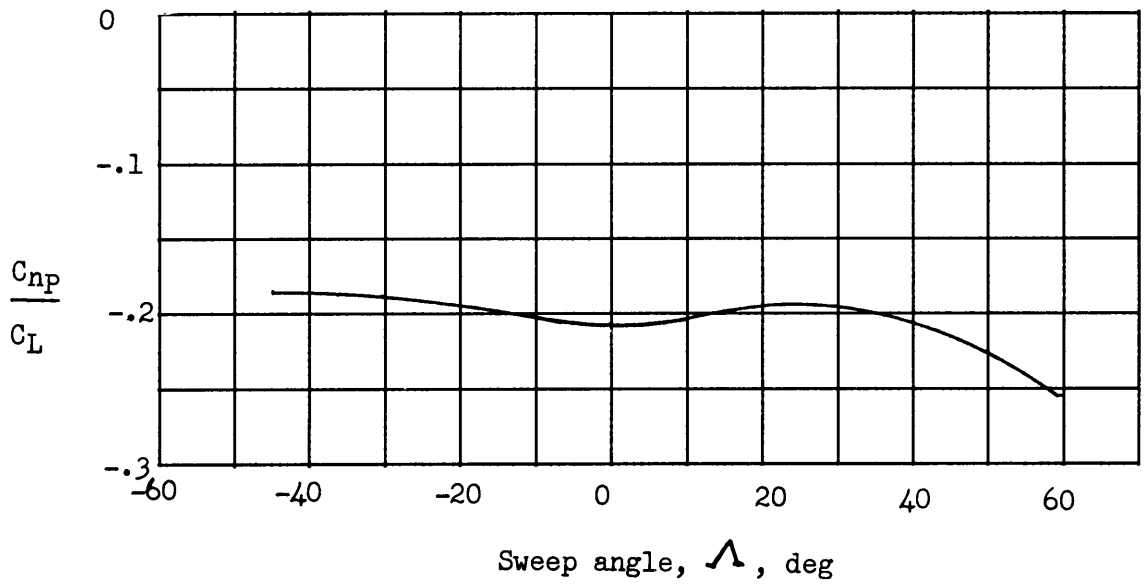

(b) M = 0.8.

Figure 56.- Variation of $\frac{C_{n_P}}{C_L}$ with sweep angle as predicted by equation (103). Results are shown only for aspect ratio 2 since $\frac{C_{n_P}}{C_L}$ is very nearly independent of aspect ratio. $\bar{X}^* = 0$; $\lambda = 1.0$.

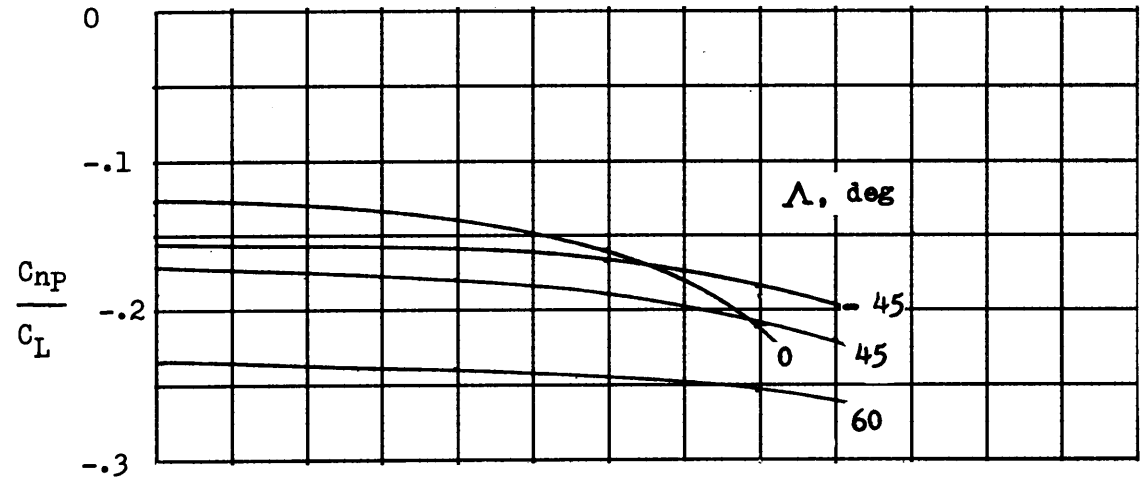

(a) A = 2.

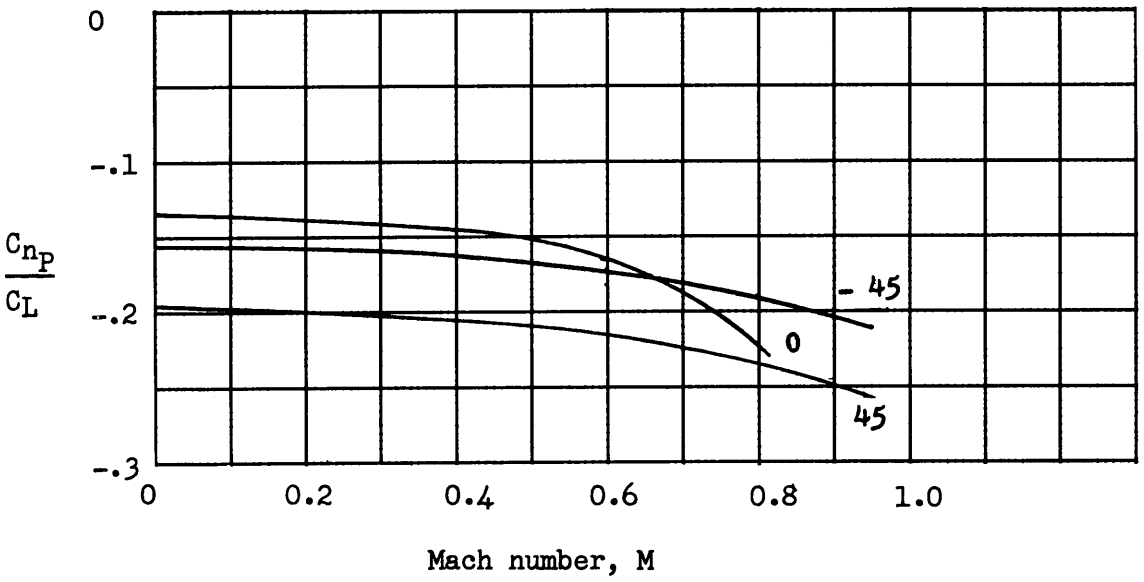

(b) A = 6.

Figure 57.- Variation of $\frac{C_{n_P}}{C_L}$ with Mach number as predicted by equation (103). $\bar{X}^* = 0$: $\lambda = 1.0$.

A THEORY AND METHOD OF PREDICTING THE STABILITY DERIVATIVES C_{l_p}, C_{l_r}, C_{n_p}, AND C_{Y_p} FOR WINGS OF ARBITRARY PLANFORM IN SUBSONIC FLOW

By M. J. Queijo

ABSTRACT

A theory and method have been developed, and charts drawn, for the estimation of certain stability derivatives for wings of arbitrary planform in subsonic flow. The derivatives obtained are those which are linearly dependent on the wing lift coefficient, and are C_{l_p}, C_{l_r}, C_{Y_p}, and C_{n_p}. The method is generally applicable to wings of any planform provided the angle-of-attack load distribution is known. Such information is available in the literature for a great variety of wing planforms, hence the requirement for this information should not be a serious limitation on the method. Further, for wings of odd planform, the angle-of-attack load distribution can be determined by straightforward methods, after which the present method is applicable for determining the above-mentioned derivatives.

The theory developed herein is based on a vortex representation of the wing. The vortex strength distribution in sideslip and yawing is justified as being the same as for the wing at angle of attack, and zero sideslip and yawing velocity. The velocity components associated with sideslip and yawing are then used with the vortex system to obtain the desired derivatives. A similar method is used for the rolling wing, however, in this case the circulation strength must be altered because

rolling velocity causes an incremental change in angle of attack across the wing span.

The derivatives estimated by the methods developed in this thesis are compared with results from other theories (where available) and also with experimental data. In general, the various theories are in agreement with regard to trends, at least for wings in incompressible flow. The present method generally appears to provide better correlation with data than other theories. The derivative which does not show very good correlation with experiment is C_{Y_p}, but fortunately this derivative is not particularly important with regard to the dynamic stability of aircraft.

Compressibility effects are also included in the method. These effects were based on the application of the Prandtl-Glauert correction to the section lift-curve slope for those parts of the derivative which were subject to a large component of the free-stream velocity. Comparisons with data for the parameter $\frac{C_{l_\beta}}{C_L}$ show that the method predicts the proper trends with regard to compressibility effects. There were no data available for verification of the theory with regard to the other derivatives.

There appears to be only one other theory published in the literature which estimates compressibility effects on the various stability derivatives. This theory also is based on application of the Prandtl-Glauert correction to the section lift-curve slope. In this case, however, the correction is applied wherever the section

lift-curve slope occurs. This procedure results in an erroneous prediction of the effects of compressibility on the derivative $\frac{C_{l_\beta}}{C_L}$. Of course the experimental variation for this derivative has been well verified.

Equations have been derived for the additional span loading associated with sideslip and yawing. There appear to be no other theories available in the literature for comparison with the present theory, and the available span load data appear to be limited to one source for loads in sideslip. In this case the present theory showed very good agreement with experiment.